



3 1176 00168 0744

NASA CR - 165185  
LYC NO. 80-27



NASA-CR-165185  
19810023604

**FINAL REPORT**

**DESIGN AND EVALUATION  
OF AN INTEGRATED  
QUIET CLEAN GENERAL AVIATION TURBOFAN  
(QCGAT)  
ENGINE AND AIRCRAFT PROPULSION SYSTEM**

by

*Jon German, Philip Fogel and Craig Wilson*

**AVCO LYCOMING DIVISION**  
**550 South Main Street**  
**Stratford, Connecticut 06497**

LIBRARY COPY

FEB 24 1981

MANLEY STARR CENTER  
LIBRARY, NASA  
HAMPTON, VIRGINIA

Prepared for

**NATIONAL AERONAUTICS AND SPACE ADMINISTRATION**

**NASA Lewis Research Center  
Cleveland, Ohio 44135**

**Contract NAS 3-20584**



NF02439

**All Blank Pages  
Intentionally Left Blank  
To Keep Document Continuity**



***FINAL REPORT***

**DESIGN AND EVALUATION  
OF AN INTEGRATED  
QUIET CLEAN GENERAL AVIATION TURBOFAN  
(QCGAT)  
ENGINE AND AIRCRAFT PROPULSION SYSTEM**

*by*

*Jon German, Philip Fogel and Craig Wilson*

**AVCO LYCOMING DIVISION  
550 South Main Street  
Stratford, Connecticut 06497**

Prepared for

**NATIONAL AERONAUTICS AND SPACE ADMINISTRATION**

**NASA Lewis Research Center  
Cleveland, Ohio 44135**

**Contract NAS 3-20584**

*N81-16057#*

1 Report No		2 Government Accession No		3 Recipient's Catalog No	
4 Title and Subtitle DESIGN AND EVALUATION OF AN INTEGRATED QUIET, CLEAN GENERAL AVIATION TURBO FAN (QCGAT) ENGINE AND AIRCRAFT PROPULSION SYSTEM				5 Report Date April 1980	
				6 Performing Organization Code	
7 Author(s) J. German, P. Fogel, C. Wilson				8 Performing Organization Report No LYC 80-27	
9 Performing Organization Name and Address Avco Lycoming Division 550 South Main Street Stratford, Connecticut 06497				10 Work Unit No	
				11 Contract or Grant No NAS 3-20584	
12 Sponsoring Agency Name and Address NASA - Lewis Research Center 2100 Brookpark Road Cleveland, Ohio 44135				13 Type of Report and Period Covered Contractor Dec. 76 - Apr. 80	
				14 Sponsoring Agency Code	
15 Supplementary Notes Program Manager, G.K. Sievers NASA - LRC, Cleveland, Ohio					
16 Abstract <p>Avco Lycoming participated in the NASA Quiet, Clean, General Aviation Turbofan (QCGAT) engine program by designing a small turbofan engine in the 7000 N(1600 lbf ) thrust class. The engine and nacelle system design was to demonstrate the applicability of large turbofan engine technology to small turbofans suitable for the general aviation market.</p> <p>The Lycoming design was based on the LTS-101 engine family for the core engine. A high bypass fan design (BPR=9.4) was incorporated to provide reduced fuel consumption for the design mission.</p> <p>All acoustic and pollutant emissions goals were achieved.</p> <p>A discussion of the preliminary design of a business jet suitable for the developed propulsion system is also included in this report.</p> <p>Large engine technology can be successfully applied to small turbofans, and noise or pollutant levels need not be constraints for the design of future small general aviation turbofan engines.</p>					
17 Key Words (Suggested by Author(s)) - General Aviation - Turbofan - QCGAT - Noise Reduction				18 Distribution Statement <del>Foreign Distribution excluded</del> <del>Source of Availability</del> NASA Industrial Applications Center	
19 Security Classif (of this report) UNCLASSIFIED		20 Security Classif (of this page) UNCLASSIFIED		21 No of Pages 219	
22 Price*					

## FOREWORD

The work described herein was conducted by the Lycoming Gas Turbine Division of Avco Corporation with support from Beech Aircraft Corporation in the preliminary aircraft design, Lockheed Aircraft Corporation in the acoustical duct treatment evaluation, and the Aerostructures Division of Avco in fabrication of the engine nacelle.

The support and technical expertise of these subcontractors in conjunction with the various Lycoming engineering department were instrumental in attaining the contract goals addressed in this document.

The authors wish to acknowledge Mr. Keith Sievers, NASA QCGAT Program Manager, and his staff for their guidance and support.



## TABLE OF CONTENTS

	<u>Page</u>
FOREWORD .....	iii
LIST OF ILLUSTRATION .....	vii
LIST OF TABLES .....	xv
1.0 SUMMARY .....	1
2.0 INTRODUCTION .....	2
3.0 AIRCRAFT AND ENGINE DESIGN OPTIMIZATION .....	2
3.1 Aircraft Design Approach .....	3
3.2 Engine Design .....	15
3.2.1 Design Considerations .....	15
3.2.2 Engine Hardware Description .....	17
3.3 Nacelle Design Approach .....	48
3.3.1 Aerodynamic Design .....	51
3.3.2 Acoustic Considerations .....	63
3.3.3 Structural Design .....	68
3.4 Mixer Nozzle Design .....	79
4.0 SUBSYSTEM TEST RESULTS .....	84
4.1 Fan Blade Analysis .....	84
4.1.1 Test Program .....	84
4.1.2 Fan Blade Test Results .....	84
4.2 Low-Pressure Turbine Blade Analysis .....	84
4.2.1 Power Turbine Blade Results .....	90
4.3 Ring Gear Frequency Analysis .....	90
4.3.1 Ring Gear Test Results .....	90
4.4 Flow Divider and Fuel Manifold System Analysis .....	97
4.5 Fan Component Test Rig .....	97
4.5.1 Fan Component Test Results .....	102
4.5.2 Distorted Inlet Test Results .....	108
4.6 Combustor Module .....	114
4.6.1 Test Rig and Facilities .....	116
4.6.2 Test Sequence .....	116
4.6.3 Test Results .....	119

## TABLE OF CONTENTS

	<u>Page</u>
5.0 ENGINE/NACELLE SYSTEMS PERFORMANCE .....	121
5.1 Overall Performance .....	121
5.1.1 Component Performance .....	121
5.1.2 Full Engine Tests .....	126
5.2 Emission Test Results .....	146
5.2.1 Design and Emissions Projections .....	146
5.2.2 Emissions Sampling .....	152
5.2.3 Emissions Summary .....	152
5.3 Acoustical Performance .....	155
5.3.1 Background .....	155
5.3.2 Engine Design and Noise Prediction ....	159
5.3.3 Sound Treatment Design .....	165
5.3.4 Wing Shielding .....	173
5.3.5 Acoustic Test Phase .....	173
5.3.6 Data Analysis ..	180
5.3.7 Conclusion .....	204
6.0 SUMMARY OF RESULTS .....	207
6.1 Objectives .....	207
6.2 Test Results .....	207
6.2.1 Overall Engine Performance Demonstrated .....	208
6.2.2 Emissions .....	208
6.2.3 Acoustics.....	209
6.3 Concluding Remarks.....	209
REFERENCES.....	210
DISTRIBUTION LIST.....	212



## LIST OF ILLUSTRATIONS

<u>Figure</u>		<u>Page</u>
1	New General Aviation Aircraft for the 1980 Decade .....	5
2	QCGAT Aircraft Design .....	6
3	Design Areas Selected for Composite Structures ....	9
4	Wing Selection .....	11
5	Best Range Versus Payload .....	14
6	Aircraft Stall Speed and Field Capacity .....	16
7	Cycle Optimization for Specific Fuel Consumption ...	18
8	Selected Fan Pressure Ratio .....	19
9	Engine Configuration .....	20
10	Engine Modules .....	21
11	Gas Generator Module .....	23
12	Circumferentially Stirred Combustor Flow Pattern .....	26
13	Airblast Fuel Injector System .....	29
14	Turbine Arrangement .....	31
15	Cooling of First Stage Rotor Blades and Turbine Nozzle .....	32
16	Power Turbine Module .....	34
17	Turbine Section Meridional Flow Path .....	36
18	Interturbine Duct Inner and Outer Wall Velocity Distribution at Sea Level Takeoff .....	37

LIST OF ILLUSTRATIONS (Cont.)

<u>Figure</u>		<u>Page</u>
19	Accessory Drive Module Installation .....	39
20	QCGAT Accessory Gearbox .....	40
21	Power Control and Fuel System Schematic .....	42
22	Fuel Control Assembly .....	44
23	Dual Compressor Flow Fence Schematic .....	45
24	Flow Fence Actuator .....	46
25	Fan Overspeed Trip System .....	47
26	Cross Section of Engine with Cutaway .....	50
27	QCGAT Nacelle External Geometry .....	52
28	QCGAT Nacelle Front Cowl Geometry .....	53
29	QCGAT Nacelle Maximum Drag Divergence Flight Speed .....	54
30	QCGAT Upper Cowl Lip Spillage Margin .....	55
31	QCGAT Inlet Flow Incidence Limits .....	57
32	Inlet Pressure Recovery .....	58
33	QCGAT Nacelle Duct Areas and Mean Mach Numbers .....	59
34	QCGAT Flight Nacelle with Sound Treated Panels Installed .....	60
35	QCGAT Lockheed Fan Exhaust Noise Treatment Design .....	61
36	Sample from Lockheed's Materials Handbook for Metal .....	67

LIST OF ILLUSTRATIONS (Cont.)

<u>Figure</u>		<u>Page</u>
37	Nacelle Sectional View .....	69
38	QCGAT Nacelle Components .....	70
39	Nacelle Materials and Weights .....	72
40	Nacelle Fire Prevention/Compartment Ventilation .....	73
41	Test Nacelle Assembly .....	75
42	QCGAT Flight Nacelle Simulation .....	76
43	Replaceable Inlet Lips .....	77
44	Bellmouth and Flight Nacelle Inlets .....	78
45	QCGAT Exhaust Nozzle System .....	80
46	Core Engine Mixer Nozzle Geometric Definition .....	81
47	Lycoming QCGAT Mixer Nozzle Design .....	82
48	Mixer Nozzle Installation .....	83
49	General Test Setup Holographic Analysis .....	85
50	Fan Blade Root Fixture .....	86
51	Fan Blade Natural Frequencies and Associated Mode Shapes - First and Second Bending Mode, First Torsional Mode .....	87
52	Fan Blade Natural Frequencies and Associated Mode Shapes - Second Torsional Mode, Third and Fourth Bending Mode .....	88
53	Fan Blade Excitation Diagram .....	89
54	Power Turbine Segment Mounted to Shaker .....	91

LIST OF ILLUSTRATIONS (Cont.)

<u>Figure</u>		<u>Page</u>
55	Power Turbine Natural Frequencies and Associated Mode Shapes .....	92
56	Power Turbine Blade Excitation Diagram at Ambient Temperature .....	93
57	Power Turbine Blade Excitation Diagram at 1250°F .....	94
58	Ring Gear Clamping Arrangement and Natural Frequencies and Associated Mode Shapes .....	95
59	Ring Gear Natural Frequencies and Associated Mode Shapes .....	96
60	QCGAT Fan Module Test Rig .....	98
61	Fan Module Instrumentation Planes - Nomenclature ..	99
62	Aerodynamic Performance Instrumentation .....	100
63	Fan Module Inlet Instrumentation Planes and Distortion Screen Position .....	101
64	QCGAT Fan Module - Testway Installation .....	103
65	QCGAT Fan Module Baseline Test - Bypass Overall Performance Map .....	104
66	QCGAT Fan Module Baseline Test - Supercharger Overall Performance Map .....	105
67	Bypass Exit Plane Profile Data .....	106
68	Supercharger Exit Plane Profile Data .....	107
69	Area Blockage (15 Percent) Inlet Distortion Plate with Resultant Total Pressure Contours .....	110
70	Distortion Index as a Function of Total Referred Airflow .....	112

LIST OF ILLUSTRATIONS (Cont.)

<u>Figure</u>		<u>Page</u>
71	Bypass Overall Performance with Inlet Distortion ...	113
72	Comparison of the LTS 101 Combustor with the QCGAT Combustor .....	115
73	Circumferentially Stirred Combustor Flow Pattern...	117
74	QCGAT Annular Combustor Test Rig and Test Cell Installation .....	118
75	NO <sub>x</sub> Versus Combustor Inlet Temperature .....	120
76	Predicted Influence of the Mixer .....	124
77	QCGAT Referee Configuration - Inlet .....	127
78	QCGAT Referee Configuration - Exit .....	128
79	QCGAT Test Nacelle .....	129
80	Replaceable Inlet Lips .....	130
81	Details of the Test Nacelle .....	131
82	Low Spool Speed Versus Net Thrust .....	134
83	High Spool Speed Versus Net Thrust .....	135
84	Thrust Specific Fuel Consumption Versus Net Thrust .....	136
85	Low Spool Speed Versus High Spool Speed .....	137
86	Fan Pressure Ratio Versus Fan Bypass Airflow .....	138
87	Total Engine Airflow Versus Low Spool Speed .....	139
88	Low Spool Speed Versus Net Thrust - Nacelle Installed .....	140

LIST OF ILLUSTRATIONS (Cont.)

<u>Figure</u>		<u>Page</u>
89	High Spool Speed Versus Net Thrust - Nacelle Installed .....	141
90	Thrust Specific Fuel Consumption Versus Net Thrust - Nacelle Installed .....	142
91	Low Spool Speed Versus High Spool Speed - Nacelle Installed .....	143
92	Fan Pressure Ratio Versus Bypass Airflow - Nacelle Installed .....	144
93	Total Engine Airflow Versus Low Spool Speed - Nacelle Installed .....	145
94	QCGAT Combustor .....	148
95	NO <sub>x</sub> Versus Combustor Inlet Temperature .....	151
96	Engine Emissions Sampling Test Probes .....	153
97	Cross Section of the Engine with Cutaway .....	156
98	QCGAT Noise Goals .....	158
99	Noise Prediction Procedures .....	160
100	Fan Noise Components .....	162
101	Core Noise Model .....	164
102	Sound Treatment Locations .....	166
103	Sound Treatment Design .....	168
104	Inlet Attenuation .....	170
105	Exhaust Attenuation .....	171
106	Sound Treatment Panels .....	172

LIST OF ILLUSTRATIONS (Cont.)

<u>Figure</u>		<u>Page</u>
107	Wing Shielding .....	174
108	Microphone Arrangement .....	176
109	Test Site .....	177
110	Instrumentation Setup for the Acquisition of the Acoustic Data .....	178
111	Barrier .....	179
112	Probe Locations .....	181
113	Reference System .....	182
114	Measurements with Predicted Fan .....	184
115	Measurements with Jet Added .....	185
116	Core Added to Measured .....	186
117	High Power Setting.....	187
118	Core Comparison .....	188
119	Revised Core Comparison .....	190
120	Core Noise Dominance .....	191
121	Fan Directivity Plots .....	192
122	High Fan Directivity .....	193
123	Final Comparison .....	194
124	Sound Treatment .....	196
125	Insertion Loss - Inlet .....	197
126	Insertion Loss - Discharge .....	198

LIST OF ILLUSTRATIONS (Cont.)

<u>Figure</u>		<u>Page</u>
127	Jet Spectra .....	199
128	Flyover Procedures .....	200
129	Component Contribution - Approach Noise .....	202
130	Component Contribution - Takeoff Noise .....	203
131	Noise Levels - QCGAT Goals .....	205
132	Noise Levels - FAA Standards .....	206



LIST OF TABLES

<u>Table</u>		<u>Page</u>
1	Benefits from Advanced Aircraft Design .....	8
2	Engine Operating Parameters .....	62
3	Results of Design Study .....	122
4	QCGAT Performance Goals .....	123
5	Engine Configurations Tested .....	132
6	QCGAT Performance .....	147
7	Initial Estimated QCGAT Emissions .....	150
8	QCGAT Emissions Results .....	154



## 1.0 SUMMARY

Avco Lycoming participated in the NASA Quiet, Clean, General Aviation Turbofan (QCGAT) engine program to design a small turbofan in the 7000N (1600 lbf) thrust class. Lycoming's engine is a high-bypass ratio, twin-spool design with a geared-fan. The core engine is a growth derivative of the Lycoming LTS 101 engine series being used in many turboshaft and turboprop applications.

The Lycoming demonstrator engine program accomplished the following goals which were the primary objectives of the NASA/QCGAT program:

- o Large engine technology can be successfully applied to general aviation-size engines to reduce noise and pollutant emissions verifying that these items are not a constraint to the general aviation market growth.
- o Pollutant-emission design goals met or exceeded stringent requirements which have since been abandoned by the EPA as part of the Clean Air Act of 1970.
- o Noise emissions were substantially below (-25 dB) the Federal Air Regulations, Part 36 limits for aircraft takeoff, approach, and side line conditions.
- o Fuel efficiency was superior when compared with presently available moderate-bypass ratio engines in the thrust class up to 11,000N (2500 lbf).

## 2.0 INTRODUCTION

The general aviation fleet has shown significant growth characteristics in the past decade, it is expected that this trend will continue throughout the 1980's. In particular, the size of the multi-engine general aviation fleet is expected to increase by 20 percent. These general aviation aircraft typically use suburban airports unprotected by commercial buffer zones. Therefore, there is a potential for general aviation traffic to create more widespread, adverse, community reaction to noise and pollution than that experienced by the commercial air carriers.

A program initiated by NASA to address this segment of general aviation aircraft industry culminated in Avco-Lycoming's receiving a contract to design, develop, and test a Quiet Clean General Aviation Turbofan (QCGAT) engine. The objective of this program was to demonstrate the applicability of available, large turbofan engine technology to small general aviation engines so as to obtain significant reductions in noise and pollutant emissions, while reducing or maintaining fuel consumption levels.

This report presents the Lycoming-QCGAT engine development study, covering design through engine test and including acoustical, pollutant emissions, and performance results. Also included is the preliminary design of an appropriate general aviation aircraft that could use the propulsion system developed.

## 3.0 AIRCRAFT AND ENGINE DESIGN OPTIMIZATION

The Avco Lycoming QCGAT engine was designed to demonstrate the latest noise-control technology. The high-bypass fan was optimized with an existing proven core engine and advances in emission reduction. The resultant design of the aircraft/propulsion system used the technical expertise of the following subcontractors:

- o Beech Aircraft Corporation..... Aircraft Design
- o Avco Aerostructures..... Nacelle Mechanical Design
- o Lockheed Aircraft Corporation... Nacelle Acoustic Treatment

These studies culminated in the preliminary design of a twin-engine, six-place, executive aircraft having an advanced propulsion system to meet the needs of the general aviation industry for a quiet-clean, efficient aircraft in the current and future decades.

### 3.1 AIRCRAFT DESIGN APPROACH

Beech Aircraft Corporation was enlisted under separate contract with Lycoming to design an aircraft based on the proposed QCGAT engine. To guide the aircraft system design, five primary objectives were established.

1. Practical, direct application of technology without significant scaling.
2. The aircraft must offer attractive range, fuel economy, and flight speed. A target of 2593 km (1400NM) was established. This exceeds the range of most current small business aircraft thereby providing a nonstop capability between opposite extremes of high-density traffic areas.
3. A cruise Mach number of 0.6, chosen as an optimal compromise between time and fuel economy, provides a 40-percent greater cruise speed than a turboprop with a 30-percent improvement in fuel economy over operation at 0.8 Mach number.
4. A balanced field length of 762 meters (2500 ft) was desired because it would permit safe operation from over 70 percent of all public airports, including those with unimproved runways.
5. Close attention to ecological characteristics of an aircraft system design was desired since they might well become primary competitive parameters for the General Aviation industry in future decades.

The initial step in aircraft preliminary design was the selection of appropriate size and design. The vast majority of general aviation aircraft operating from airfields located in suburban communities are in the size class below 5450 kg (12,000 lb) gross

weight. In the lower extremity of the gross weight spectrum, small private aircraft in the range below 1800 kg (4,000 lb) are generally powered by single reciprocating engines. It is expected that market constraints for very low-cost aircraft in this class will dictate continued usage of reciprocating engines for the foreseeable future. It, therefore, follows that the greatest public ecological benefits can be realized by introduction of a quiet clean aircraft system in the 1814 - 5433 kg (4,000 - 12,000 lb) gross weight class. Figure 1 shows the projected market volume for various sizes of general aviation aircraft.

As with the passenger car trend toward smaller, more sophisticated cars to perform the same function, it is expected that the 1980's will see a similar general aviation trend towards reduced aircraft weight and smaller engines size for the same mission. Because noise, emissions, and fuel consumption reduce with engine size, subsequent improvement in ecological characteristics can be anticipated. Using technologies such as turbofan propulsion, high aspect-ratio super critical wing, and lightweight composite structures, it is expected that a new class of small general aviation aircraft will emerge in the eighties. A target of 30 percent weight reduction was considered achievable.

For selection of aircraft size, our target was the largest segment of general aviation aircraft where cost of turbofan propulsion does not preclude its introduction.

Figure 1 presents a composite plot of aircraft gross weight versus both "The Number of New Aircraft to be Built" and "The Current Estimated Nominal Aircraft Cost". The number of aircraft is based on General Aviation Manufacturers Association data. The expected trend toward lighter weight and higher cost for the same mission has not been reflected to ensure conservative engine sizing. The range of 3175 - 4536 kg (7,000 to 10,000 lb) gross weight appeared attractive, with 3629 kg (8,000 lb) selected as our goal.

With the defined aircraft goals and Lycoming's estimates for engine performance, Beech Aircraft Corporation conducted parametric studies to optimize the aircraft preliminary design.

### 3.1.1 Final Aircraft Design Optimization

The evolved aircraft (Figure 2) is a sleek, advanced design, six-place aircraft with 3538 kg (7800 lb) maximum gross weight.

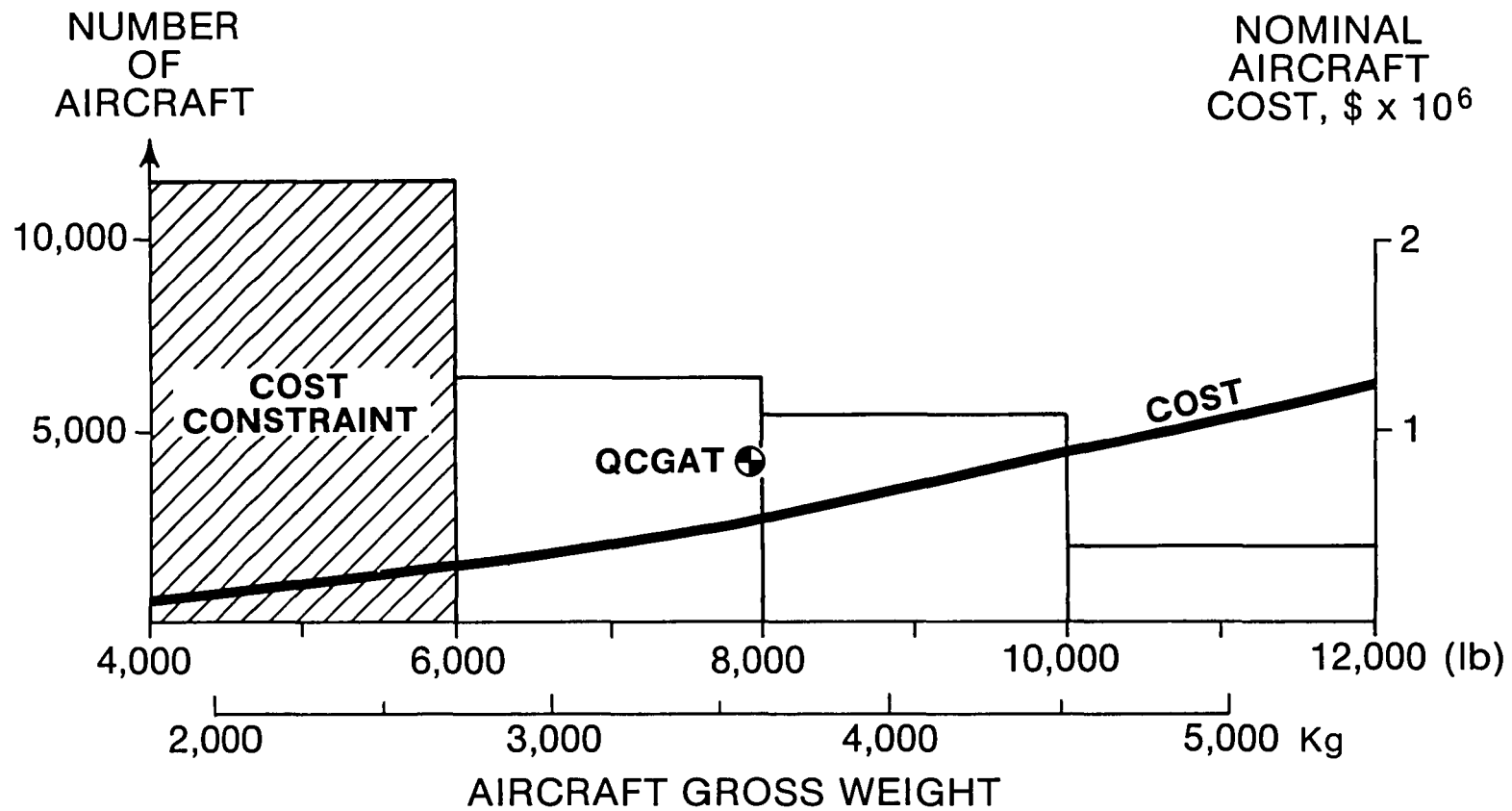


Figure 1. New General Aviation Aircraft For The 1980 Decade.

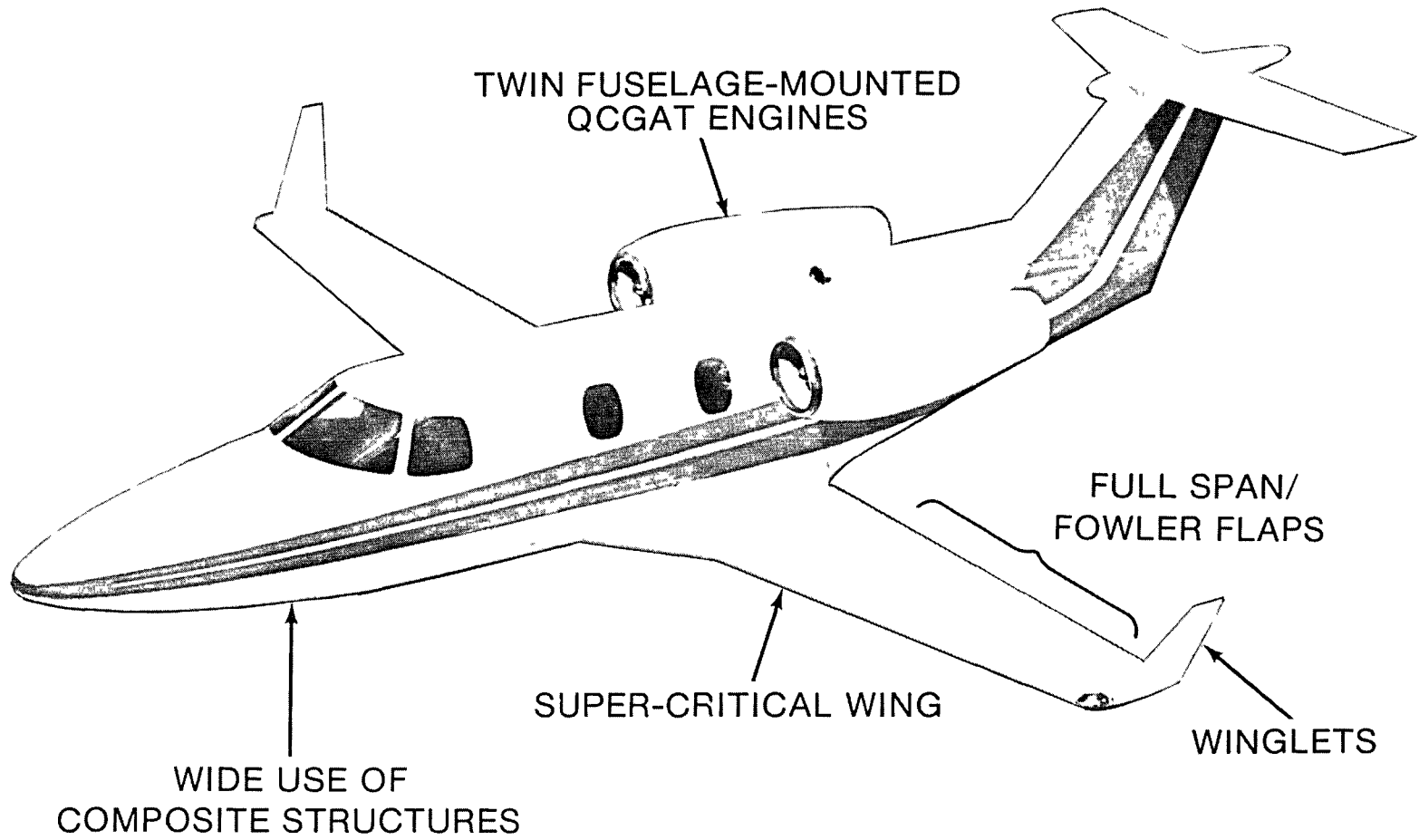


Figure 2. QCGAT Aircraft Design.



It offers a 2778 kilometer (1500 nautical mile) range with cruise speed of 0.6 Mach number, and will takeoff and land on a majority of general aviation airfields. Advanced features include broad application of composite materials and a supercritical wing design with winglets. Full-span fowler flaps have been introduced to improve landing capability. Engines are fuselage-mounted with inlets over the wing to provide shielding of fan noise by the wing surfaces.

The high bypass-ratio QCGAT engine plays an important role in shaping the aircraft design. It offers a dramatic reduction in specific fuel consumption compared with current pure jets and low-to-moderate bypass ratio turbofans. Table 1 provides this comparison, reflecting a 22 percent improvement in fuel economy.

This lower fuel consumption may be used in either of two ways or in combination:

1. It can substantially reduce aircraft gross weight for the same range. The reduced weight provides compound interest on the fuel economy. It also requires lower thrust which favors reduction of noise and emissions.
2. If preferred, the lower fuel consumption can be translated into longer range for the original gross weight.

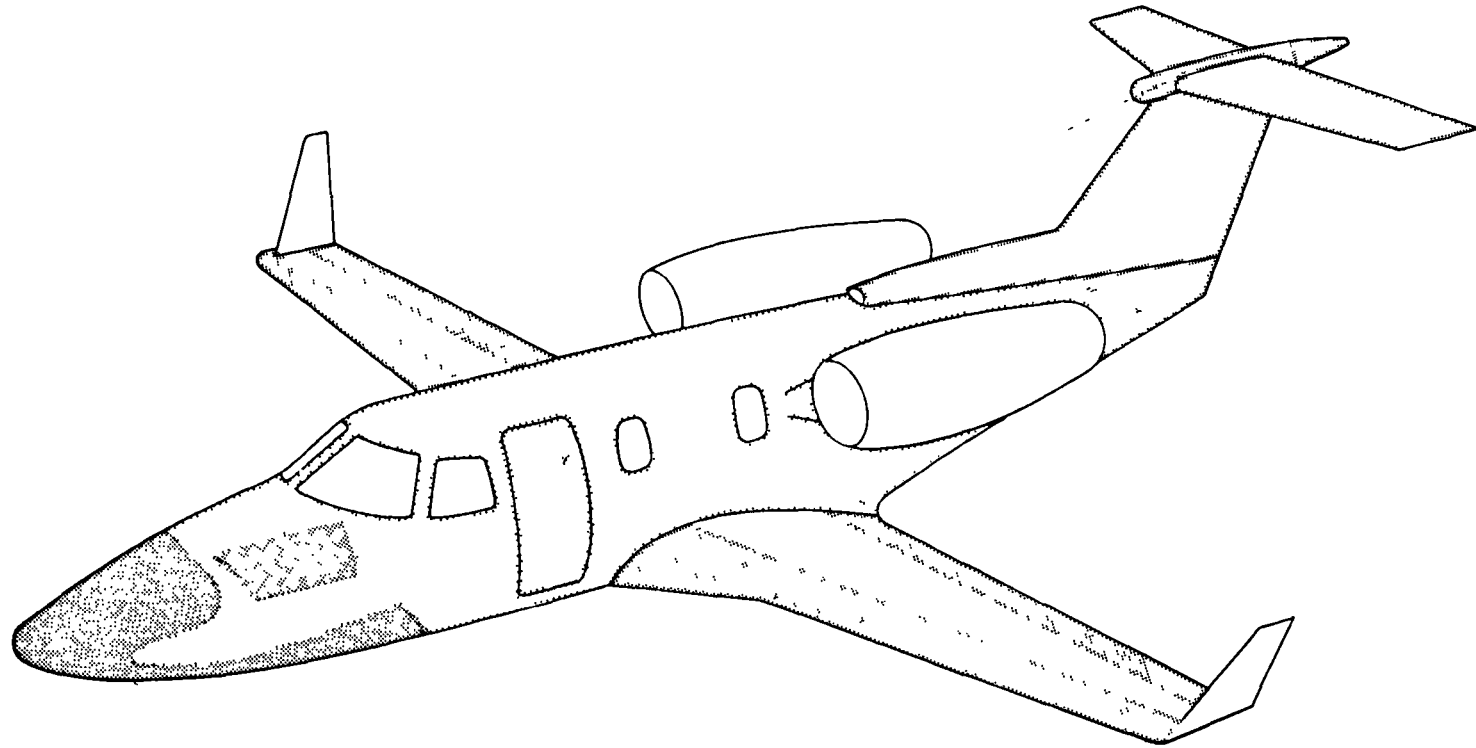
We chose to reduce gross weight and favor ecological characteristics.



Composite structures have been used extensively in the aircraft preliminary design to further reduce gross weight. Areas selected by Beech for the application of composite materials are shown in Figure 3. Kevlar graphite composites were used for aircraft weight estimates. Further potential for weight savings exists in the engine nacelles. A conventional design was used to reflect the low-cost test nacelle. Critical load carrying members, such as the wing spar, are of conventional aluminum construction.

Approximately 40 percent of the structure is of fiber epoxy or honeycomb-bonded structure. The use of composite structure in aircraft design provides a decreasing rate of benefit as the application of composites becomes more widespread in the design. Initial selection of applications is in noncritical areas. As the stress in selected areas increases, the design safety factor also increases to compensate for uncertainties resulting from advance technological use of the composite application.

TABLE 1. BENEFITS FROM ADVANCED AIRCRAFT DESIGN

AIRCRAFT CONFIGURATION	FUEL WEIGHT, kg (lbm)	STRUCTURE AND PROPULSION WEIGHT, kg (lbm)	GROSS WEIGHT, kg (lbm)
CURRENT AIRCRAFT	1370 (3,016)	2520 (5,551)	4522 (9,960)
INTRODUCE QCGAT ENGINE	992 (2,186)	2392 (5,268)	4017 (8,848)
USE COMPOSITES AND SUPERCRITICAL WING	932 (2,053)	1979 (4,360)	3541 (7,800)
SAVINGS	32%	23%	22%



	GRAPHITE REINFORCED KEVLAR SKIN
	ALUMINUM SKIN HONEYCOMB CORE

 **AVCO** LYCOMING DIVISION  
STRATFORD, CONN.

Figure 3. Design Areas Selected for Composite Structures.

Structural design is in accordance with Federal Aviation Regulation, Part 23, airworthiness standards for normal category airplanes.

A 17 percent thickness-to-chord ratio supercritical wing shape was selected because it offers a number of advantages over the conventional 12 percent NACA shape. These advantages are summarized in Figure 4.

- o From the cross-sectional comparison shown here, it can be concluded that the supercritical wing provides larger volume for fuel storage for the same chord width. The thickness increase has the supplementary benefit of higher-section modulus, permitting lighter construction for equivalent bending loads.
- o The two shapes have comparable drag characteristics in the cruise mode. Increasing the NACA airfoil thickness in an attempt to achieve similar volume is impractical, because it results in a significant reduction in useful flight speed combined with an overall drag increase at lower speeds.
- o Iterative design studies show a 25 percent increase in fuel capacity combined with a 3 percent decrease in aircraft gross weight. These savings are for an equivalent aspect ratio of 10 and a design wing loading of  $2250 \text{ N/m}^2$  (47 lb/sq ft) of wing area.
- o Prior test data have shown an appreciable increase in lift capability as depicted in this comparison. This promises a more forgiving aircraft for variations in angle of attack and enhances safety. For equivalent sophistication of flap systems, reduced landing speeds are achievable, thus resulting in shorter landing-field length capability.

The airfoil selected by Beech is similar to the NASA GA (W) -1 airfoil but is tailored specifically for the high-speed, high fuel volume, and the high lift requirements of the QCGAT configuration.

Major lift parameters are summarized below. Establishing optimum flap settings was beyond the scope of this study. However, experience indicates that a full flap deflection of 40 degrees for

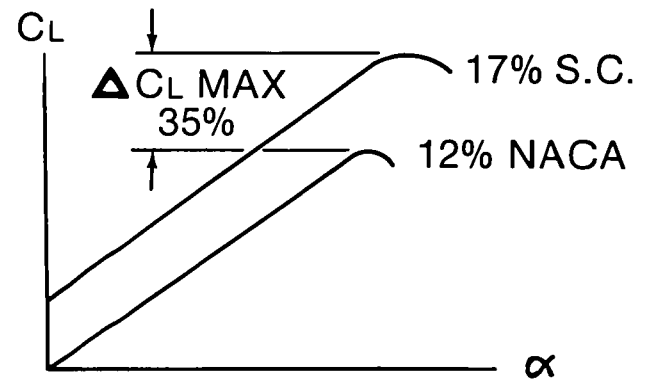
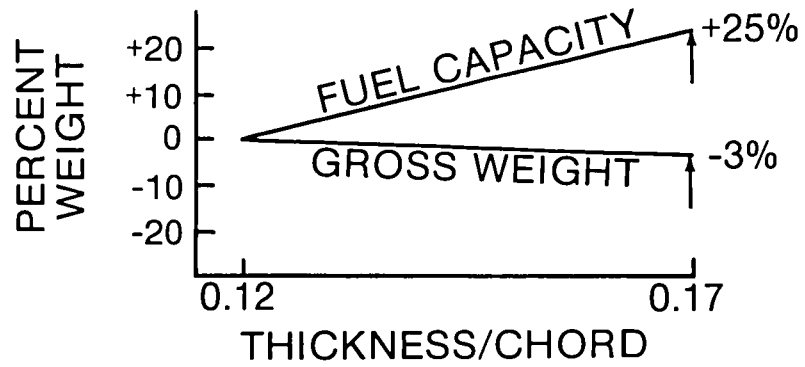
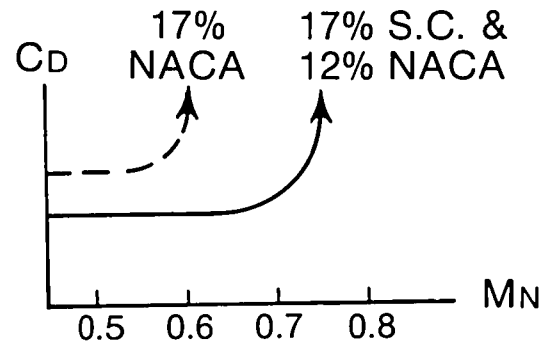
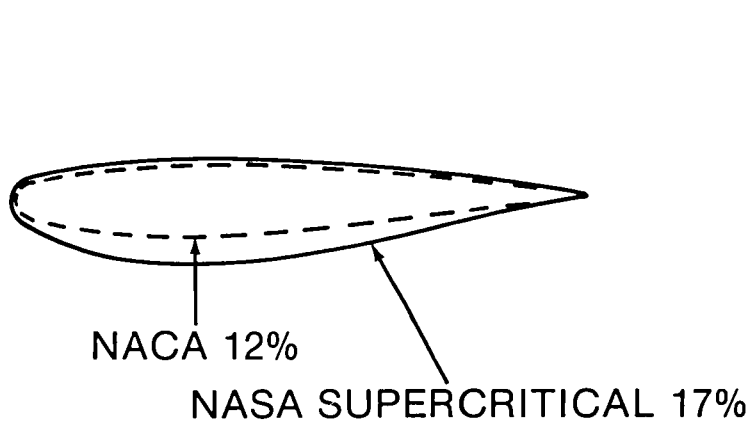


Figure 4. Wing Selection.

landing and a take-off flap setting of 40 percent of full deflection are appropriate for Fowler flap design. These values of  $C_{L_{max}}$  represent available state-of-the art with advanced airfoils.

<u>Flap Position</u>	<u><math>C_L</math> @ <math>L = 0</math></u>	<u><math>\frac{d C_L}{d \alpha}</math></u>	<u><math>C_{L_{max}}</math></u>
Up	0.132	0.088	1.6
40% (Take-off)	0.98	0.088	2.35
Down	2.13	0.088	3.45

Full-span fowler flaps and spoilers have been introduced to achieve the desired 762 meter (2500 feet) take-off field length and landing distances with reduced wing area. Winglets have also been added to reduce actual span and wing structural weight, while maintaining a high effective aspect ratio.

Many drag-influencing design details of the QCGAT airplane are not established at this time, because the airplane is as yet a preliminary design study. For drag analysis, ambitious estimates were made for the various items. Achievement of total airplane drag coefficients will require exacting efforts in the practical development of the airplane. The resulting QCGAT aircraft drag compares with that of Learjet Model 24, which is an extremely clean airplane. Allowances have been made for differences in wing thickness, component size; etc. Drag coefficients used are summarized below.

Total $C_{D_P}$	Flaps and gear up	0.02661, 0.02534 cruise
Incremental	$C_{D_P}$ for landing gear	0.0164
Incremental	$C_{D_P}$ for full flap	0.04066
Incremental	$C_{D_P}$ for T.O. flap	0.0163
Incremental	$C_{D_P}$ for one engine out	0.01209

Four major aircraft variables considered in the parametric study to optimize the wing configuration are:

1. Wing area
2. Wing aspect ratio
3. Fuel weight
4. Takeoff weight

For each performance goal in this study, the limiting aspect ratio versus wing area is plotted for several takeoff weights, including the effects of wing geometry on wing weight. These limits for each of the performance goals are then summarized on a graph so that the best compromise could be selected. A design point of 15.33 square meters (165 square feet) wing area and an effective aspect ratio of 10 were selected.

The expected weights are summarized for fuel, structure-plus-propulsion, and complete aircraft with payload for both conventional and QCGAT aircraft designs in Table 1.

The first line of Table 1 represents a hypothetical aircraft of current vintage design with low bypass turbofan propulsion. Introduction of a QCGAT high-bypass turbofan reduces fuel consumption by 22 percent. When this savings is iterated through the aircraft design, structure and gross weight reduce, providing an additional 5.5 percent in fuel economy. Similar iterations with weight savings from composite materials and supercritical wing result in an additional 4.4 percent savings in fuel. The combined engine and aircraft changes provide 32 percent better fuel economy. The 22 percent reduction in gross weight permits the use of a smaller engine with 22 percent lower thrust and, therefore, lower absolute emissions and noise.

The aircraft study projected the maximum ranges shown in Figure 5 for various payloads. While 1134 kg (2500 lb) is depicted as maximum payload for the aircraft, only 753 kg (1660 lb) is required to accommodate six people with their baggage. At this payload, the achievable range is in excess of 2963 kilometers (1600 nautical miles). Flight conditions are 10058 meters (33,000 feet) and an average flight speed of approximately 0.5 Mach number.

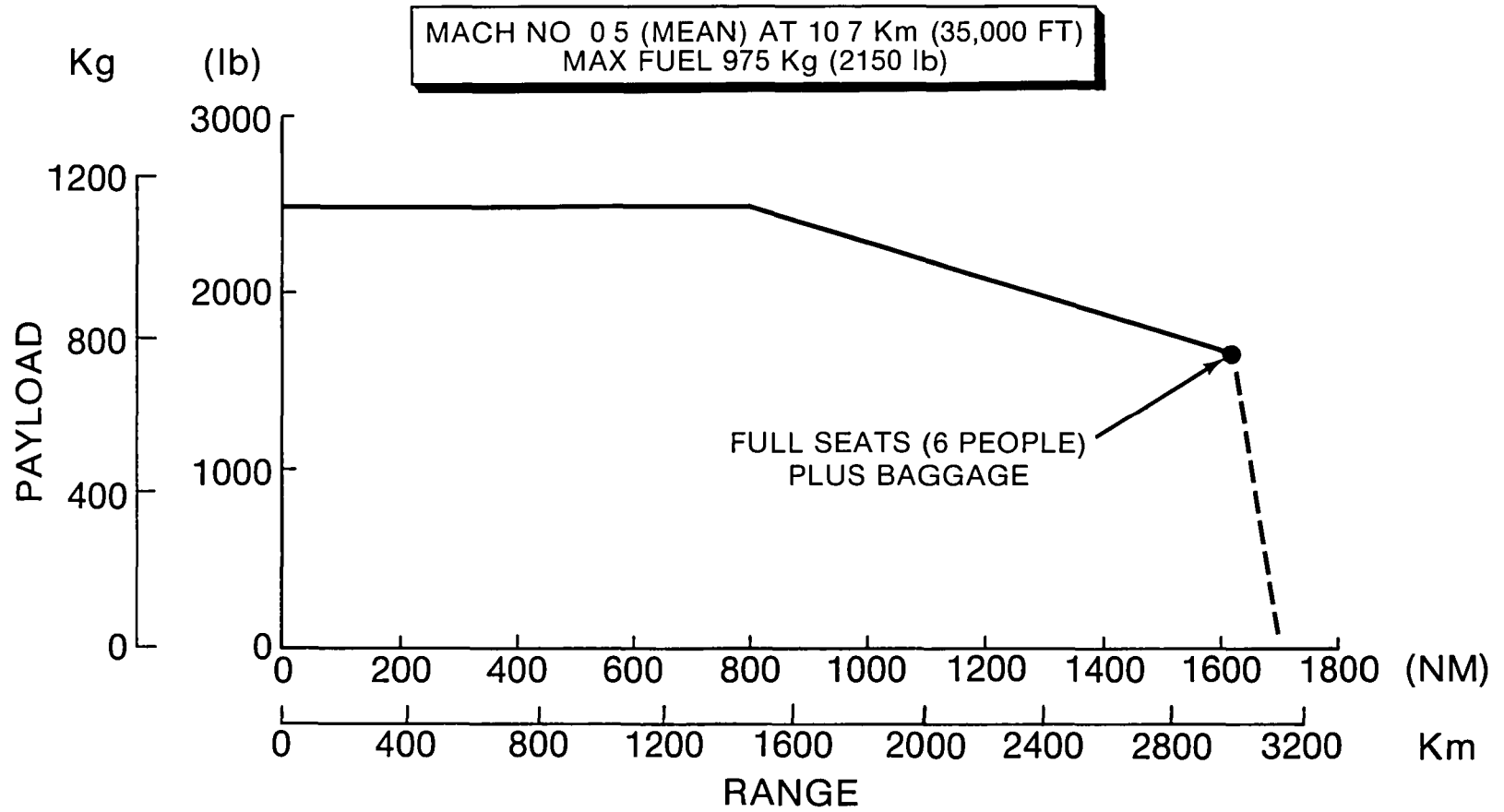


Figure 5. Best Range Versus Payload.



In our QCGAT aircraft study, landing distance, rather than take-off capability, set the minimum usable airfield length. Introduction of full-span fowler flaps with moderate wing loading results in a very low "landing configuration" stall speed. The 32 meters/sec (62 knot) stall speed compares with 41 - 46 meters/sec (80--90 knots) for current typical jet and turbofan aircraft. Since landing distance is proportional to stall speed squared, this low landing speed provides an attractive sea level FAR landing field length of 811 meters (2660) feet.

Figure 6 shows a representative sample of general aviation airfields plotted on coordinates of field elevation and field length. The Beech QCGAT aircraft with full useful payload has a landing capability consistent with the majority of these fields.

The expected stall speeds promise a very forgiving aircraft in both the take-off and landing modes where most accidents occur.

### 3.2 ENGINE DESIGN

The NASA QCGAT engine was designed using existing advance technology in the fields of noise and pollutant emissions control. Stringent noise goals that were set required both attenuation techniques and design considerations for the major noise sources. Similar goals were set for emissions levels based on the 1979 EPA standards. These standards were later abandoned by the EPA as being excessively strict; however, they were retained as the QCGAT program goals.

Work has been performed in these technologies for large commercial applications; however, little benefit has filtered through to the general aviation industry.

While not specifically stated as a program goal, low acquisition and operating costs are of unquestionable importance to the general aviation marketplace and are the key ingredients to widespread acceptance.

The Lycoming QCGAT engine was developed to specifically satisfy the program goals of low noise and emissions. This was accomplished without incurring the excessive complexity and cost which normally are associated with advanced technology systems.

#### 3.2.1 Design Considerations

In order to achieve all of the preceding goals, a multifaceted design approach was required to optimize each component for its task without placing an excessive penalty on other components.

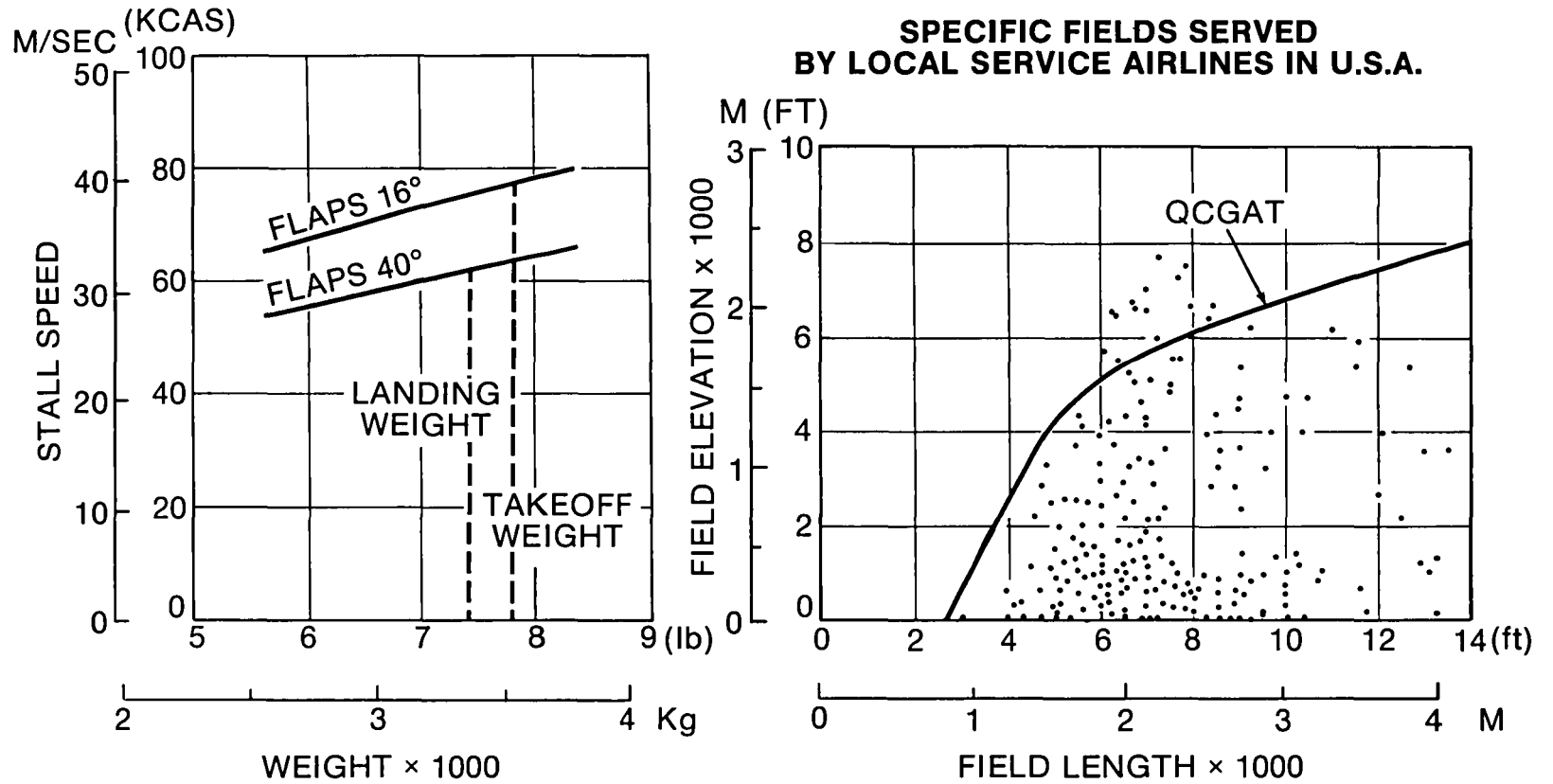


Figure 6. Aircraft Stall Speed and Field Capacity.

### 3.2.1.1 Operating Cycle

Preliminary engine cycle definitions were based on the power requirements of the proposed airframe and the fuel consumption. Figure 7 illustrates the relation of fuel consumption-to-bypass ratio as a function of the compressor pressure ratio. Pressure ratios ( $P_r H_c$ ) above approximately 10.4 would have necessitated a multi-stage power turbine that would impact the engine complexity and cost. In addition, increasing bypass ratio above 9.6 tends to result in reduced performance at altitude caused by off-design fan loading. By selecting a bypass ratio of 9.4 (at 25,000 feet altitude) and a compressor pressure ratio of 10.2, engine simplicity can be maintained with minimum fuel consumption. The effect of bypass ratio on fan pressure ratio is given in Figure 8. Overall engine sizing is based on FAA regulations which require the capability of an aircraft to successfully climb after takeoff with one engine inoperative on a hot day.

This thrust level also ensures that the aircraft will be capable of serving a majority of small, general-aviation airfields, including many remote, unpaved runways.

### 3.2.1.2 Low Cost and Simplicity

The Avco Lycoming LTS 101 series engines selected as a building block for the QCGAT engine is a strong contender in the general-aviation market in both turboshaft and turboprop configurations. The use of this engine as a base allows the maximum use of existing technology and proven design concepts. One feature, which is especially attractive to the general aviation operation, is the modular design concept. Although ideally no major maintenance would be specified for an engine during its service life, maintenance and repair are an inevitable necessity and can cause significantly rapid escalating downtime operating costs.

Modular maintenance allows the expeditious removal of any major component for inspection or repair without removal of the entire engine. Interchangeability of modules promotes a fast return to service and decreases the spares requirements and life-cycle costs.

### 3.2.2 Engine Hardware Description

The final QCGAT engine configuration shown in Figure 9 consists of four basic modules. (See Figure 10.) These modules are the fan, the gas generator or core engine, the power turbine, and the accessory gearbox.

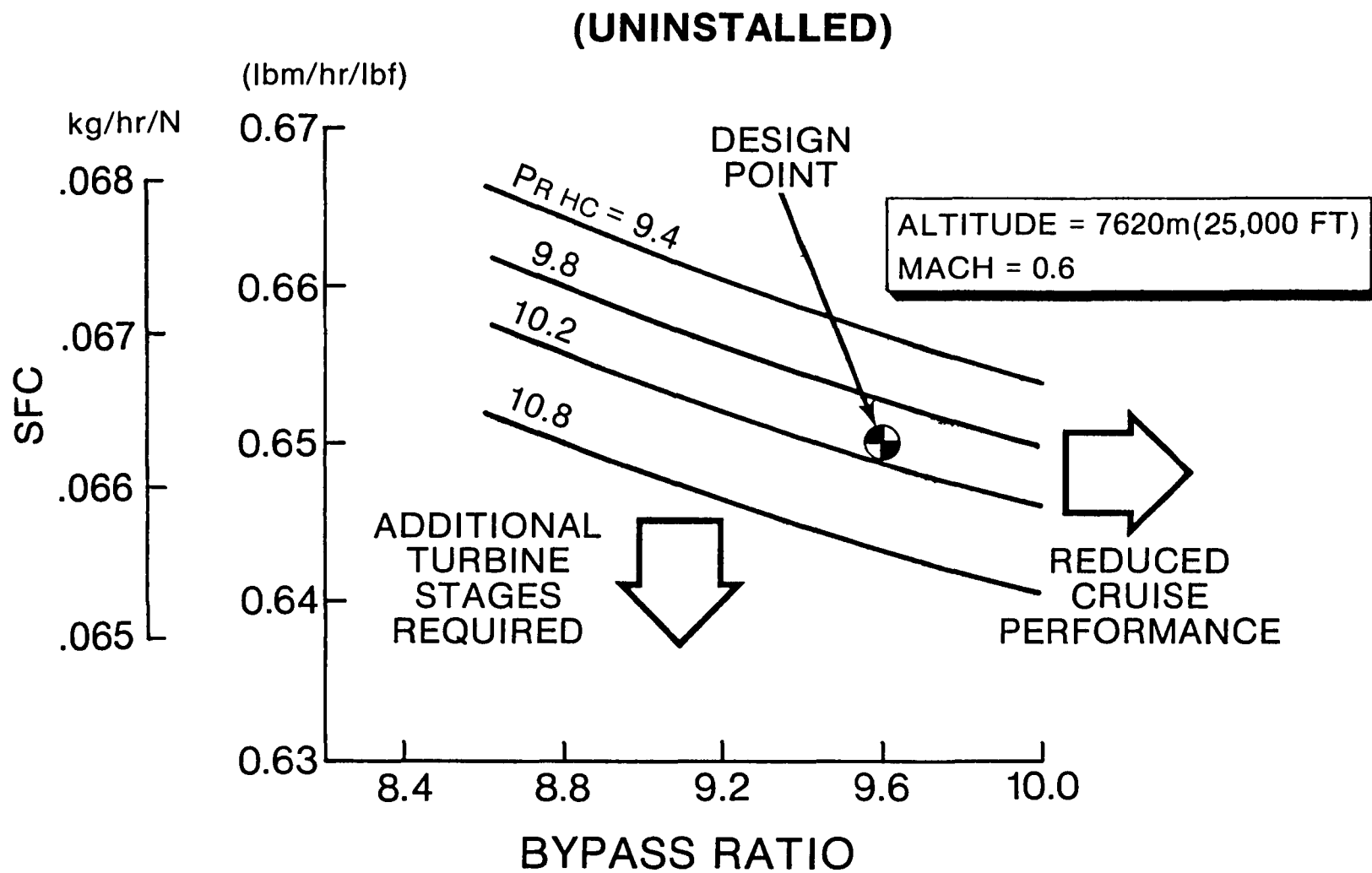


Figure 7. Cycle Optimization for Specific Fuel Consumption.

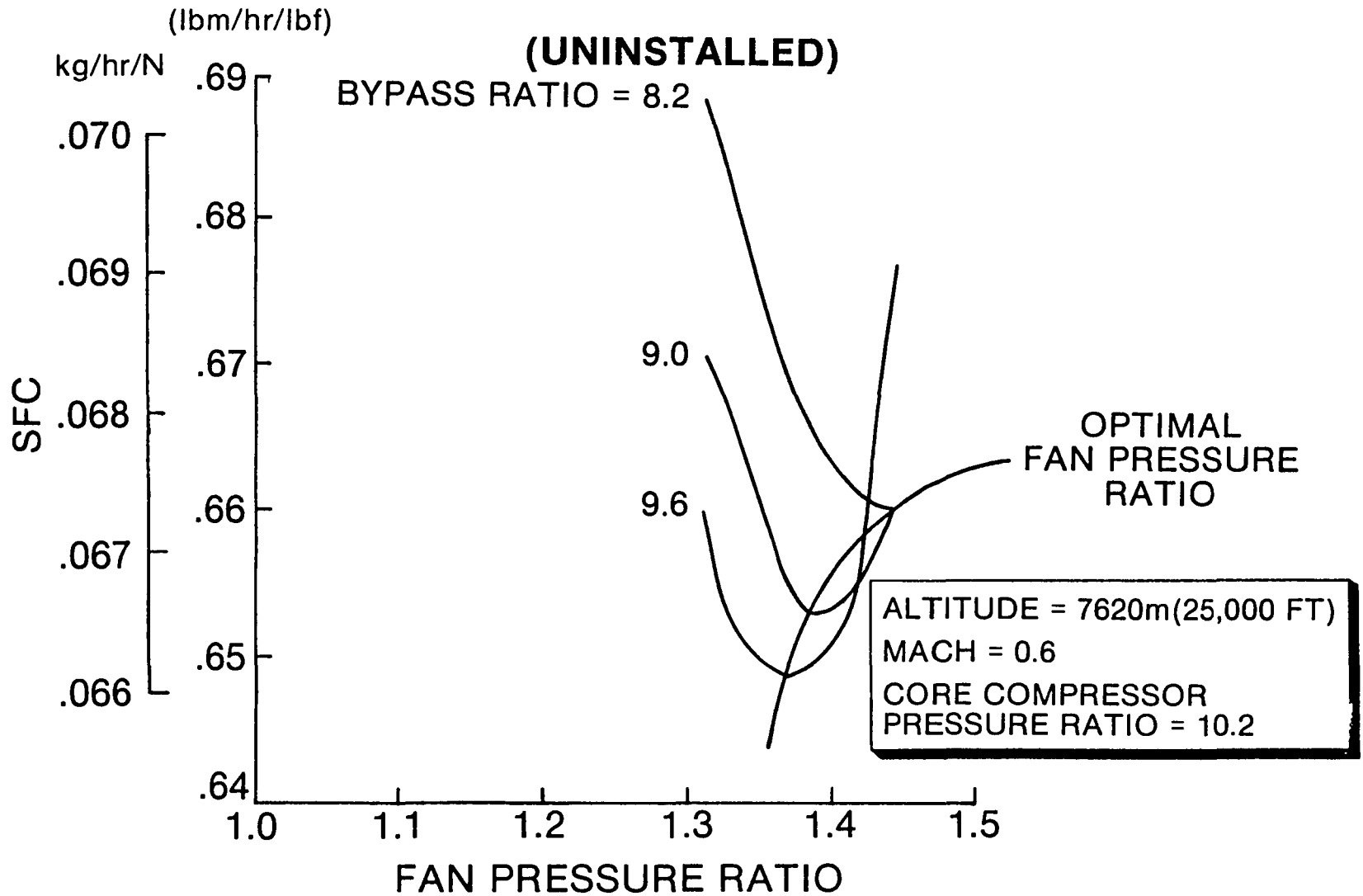


Figure 8. Selected Fan Pressure Ratio.

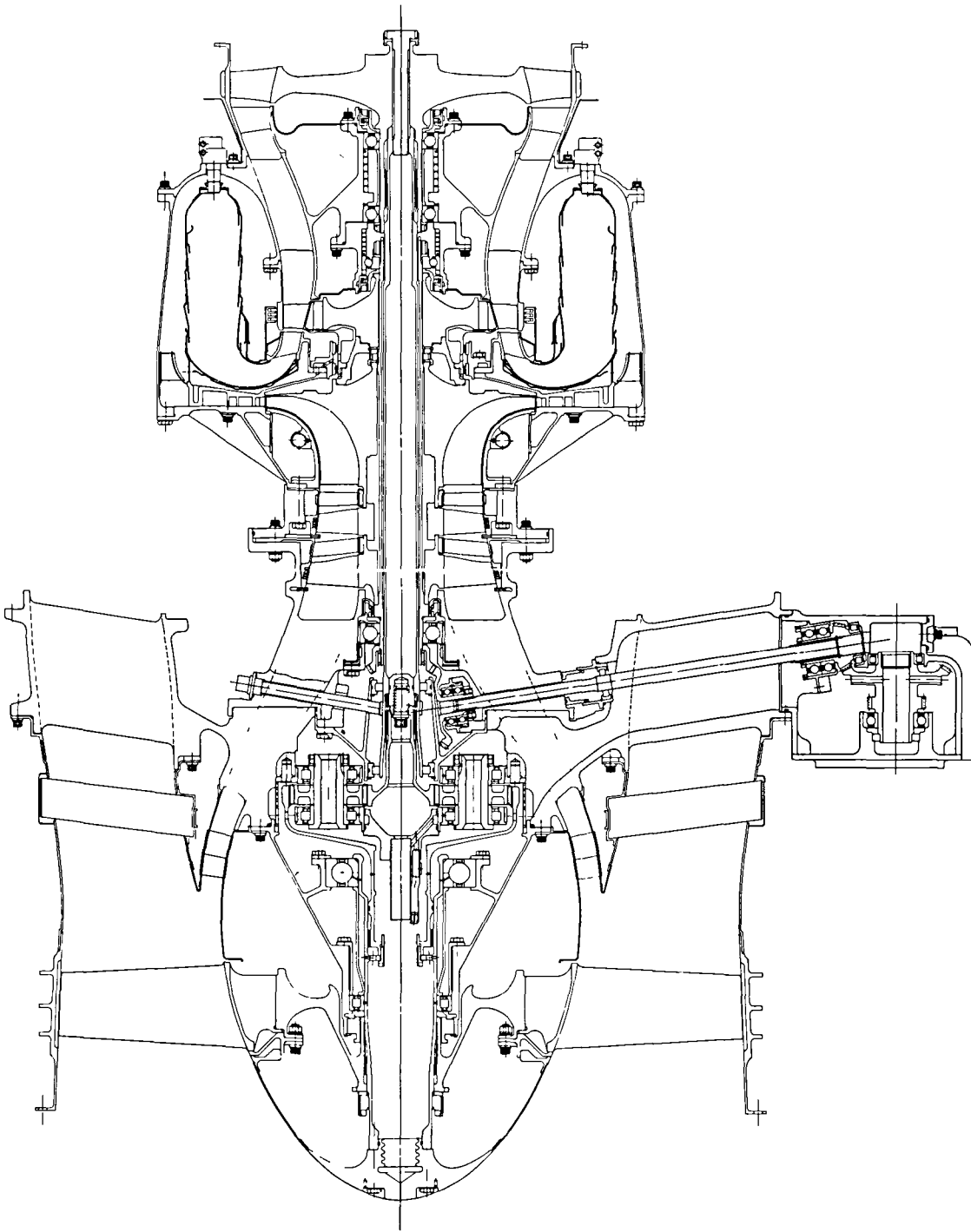


Figure 9. Engine Configuration.

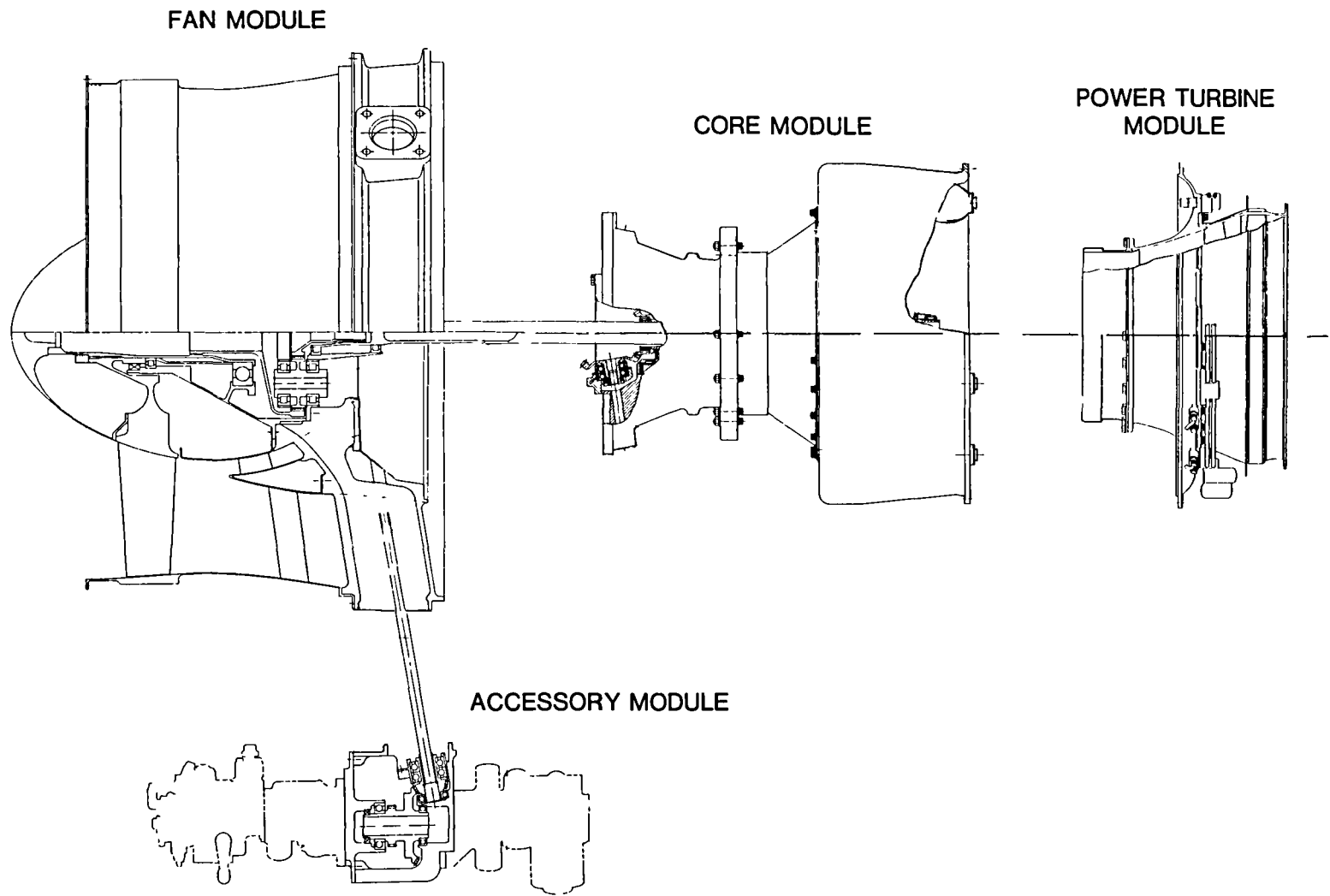


Figure 10. Engine Modules.

### 3.2.2.1 Fan Module

Design of the QCGAT engine fan module is similar to that of the Lycoming ALF 502. This module comprises a main support frame that features provisions for engine mounting and supports the fan, reduction gearing, and the power producer. The fan is driven on its splined shaft by a bell gear which is, in turn, driven by the power turbine rotor through a connecting shaft to a sun gear and five fixed planet gears. The power turbine input speed is reduced by a 3.102 ratio by the reduction gear system.

The relatively wide-chord, low aspect ratio (1.6) design of the fan blades avoided the need for midspan dampers. This elimination of dampers resulted in an efficient design, both from a noise reduction and performance viewpoint. The fan rotor consists of 24 multiple circular-arc airfoil blades and has a tip diameter of 57.7 cm (22.72 in.). The inlet hub-to-tip ratio is 0.45.

The single-stage fan is followed by a splitter in order to separate the airflow into the bypass and core engine flow channels. In the bypass channel, a single-row stator vane assembly having 59 double circular-arc airfoils is used to remove all whirl from the flow before it enters the main frame duct. The number of vanes was selected on the basis of noise considerations because large-engine technology indicated a quantity in excess of twice the rotor blade number. The bypass stator vanes have the unique capability, as does the fan rotor, to individually replace either a single vane or all vanes if they are inadvertently damaged.

In the supercharger channel that leads to the core engine, a double-row stator assembly was used. This configuration reduced the inlet velocity to the supercharger duct; this reduced velocity, which could not have been achieved with a single-row assembly, allows higher diffusion and lower losses. There are 53 double circular-arc vanes in each row with an average inlet Mach number and diffusion factor of 0.76 and 0.35, respectively.

### 3.2.2.2 Gas Generator Module

A cross section of the gas generator module is shown in Figure 11. The main components are the high-pressure compressor, the combustor, and the high-pressure turbine assemblies. This gas generator, also referred to as the core engine, is a growth version of the proven



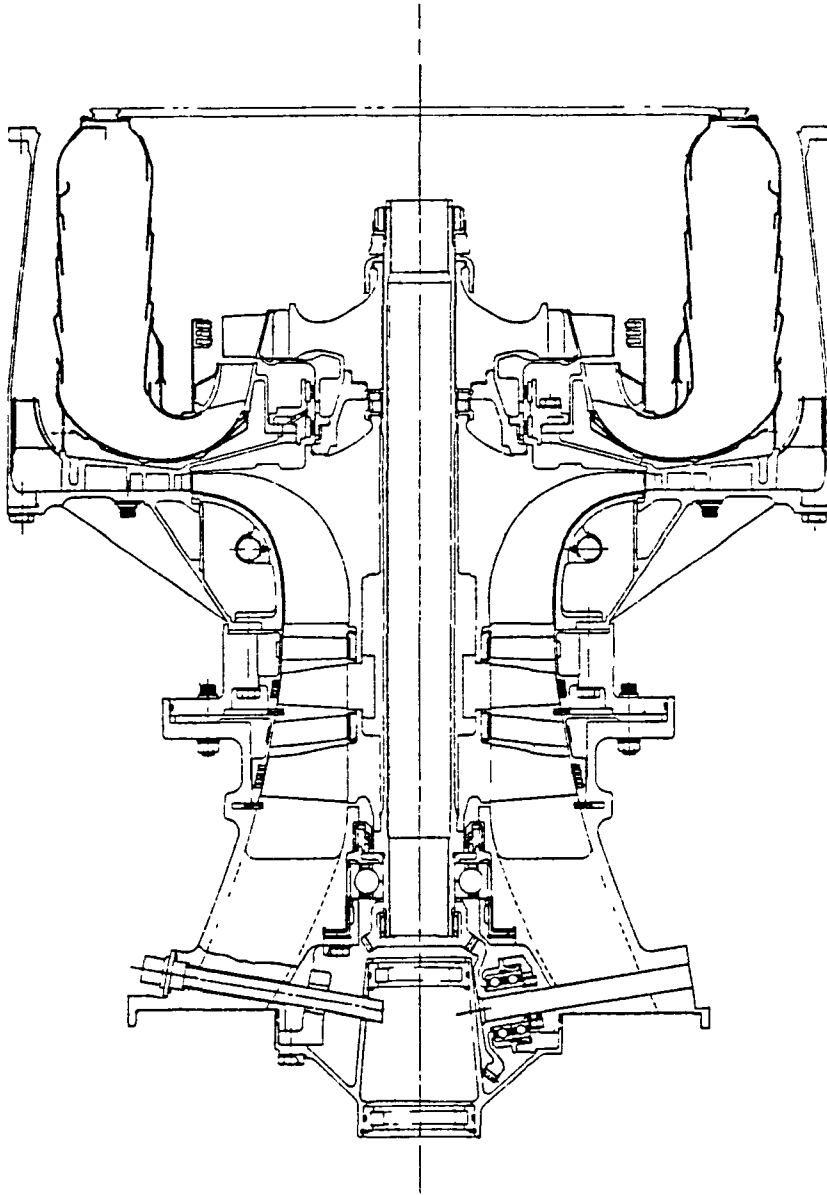


Figure 11. Gas Generator Module.

and certified LTS 101 basic design which has both turboshaft and turbo-prop configurations currently in production in the 500 to 750 horsepower class. Taking advantage of the latest technology in compressor, low-loss combustor, and high-temperature turbine design, a viable core engine suitable for the turbofan was developed.

The inside rear surface of the fan frame provides the interface for the gas generator module (Figure 9). The compressor section, which is a stacked assembly, contains two axial stages and one centrifugal stage clamped together on the gas producer shaft by a nut located at the rear of the centrifugal stage. The gas producer turbine assembly, consisting of a spacer seal assembly and a disc-blade assembly, is located at the rear of the gas producer shaft and completes the shaft assembly for the module.

The compressor assembly and the turbine assembly are each individually balanced; this permits removal of the turbine and reinstallation and eliminates rebalancing of the total assembly.

Buildup of the rotor system is accomplished by sliding the rotational components of the compressor section onto the gas producer shaft and seating them in place, on their piloting surfaces, with the clamping force applied by the nut located at the rear of the centrifugal stage. This clamped assembly is then balanced as a unit.

When the modular buildup is completed, the compressor nut clamping force that was initially applied across the axial and centrifugal stages is relieved because the clamping force applied by the nut at the rear of the turbine disc causes enough stretch of the gas producer shaft to relieve the initial load of this intermediate nut. The shaft then acts only as a bolt applying a clamping force across the rotor interfaces.

#### 3.2.2.2.1 High-Pressure Compressor

The high-pressure compressor for the QCGAT engine consists of a zero-staged LTP 101-700 unit. As such, it contains two axial stages and one centrifugal stage. "Zero staging" of the -700 compressor required small modifications to the original axial stage to compensate for inlet air angle variations caused by the addition of a preceding stage. Blade chord width was increased 16 percent so as to alter natural frequency and provide additional margin from vibratory excitation. No changes were required for the original axial exit stator, centrifugal compressor rotor, or air diffuser.

The new first-stage (zero stage) was designed at modest stage pressure ratio to favor part-speed operation for the QCGAT design. The strip stock for the new stator is identical to that used on the second stage.

The first-stage axial compressor is an integral casting containing multiple circular-arc blades designed to maximize the tip section efficiency at the high rotor tip relative Mach numbers at which the blades operate. This compressor stage is cast in an alloy that is a proprietary martensitic, age-hardenable stainless steel.

This rotor is followed by the first-stage stator which is a split and brazed assembly. These vanes are made of strip stock for the benefit of low cost and have double circular-arc profiles. The stator incidence angles were set based on an off-design analysis to provide a wide operating range.

The second axial stage is a similar design to the first stage, but at slightly different solidities.

The centrifugal compressor stage following the two axial stages is an integral casting and is identical to units operating in the LTS 101 engines.

#### 3.2.2.2.2 Combustor

Selection of the LTS 101 combustor style for a small, low-pollution turbofan engine was based in part on the unique features of the circumferentially stirred or "horseshoe" vortex annular combustor configuration.

Figure 12 illustrates the aerodynamic concept embodied in the combustor design. Primary air is admitted through slots in the liner header to produce flow circulation about a circumferential mean line. Air jets ("folding jets"), entering through the inner wall, force primary zone recirculation. Since the secondary holes exist only on the inner wall, the vortex fills the full annular height of the liner and produces adequate flame stabilization within a smaller cross-sectional space.

With the folding jet in line with the fuel injector, initial flow circulation is in a circumferential direction. The vortex is permitted to turn to the axial direction on either side of the folding jet. As a result, the mean path of the combustion zone flow vortex takes the shape of a horseshoe centered on the injector and folding jet axial centerline.

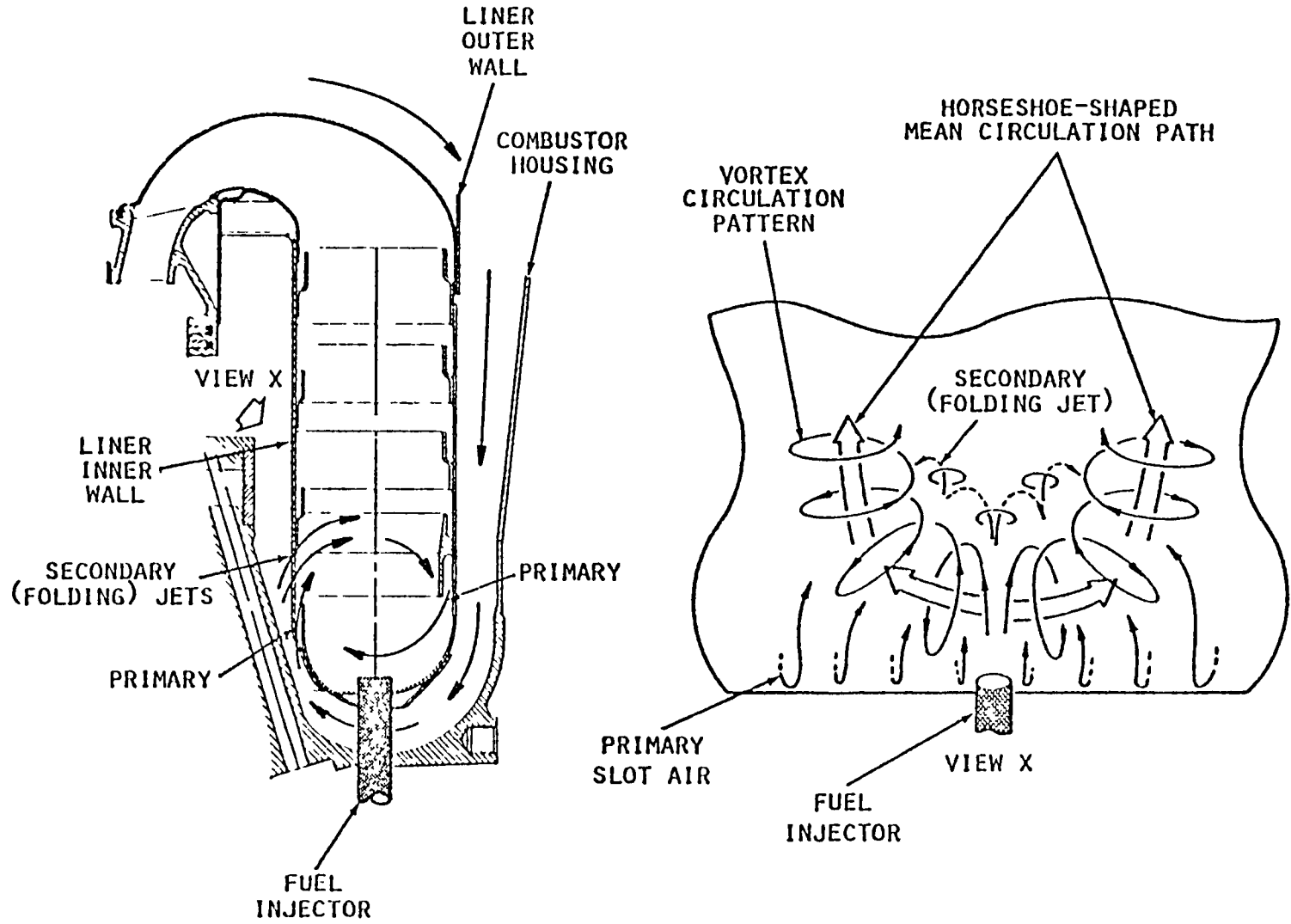


Figure 12. Circumferentially Stirred Combustor Flow Pattern.

The number of fuel injectors is reduced by one half, compared with normal practice, because of this unique combustor primary zone aerodynamic concept.

Primary air, entering in two stages from the outer liner, is directed along the dome of the liner to provide cooling and is then diffused into the vortex created by the folding jets. The baffle which deflects the first-stage primary air is cooled by jet impingement. The second-stage of primary air enters the burner on the injector centerline through a step formed by the double liner end.

Two spark igniters located in line with the lower two fuel injectors penetrate through the primary air baffle. Since this location has been found to be optimum in the LTS 101 engine, the QCGAT combustor housing has been designed to maintain the location.

Eight airblast fuel injectors equally spaced in the liner end straddle the vertical engine centerline. Each injector has a self-aligning air seal at the liner and penetrates past the second-stage primary air step. The fuel manifold consists of two halves to allow easy removal. A flow divider mounted under the engine has separate primary and secondary lines to feed each manifold half.

The liner walls are designed for maximum structural integrity and wall cooling efficiency. Splash-cooling rings are formed by the overlap of each cone, which provides a cooling effectiveness advantage over the standard LTS 101-type cooling ring inserts. Cooling air is metered through holes drilled in the outer cone so that air jets impinge on the splash ring, thus providing cooling of the splash ring lip; this air then spreads to become a lower velocity film at the discharge of the splash ring. Air quantity and conical step length are designed so that adequate cooling effectiveness persists until the next joint is reached. To minimize buckling caused by uneven heating and thermal expansion, the joints are spot welded and then back-brazed to provide good conduction of heat into the colder, outer cone. In addition, the lips on the outer liner are slotted to prevent compression buckling.

Inner and outer liner-to-curl seals are the "fishmouth"-type used on most Lycoming engines to insure a seal regardless of local liner or curl warpage. These curls are cooled by air films, similar to those at the liner walls. In addition, the outer curl is of double-wall construction with turbine inner shrouds cooling air flowing through it, and the hot side wall is coated with thermal barrier coating. This additional cooling provides margin for the higher temperatures of the QCGAT, as compared

with the single-wall LTS 101. Liner mounting is accomplished by means of four radial mounting pins which make the liner free floating, while providing complete centering and axial retention.

The design configuration selected for the QCGAT liner produces a unique CO/NO<sub>x</sub> relationship which permits trade-offs to meet EPA emission requirements (low NO<sub>x</sub> at high power settings). Furthermore, the use of ALF 502 airblast injectors improves combustion efficiency at idle over the LTS 101-type dual-orifice injectors with a resulting reduction of UHC and CO. The fuel injection system used for this engine is similar to the airblast system used on the ALF 502 engine. Eight standard-production ALF 502 injectors are used. Flow divider orificing has been changed from the ALF 502 to accommodate the fewer number of injectors in the QCGAT engine. The fuel injector manifold has been split in two halves to provide easy removal and installation on the QCGAT engine.

The airblast injector flow system is depicted schematically in Figure 13. This system provides an optimum trade-off for fuel contamination resistance, cold starting capability, simplicity, and reliability. Fuel flow entering the flow divider, under starting conditions passes through a wash-flow filter and into the eight pilot injectors, which are low-flow/high-pressure drop orifices used to provide good starting fuel spray. As inlet fuel flow increases, the airblast portion of the injector starts to "cut-in"; as this flow increases, the pilot flow decreases. This arrangement minimizes the increase in fuel pump back pressure, yet still keeps the pilot injector cool enough to minimize internal coking. The mixing of pilot and airblast fuel flows at idle was chosen to produce good combustion efficiency and minimize CO and UHC. A reference pressure line from the spring-side of the flow divider vents to engine fuel pump inlet pressure, thus preventing fluid lock of the piston.

During starting, there are, in effect, eight starting fuel injectors (pilot injectors) and, because they are placed in the center of the airblast injector (Figure 13), atomization and droplet distribution is superior to merely pressure-atomized spray. This system demonstrated an outstanding improvement in cold starting, altitude relight capability, and higher combustion efficiency at idle operation in other Avco engines.

This type of combustor is applied to the standard Avco Lycoming reverse-flow annular combustor design to effect a short, compact, lightweight engine having no critical shaft speed in the operating range.

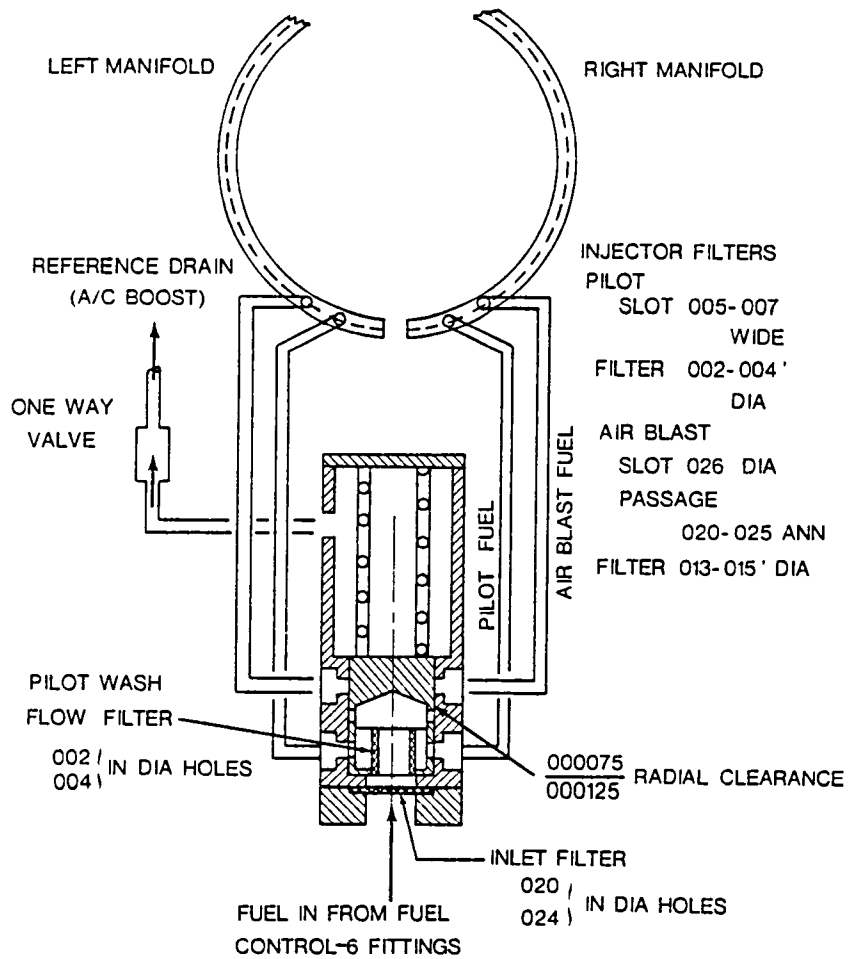
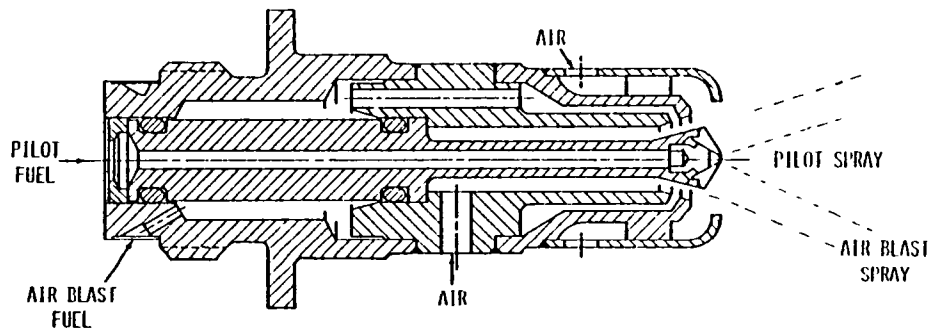


Figure 13. Airblast Fuel Injector System.

### 3.2.2.2.3 High-Pressure Turbine

The gas generator turbine consists of a single-stage axial turbine that powers the compressor. This high-pressure turbine is similar to the LTS 101-600/700 gas generator turbine except for modifications that optimize it for the higher cycle pressure ratio and temperature of the engine. The turbine arrangement is depicted in Figure 14. The gas generator turbine stator and rotor are cooled by compressor discharge air. Stator cooling air is discharged through slots on the pressure-side near the trailing edge, while rotor cooling air is discharged by means of trailing-edge ejection.

The vanes in the first-stage turbine nozzle have a generous leading edge radius and relatively thin trailing edge in order to obtain a low leading edge gas-side heat-transfer coefficient and low trailing edge wake losses. The vanes are cooled by a two-pass cooling configuration by means of internal convection cooling at the main body of the vane and external film cooling at the vane's trailing edge. The two-pass cooling design provides a long in-line passage length for good use of the cooling-air thermal capacity. Passage flow areas are varied to maintain a high mass velocity flow rate to match the local heat input rate at the vane's outside surface to achieve a near-uniform vane temperature.

Cooling air to the internal air passages of the vane is supplied through an opening at the vane's leading-edge hub section. Cooling air in the vane's leading-edge passage flows radially outboard. At the vane tip, the air makes a 180-degree turn and enters the vane's tail passage. In the tail passage, the air flows inboard radially, and, at the same time, it discharges gradually to the gas stream through three slots in the vane's trailing edge pressure-side wall. A schematic representation is presented in Figure 15.

The gas producer rotor blades are cooled by a two-pass cooling configuration similar to that of the gas producer nozzle vane. However, two separate cooling air passages are used in the rotor blade cooling design, as can be seen in Figure 15.

One branch of cooling air enters the blades' leading-edge passage through an opening at the front face of the blade root. This air flows radially outboard in the leading edge passage and turns to the tail passage at the blade tip. In the tail passage, the air flows radially inboard, and, at the same time, discharges gradually to the gas stream through a trailing edge "through slot". This flow path terminates



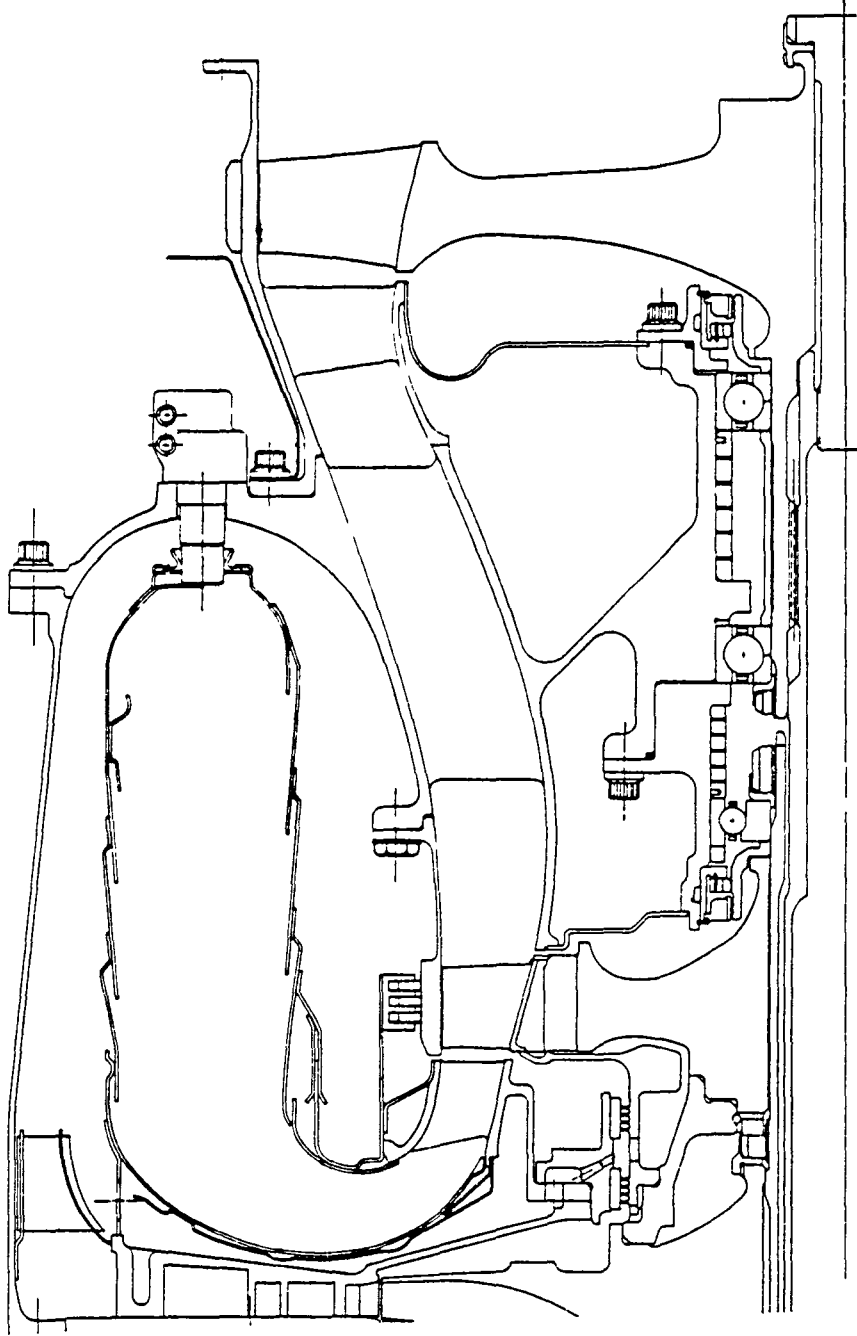


Figure 14. Turbine Arrangement.

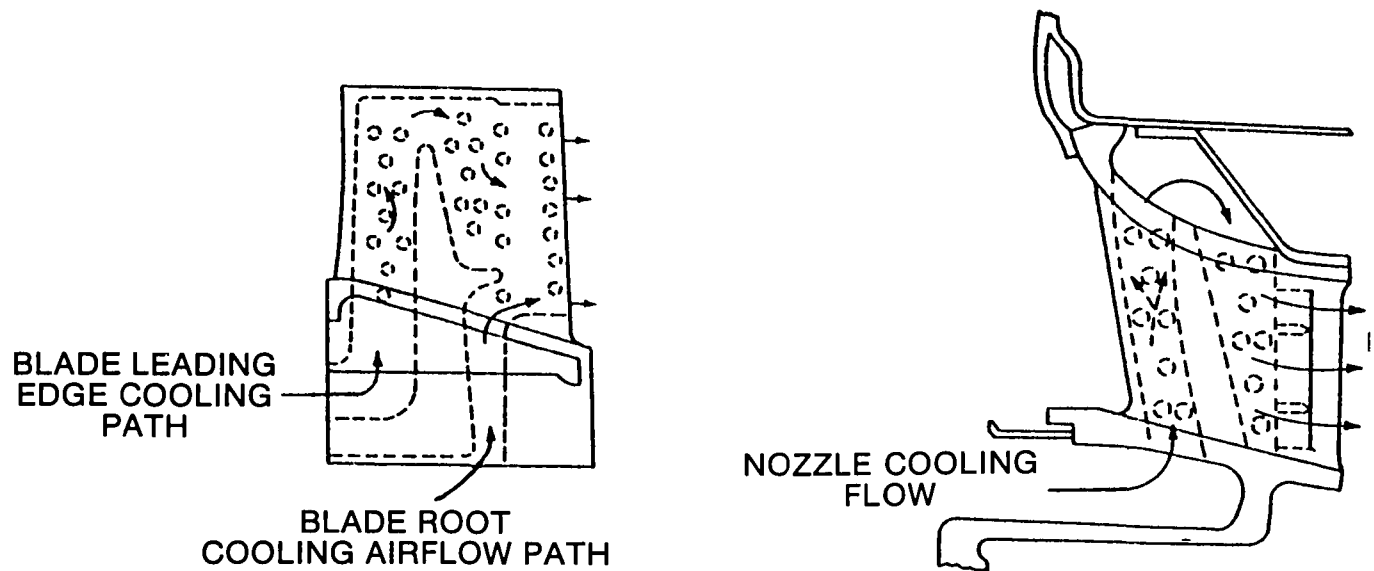


Figure 15. Cooling of First Stage Rotor Blades and Turbine Nozzle.

just short of the blade's hub section. The other branch of cooling air enters the blade at the blade root where it flows first axially rearward between the blade root and the disc rim and then radially outboard through the rear portion of the blade shank to the blade hub section. At the blade hub section, the air discharges to the gas stream through the trailing edge "through slot". By flowing through the blade root and rear shank, the second branch serves to cool both the blade root and disc rim. The blade cooling air passages are designed with variable flow areas to obtain optimal local mass velocity flow rates and cooling effectiveness.

### 3.2.2.3 Power Turbine Module

The QCGAT low-pressure power turbine (Figure 16) is a single, axial stage with moderate stage loading and non-free vortex design. An outward flowing, diffusing duct connects the low and high pressure turbines and provides bearing support. The low-pressure rotor is integrally cast, with unshrouded, medium aspect ratio, constant tip diameter blades.

The high-speed, single-stage configuration was chosen as the best combination of performance, mechanical simplicity, weight, and cost. The reduction gear between fan and low-pressure turbine allows rotational speeds nearly optimum for both components, while maintaining low fan tip speed and turbine blade passing frequency beyond the audible range for reduced engine noise. The low-pressure turbine design point is between sea level takeoff and  $M=0.6$ , 7620 m (25,000 ft) maximum cruise operating points.

The rear flange of the combustor casing on the gas producer module, Figure 14, provides the forward interface for the power turbine module, Figure 16. The two major components of this module are the rear bearing support housing and the power turbine rotor, which it supports. The rear bearing support housing, which is the module's main structural member, is a segmented investment casting. This housing, which supports and transfers the power turbine loads, also functions as the main artery to ensure proper operation of the power turbine module.

An area-compensated aerodynamic diffuser flow path in this housing interconnects the gas producer turbine with the single-stage power turbine. This duct is divided by four hollow airfoil-shaped struts which serve as the access corridors for lubrication and ventilation, as well as the structural supports for the rear bearing housing.

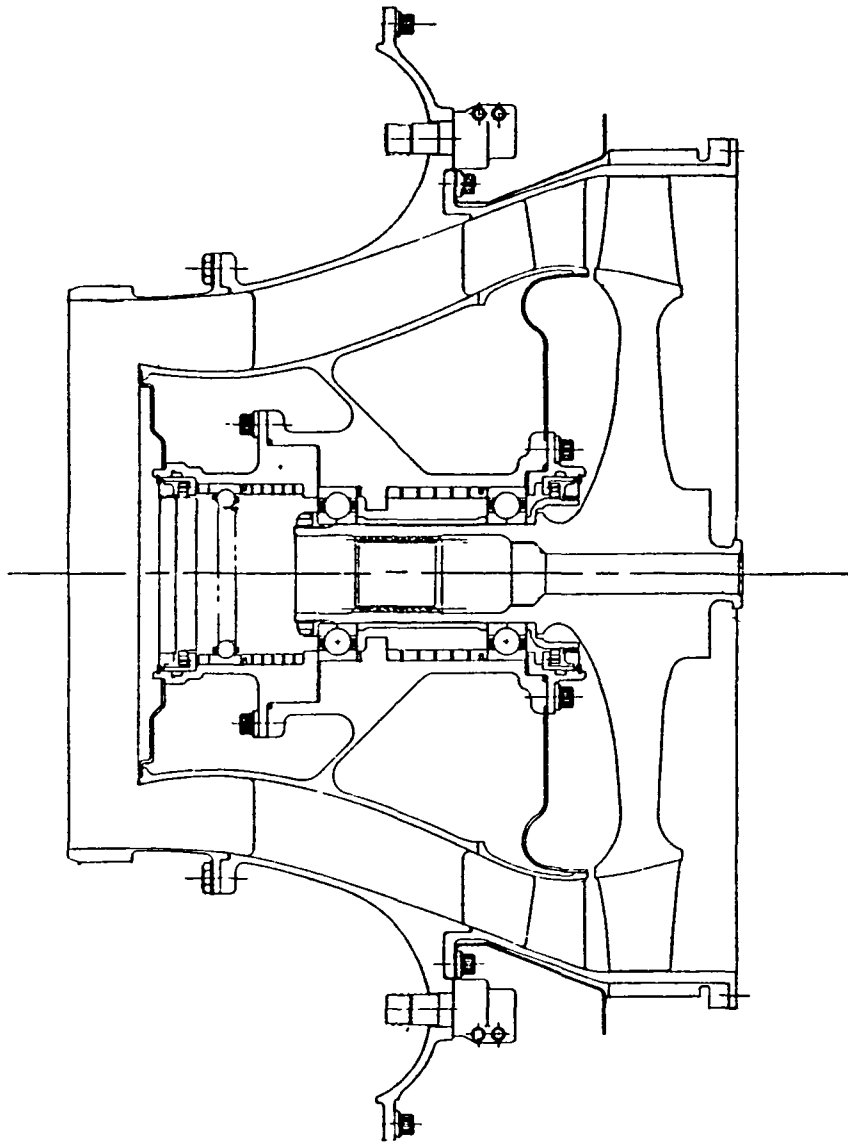


Figure 16. Power Turbine Module.

The support housing's inner cylinders, which are supported by the access struts, contain the bearings and seals necessary for the rear of the compressor shaft and the power turbine stub shaft. Spring pre-loading of the aft bearings on both of these shafts assures a constant axial bearing load application. This bearing compartment is sealed from hot combustion gases by fore and aft heat shields, which extend from the diffuser duct inner wall to the bearing housings, and by fore and aft controlled gap seals.

The periphery of this housing, which bolts to the rear of the gas producer module transmits the power turbine reaction loads, seals the burner cavity, and contains the necessary service bosses. The cast power turbine nozzle and brazed rear heat shield assembly, and at a larger radius, the fuel manifold assembly, bolt to the rear of the casting. Thermocouples that measure the gas temperatures entering the power turbine insert radially through bosses next to the module connection flange. Opening this main flange connection and the power turbine shaft lock, permits withdrawal of this module from the core engine for hot-end inspection.

The power turbine rotor consists of a cylindrical stub shaft and an integrally cast, inertia-welded rotor assembly. This assembly pilots on and is clamped to the two split ball bearings in the rear bearing support housing.

A schematic of the meridional flow path of the turbine sections is shown in Figure 17.

#### 3.2.2.3.1 Interturbine Duct

The interturbine duct moves from the high-pressure turbine exit gradually outward following the lower contour of the combustor to reach the larger diameter of the low-pressure turbine. A moderate diffusion is tolerated throughout the duct in order to enhance the flow acceleration rates across the low-pressure turbine blade rows.

Figure 18 shows in solid line the velocity distribution along inner and outer duct wall, respectively, as calculated by axisymmetric analysis. The dashed line indicates the strut surface velocity distribution obtained by superimposition of the two-dimensional cascade flow on the meridional flow velocity.

Four struts provide the load carrying structure for the turbine bearings and rigidly connect the duct walls. These struts have an axial

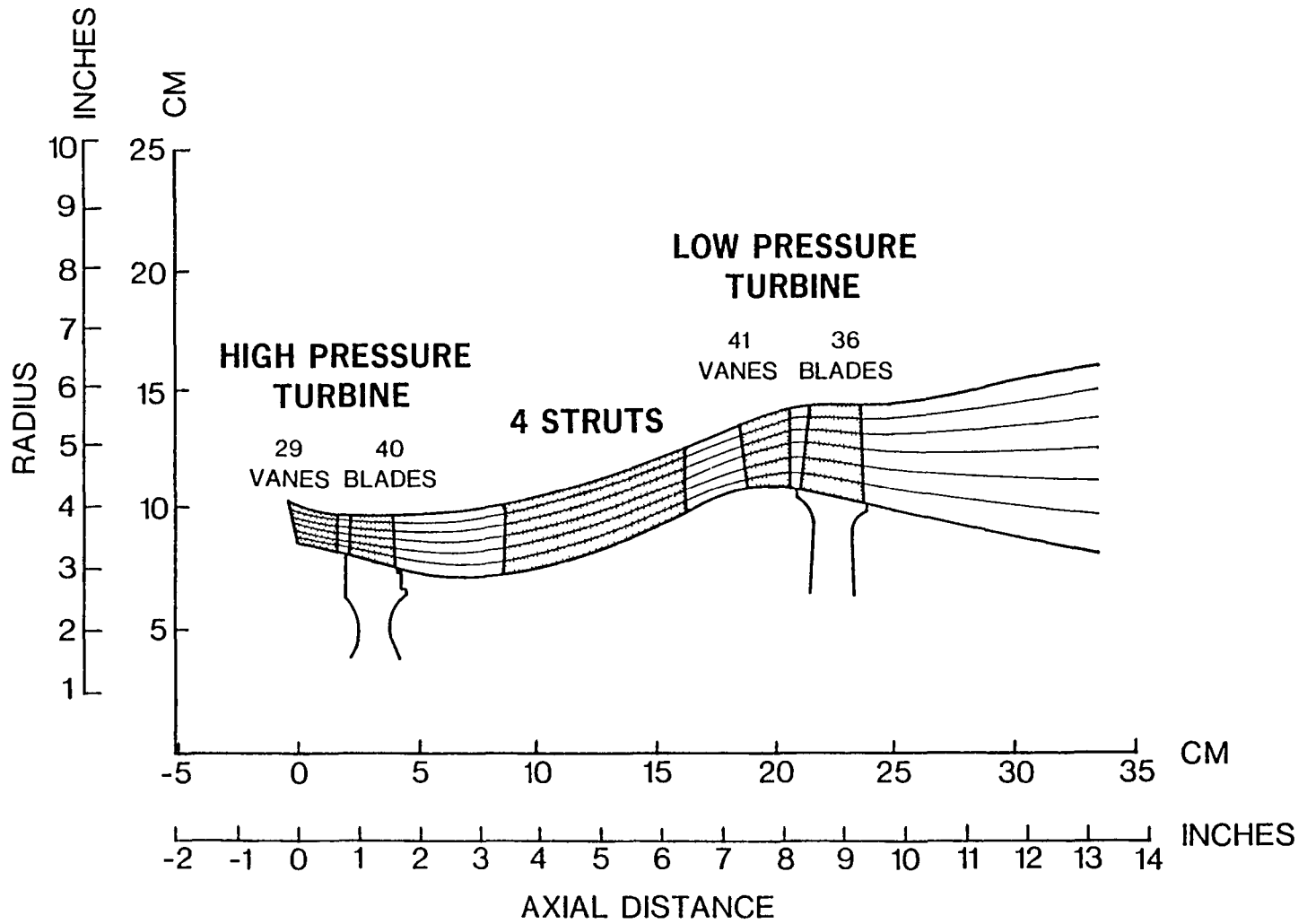


Figure 17. Turbine Section Meridional Flow Path.

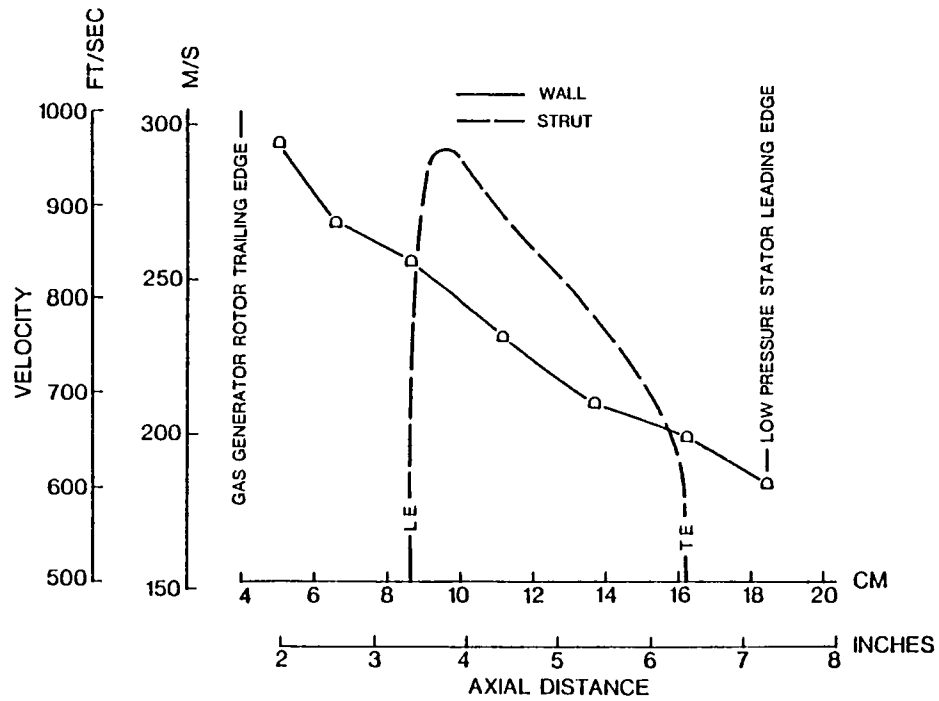
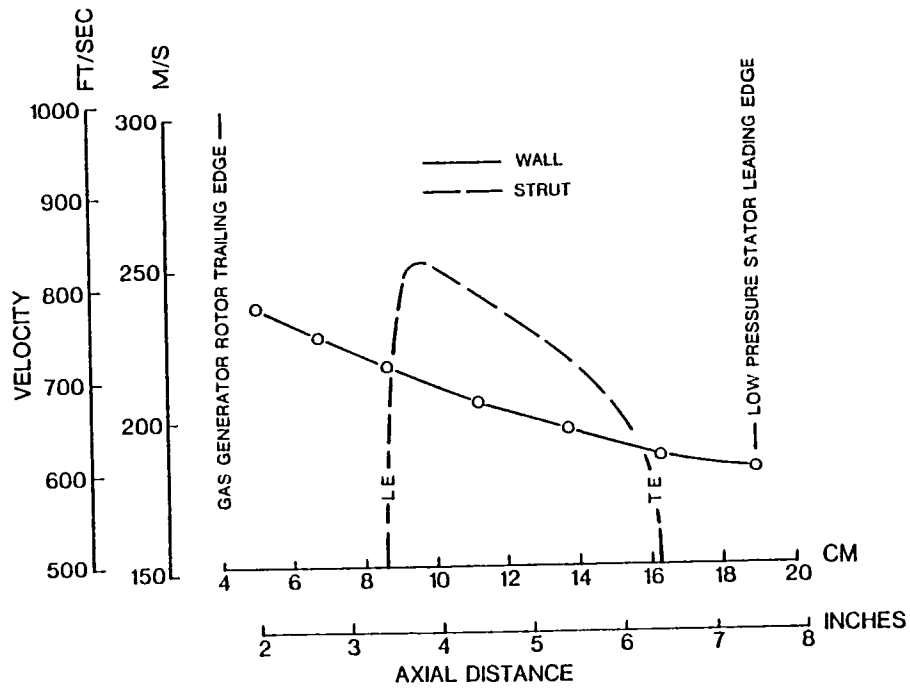


Figure 18. Interturbine Duct Inner and Outer Wall Velocity Distribution at Sea Level Takeoff

length of 7.6 cm (3.0 in.) and a maximum thickness of 1.2 cm (0.47 in.) to allow internal passage of the rear bearing cavity service lines.

To minimize strut blockage losses, channel contour in between the struts has been adjusted to compensate for strut blockage by locally tailoring the flow path in the strut region.

#### 3.2.2.4 Accessory Drive Module

As there were no contractual requirements for the gearbox design, it was sized for available bearing size's and therefore represents a basic boiler plate design concept. Each particular airframe application would specify its accessory load requirements and the appropriate flight weight housing and gearing system would then be designed.

The accessory drive module is mounted at the bottom of the fan frame and connected to the gas generator core through a steel turret shaft as shown in Figure 19.

The module is easily removed by removing the plug, extracting the turret shaft and unbolting the housing (4 bolts). A cross section of accessory gearbox is depicted in Figure 20.

The gearbox housing is a two-part design and consists of the housing and a front cover. Scavenge oil, which drains from the fan module through a hollow strut into the gearbox module, is removed from the gearbox by an externally mounted scavenge pump (oil pump pad). Pump, scavenge, and drain ducts have been sized to permit safe oil removal under any operating condition. A rotating oil-air separator is used to dump engine seal pressurization air overboard via a vent located in the gearbox forward face. All gears and bearings are oil mist lubricated.

The gearbox also contains the gas generator speed pickup as well as a chip detector and oil drain plug.

#### 3.2.2.5 Engine Control System

The majority of fuel and power control components are grouped around the main fan frame and are accessible for ground maintenance.

The gas producer fuel control is installed directly on the fuel pump, which in turn, is mounted on the accessory gearbox. This



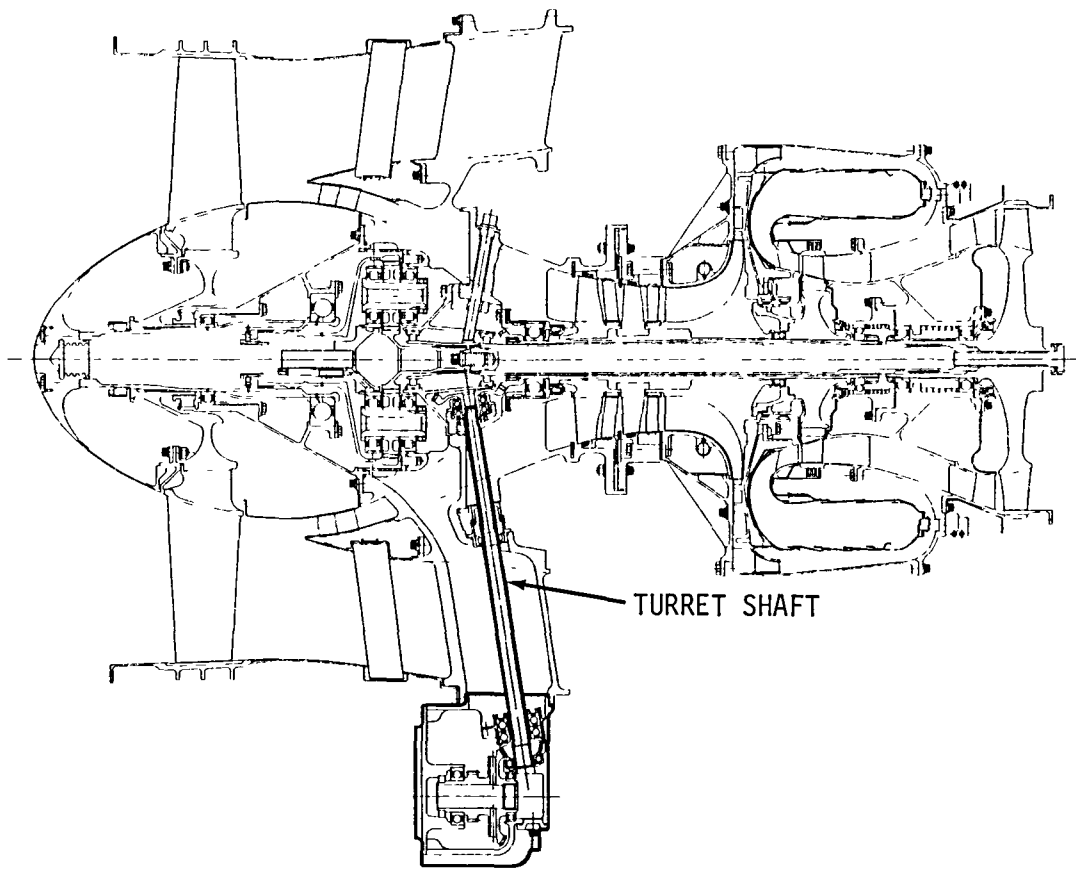


Figure 19. Accessory Drive Module Installation.

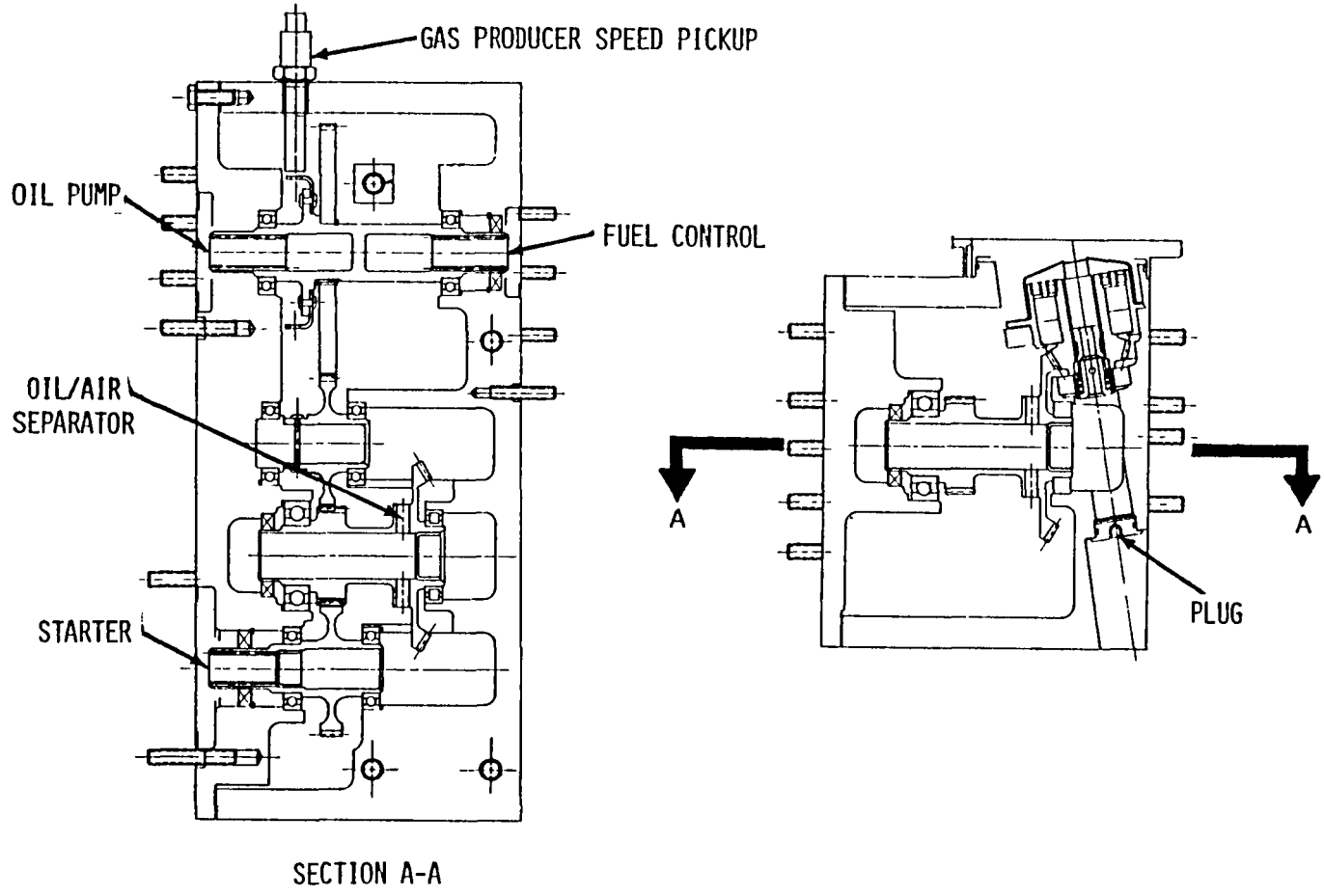


Figure 20. QCGAT Accessory Gearbox.

external arrangement eliminates vulnerable external pressure and return lines to the fuel metering section of the control and saves an additional pad and gearing on the accessory gearbox. Both the pump and control filter screen assemblies are designed so that they may be easily removed for cleaning or replacement with the control mounted on the engine. Local screening is used within the control in order to provide protection for orifices and valves.

The ambient temperature signal at the engine inlet is directed to and from the gas producer control by two flexible hoses mounted at the entrance to the engine fan stage.

The fuel and engine control system for the QCGAT application were selected to achieve important design criteria such as reliability, durability, and simplicity without compromising functional requirements of the engine. The engine control system performs the basic functions of metering the required amount of fuel flow to the engine during starting, acceleration, deceleration, and steady-state operation. In addition, it also controls the operation of the compressor inlet flow fence assembly during steady-state and transient maneuvers. The QCGAT engine control system consists of the following major components: Fuel control, fuel pump, flow fence actuator and temperature compensator.

The high-pressure fuel pump incorporates a pumping element and gear set used on Lycoming T53 engines which has been repackaged in a new housing for utilization on LTS/LTP 101 power plants.

The gas producer control and ambient temperature compensator are substantially identical to systems that are in production for the Lycoming LTS/LTP 101 engine.

The inlet flow fence actuator was specifically designed for the LTS/LTP 101 engine and with the exception of a few minor changes, is directly applicable for the QCGAT application.

#### 3.2.2.5.1 Fuel System Operation

A schematic flow diagram of the engine power control and fuel system is shown in Figure 21. The fuel from the airframe supply system is supplied to the fuel inlet port on the engine fuel pump. A 10-micron barrier filter is required in the airframe fuel system to protect the engine fuel system against contamination. The inlet pressure is increased by the engine-driven fuel pump to the level required for fuel nozzle injection. The pump output flow enters the gas producer control

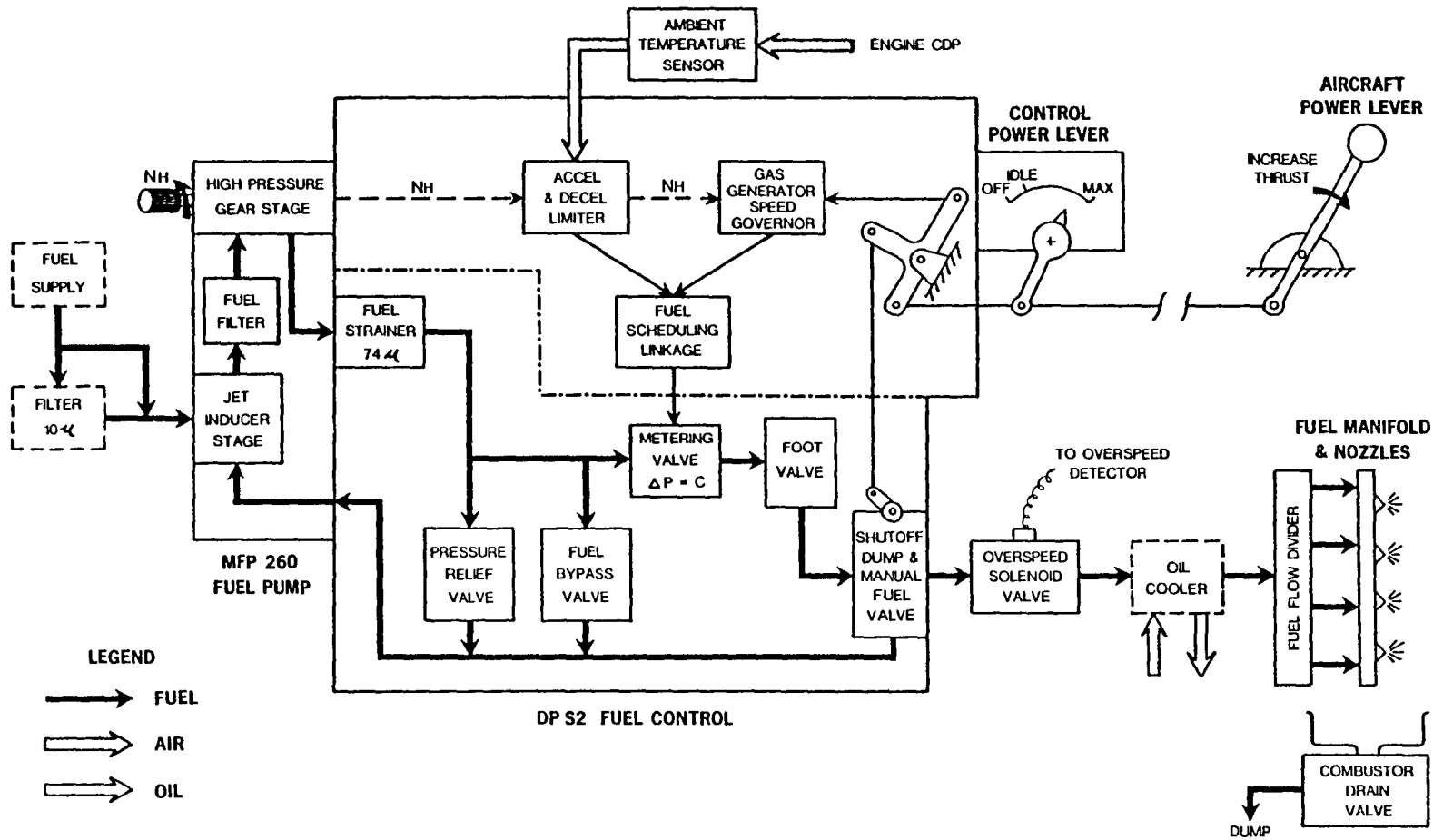


Figure 21. Power Control and Fuel System Schematic.

from where the engine demand flow is metered to the low pressure turbine fan overspeed solenoid valve, engine oil cooler, and finally into the fuel flow divider. Here the flow is split into a primary path and a secondary path injected into the combustor by eight dual orifice injectors. The pump flow in excess of the engine demand is internally returned from the control to the pump inlet.

The fuel control performs the following functions:

- o Maintains the engine speed condition as demanded by inputs from the operator via the power lever.
- o Schedules the proper amount of fuel flow for accelerations and decelerations.
- o Schedules the fuel flow required for engine starting.

The ambient temperature compensator, which is physically a separate unit mounted in the engine inlet, is functionally a part of the control and serves primarily to bias the acceleration schedule with ambient temperature. The control is pictorially shown in Figure 22.

#### 3.2.2.5.2 Inlet Flow Fence Control and Actuator

A pair of retractable rings are located in the engine inlet housing in front of the compressor. The rings are mechanically operated by a pneumatic actuator whose output stroke is scheduled by a closed-loop, integral pressure ratio ( $P_c/P_{in}$  or  $P_3/P_{2.1}$ ) controller. Refer to Figure 23 for a schematic representation of the complete assembly. The actuator and controller are mounted on the compressor diffuser and are shown in Figure 24.

At speeds up to approximately 80 percent  $N_H$ , the rings are extended into the inlet air stream to prevent low-speed rotating compressor stall. Above 80 percent  $N_H$ , which corresponds to a particular engine pressure ratio ( $P_c/P_{in}$ ), the actuator begins to move and gradually retracts the flow fence rings. Above 90 percent  $N_H$ , which corresponds to another  $P_c/P_{in}$ , the fences are completely retracted out of the air stream. This action permits surge-free gas producer accelerations of approximately 5 seconds from flight idle and to achieve maximum rated thrust for takeoff conditions.

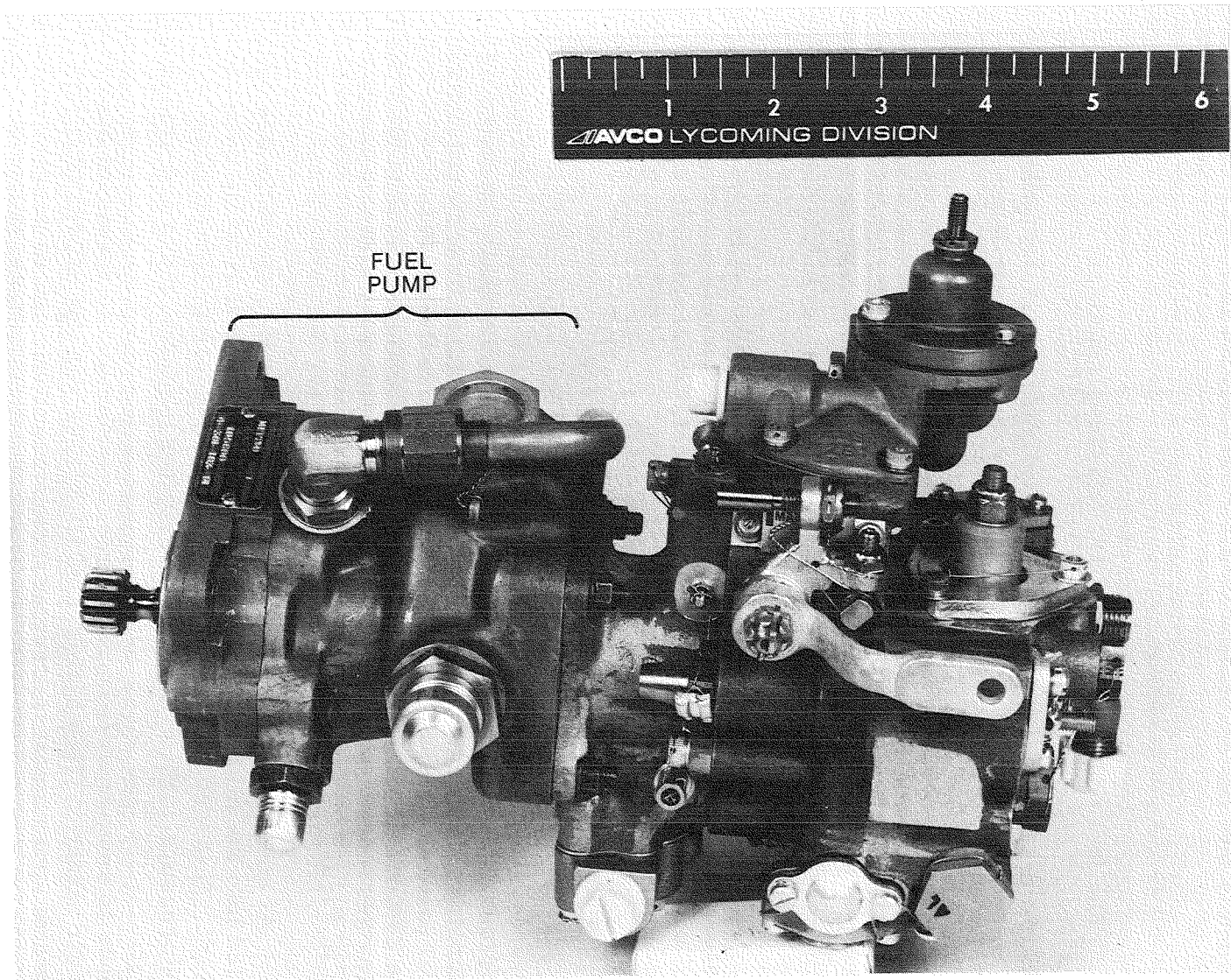


Figure 22. Fuel Control Assembly.

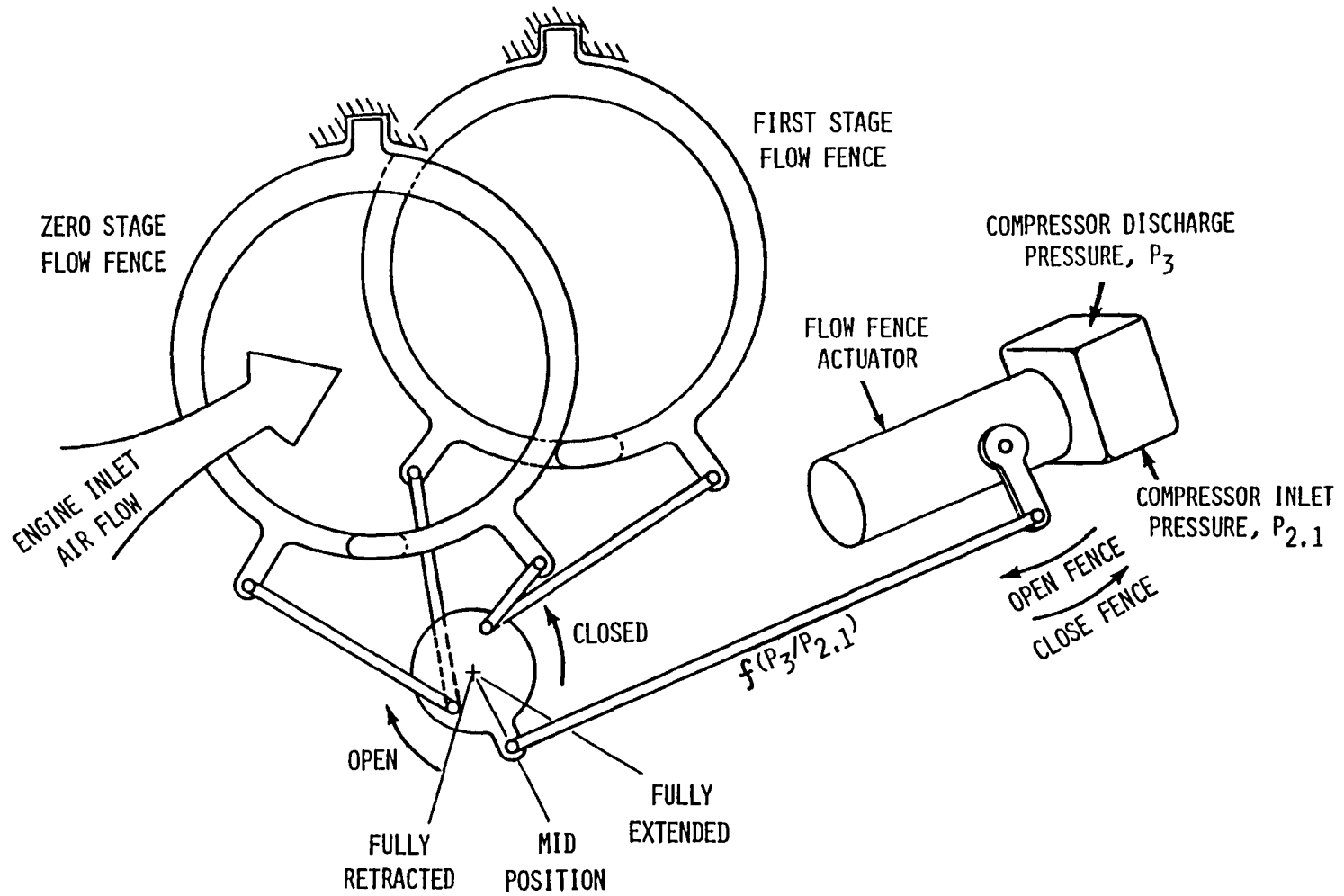


Figure 23. Dual Compressor Flow Fence Schematic.

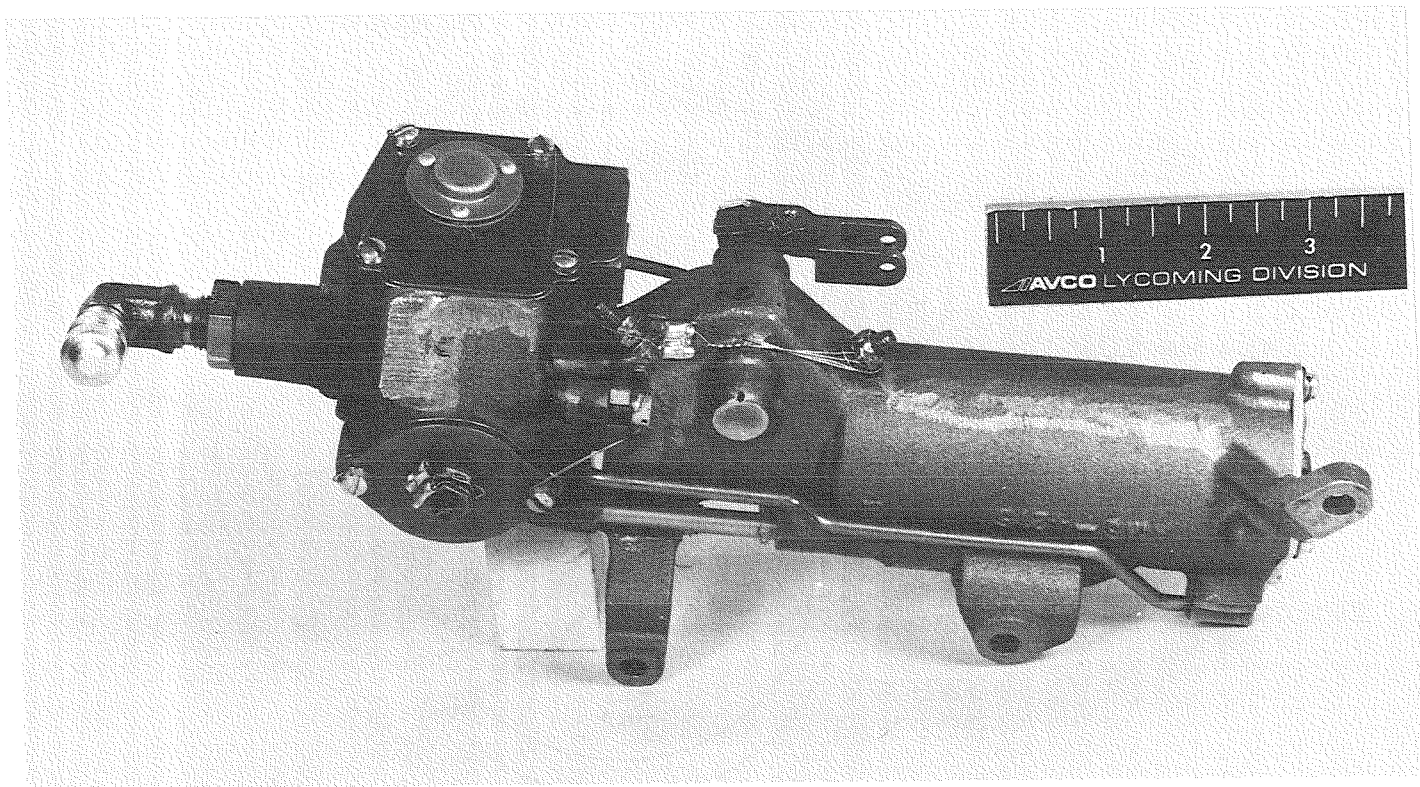


Figure 24. Flow Fence Actuator.



The unit is self-contained with mechanical closed-loop positioning of the actuator piston. The only input required is compressor discharge pressure (Pc).

### 3.2.2.5.3 Engine Overspeed Protection

The overspeed trip utilized here is the same unit, with modified trip point frequencies as that used on the Lycoming LTS 101 commercial engine. The design was taken in total from the engine protection/sequence control developed for Lycoming's AGT 1500 gas turbine army tank engine.

The system particulars are as follows:

Trip Speed:	108% of Power Turbine, Takeoff Speed, RPM
Reset Speed:	95% of Power Turbine, Takeoff Speed, RPM
Response Time:	Less than 6 milliseconds for the trip, less than 45 milliseconds for the total system
Input Power Supply:	16 to 30 VDC per MIL-STD-704
Switched Output:	1.5 amps
Input Signal Volts:	+4.5, -2.0 min at trip speed +2.5, -2.0 min at 1/2 test
Temperature:	-65° to +250°F
Altitude:	-1,000 to 50,000 feet
Vibration:	20 g's 5 to 500 Hz
Shock:	30 g's 11 MS
EMI:	Tested to MIL-STD-461, Notice 4

Engine power turbine overspeed protection is provided by an electronic overspeed trip unit via the engine's main fuel flow. The overspeed protection system is schematically shown in Figure 25. Protection is accomplished by monitoring the engine power turbine speed with a variable reluctance magnetic speed pickup which senses the shaft speed directly. The resultant output signal is an output pulse repetition rate which is proportional to the shaft speed and having a minimum voltage amplitude. This signal is supplied to the overspeed trip unit which conditions it into a fixed geometry pulse train whose frequency/shaft speed information has been carefully preserved.

### 3.3 NACELLE DESIGN APPROACH

A preliminary design of the flight nacelle was defined to establish a realistic baseline from which a ground test nacelle could duplicate the important features at reduced program cost. However, only a ground test nacelle was fabricated.

The flight nacelle conception shown in Figure 26 comprises the following sections:

1. An inlet duct to provide uniform flow into the engine
2. A fan outer duct and core cowl to guide the bypass air around the engine
3. A mixer assembly to force the mixing of hot, higher velocity core engine exhaust with the cooler, lower velocity fan stream
4. A mixing chamber preceding the final nacelle exit nozzle
5. An aerodynamically shaped outer skin designed to minimize drag at the higher flight speeds.

A mixed-flow exhaust system was selected because it reduces the peak exit velocity which improves propulsive efficiency and reduces jet noise.

Noise attenuation treatment in the form of perforated acoustic panels was introduced in the air intake section and the fan duct outer wall.

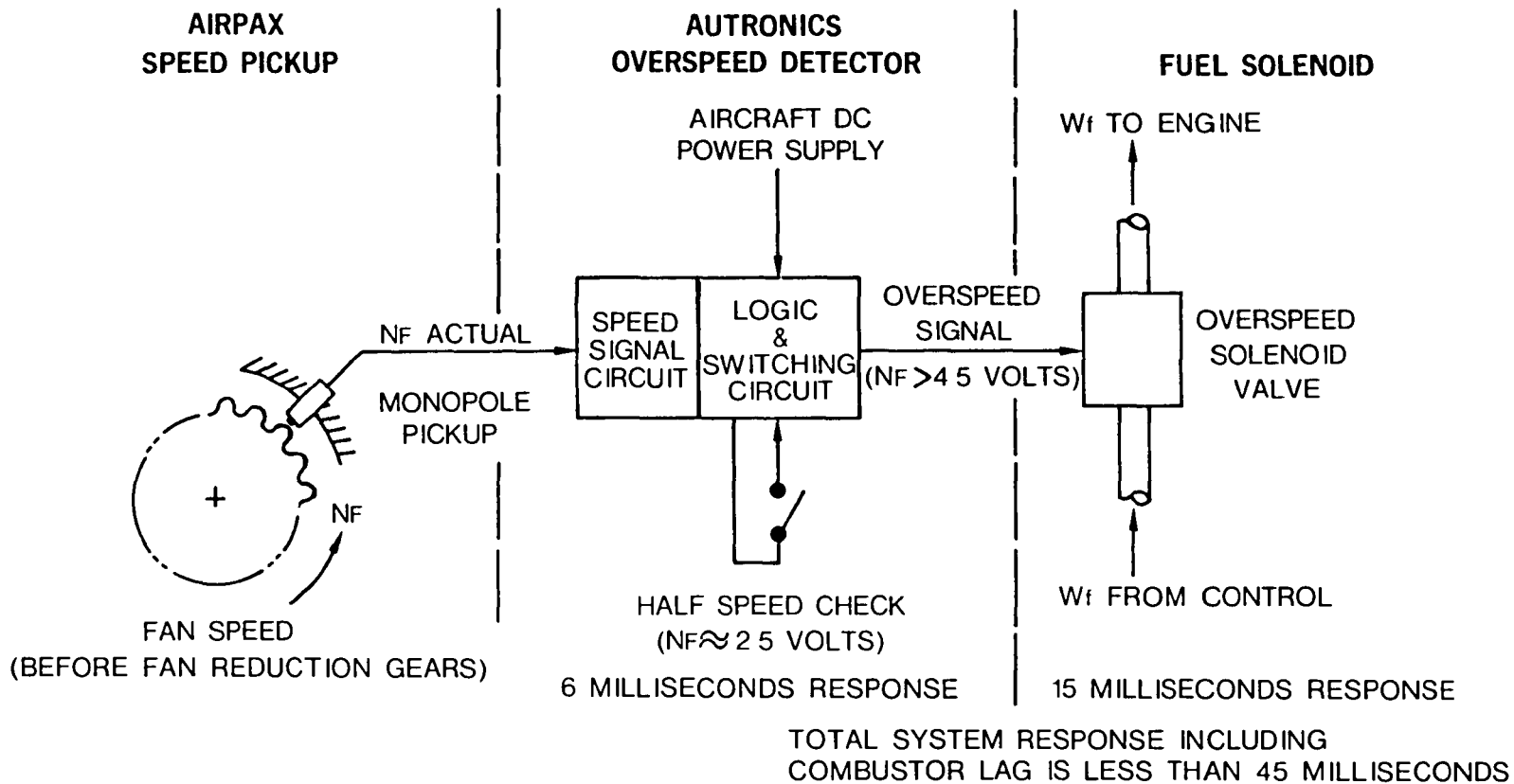


Figure 25. Fan Overspeed Trip System

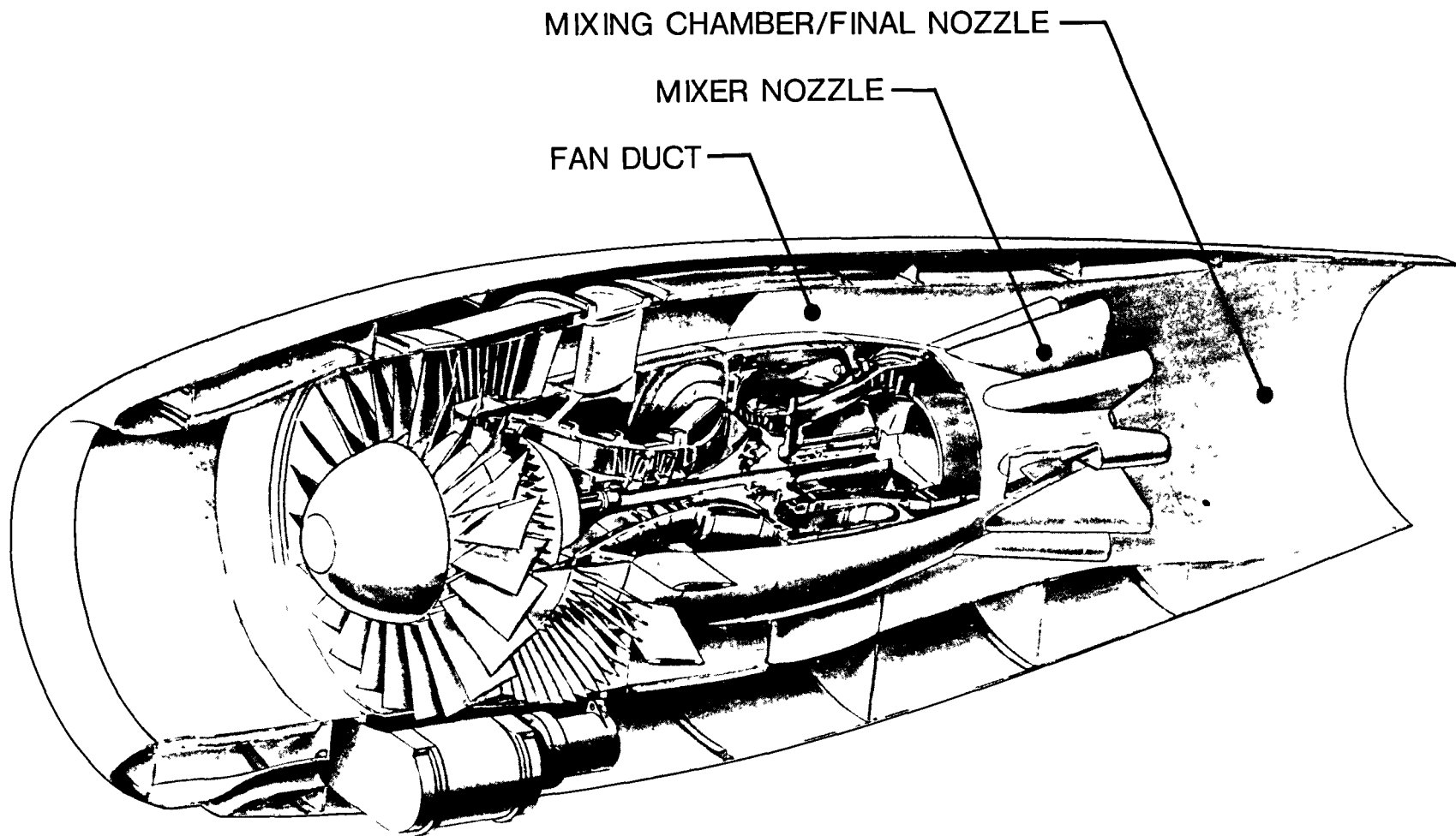


Figure 26. Cross Section of Engine With Cutaway.

The flight nacelle is designed for optimum cruise performance at 0.6 to 0.65 Mach no. at 7620 meters (25,000 feet) altitude and is adaptable to pylon mounting on the side of the fuselage or top mounting for underwing installations.

Conventional metal construction (mainly aluminum) that is consistent with simplicity and the low cost required to general aviation application was used throughout the design. The main design objectives have been low noise (low internal and external tones), ease of accessibility, low weight, and low cost. The air inlet is designed to provide high-pressure recovery and inflow incidence tolerance.

### 3.3.1 Aerodynamic Design

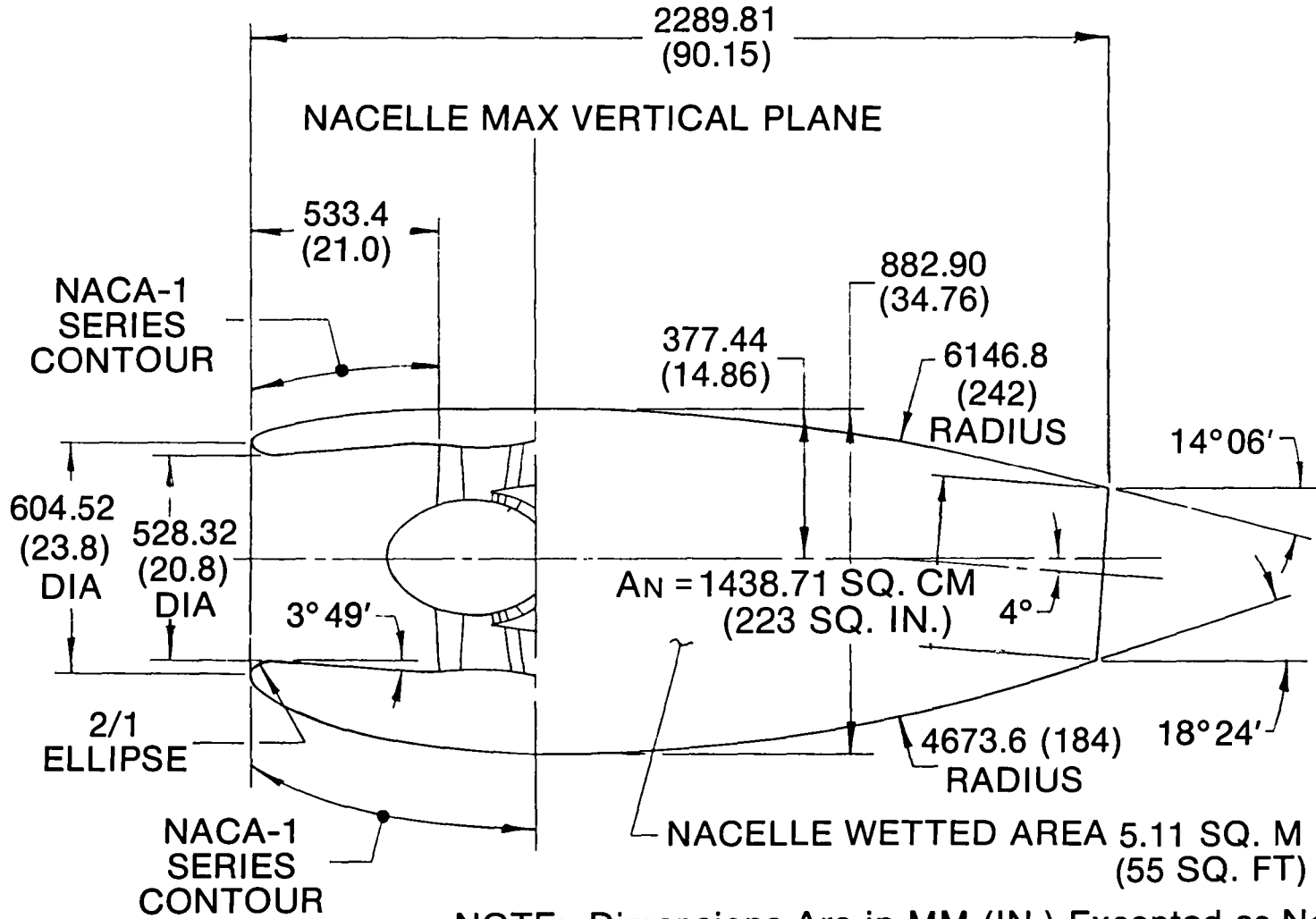
The overall aerodynamic contours of the flight nacelle are shown in Figure 27. A separate evaluation of drooped inlets having reduced curvature over the front lower contour indicated no improvement in the external aerodynamic drag when compared with a straight inlet. As a result, the lower cost axisymmetric inlet was chosen.

Basic design considerations and front cowl geometry are shown in Figure 28. The inlet throat denoted  $R_t$  in the figure has been designed for a low Mach number to efficiently accommodate up to 20 percent mass-flow growth. Front cowl external geometry ratios  $L_{EXT}/R_{MAX}$ ,  $R_{\infty}/R_{HL}$  and  $R_{MAX}/R_{HL}$  have been checked to ensure zero compressibility drag divergence and zero spillage drag over the full range of cruise power settings.

The drag divergence Mach number of the front cowl shown in Figure 29 is substantially above 0.65 Mach number for the upper and lower contours of the nacelle. The criterion used was based on tests of various geometry NASA Series 1 cowl shapes that relate dimensions and cowl curvature to drag divergence Mach number.

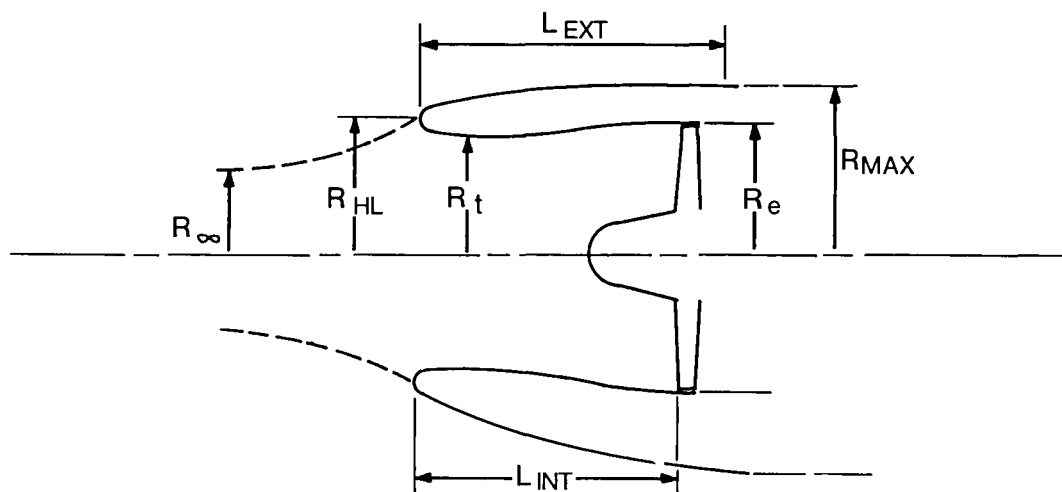
Spillage drag margin shown in Figure 30 relates cowl curvature determining dimensions and mass flow ratio  $(R_{\infty}/R_{HL})^2$  to a limit line that defines onset of spillage.

The criteria shown for cruise on the critical upper lip at 0.65 Mach number at 7620 m (25,000 ft) with the engine operating at maximum cruise power would permit an aircraft incidence of 2 degrees before the onset of spillage drag. This incidence margin is higher than that which would be experienced in steady-state cruise. Some spillage



NOTE: Dimensions Are in MM (IN.) Excepted as Noted

Figure 27. QCGAT Nacelle External Geometry.



RATIOS	UPPER LIP	LOWER LIP	CONSIDERATION
$L_{EXT}/R_{MAX}$	1 413	1 558	AVOIDANCE OF SPILLAGE OF COMPRESSIBILITY DRAG DIVERGENCE
$R_{MAX}/R_{HL}$	1 252	1 676	
$(1)R_{\infty}/R_t$	0 761		
$R_{HL}/R_t$	1 14		INCIDENCE OF CROSSWIND TOLERANCE
$R_e/R_t$	1 1		PROVIDE INTERNAL DIFFUSION WITH MINIMUM DISTORTION
$L_{INT}/R_t$	2 056		

DIMENSIONS CM (IN.)		
SYMBOL	UPPER LIP	LOWER LIP
$R_{MAX}$	37 74 (14 86)	50 55 (19 90)
$R_t$	26 44 (10 41)	
$R_{HL}$	30 15 (11 87)	
$R_e$	29 08 (11 45)	
$L_{EXT}$	53 34 (21)	78 74 (31)
$L_{INT}$	54 36 (21 4)	
$(1)R_{\infty}$	22 94 (9 03)	

(1) Cruise Max Continuous Rating at 7,600 M (25,000 FT), 0.65 Mach No, Standard Day

Figure 28. QCGAT Nacelle Front Cowl Geometry.

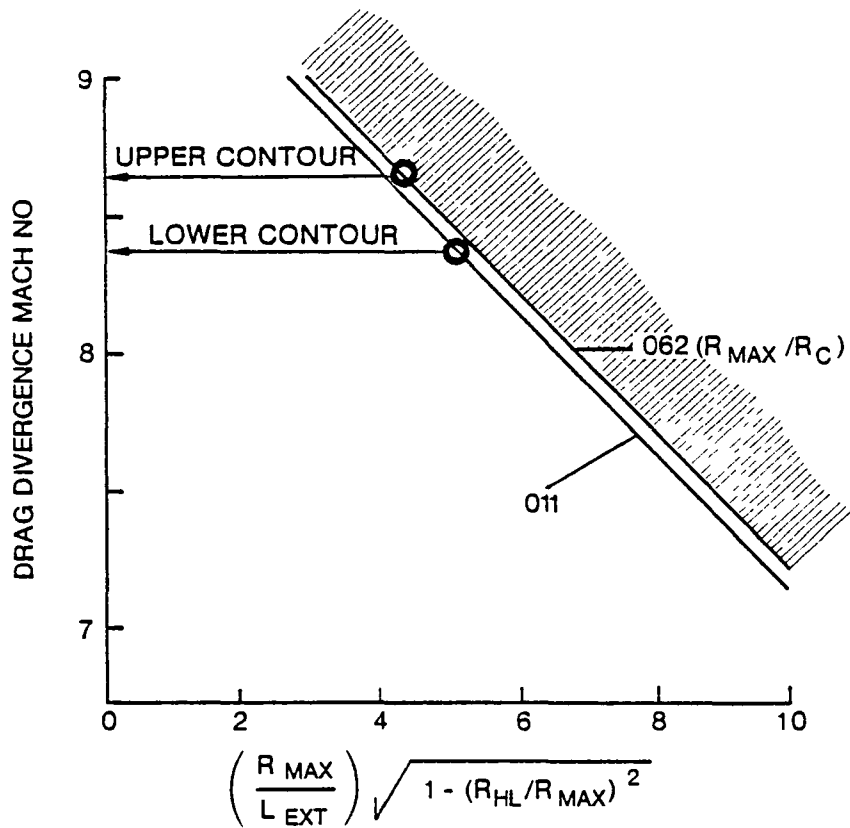
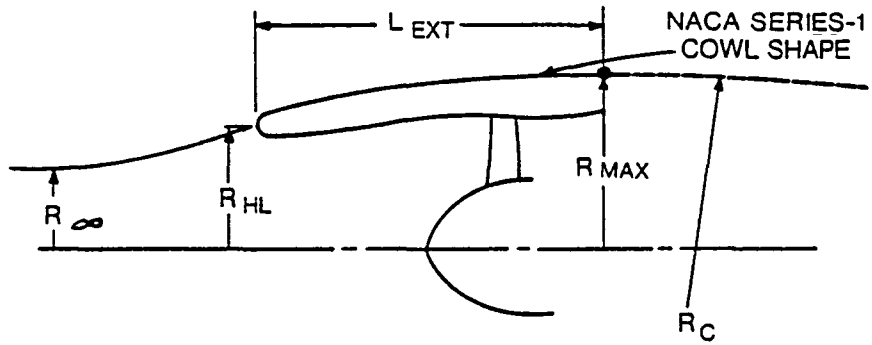
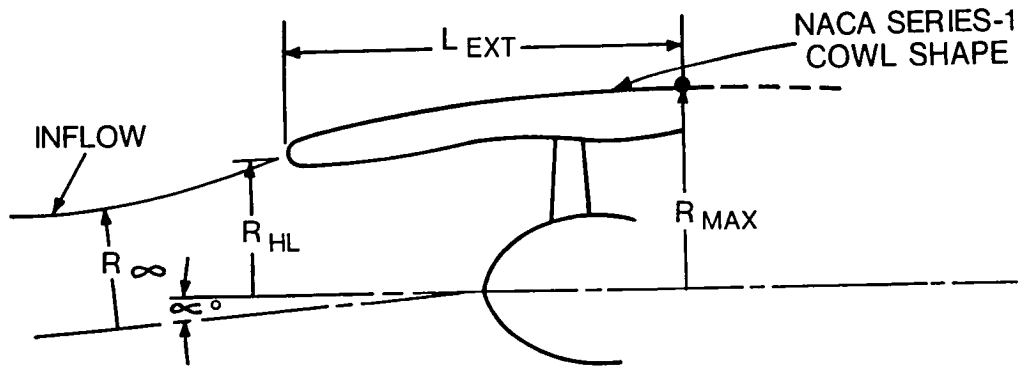


Figure 29. QCGAT Nacelle Maximum Drag Divergence Flight Speed





CRITICAL MASS  
FLOW RATIO

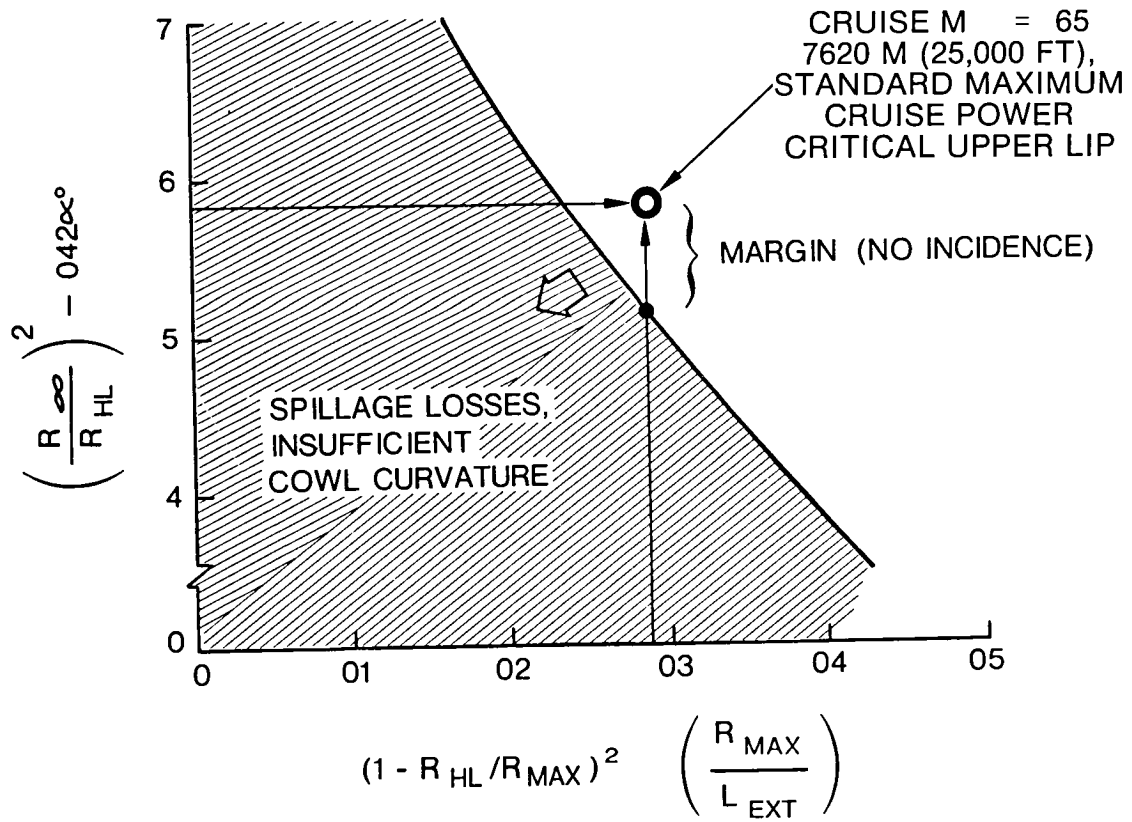


Figure 30. QCGAT Upper Cowl Lip Spillage Margin.

permissible for transient maneuvers will not impact mission fuel economy. The lower lip with its high external lip curvature gives substantially more margin.

The incidence tolerance of the inlet for takeoff and landing approach conditions is shown in Figure 31. With a contraction ratio ( $R_{HL}/R_t$ ) equal to 1.14, the inlet maintains acceptable flow distribution to the fan for an inflow incidence over 30 degrees for approach and over 40 degrees for takeoff. This provides at least a 20.6 m/sec (40-knot) crosswind tolerance.

The ratio of the inlet length (Figure 28) to the throat radius  $L_{INT}/R_t$  is slightly above 2.0; this ensures minimum inlet distortion and provides sufficient space for effective inlet noise attenuation panels. The inlet diffusion half angle is below 4 degrees as shown in Figure 27.

The inlet cowl shape which has a leading edge radius equal to 1.5 percent of the highlight radius ( $R_{HL}$ ) blends into a NASA Series 1 outer cowl contour and a 2:1 aspect ratio ellipse that forms the inner lip shape.

Estimated inlet pressure recovery ( $P_{T1}/P_{T\infty}$ ) at the fan inlet face is shown in Figure 32 with both noise attenuation panels and hard wall panels. At flight Mach numbers greater than 0.15, the pressure recovery is approximately 0.997 for a hard-panel duct and 0.995 with noise-attenuation panels.

The external geometry of the nacelle is shown in Figure 27. The boat tail angle at the lower fan contour has been limited to 18 degrees to ensure separation-free operation for steady-state flight throughout the aircraft flight envelope. The side and upper contours have a boat tail angle of about 14 degrees and a curvature ( $R_c/R_{MAX}$ ) of 16. The total wetted area of the nacelle is 5.1 square meters (55 square feet). The nacelle drag area is .015 square meter (0.158 square feet) assuming a drag coefficient ( $C_{Dwet}$ ) of 0.0024 based on total wetted area and a body fineness ratio form factor of 1.2.

Flow areas and mass-flow averaged Mach numbers along the air inlet and fan flowpaths are shown in Figure 33 for sea level takeoff conditions. Duct mach numbers at all stations are below 0.4. Fan and primary exhaust flows are mixed by means of a multi-lobed mixer nozzle as indicated in the Figure 32.

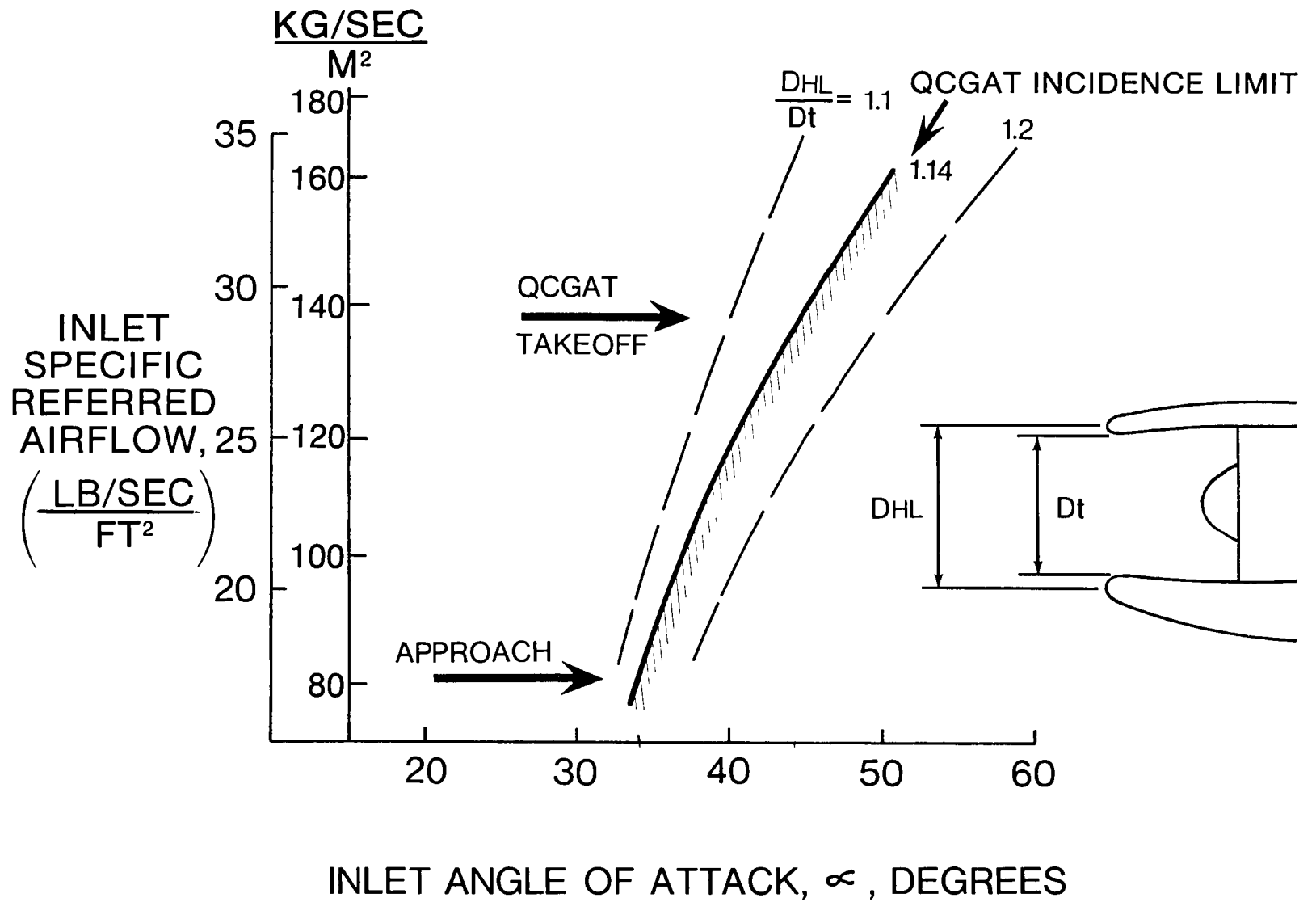


Figure 31. QCGAT Inlet Flow Incidence Limits.

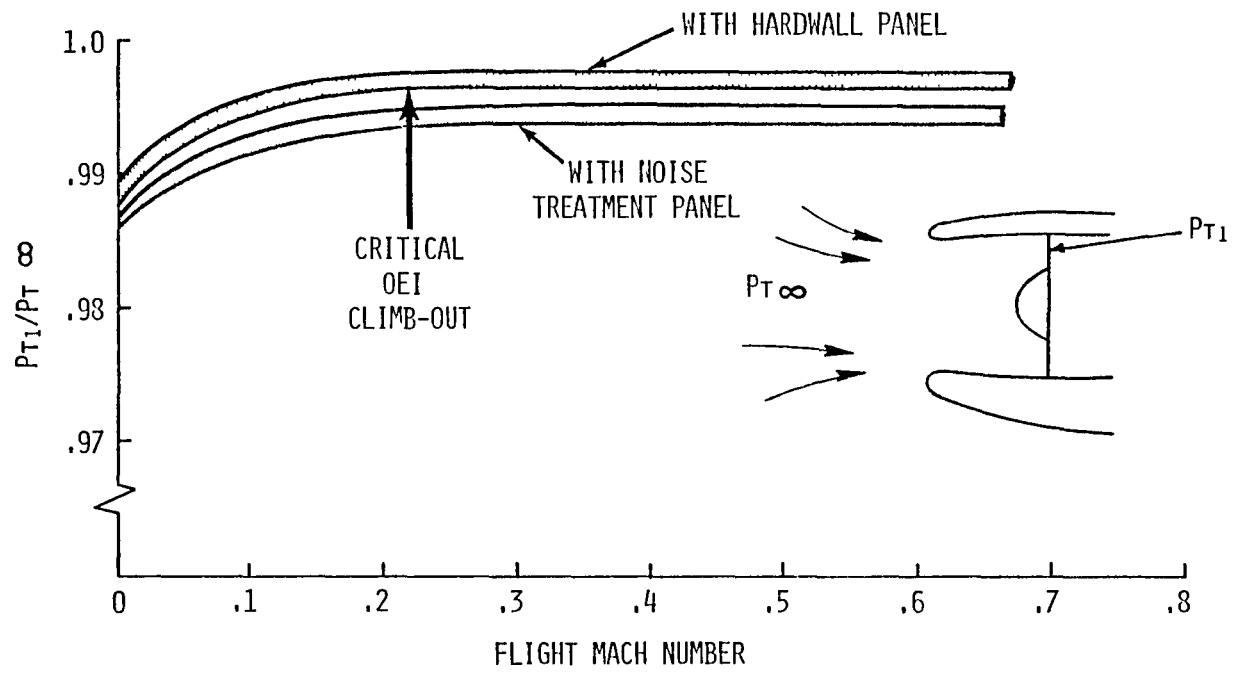


Figure 32. Inlet Pressure Recovery.

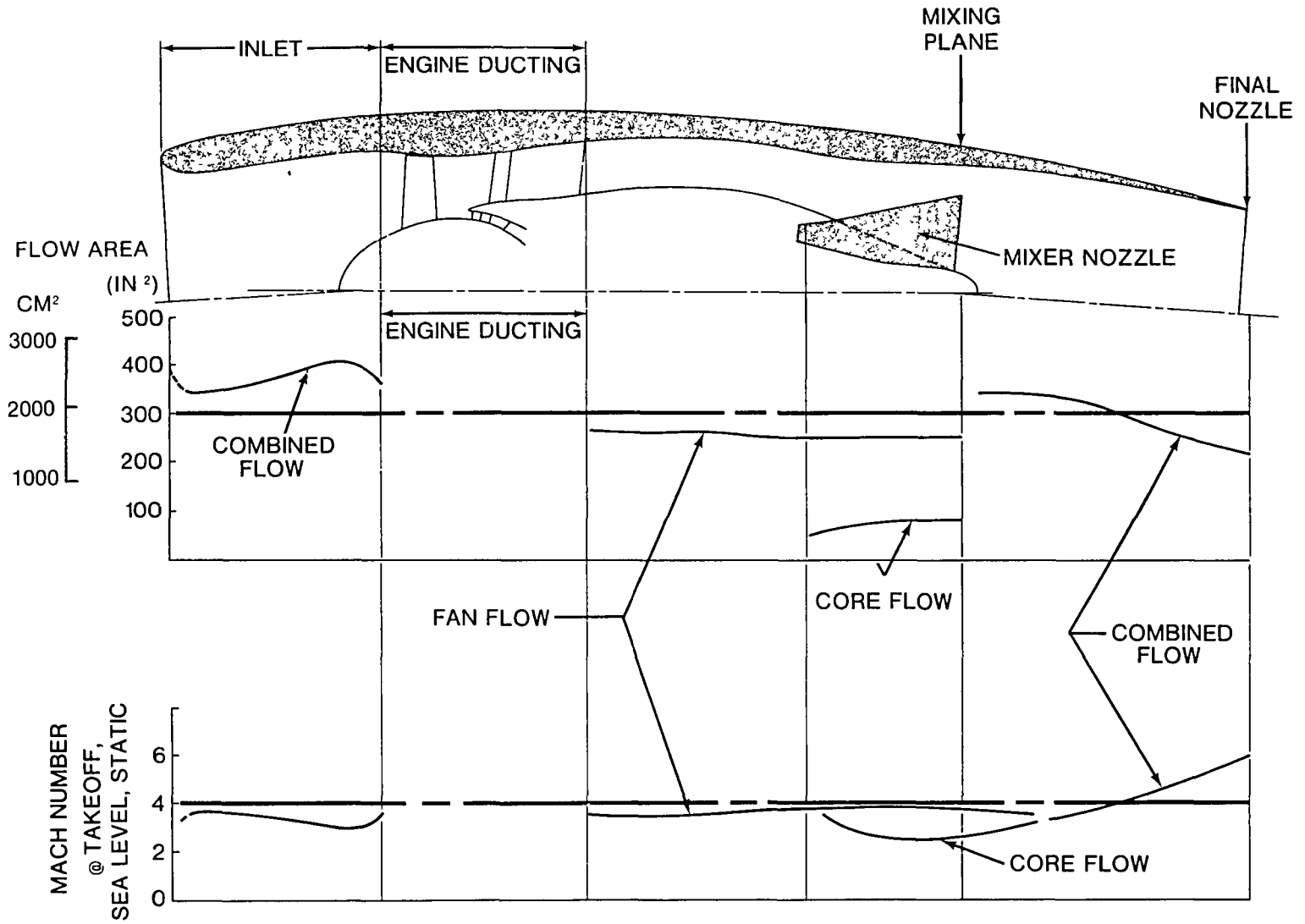


Figure 33. QCGAT Nacelle Duct Areas and Mean Mach Numbers.

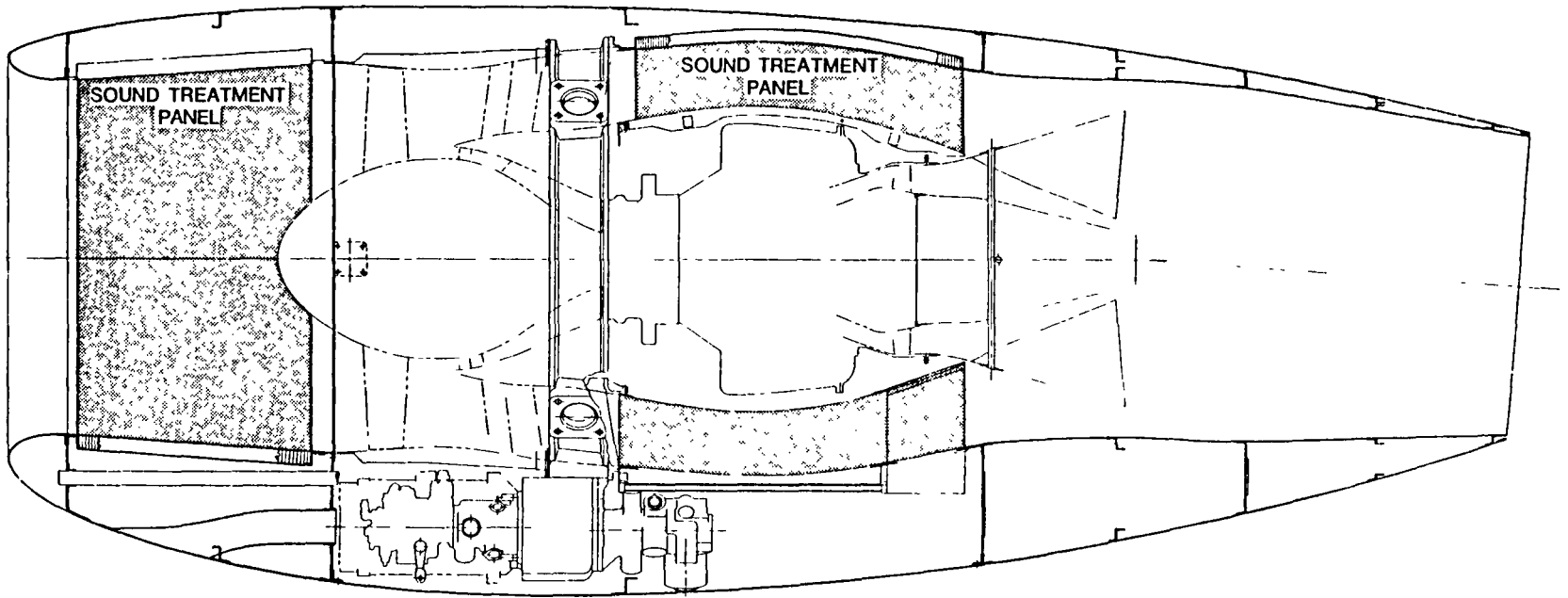


Figure 34. QCGAT Flight Nacelle With Sound Treated Panels Installed.

- Designed at Approach Power Setting
- Effective Off-Design Performance

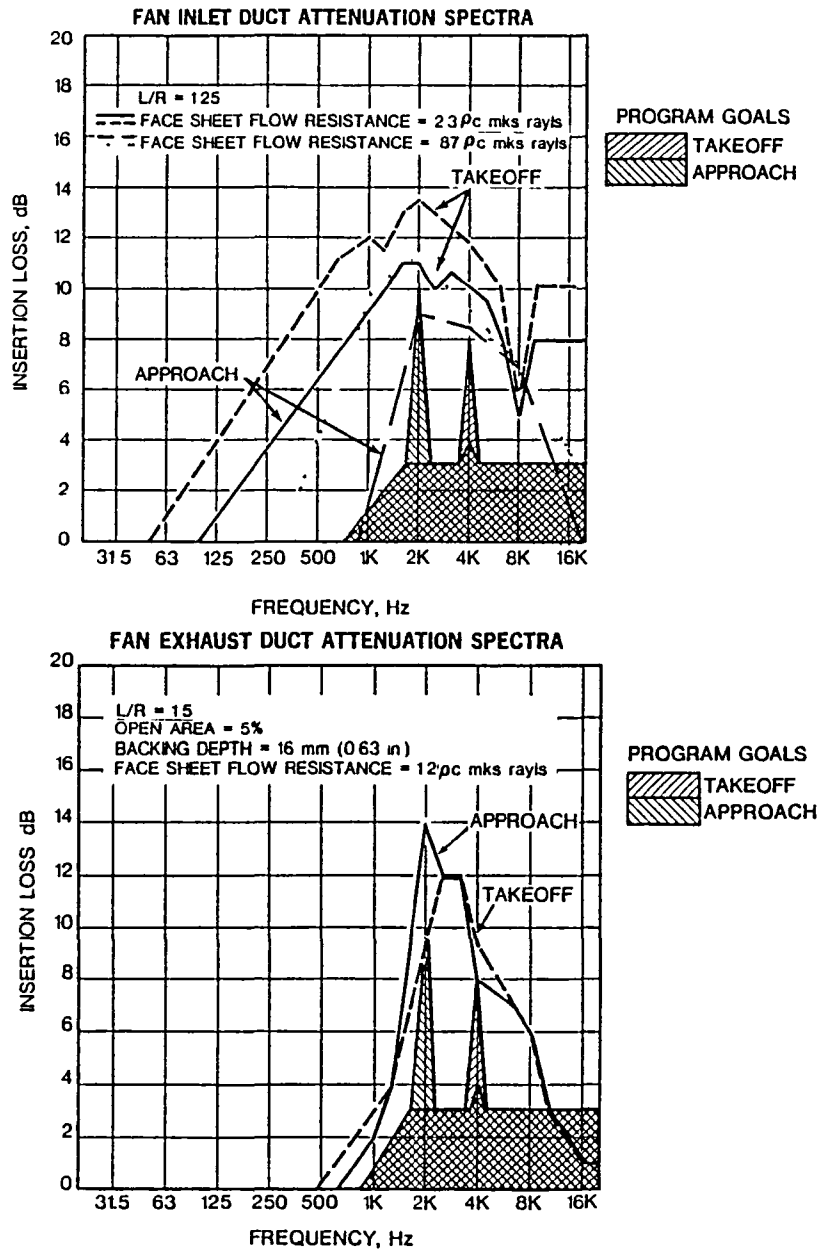


Figure 35. QCGAT Lockheed Fan Exhaust Noise Treatment Design.

TABLE 2. ENGINE OPERATING PARAMETERS

Parameter	Design Point	Off-Design Point
Power Setting	Approach	Takeoff
Altitude	112.8m (370 ft)	1105.2 m (3626 ft)
Forward Air Speed	91 knots	103 knots
<u>Number of</u>		
Fan Blades	24	24
Inlet Guide Vanes	0	0
Exit Guide Vanes	59	59
Support Struts	8	8
Ratio of Distance Separating Blades from Vanes to Axial Blade Length	2.35	2.35
Fan Rotor Speed	5400 rpm	9928 rpm
Blade Tip Relative Mach Number	0.5117	0.995
Inlet Temperature	298.5°C (537.3°F)	292.5°C (526.3°R)
Exit Temperature	306.2°C (550.9°R)	318.4°C (573.0°R)
Inlet Pressure	99.9 kPa (14.5 psia)	88.7 kPa (12.87 psia)
Exit Pressure	107.9 kPa (15.7 psia)	116.5 kPa (16.89 psia)
<u>Average Mach No.</u>		
Inlet Duct	0.2	0.36
Discharge Duct	0.22	0.38



### 3.3.2 Acoustic Considerations

It has been recognized for sometime that the fan inlet and discharge ducts of the engine nacelle offer ideal locations for installation of sound treatment material to absorb much of the noise generated by the fan. Absorptive materials are particularly efficient in absorbing sound energy in the high-frequency region where much of the acoustical power radiated by the fan is concentrated. In addition, sound treatment can be accomplished in the use of flight-worthy materials that add little weight to the aircraft. Finally, the theory and experience of designing sound-treatment panels are sufficiently sophisticated to accurately predict the results that will be achieved from a particular design. Consequently, sound-treatment panels for the QCGAT engine nacelle were investigated to determine the benefit that would be derived from their incorporation in the aircraft design. The treated areas are depicted in Figure 34.

The acoustical problem statement comprised a set of attenuation requirements, a description of relevant engine and nacelle geometry and operating parameters, and estimates of the acoustical conditions in the ducts. The attenuation requirements are shown superimposed on the insertion-loss prediction graphs and are broken down into 1/3 octave spectra for approach and take-off conditions. (See Figure 35 ). These spectra are dominated by the requirements at blade passage fundamental. The geometry of the air passages was presented as scalable line drawings, and the operating conditions defining approach and takeoff are summarized in Table 2.

The inlet duct was modeled as a simple cylinder, 533 millimeters (21 inches) in diameter. Lengths of 1 radius and 1.25 radius were considered. The inner wall is considered to have an in-place acoustic impedance  $Z$ , where  $Z$  is a function of airspace depth, facing sheet throughflow resistance, inertance, mean grazing flow, the sound pressure level, and sound pressure spectrum.

The discharge duct was modeled as a straight annular duct having larger diameter, 610 mm (24 in.), and inner diameter, 355 mm (14 in.). The inner duct wall is nonabsorptive. The outer wall has a finite acoustic impedance  $Z$ . Inlet flow is described by its mean Mach number (-M) and discharge flow by its mean Mach number (+M). The convention of signed Mach numbers is peculiar to acoustical analysis.

The theory of the transmission of sound in ducts containing flow leads to a general governing equation known as the convected wave equation. Its solutions are infinite in number, but only a small group represent the propagation of energy along the duct, the so-called propagating modes. The remainder (nonpropagating modes) represents pressure disturbances that cannot propagate energy even along a nonabsorptive duct. These pressure disturbances decay along the duct, usually very rapidly. In the case of circular or annular ducts, each mode, except the zero-order mode, is represented by a rotating pressure pattern having sinusoidal lobes ( $m$ ) and radial nodes ( $q$ ) called spinning modes. Whether or not the  $m$ ,  $q$ th mode can propagate at any given frequency is precisely calculable, and the details of the noise source mechanism determine the modal content of the sound in the duct. Aerodynamic noise is likely to contain all possible propagating modes. The actual energy distribution among the modes is seldom, if ever, known, but a reasonable assumption is equipartition among the allowed lobe counts 0 to  $m$  and equipartition of the energy in the  $m$ th lobe count among its  $q$  radial modes.

The pure tones generated by rotor blade-stator vane interaction, are a very restricted set of "allowed" modes. As first shown by Tyler and Sofrin (Reference 2), a mode is "allowed" only if  $m = nB - kV$ , where  $n$  is the harmonic number of blade passage frequency,  $k$  is any positive or negative integer or zero,  $B$  is the rotor blade count, and  $V$  is the stator vane count. Negative  $m$  simply means rotation opposite to shaft rotation. It also is shown that for blade-tip circumferential velocities up to sonic, propagation can occur only if  $nB > m$ . Thus, so long as  $V > 2B$ , the fundamental blade passage tone due to blade-vane interaction, is suppressed. Any such tone appreciably present must then be due to an aerodynamic process such as blade chopping of inlet distortion. This acts analogously to a single inlet guide vane  $V = 1$ , making all propagating modes possible. This was the modal distribution previously ascribed to aerodynamic noise.

Aerodynamic noise was assigned the classic equipartition of energy among the  $\bar{m}$  propagating lobe counts. This, in turn, was subdivided equally among the  $\bar{q}$  radial modes for each value of  $m$ , where the bars signify maximum possible values of the indices  $m$  or  $q$ .

Pure tone fundamentals of the blade passage were formally inserted into the wave equation, even though the presence of no propagating allowed modes was assured by the criteria previously mentioned. It was assumed that the fundamental tones were ascribed to inlet distortion. They were, therefore, represented by the same modal energy dis-

tribution used for the broadband noise. The second harmonic, a propagating pure tone, was considered. Still higher harmonics of blade passage frequency were disregarded for two reasons. First, the harmonics are above the audible range and, hence, no attenuation requirements were identified. Secondly, except for certain rare occurrences that are not pertinent to this design, the harmonics are in the high frequency range that attenuate rapidly.

In the absence of detailed boundary layer definition, plug flow (zero boundary layer thickness) was initially assumed for all four conditions. It is well known that shear flow which has a negligible effect on discharge duct attenuation, and what effect is present is constructive as sheared flow tends to refract sound outward into the liner (Reference 3).

In addition, marked differences in optimum impedance and moderate differences in attenuation predictions can occur for individual modes at fairly high Mach numbers (Reference 4). However, the variations in optimum impedance and attenuation predictions for the ensemble of modes that constitute an aerodynamic noise are much less pronounced. Furthermore, the effects of shear are opposite to the effects of redistributing the modal energy due to roll-off at the highest order modes. It is quite likely that such a roll-off is actually present. It is, therefore, concluded that for the aerodynamic type of modal distribution, which in the case of the subject engine includes the blade-passage fundamental tone, the effects of shear are less than the possible effects of the uncertainty of modal energy distribution (Reference 5). For these reasons, the plug-flow assumption is considered justified.

The duct-analysis computer program used by Lockheed (Reference 1) solves the chosen form of the convected wave equation by an iterative method which calculates insertion loss (ratio of sound power in a treated duct to that in an untreated duct in dB) for any given round-duct geometry, flow, and in-place wall impedance for each propagating mode. These individual mode solutions are assembled into an attenuation prediction for any chosen modal energy distribution.

Rarely, however, will material that is available to the designer exhibit the properties necessary to achieve the optimum design. Rather, it becomes the case of selecting the material that comes closest to the requirement. In the QCGAT design, two materials exhibit properties closest to the desired parameters. The first is a fibermetal, a mesh

of stainless steel filaments rolled and compressed into a porous sheet and laid over a perforated sheet that offers the advantage of approaching the optimum design where the change in attenuation due to change in flow resistance is less critical. Figure 36 depicts the flow resistance of this material. The second material, a plain perforated sheet having a small percentage of open area, offers the advantage of proven design and simplicity of fabrication. The figure also shows the flow resistance of this material.

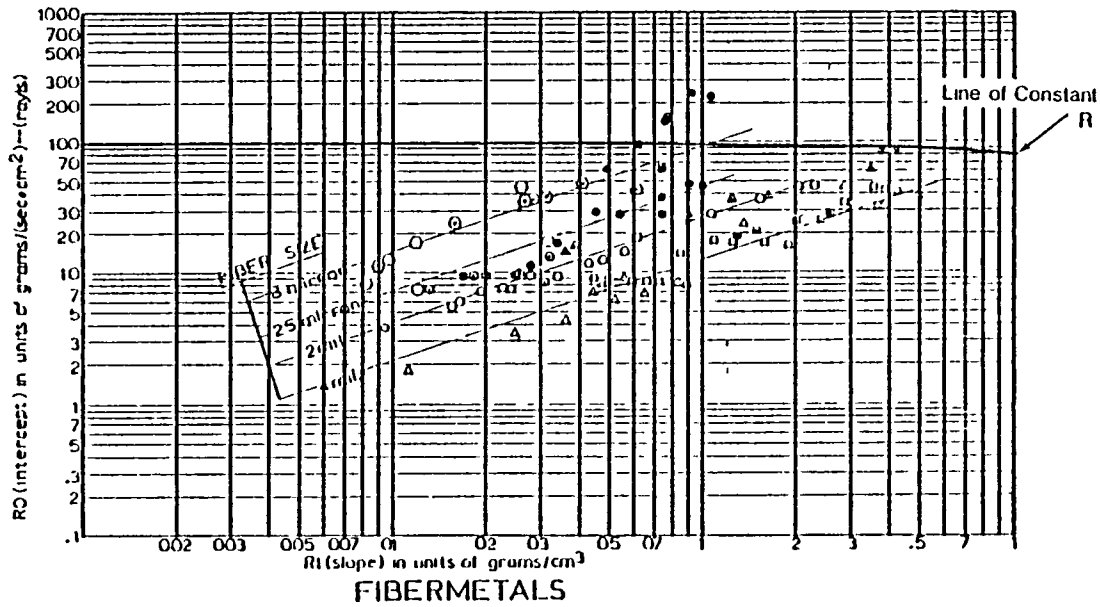
For reasons of flightworthiness, the plain perforated-face-sheet was selected for the inlet and discharge duct sound-treatment panels. Figure 36 shows that for the relatively low flows and sound pressure levels expected in the inlet duct, a low-percentage open-area perforate will be required. A 5 percent open-area perforate is considered the lower practical limit for a perforate-open area. Below this value, the rapidly increasing inertance renders the tuning both narrow and capricious, manufacturing tolerance then become critical. With small percentage open-area perforates, hole size becomes a limiting factor. Limitations in the perforator's art preclude holes whose diameter is less than metal thickness. The perforate used is manufactured from a 0.636 mm (0.025 in.) thick 2024 aluminum panel with 0.838 mm (0.033 in.) diametric holes on 2.85 mm (0.112 in.) centers. This design yields a 6.8 percent preassembled open area with 12 holes per square centimeter (79 holes per square inch).

The core will be fabricated of Hexcel 5056 F-40, with a foil thickness of 0.066 mm (0.0026 in.). Blockage of the holes by the foil is expected to reduce the open area to 5 percent. The Hexcel which has 0.95 cells per square centimeter (6.11 cells per square inch) yields approximately 12 holes per cell.

For the QCGAT design, it was possible to accomplish the dual tuning at 2160 and 3971 Hz with a liner depth of less than 25.4 mm (1 in.). The optimum values of reactance are  $0.6\rho c$  for approach and  $0.7\rho c$  for takeoff. The inertance of the selected inlet and discharge facing sheet is known to be less than  $4.5 \times 10^{-5}$  seconds. Thus, values of  $-0.8\rho c$  for approach and  $0.1\rho c$  for takeoff can be achieved with an airspace of 16 mm (0.63 in.). These values are sufficiently near optimum.

Using these design parameters, the attenuation graphs are reentered to predict the insertion loss of the panels for various treatment lengths. A treatment length of 1.25 times the average inlet duct radius and 1.5 times the average discharge duct radius were selected to yield an insertion loss within 2 dB of the attenuation goals. The predicted fan inlet and discharge duct insertion losses are shown in Figure 35.

FLOW RESISTANCE  $R = R_0 + R_I(u)$



THE RELATION BETWEEN  $R_0$  AND  $R_I$  FOR FIBERMETALS

Ref Lockheed Report #LR 28254

FLOW RESISTANCE  $R = R_0 + R_I(u)$

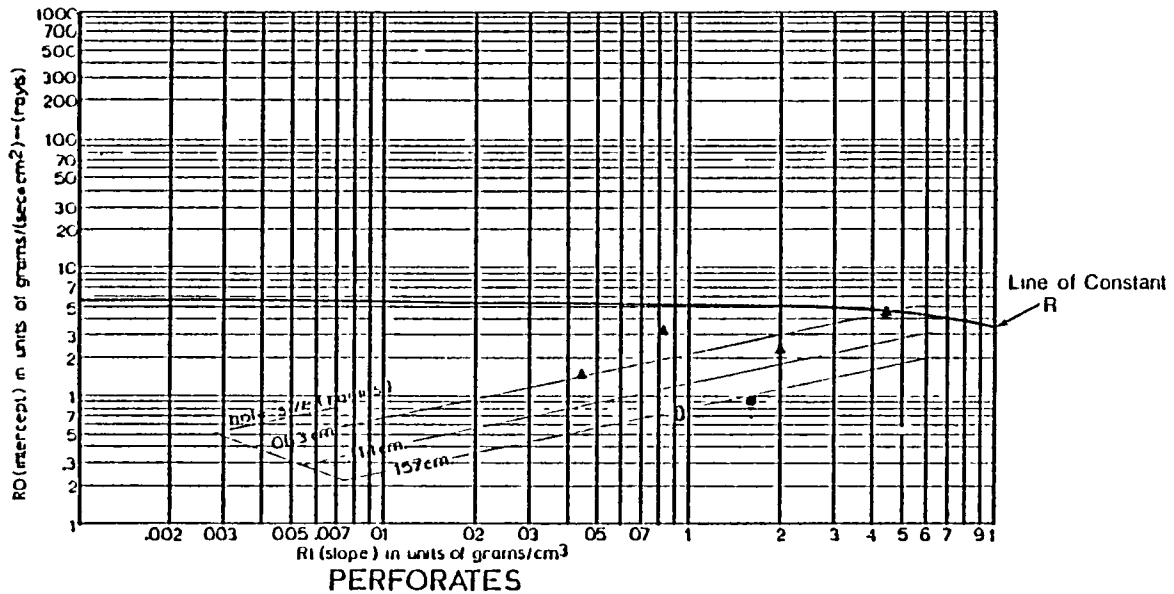


Figure 36. Sample From Lockheed's Materials Handbook for Metal.

### 3.3.3 Structural Design

Mechanical design of the flight nacelle incorporates current state-of-the-art lightweight skin-on-frame structure and acoustic suppression panels that are integrated into the air intake duct and fan exit duct.

The test nacelle retains flow channel contours identical to those of the flight nacelle. The structural design is based on the requirement to readily change duct flow panels from acoustic suppression panels to hardwall and air intake lips from conventional flight lips to bellmouth and approach simulator. This requirement resulted in departures in structural design from those used in the flight nacelle design.

Except for the removable inlet lips which are of fiberglass construction, the nacelle's basic structure consists of metal skin and frame.

The fan's main frame, which contains four main mounting pads, serves as the foundation for the nacelle structure of both the flight and test configurations.

The mixer nozzle, bolted to the turbine exit casing, is identical for both flight and test configurations; however, the sheet metal of the test nozzle is slightly thicker to allow for local material thinning that is anticipated for one of a kind stretch-form manufacturing techniques.

Design details of the flight and test nacelles are described below.

#### 3.3.3.1 Flight Nacelle

The design profile of the flight nacelle shown in Figure 34 illustrates the basic internal and external structure. Figure 37 is a sectional view of the main engine mounting station.

Basic components of the nacelle shown in Figure 38 are as follows:

- o The nose cowl contains the air intake and nacelle forward cowl and is bolted to the engine inlet flange on the fan front frame.
- o The cowl tail section contains the fan duct outer wall and the rear contour of the nacelle and is bolted to the inner aft flange of the fan main frame.

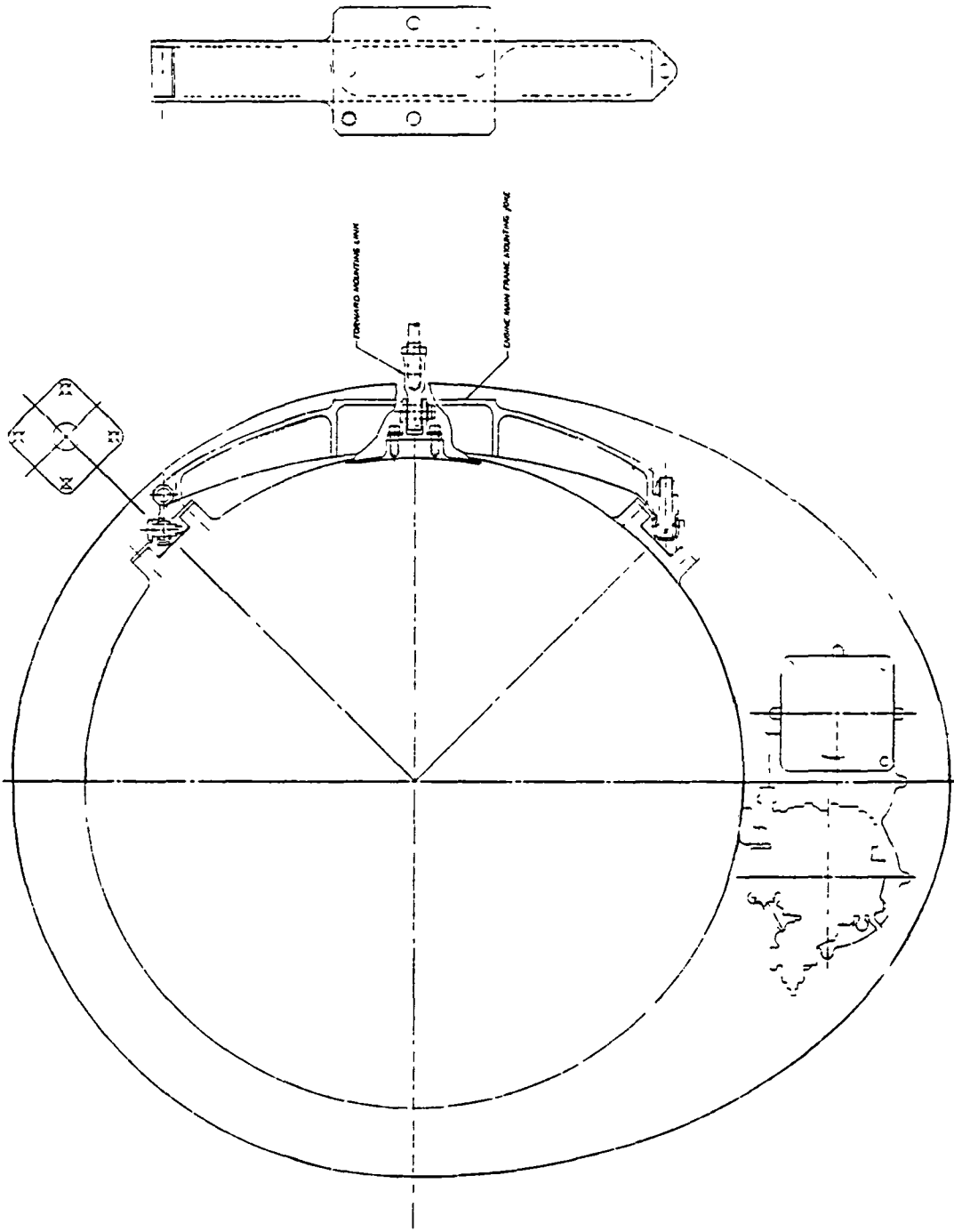


Figure 37. Nacelle Sectional View.

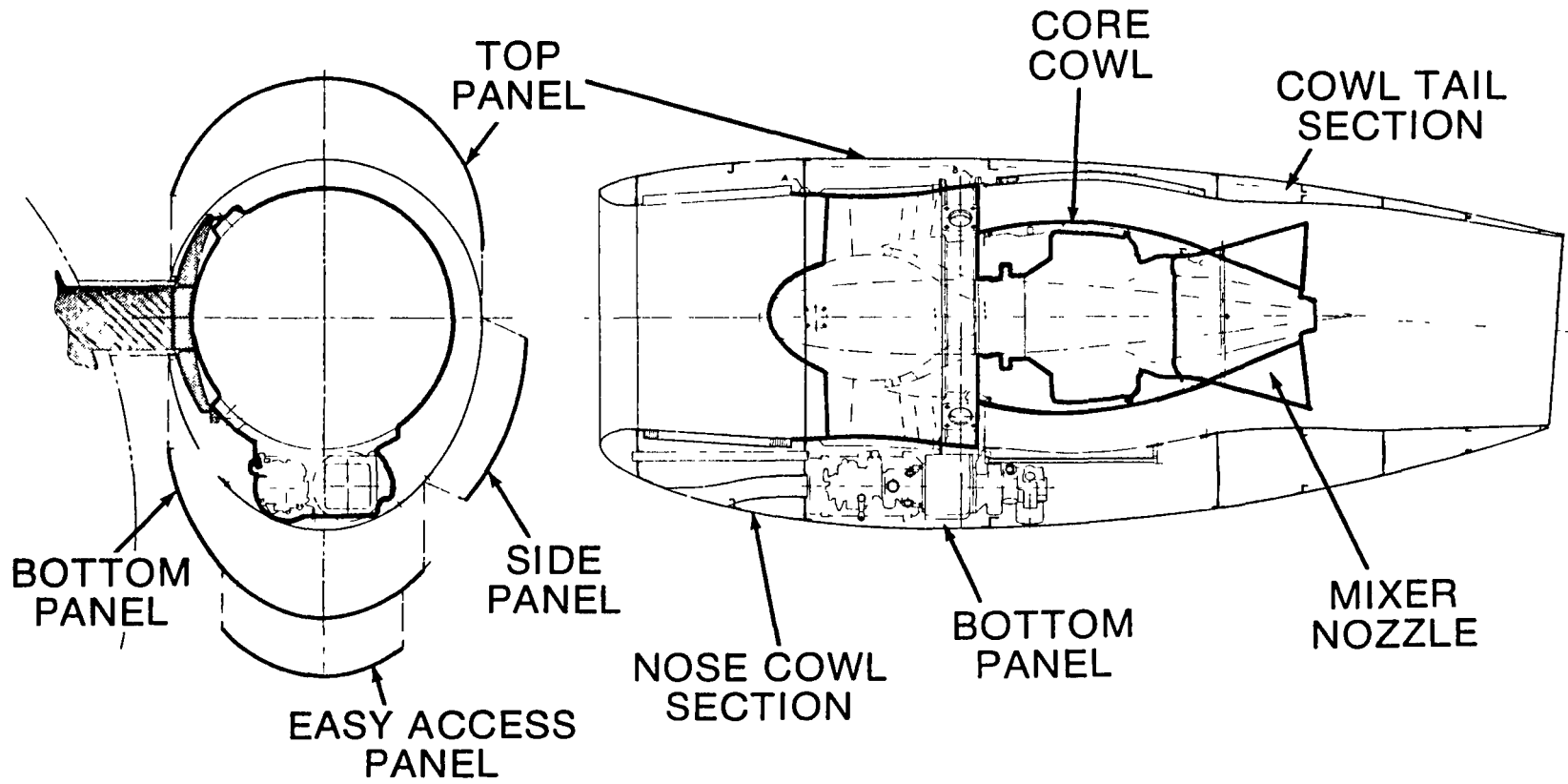


Figure 38. QCGAT Nacelle Components.



- o The core cowl forms the inner fan flowpath and provides a firewall over the core engine combustion chamber and fuel nozzles. The cowl which is cantilevered from the aft flange of the fan main frame, also contains the walls of a service strut across the fan flow channel.
- o The mixer nozzle forms the core exit nozzle and is cantilevered from the rear flange of the turbine casing.
- o The removable access panels are fastened to the fixed structure of the nacelle as shown in Figure 38.

The engine is installed in the airframe to a main engine mounting yoke which picks up two of the engine's main mounting pads on the fan's main frame (Figure 37 ). A front mounting strut attached to the containment ring assembly offers only lateral support. The structure of the nacelle front cowl and inlet consists basically of aluminum skin frame with an integral honeycomb noise-suppression panel that forms the inlet duct wall. The inlet lip which is de-iced by hot air from the engine compressor has sufficient thickness to resist hail damage and erosion. The rear bulkhead forward of the accessories serves as a firewall and support frame. The intermediate bulkhead is used only for external skin support.

The forward portion of the tail cowl is an integrated honeycomb noise-suppression panel that forms the outer wall of the fan flow channel. The cowl bolted to the fan main frame flange supports the tail section that comprises the outer wall of the fan exit duct and the external boat tail cowl.

The cowl is split into two halves that are fastened together by bolts at the top and clamped at the access strut fairing at the bottom. All external access panels are of formed and welded aluminum sheet and equipped with quick-release fasteners for ease of removal.

The weight of the nacelle, excluding engine mounts, is 106.7 pounds. A breakdown of the weight, material selection, and nacelle center-of-gravity are shown in Figure 39.

### 3.3.3.1.1 Fire Prevention and Compartment Ventilation

The section of the core engine between the rear flange of the engine main frame and the mixer nozzle attachment flange, as shown in Figure 40 is the prime fire-protected area because it contains a hot

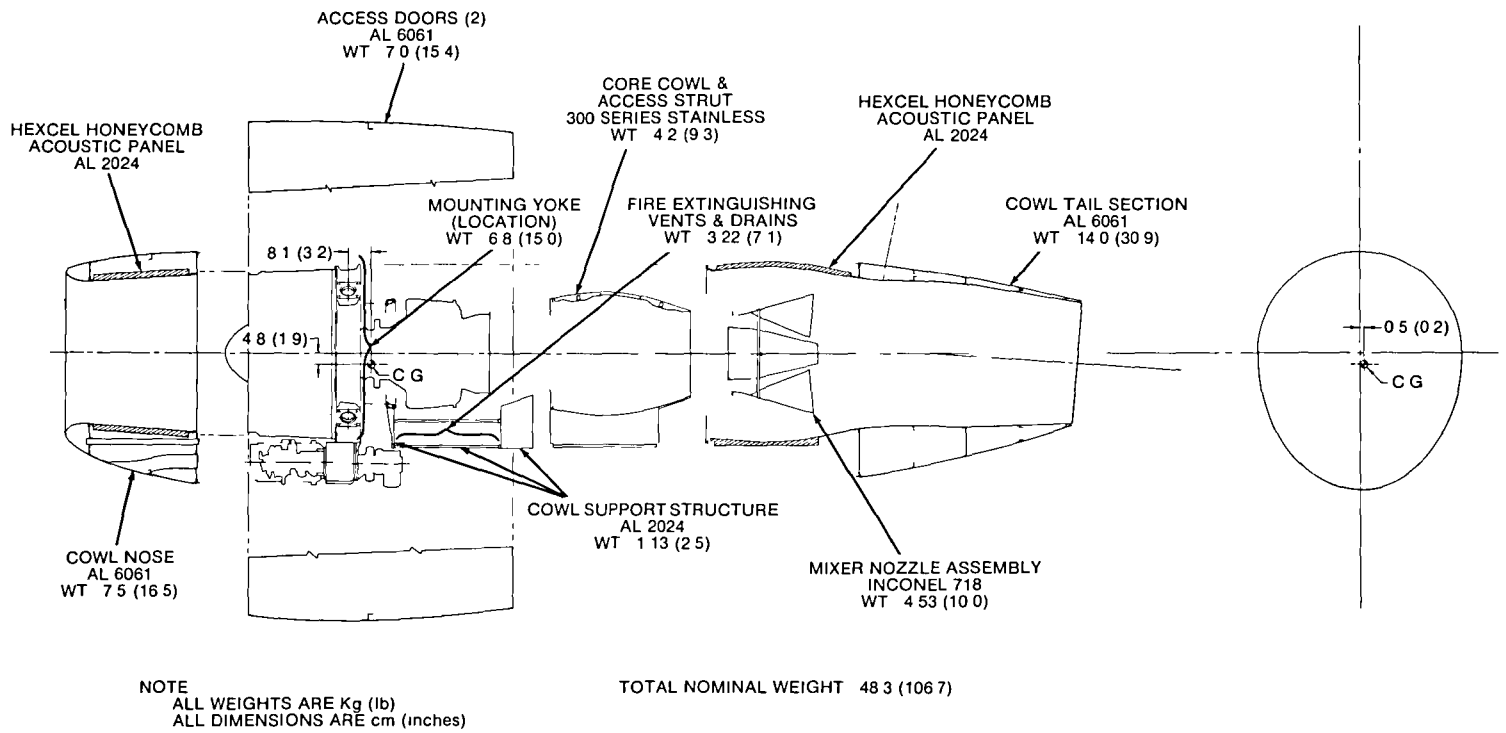


Figure 39. Nacelle Materials and Weights.

Ventilation Rate — 100 Changes/Minute  
Surface Velocities > 1ft/sec

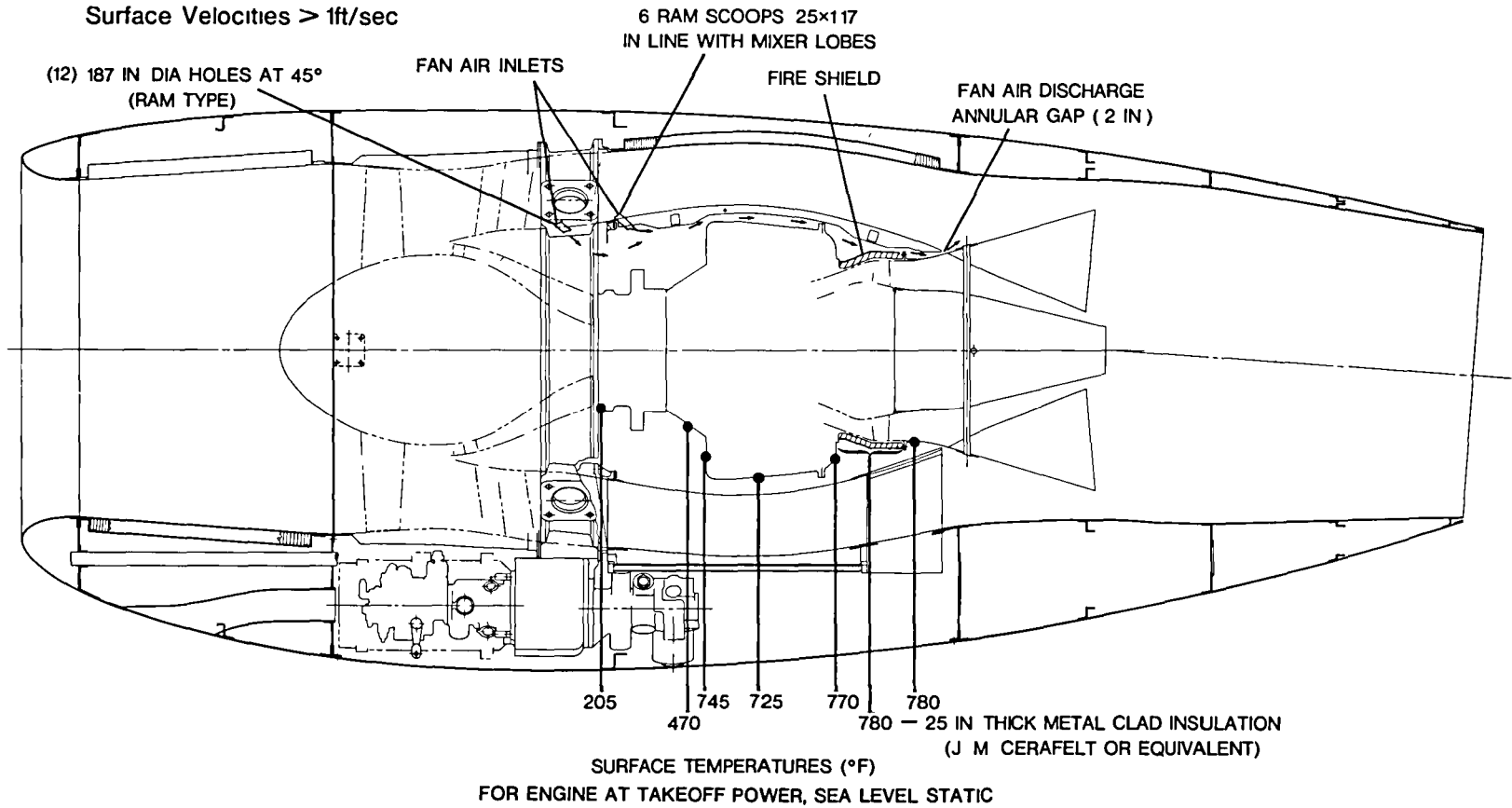


Figure 40. Nacelle Fire Prevention/Compartment Ventilation.

engine casing and fuel lines. For the critical hot-day static operation at takeoff power, surface temperatures over the combustion chamber casing are below 780°F, and surface temperatures over the turbine casing and rear portion of the mixer nozzle are kept below 780°F by thick metal-clad insulation. The steel-core cowl forms a fire-resistant wall around this portion of the core engine casing. Ventilative airflow for the fan is provided into the core zone by means of 6 scoop inlets located at the forward part of the core cowl and through 3/16-inch diameter holes through the main frame struts. The airflow reenters the fan air stream through the annulus formed between the rear edge of the core cowl and the outer surface of the mixer nozzle. The ventilative airflow circulates circumferentially through the core cowl compartment at a rate of 100 air changes per minute; the lowest surface velocity in the zone is greater than 1 foot per second. These criteria are known to be safe in the prevention of fire. This ventilative airflow reduces the ambient temperature in the core zone and represses ignition of leaking flammables upon hot surfaces.

Considering the unlikely occurrence of fire in the core zone, a fire detecting and an extinguishing system with airframe-mounted fire-suppression fluid would be provided.

### 3.3.3.2 Test Nacelle

The test nacelle configuration is shown in Figures 41 and 42. All internal ducting contours from the air inlet to the final exit plane of the nozzle are identical to those of the flight nacelle.

Except for two short front and rear boat-tail cowl portions, external skins are excluded so as to reduce costs and improve accessibility without affecting the attainment of QCGAT goals.

The design permits adaptation to the test nacelle of three distinctly different air inlet configurations -- one bellmouth, one regular inlet designed for minimum loss at cruise condition, and one inlet designed to statically simulate fan inflow conditions corresponding to an inflight approach condition (Figures 43 and 44). The acoustic suppression panels in the air intake and fan ducts are of the same construction as those used in the flight nacelle but are designed to facilitate replacement with hardwall panels.

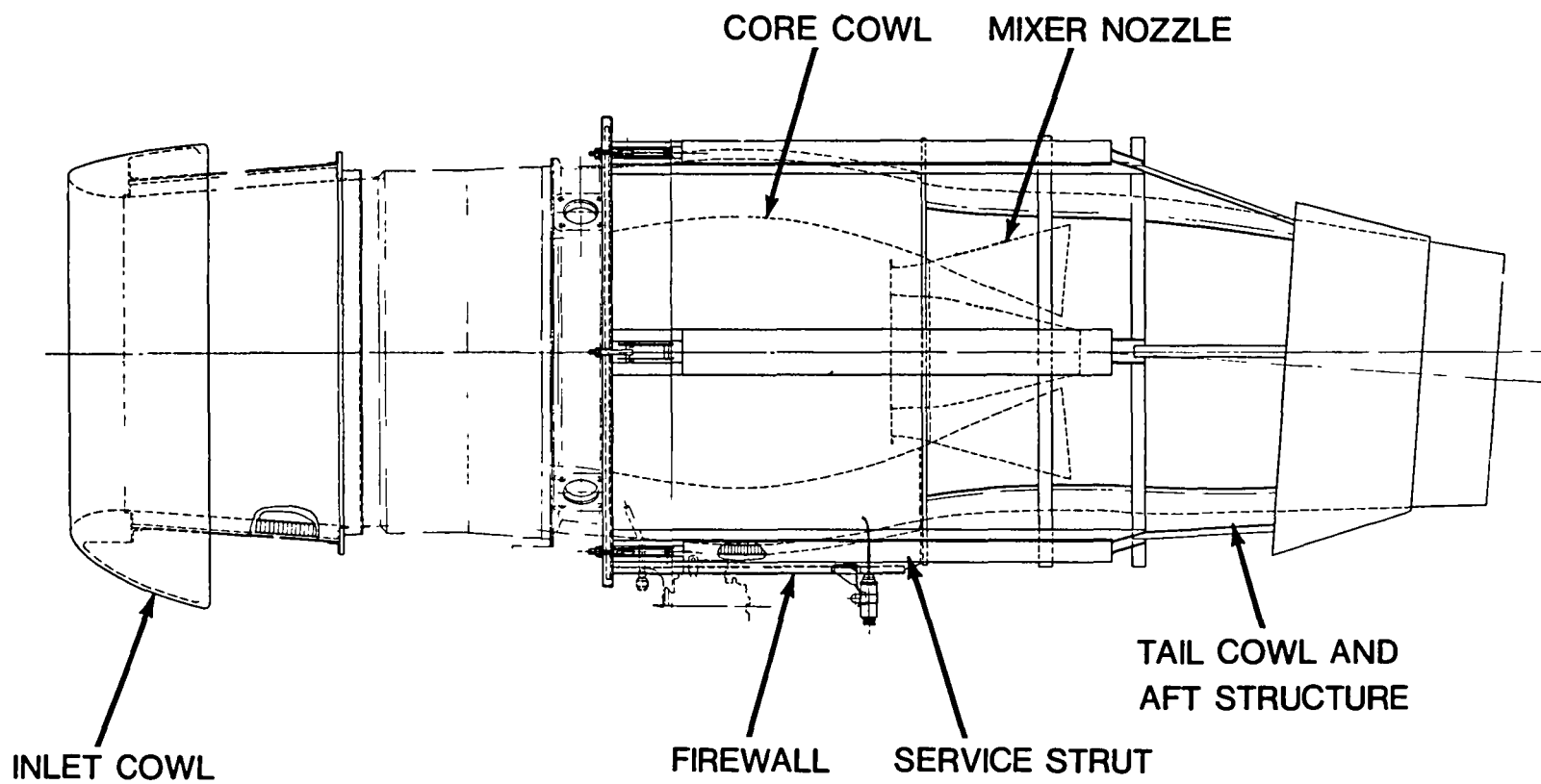


Figure 41. Test Nacelle Assembly.

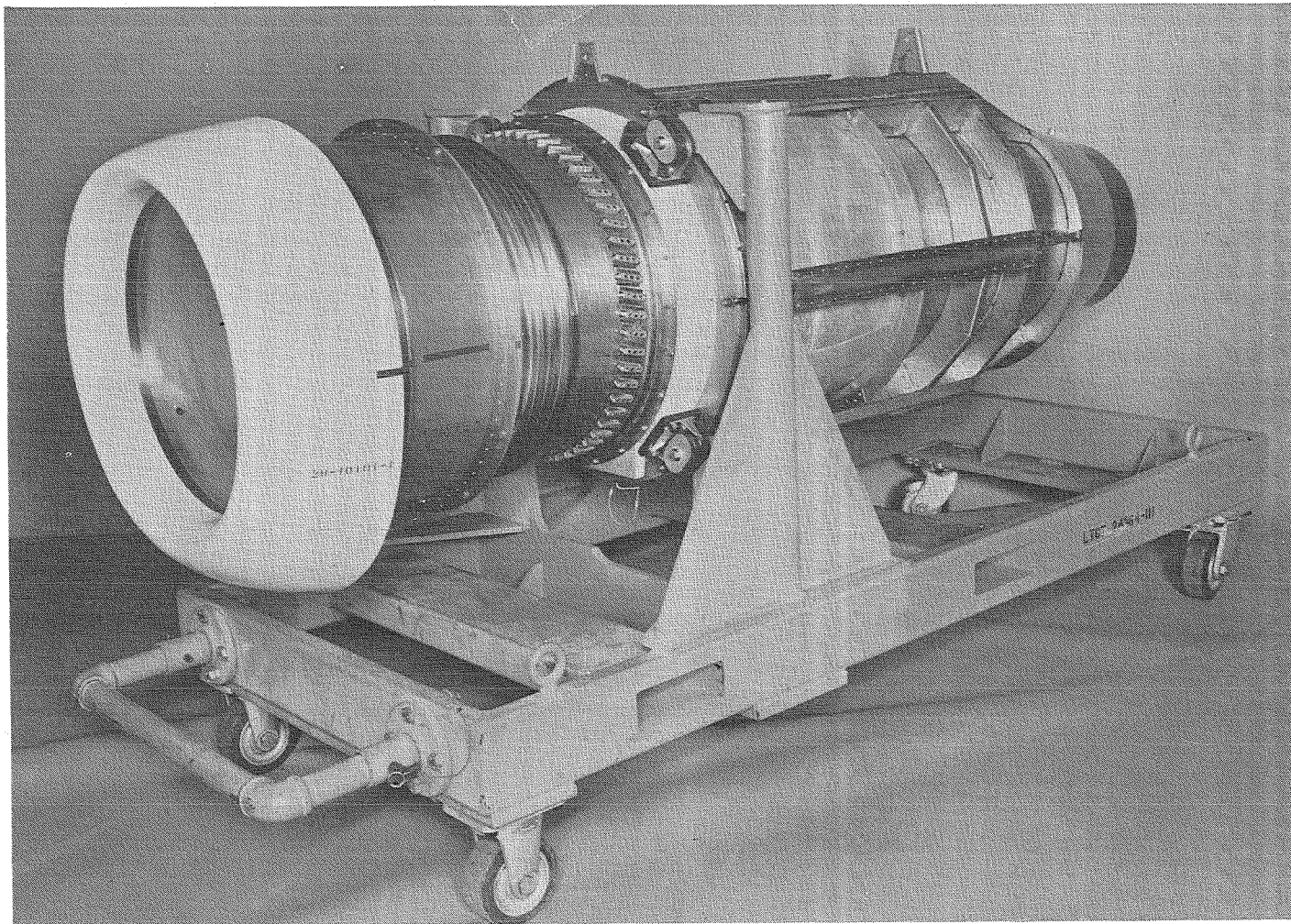


Figure 42. QCGAT Flight Nacelle Simulation.

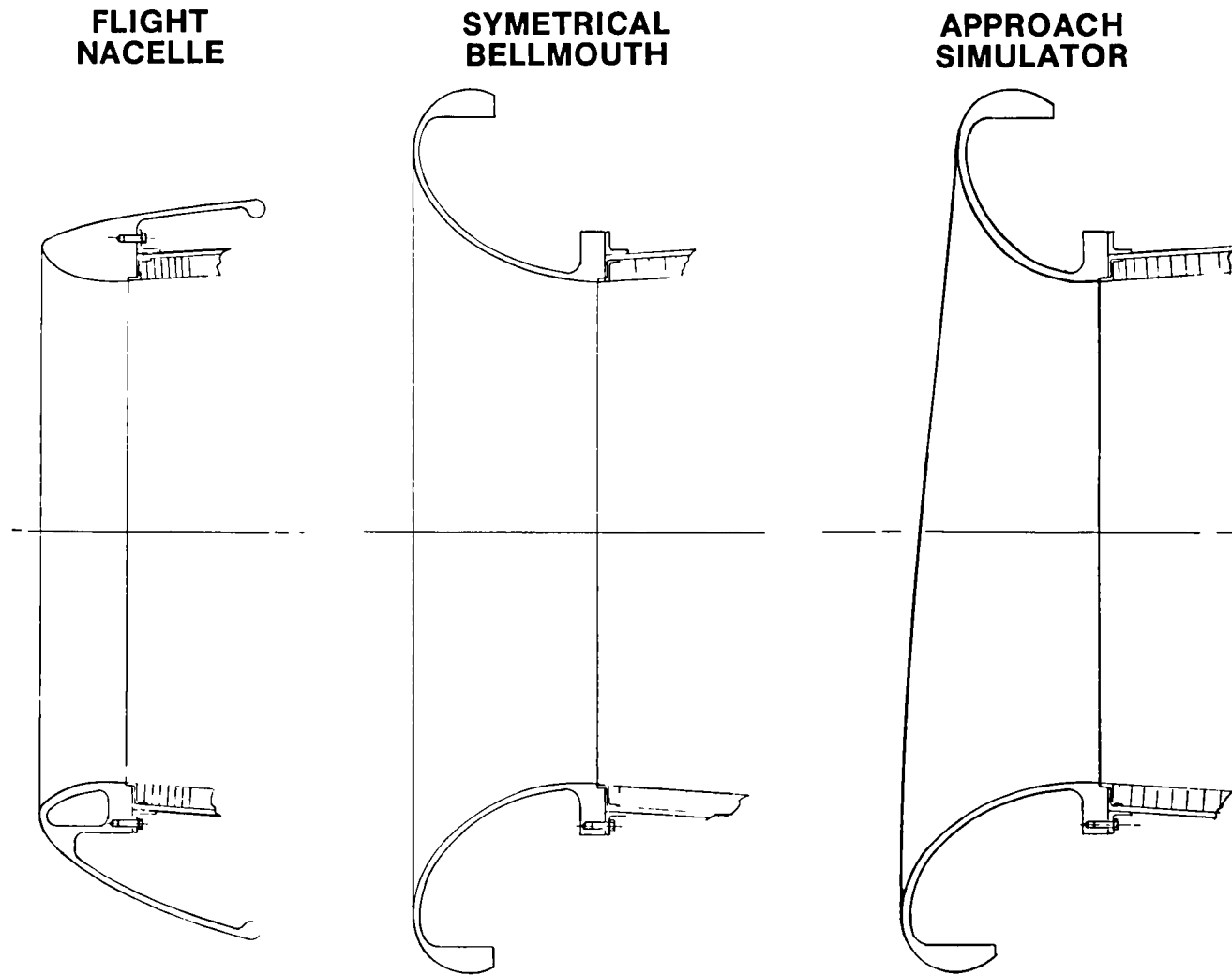
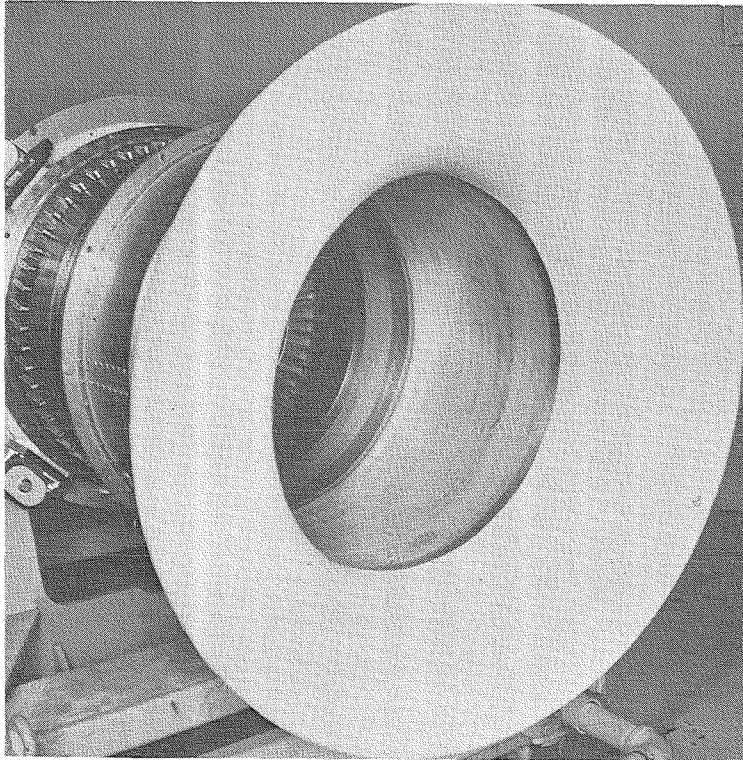


Figure 43. Replaceable Inlet Lips.

## BELLMOUTH INLET



## FLIGHT NACELLE INLET

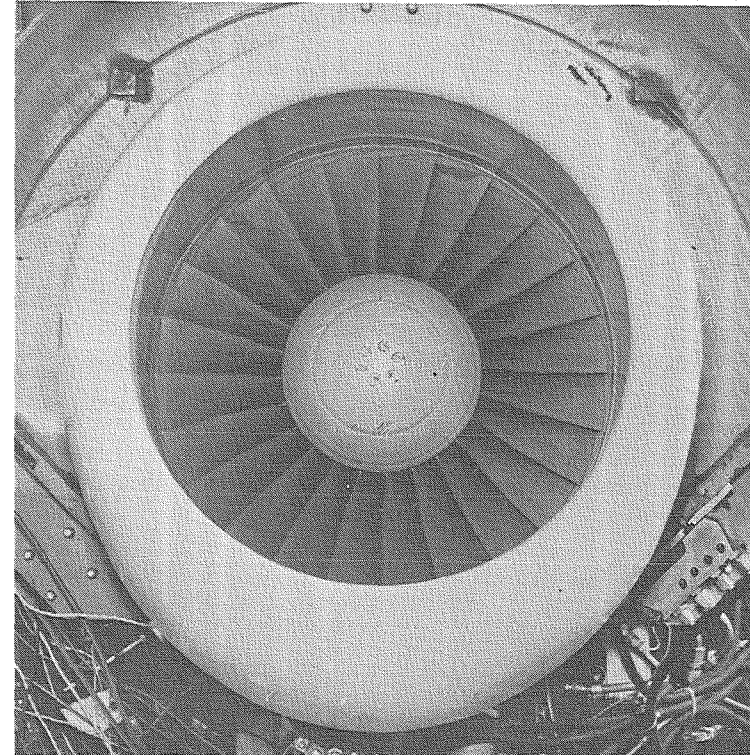


Figure 44. Bellmouth and Flight Nacelle Inlets.



Since ease of replacement of fan duct panels precludes integrating the panels into the rear cowl support structure, the rear duct section is supported by a frame comprised of barrel ringframes and longerons. This structure is cantilevered from the rear flange of the fan main frame.

The core cowl and mixer nozzle and their attachment are similar to those for the flight nacelle design.

The front cowl lips and air inlet ducting are supported by a barrel structure that is cantilevered from the engine inlet flange. The acoustic suppression panel in the inlet can be removed and replaced with a hardwall panel, and the inlet lips can be replaced without disconnecting the barrel support structure. Other details are discussed in Paragraph 5.3.3.

#### 3.4. MIXER NOZZLE DESIGN

The Lycoming QCGAT exhaust nozzle system shown in Figure 45 comprises a fan duct, a multilobe mixer nozzle, and a mixing chamber/final nozzle. This type of exhaust mixing system was chosen because of its propulsive efficiency and reduced noise-benefits. Multilobe mixer nozzles such as that shown in Figure 45 have been reported (Reference 8) to yield a considerable amount of noise suppression when compared with the more conventional split-flow nozzles. The suppression is believed to result from reduced jet turbulence levels and a reduction in the mean-relative jet-velocity gradients (Reference 2).

A parametric study was evaluated to optimize the mixer nozzle with considerations for reduced noise emissions and improved cruise fuel **economy**. These details are documented in Reference 8. The resulting design is shown in Figures 46 and 47. The mixer nozzle installation on the engine is shown in Figure 48.

Shaker test performed on the nozzle and turbofan engine strain gage testing indicated satisfactory dynamic characteristics.

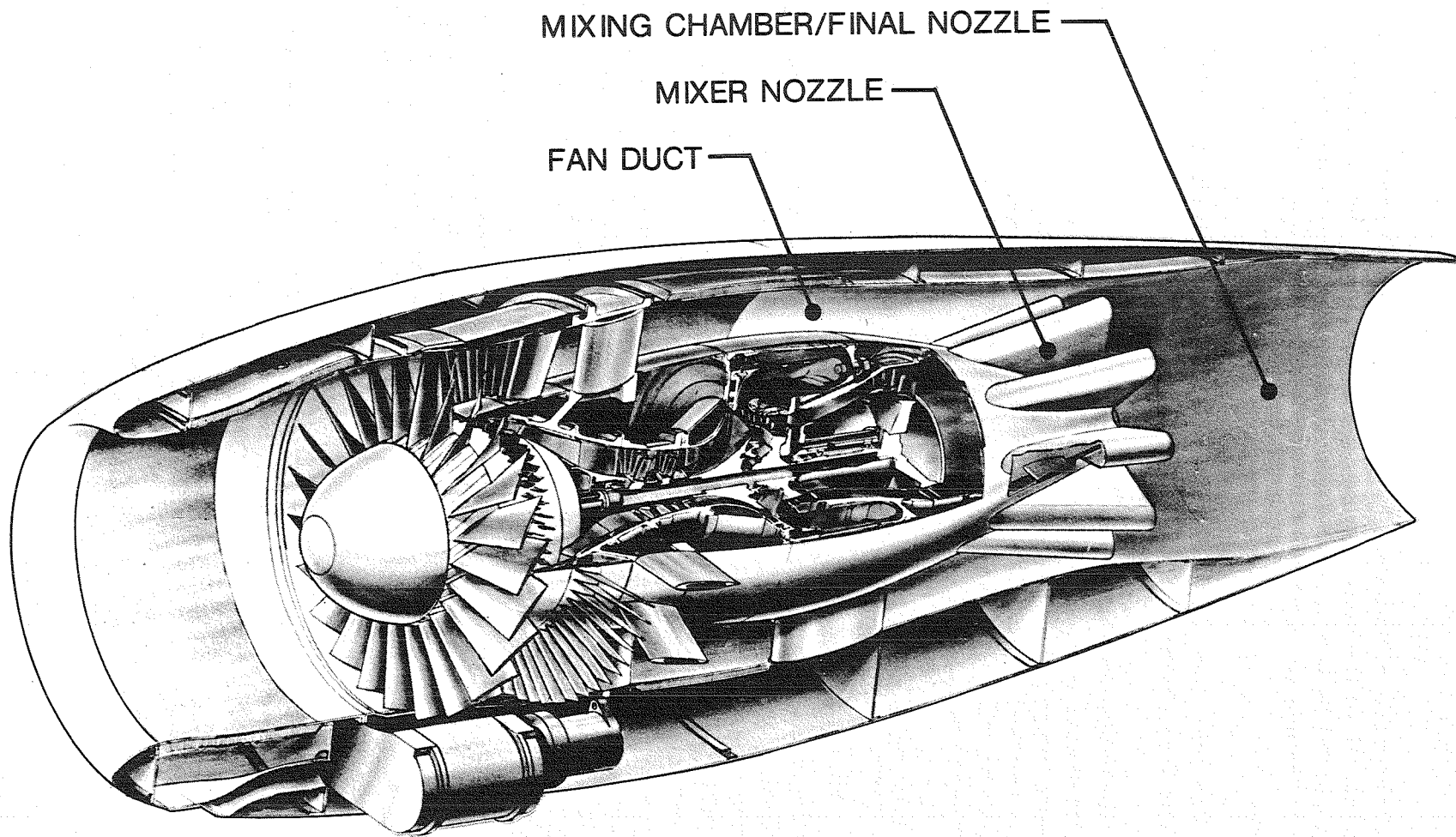


Figure 45. QCGAT Exhaust Nozzle System.

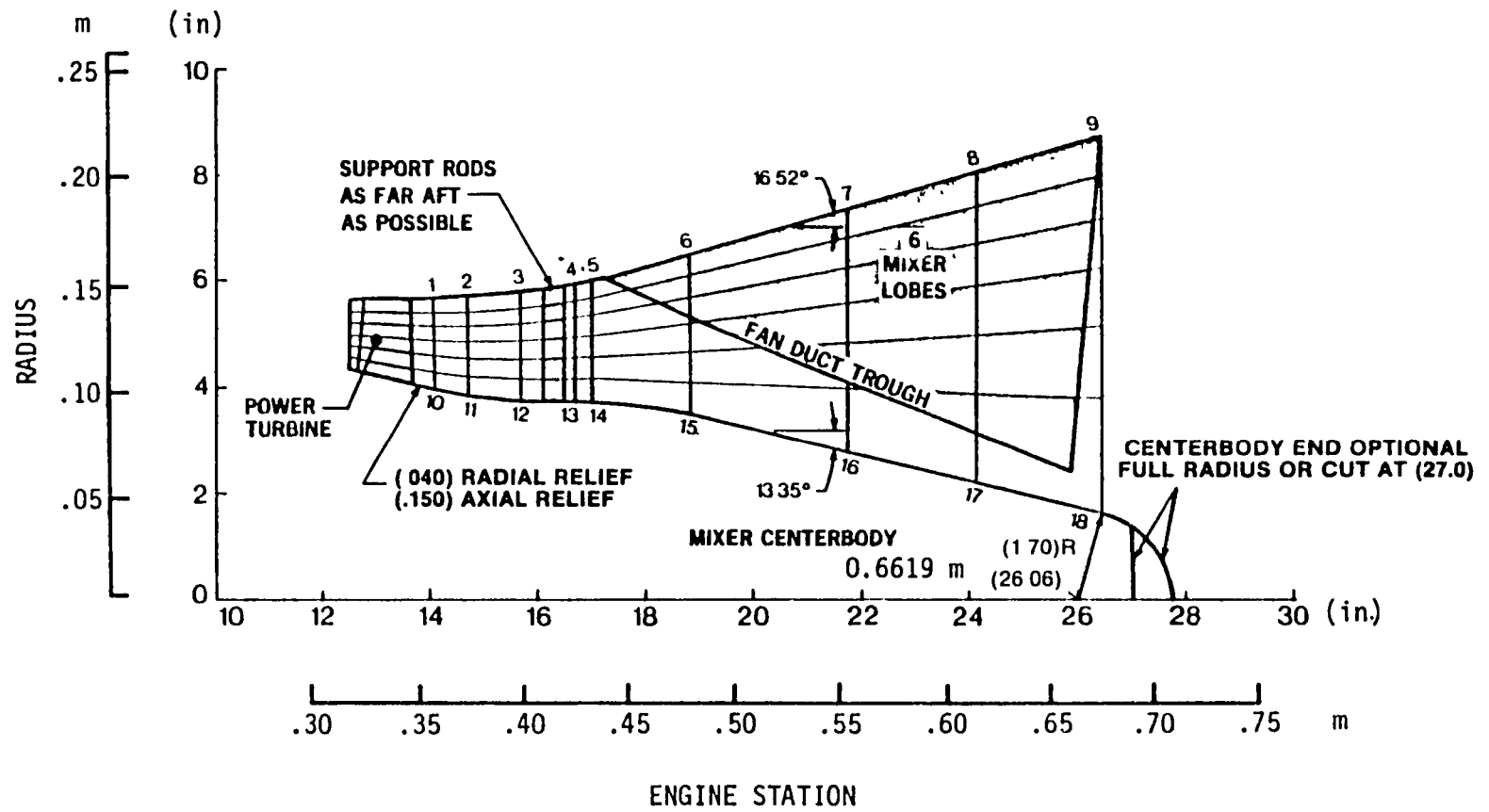


Figure 46. Core Engine Mixer Nozzle Geometric Definition.

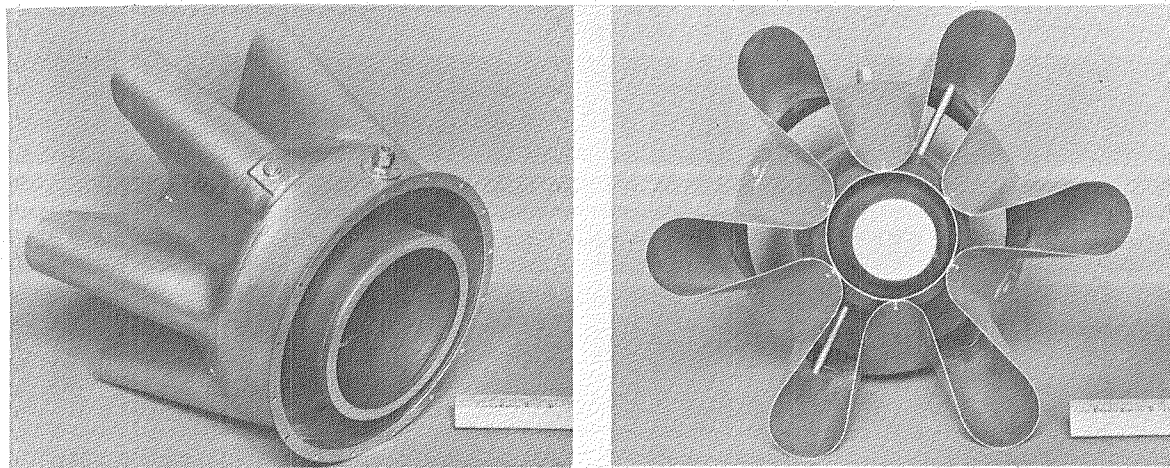
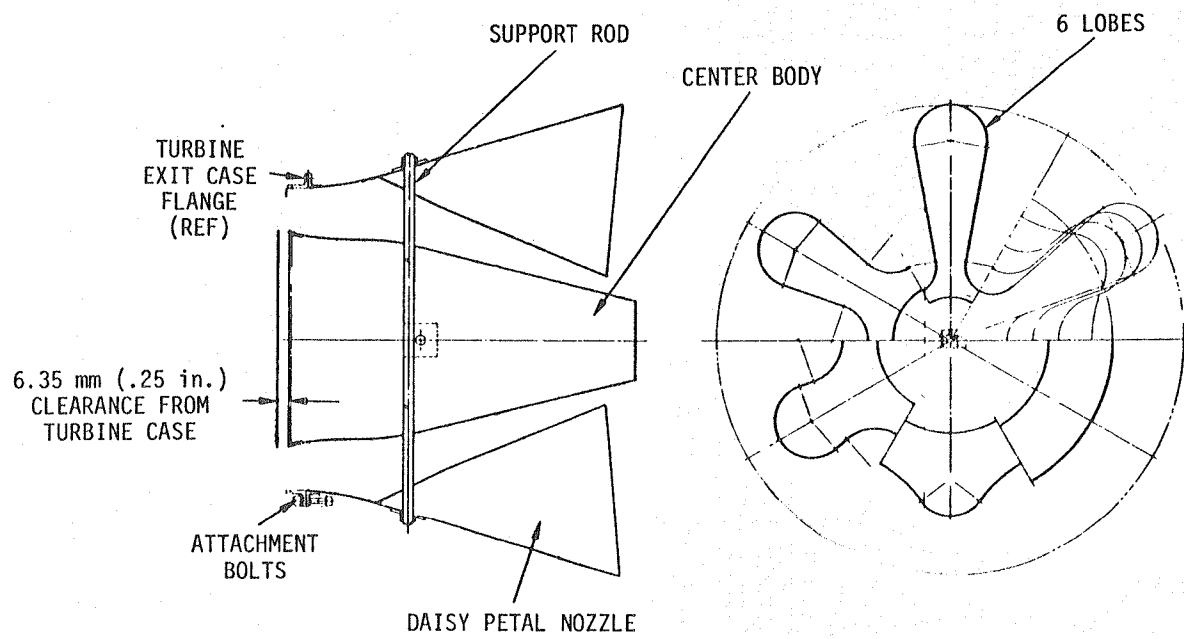


Figure 47. Lycoming QCGAT Mixer Nozzle Design.

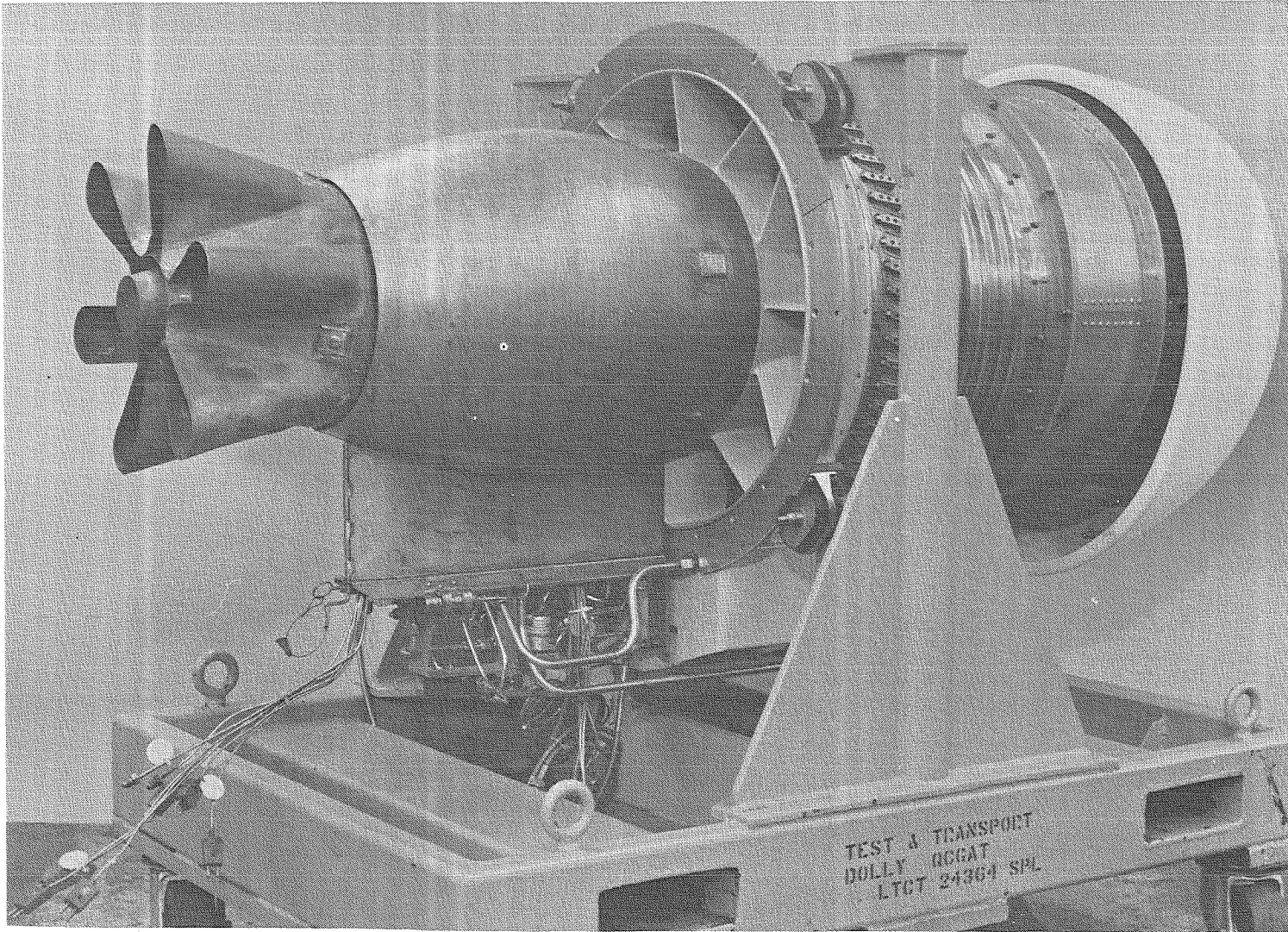


Figure 48. Mixer Nozzle Installation.

## 4.0 SUBSYSTEM TEST RESULTS

As part of the NASA/QCGAT contract, component test rigs were used in the design development of the fan and combustor modules. Additionally, laboratory tests using laser-holography techniques were used to evaluate the frequency response and mode shapes encountered on the fan blade and of the reduction gear assembly.

### 4.1 FAN BLADE ANALYSIS

Aerodynamic design of the QCGAT fan blade is the same as that used in the successful ALF-502 turbofan program. To determine and evaluate blade natural frequencies and mode shapes, a holographic interferometry analysis was conducted.

#### 4.1.1 Test Program

Figure 49 shows the general test setup used. Engine level hardware was used as test items.

A special fixture was made to allow clamping of a finished machined fan blade at the dovetail root and mounting the fixture to the piezoelectric vibration exciter. The design of this fixture and the blade attached to the fixture are depicted in Figure 59. A real time hologram was made of the blade at rest and at predominant modes up to 5000 Hz. All mode shapes were identified, photographed, and documented.

#### 4.1.2 Fan Blade Test Results

The natural frequencies of the fan blade as determined experimentally, along with their associated mode shapes, are identified in Figures 51 and 52. A diagram is presented in Figure 53. Measured frequencies are identified at the ordinate. Frequency characteristics for other than "Zero" rpm condition are based on analytical predictions. The experimental analysis verified analytical prediction of second order of the first bending mode as a potential blade excitation.

### 4.2 LOW-PRESSURE TURBINE BLADE ANALYSIS

A similar procedure was used for the QCGAT power turbine blade. Since the blade and disc are integral, the test required cutting a blade with the attached disc section from a final tip-ground turbine wheel

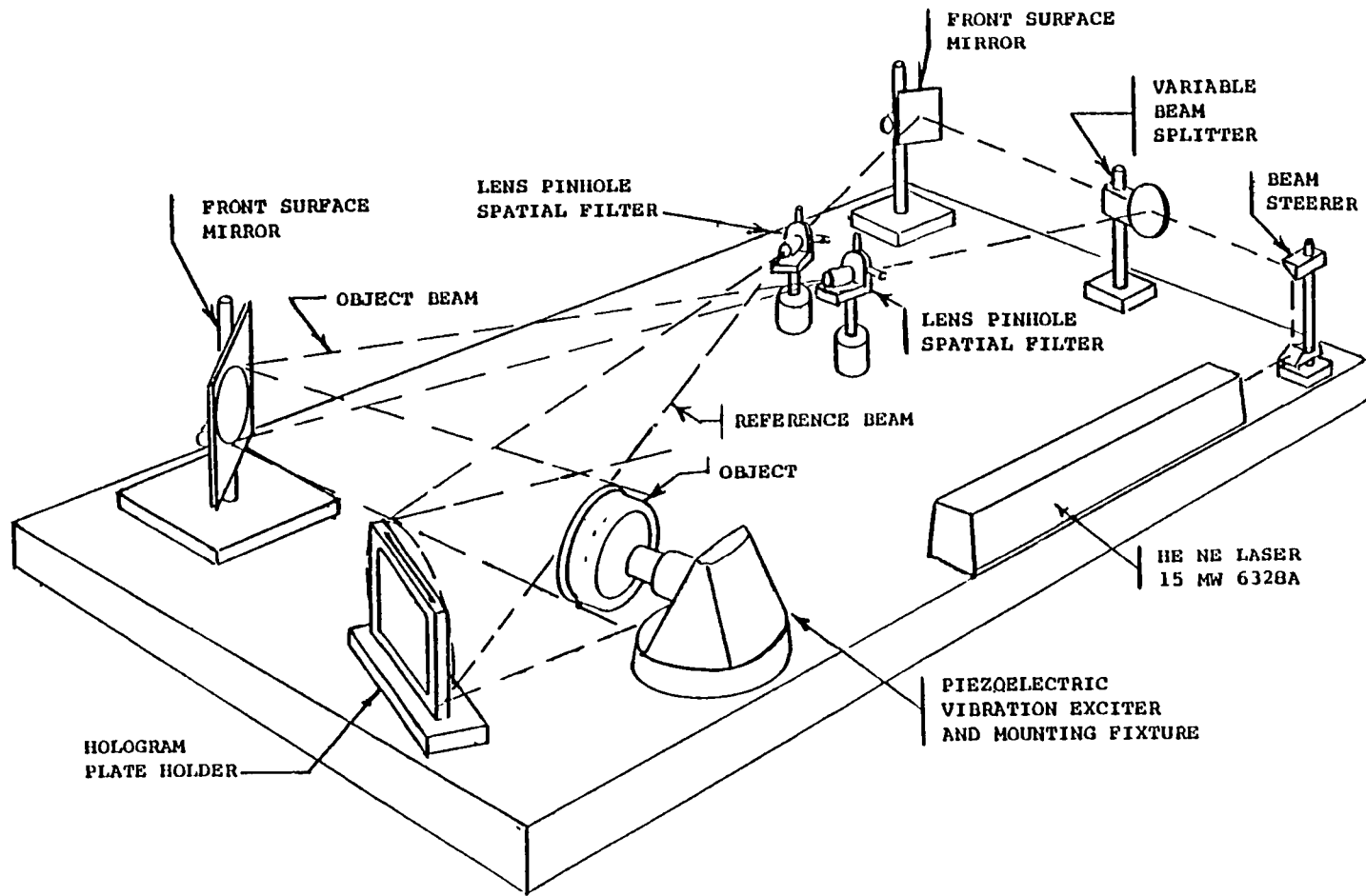


Figure 49. General Test Setup Holographic Analysis.

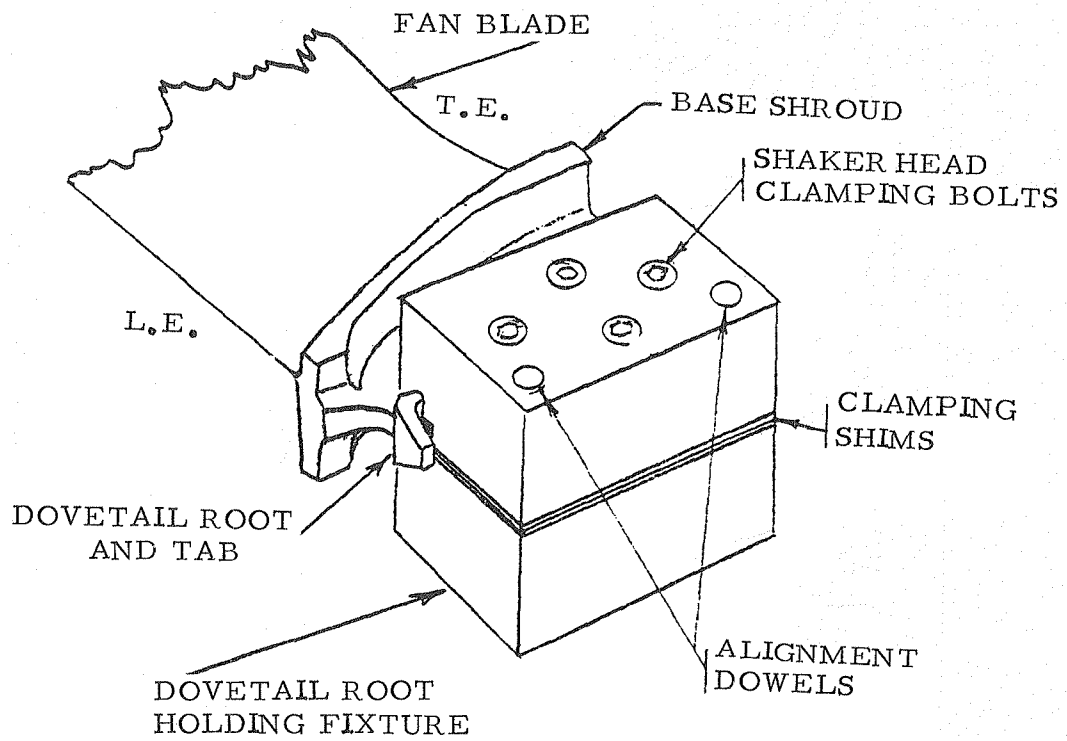
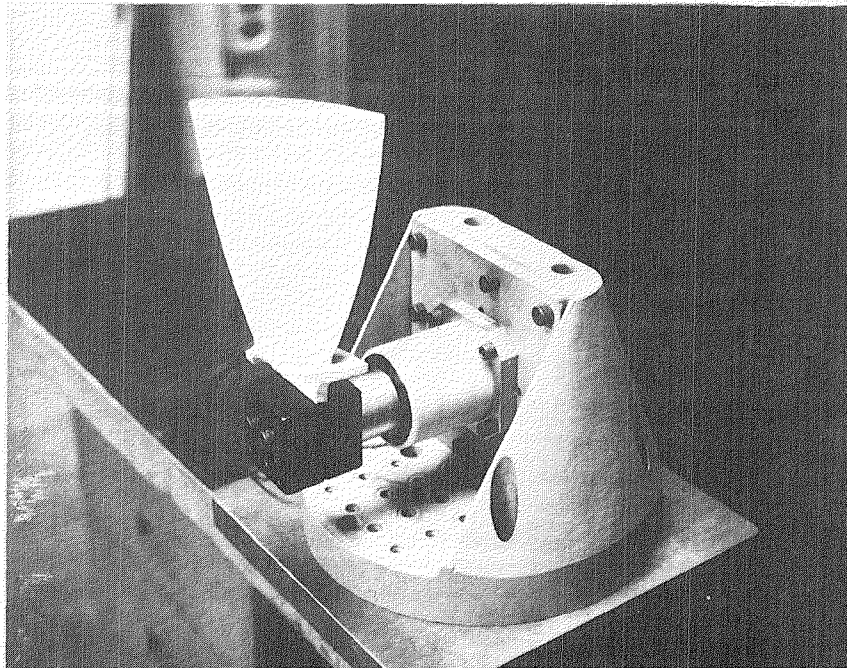
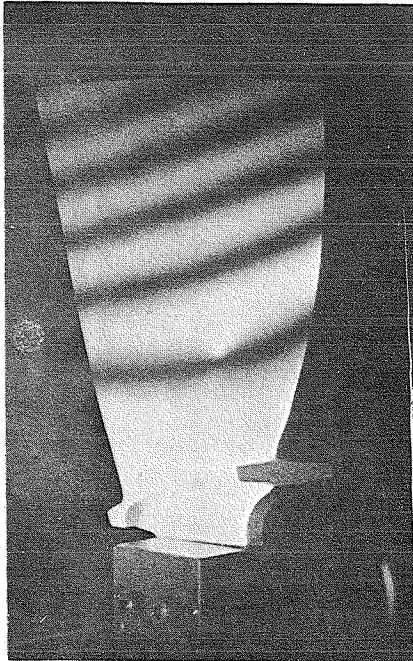
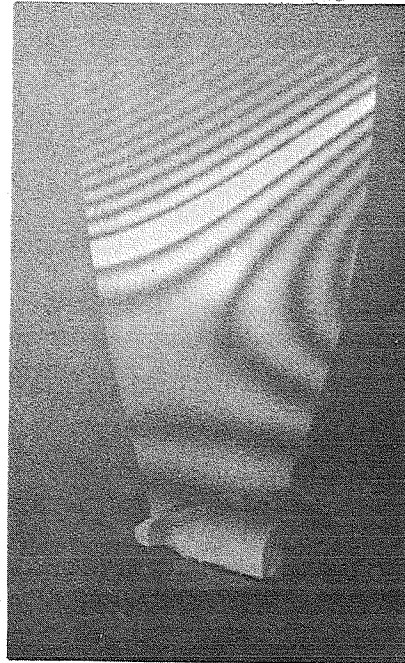


Figure 50. Fan Blade Root Fixture.

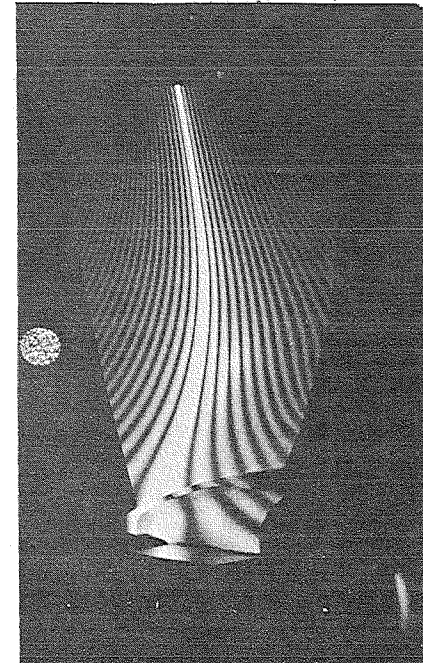




1st Bending Mode  
(214 Hz)

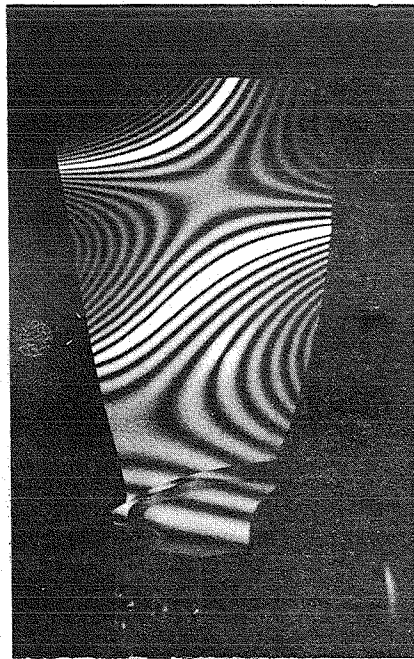


2nd Bending Mode  
(538 Hz)

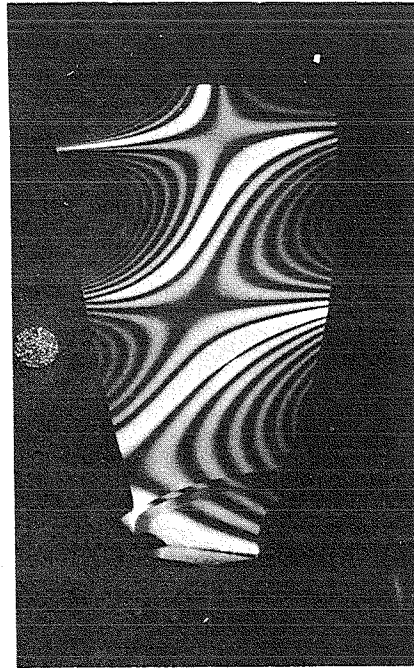


1st Torsional Mode  
(110 Hz)

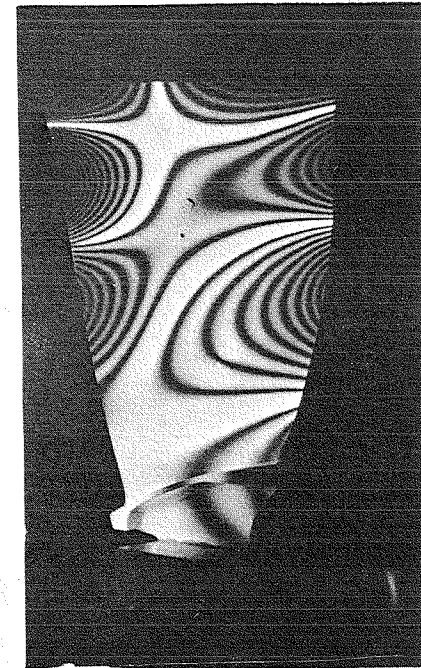
Figure 51. Fan Blade Natural Frequencies and Associated Mode Shapes--  
First and Second Bending Mode, First Torsional Mode.



1804 Hz  
3rd Bending



3140 Hz  
4th Bending



4527 Hz  
2nd Torsional

Figure 52. Fan Blade Natural Frequencies and Associated Mode Shapes--  
Second Torsional Mode, Third and Fourth Bending Mode.

# QCGAT FAN BLADE

IDENTIFIABLE MODES ARE INDICATED

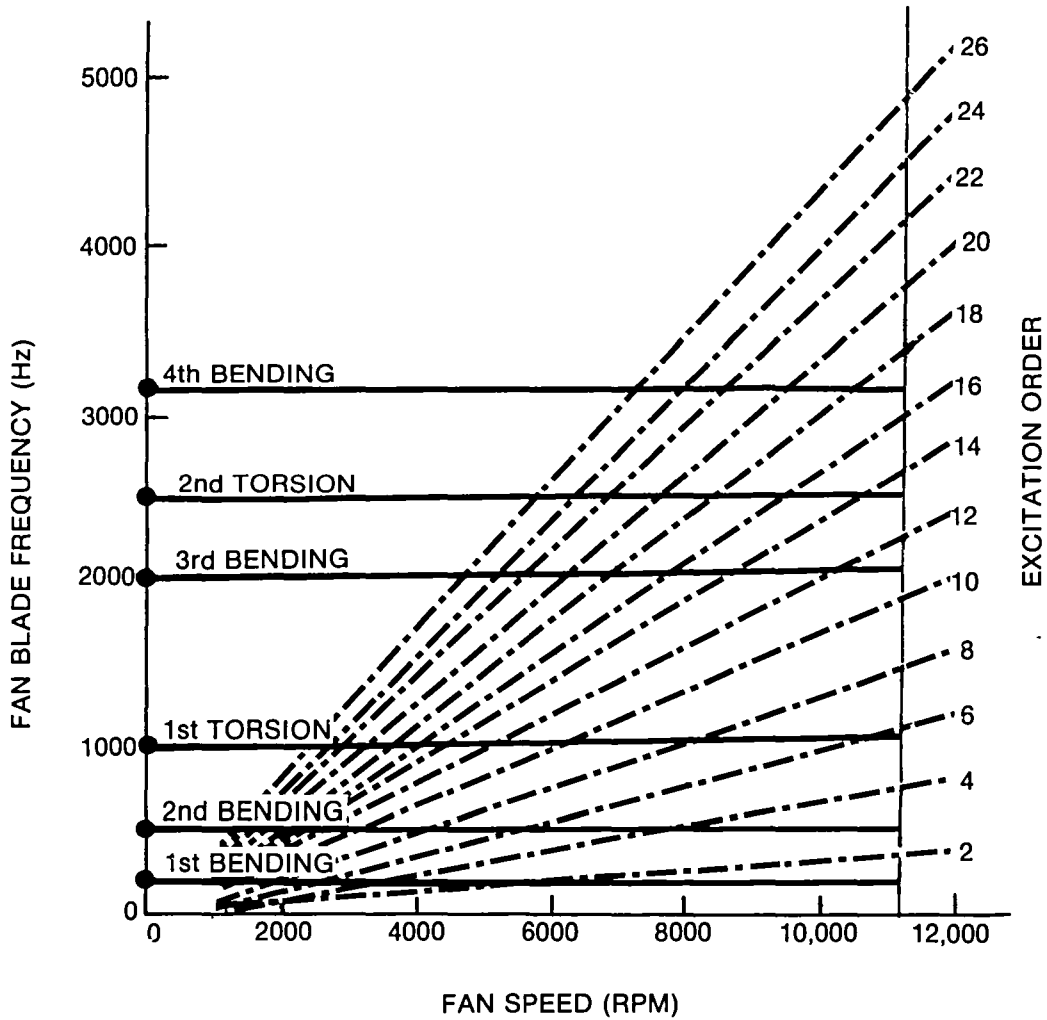


Figure 53. Fan Blade Excitation Diagram.

assembly. This segment was then bolted directly to the vibration exciter as shown in Figure 54. Real-time holograms were obtained up to 24,000 Hz covering the turbine blade frequency spectrum.

#### 4.2.1 Power Turbine Blade Results

The typical natural frequencies and associated mode shapes of the power turbine blade are identified in Figure 55. Several modes could be identified in the frequency range under consideration (0 to 24,000 Hz). A blade-frequency diagram of the power turbine blade is shown in Figure 56 for ambient test temperature conditions and Figure 57 for 1250°F (engine operating condition).

### 4.3 RING GEAR FREQUENCY ANALYSIS

A similar setup using the holographic interferometry techniques was used on the ring gear with the exception that different fixtures were required. The ring gear was bolted to the piezoelectric vibration exciter by means of a mounting adapter sized to interface with the external spline and internal bearing shoulder at the shank end of the gear. This clamping arrangement (Figure 58) considers a simply supported constraint at the bearing location and a free-free condition at the ring gear's open end.

A real-time hologram was made with the ring gear at rest, i.e., with no input excitation. The gear was excited axially (sine-wave excitation) at varying frequencies up to 24,000 Hz (limit of present exciter setup), and then the predominant natural frequencies were determined and recorded. A time-average hologram was taken at each of these recorded frequencies to identify the respective mode shapes. Each hologram was then documented by photograph.

#### 4.3.1 Ring Gear Test Results

Many diametrical and circumferential modes can be encountered over the frequency range experienced by the ring gear. Example of several modes are shown in Figure 59 showing front and aft views.

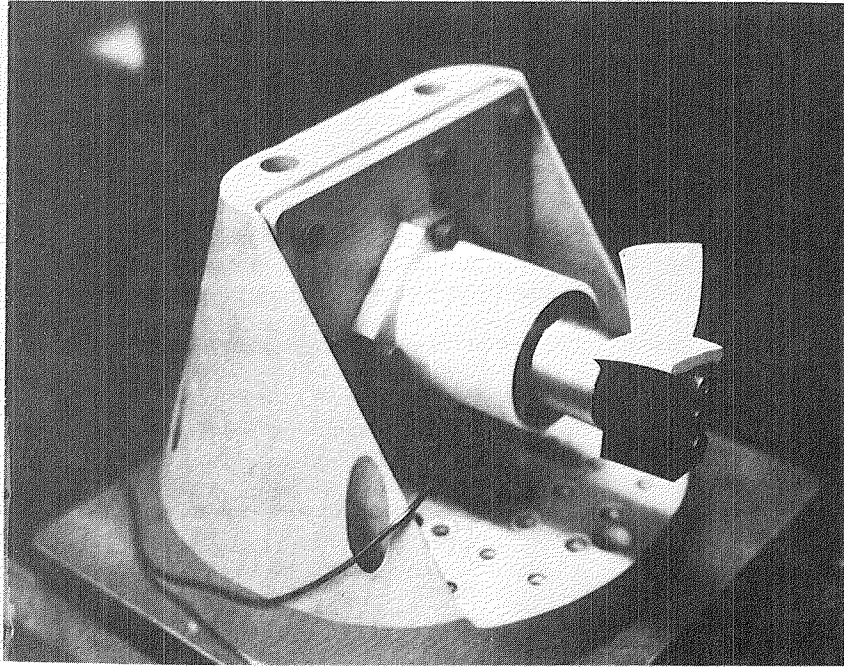


Figure 54. Power Turbine Segment Mounted to Shaker.

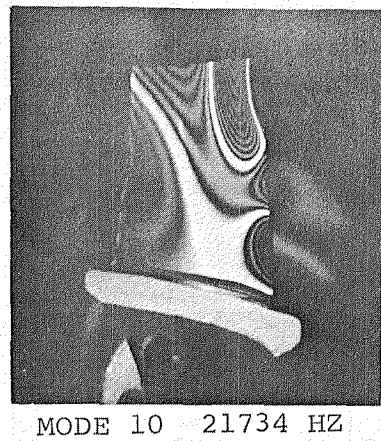
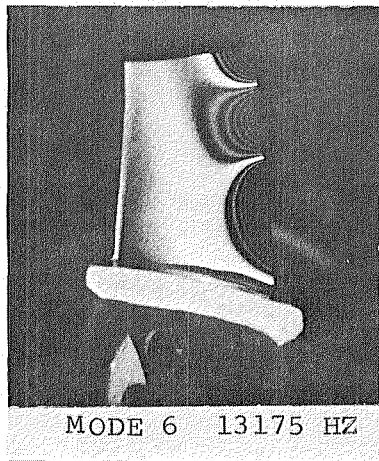
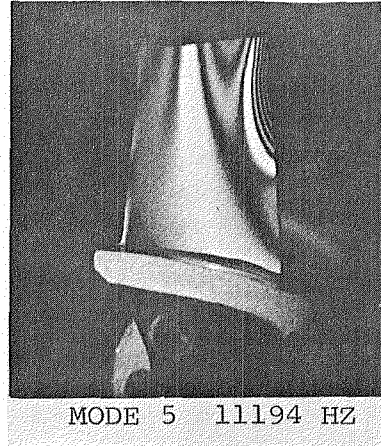
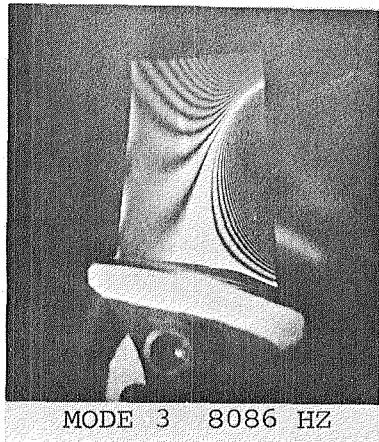


Figure 55. Power Turbine Natural Frequencies and Associated Mode Shapes.

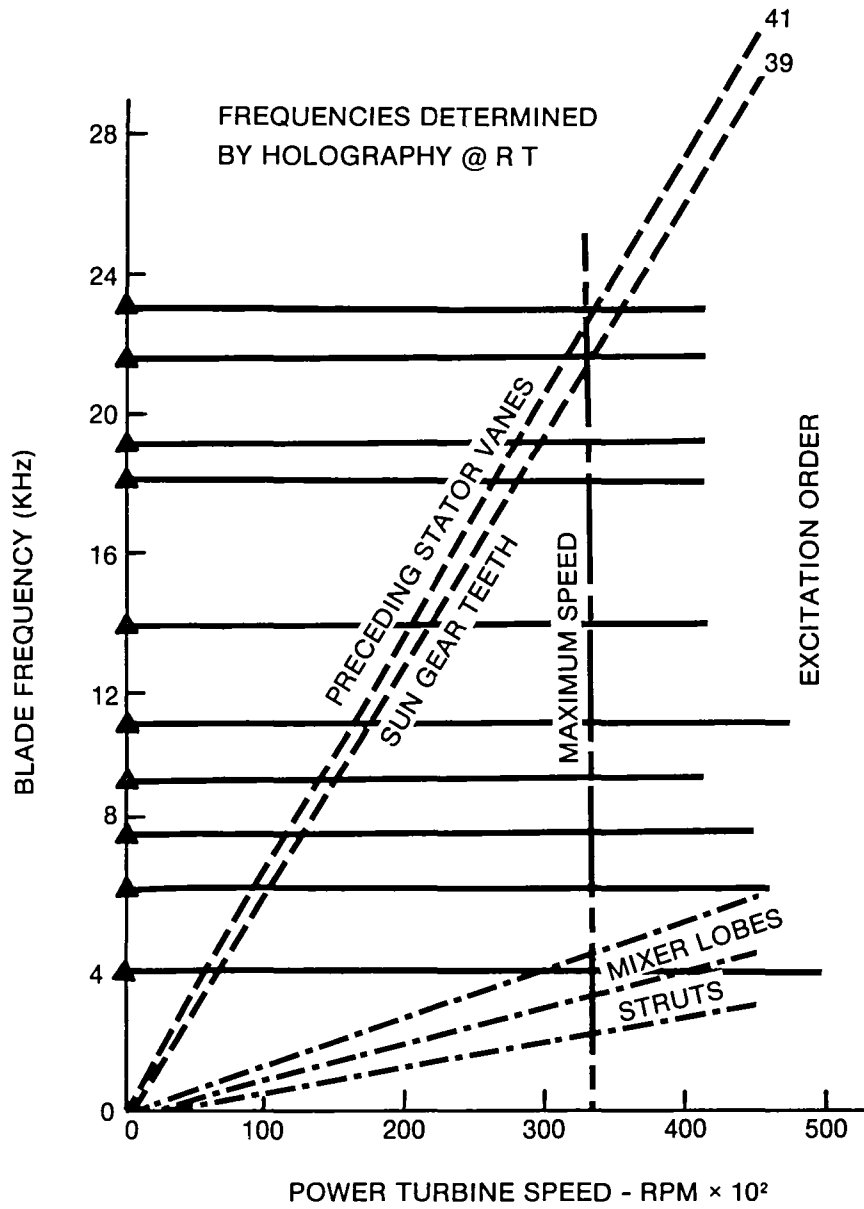


Figure 56. Power Turbine Blade Excitation Diagram at Ambient Temperature.

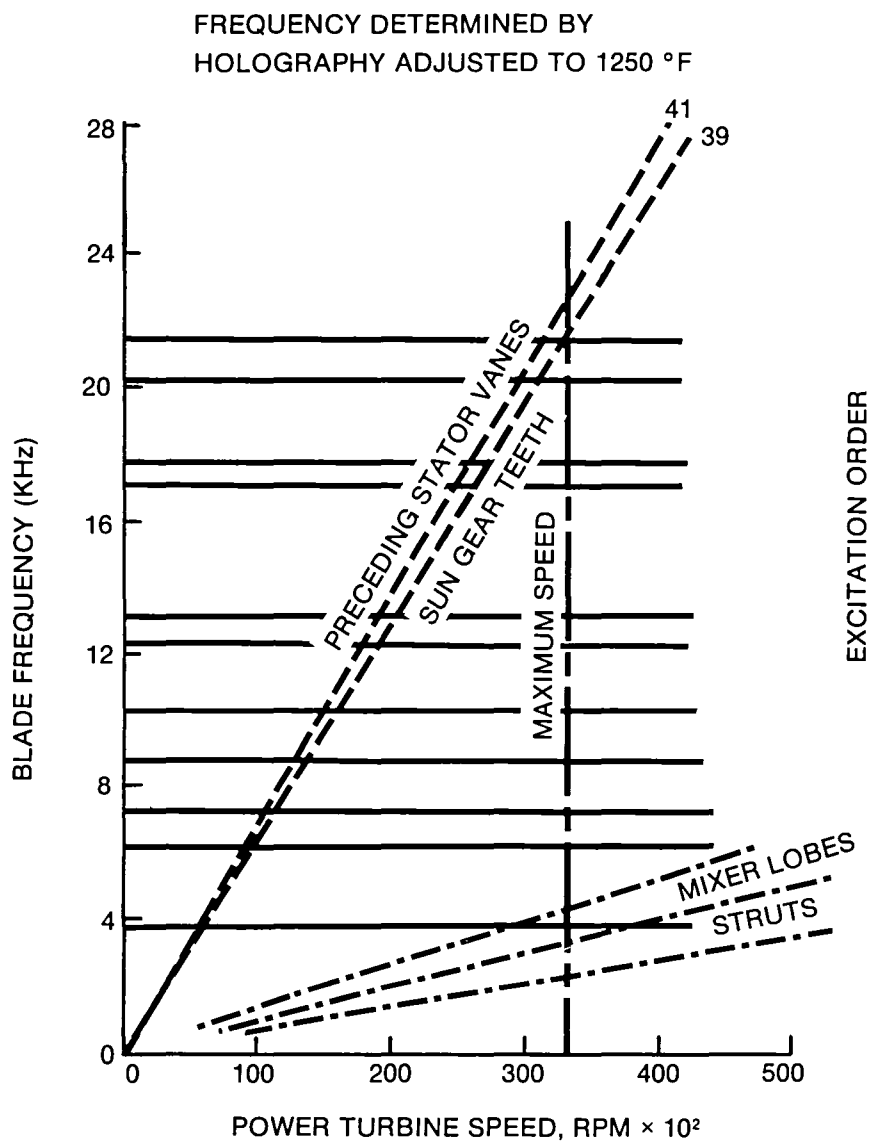


Figure 57. Power Turbine Blade Excitation Diagram at 1250°F.



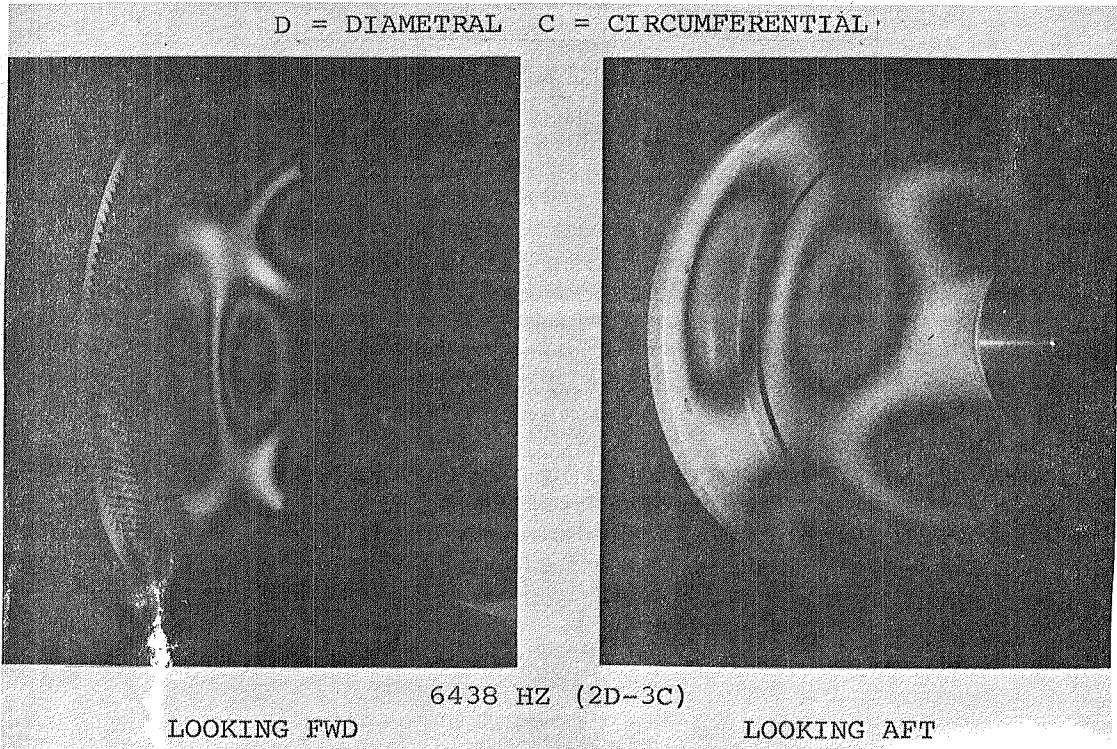
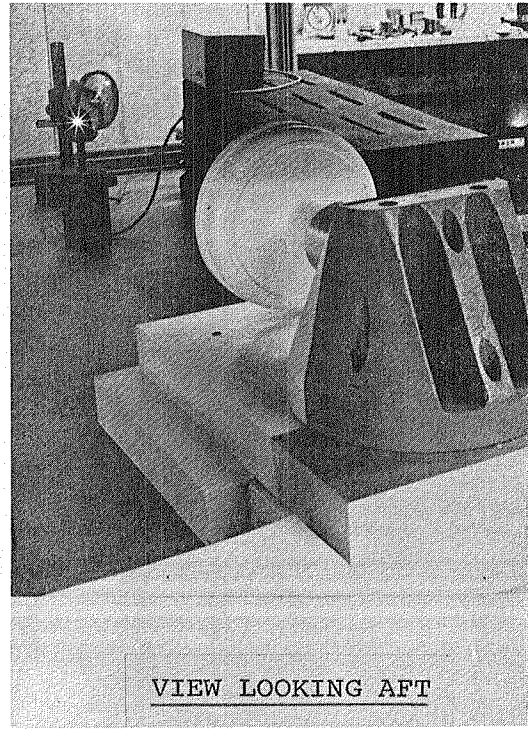
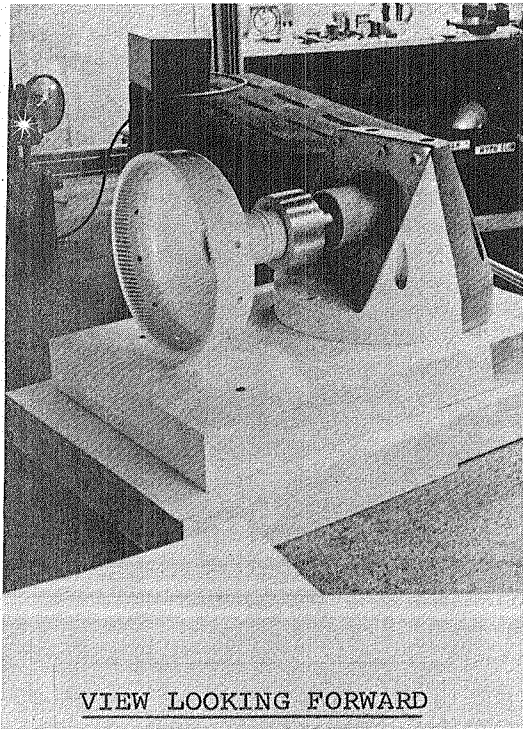


Figure 58. Ring Gear Clamping Arrangement and Natural Frequencies and Associated Mode Shapes.

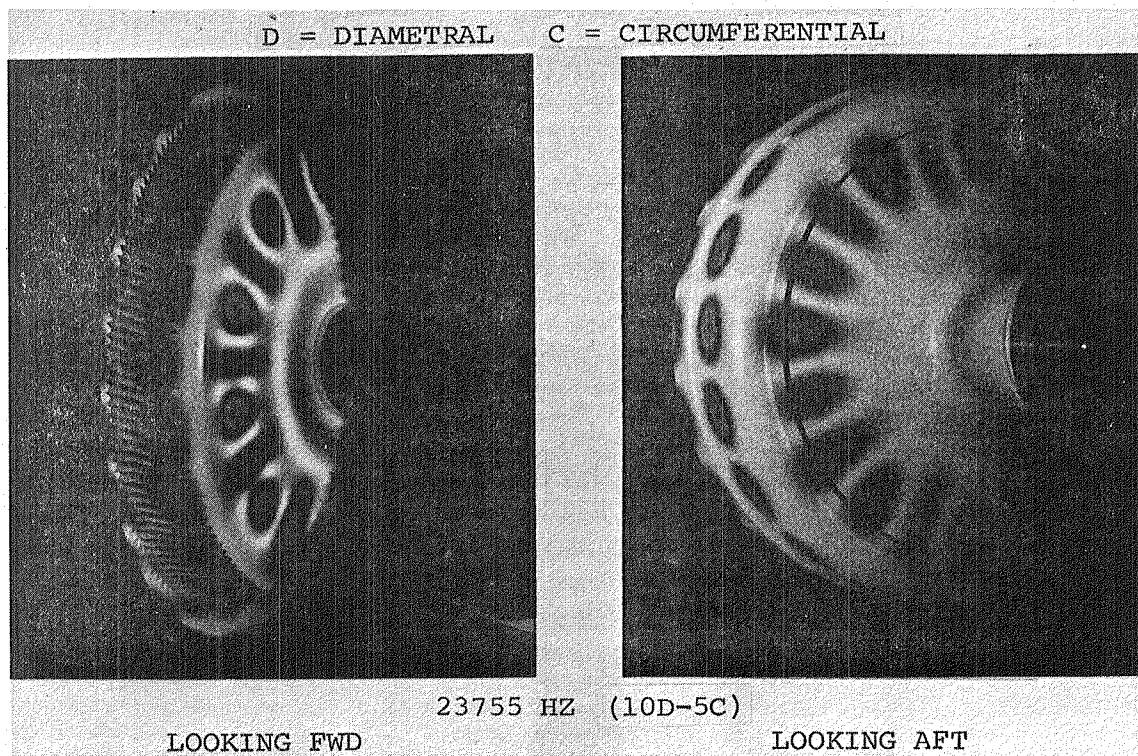
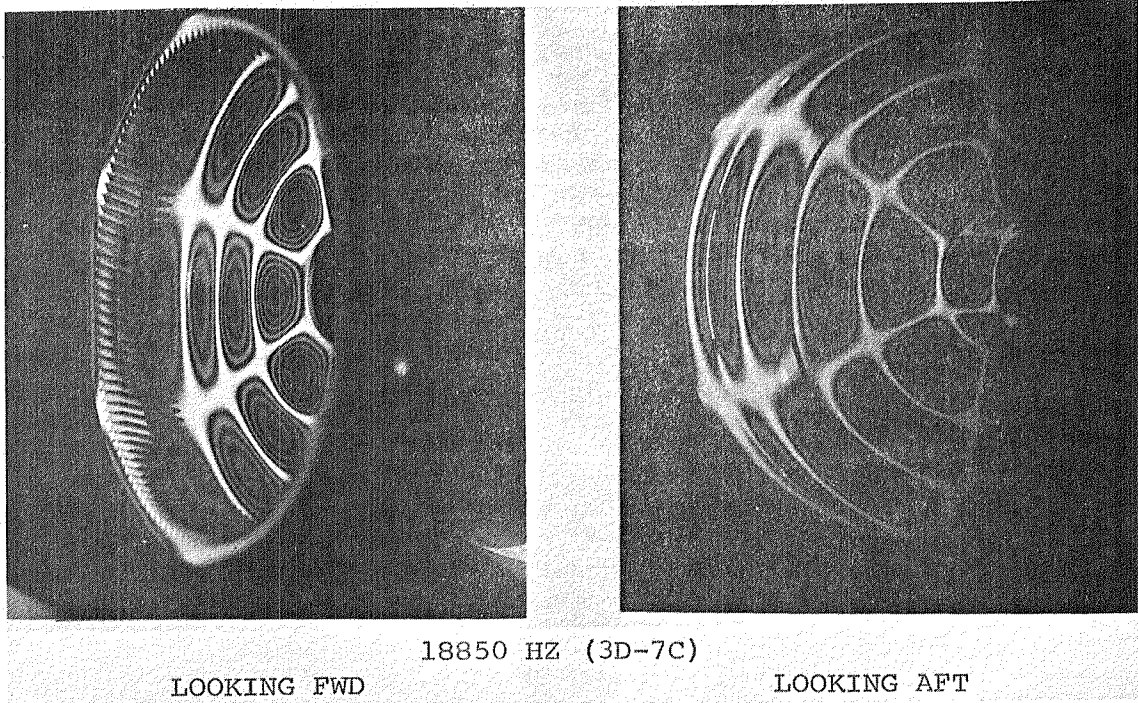


Figure 59. Ring Gear Natural Frequencies and Associated Mode Shapes.

#### 4.4 FLOW DIVIDER AND FUEL MANIFOLD SYSTEM ANALYSIS

The purpose of this component laboratory test was to determine the effect of usage on the QCGAT flow divider/fuel manifold assembly. This assembly consists of two manifold segments, each containing four ALF 502 airblast fuel injectors. The two manifold segments are made up of LTS 101 manifold bosses and tubing, except that the flow divider boss has been changed to accept the airblast flow divider.

The test was defined at 500 cycles with each cycle providing one step excursion from take-off fuel flow to below idle and one transient excursion to take-off and shut off. This series provides maximum wear and fatigue testing for the time involved. Results show the effect of wear and spring relaxation on plunger leakage, stickage, hysteresis, and flow schedule with either small-incremental or full-range transient flow changes. Injector spray quality was observed and monitored throughout the test cycles.

Flow divider performance, in terms of flow schedule, reference port leakage, and hysteresis was not adversely affected by this test. The fuel injectors also performed satisfactorily with excellent spray quality.

#### 4.5 FAN COMPONENT TEST RIG

The purpose of the fan module subsystem test was to provide measurements of aerodynamic performance necessary for successful matching to the core engine and power turbine modules and to demonstrate mechanical integrity of the fan component, including satisfactory vibration stress levels.

A cross-sectional view of the test rig is shown in Figure 60. All engine level hardware are used with the exception that the fan rotor was a direct drive, in lieu of the reduction gearing, with the test facility. Measurement planes for detailed stage-performance evaluation were defined as depicted in Figure 61, and a breakdown of the instrumentation installed is given in Figure 62.

The inlet section to the test rig consists of an airflow measurement bellmouth, optional distortion screen holder, and a six-strut distortion instrumentation housing, which also carries a freon-cooled slip ring for strain-gage testing. The rig bellmouth serves as a secondary air flow measurement and is calibrated with an ASME nozzle located at the entrance of the plenum chamber. Figure 63 is a schematic of the

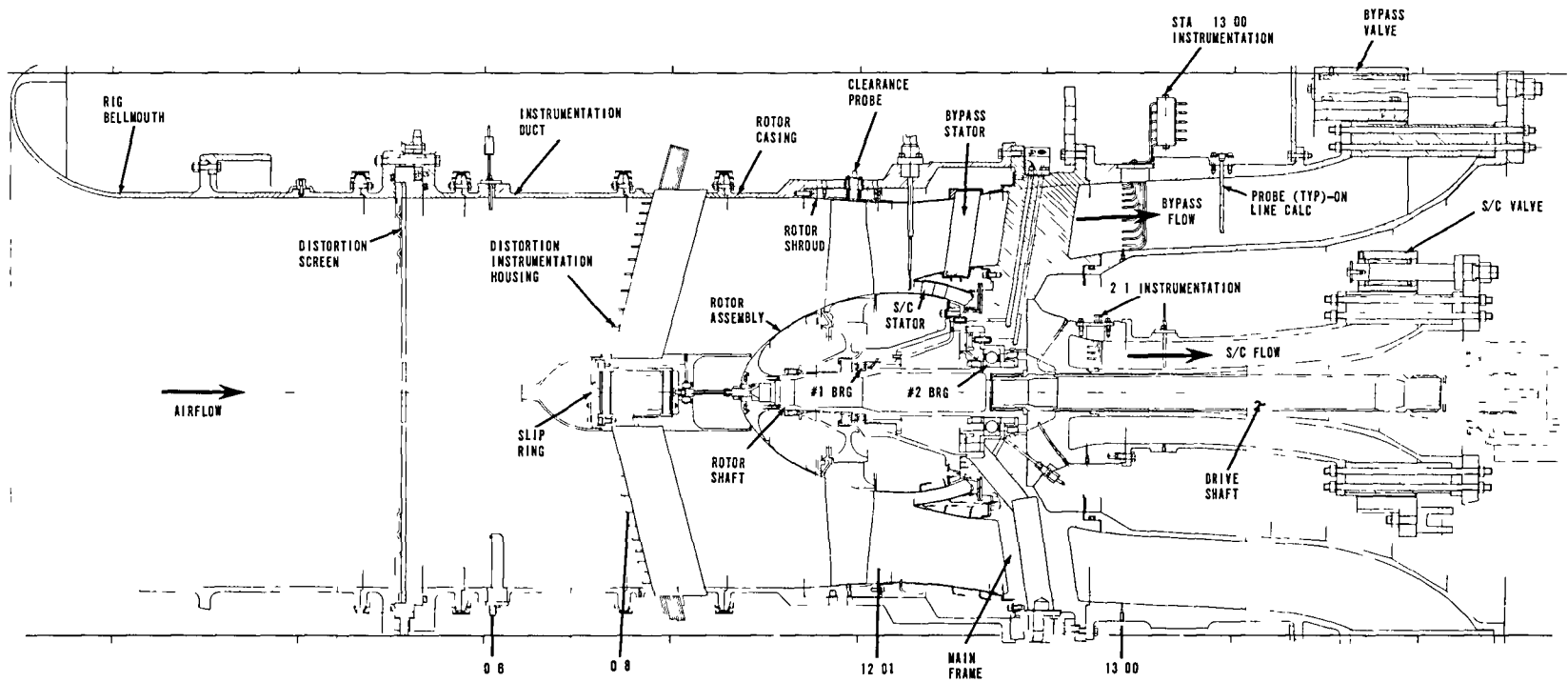
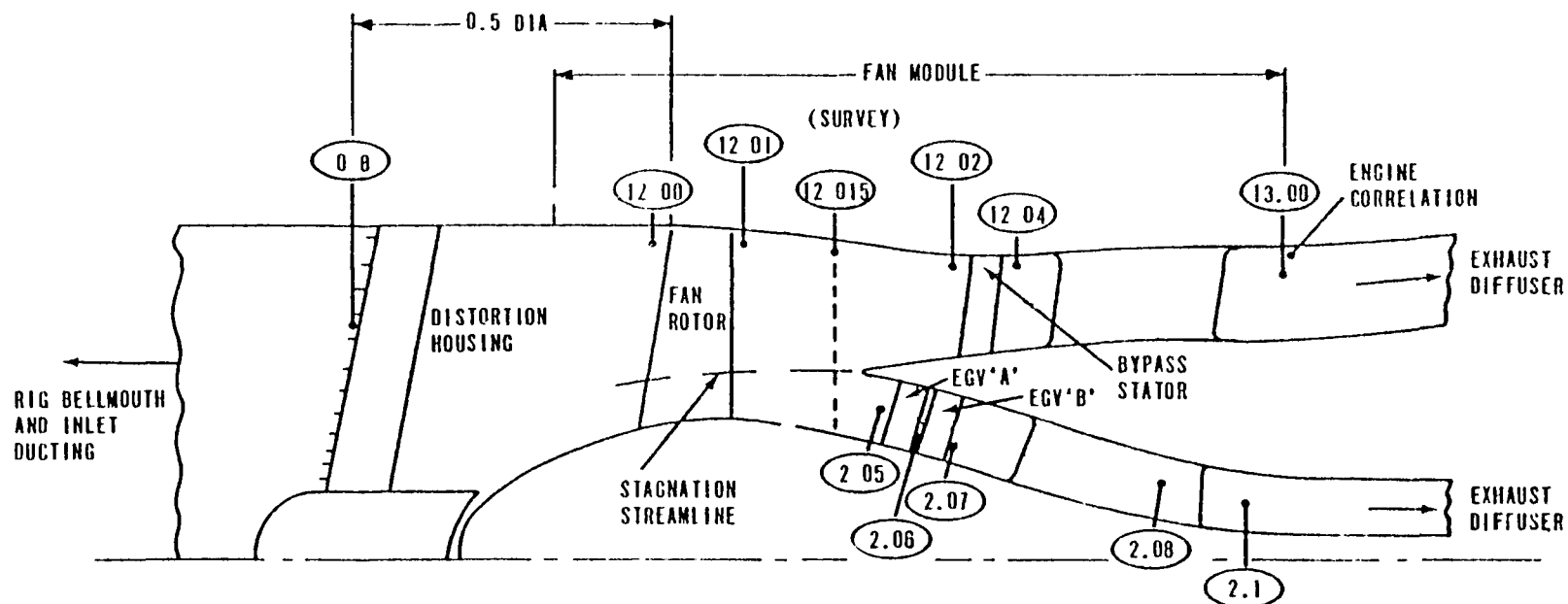


Figure 60. QCGAT Fan Module Test Rig.



Note Circumferential orientation of exit plane instrumentation (Ref. 1) is free-stream with respect to bypass struts (12) and core channel struts (4).

Figure 61. Fan Module Instrumentation Planes - Nomenclature.

STATION DESIGNATION	LOCATION	INSTRUMENT
-4	PLENUM NOZZLE	4 P <sub>T</sub> 8 P <sub>S</sub>
0	PLENUM CHAMBER	8 P <sub>T</sub> 12 T <sub>T</sub>
0.6	RIG BELLMOUTH/DUCT	4 P <sub>T</sub> 8 P <sub>S</sub> 4 T <sub>T</sub> (ENGINE ONLY)
0.8	INLET DISTORTION HOUSING	72 P <sub>T</sub> (DISTN ONLY) 6 P <sub>S</sub> (a)
12.00	ROTOR INLET PLANE	4 P <sub>S</sub> (a)
12.01	ROTOR EXIT PLANE	4 P <sub>S</sub> (a)
12.015	ROTOR EXIT SURVEY PLANE	3 RAD ACTUATORS 4 P <sub>S</sub> (a) 4 P <sub>S</sub> (c)
12.02	BYPASS STATOR INLET PLANE	4 P <sub>S</sub> (a) 4 P <sub>S</sub> (c)
12.04	BYPASS STATOR EXIT PLANE	4 P <sub>S</sub> (a) 4 P <sub>S</sub> (c)
2.05	EGV 'A' INLET (SUPERCHARGER CHANNEL)	4 P <sub>S</sub> (a) 4 P <sub>S</sub> (c)
2.06	EGV 'B' INLET	4 P <sub>S</sub> (a)
2.07	EGV 'B' EXIT	4 P <sub>S</sub> (a) 4 P <sub>S</sub> (c)
2.08	ENGINE CORRELATION PLANE - SUPERCHARGER CHANNEL	2 P <sub>T</sub> 2 T <sub>T</sub> 2 P <sub>S</sub> (a)
2.1	SUPERCHARGER EXIT PLANE	40 P <sub>T</sub> 40 T <sub>T</sub> 4 P <sub>S</sub> (a) 4 P <sub>S</sub> (c)
13.00	BYPASS EXIT PLANE	80 P <sub>T</sub> 80 T <sub>T</sub> 8 P <sub>S</sub> (a) 8 P <sub>S</sub> (c)
13.00	BYPASS EXIT - ENGINE CORRELATION	4 P <sub>T</sub> (INTEG) 4 T <sub>T</sub> 4 P <sub>S</sub> (a)

NOTE: (a) = OUTER WALL  
(c) = INNER WALL

Figure 62. Aerodynamic Performance Instrumentation.

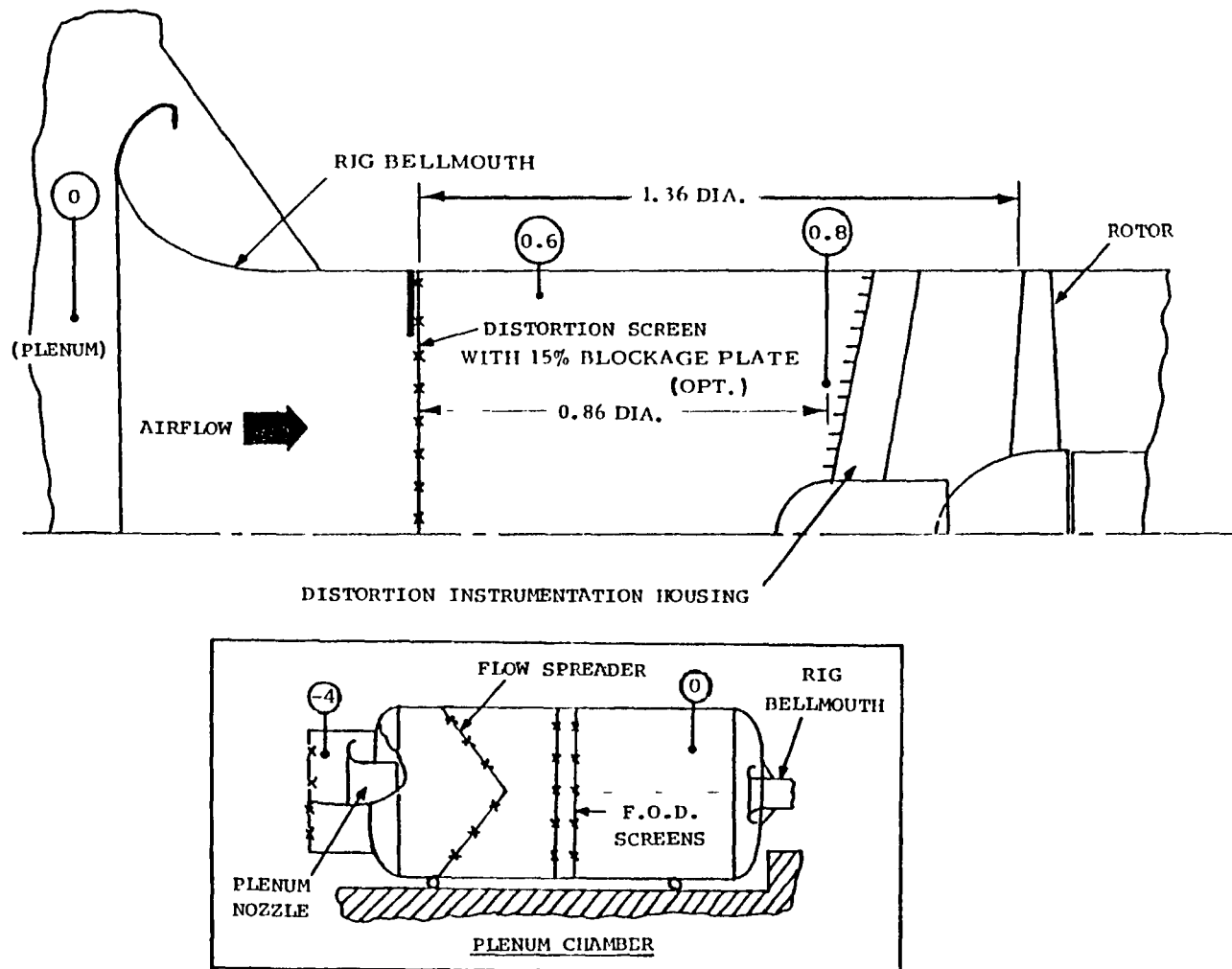


Figure 63. Fan Module Inlet Instrumentation Planes and Distortion Screen Position.

inlet duct and plenum system. Downstream of the main fan support frame are low-loss diffusing ducts to exhaust the bypass and supercharger flows to ambient pressure. Both exhaust channels are independently throttle-able to permit selection of any desired component loading thru cylindrical, actuator-driven exhaust valves. Loadings over the flow range from choke to stall can be evaluated. The QCGAT fan rig cell installation is shown in Figure 64.

#### 4.5.1 Fan Component Test Results

The development test program that was conducted consisted of three phases: steady-state base performance, diagnostic, and distorted inlet. The baseline performance for the bypass and supercharger is given in Figures 65 and 66. Both the bypass and supercharger were mapped from 50 to 105 percent of design referred speed. The overall test results are compared with design goals as tabulated below:

##### Bypass Performance (Sea Level Static)

	<u>Pressure Ratio</u>	<u>Referred Flow Kg/sec(lb/sec)</u>	<u>Polytropic Efficiency</u>	<u>Referred Speed (rpm)</u>
Design	1.380	33.70 (74.0)	0.870	11,200
Test	1.380	33.75 (74.1)	0.870	11,200

##### Supercharger Performance (Sea Level Static)

	<u>Pressure Ratio</u>	<u>Referred Flow Kg/sec (lb/sec)</u>	<u>Polytropic Efficiency</u>	<u>Referred Speed (rpm)</u>
Design	1.350	3.63 (8.00)	0.850	11,200
Test	1.308	3.63 (8.00)	0.715*	11,200

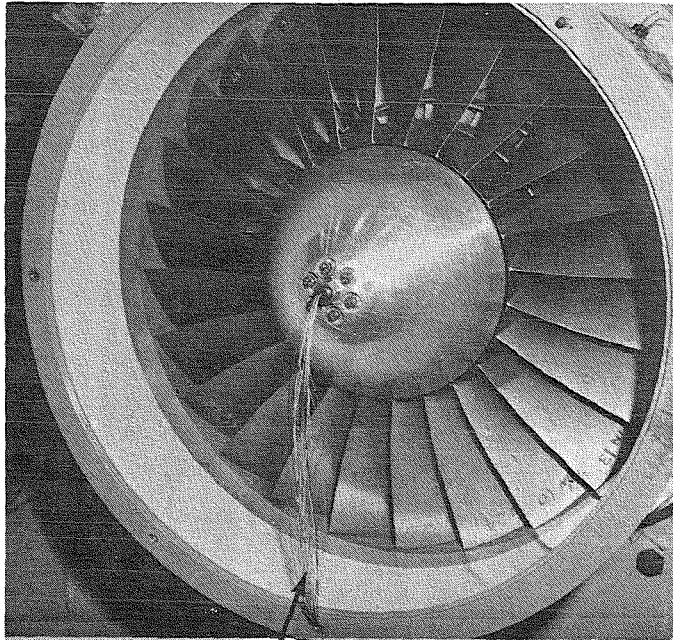
##### At Peak Efficiency

	1.324	3.41 (7.50)	0.732	11,200
--	-------	-------------	-------	--------

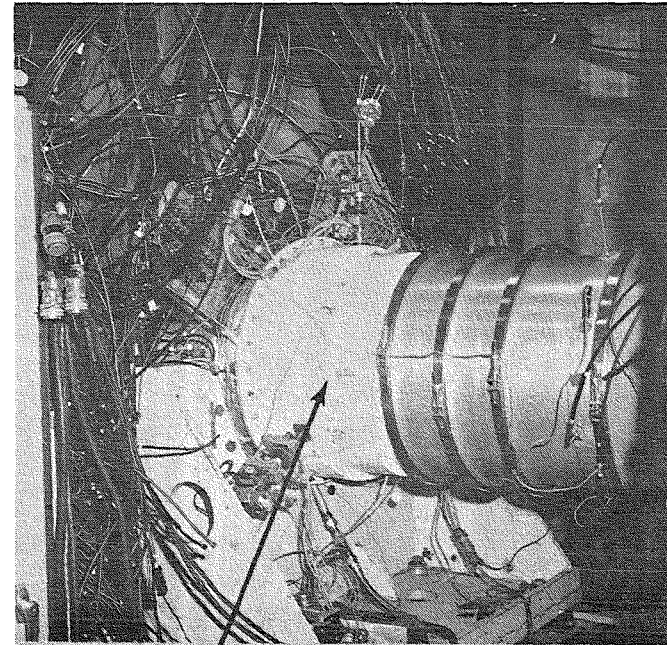
\*The supercharger was redesigned and resulted in a 8-point gain in efficiency based on engine performance data.

The bypass component met or exceeded all design goals; whereas, the supercharger performance was lower than the desired goal. Bypass and supercharger exit profiles are shown in Figures 67 and 68. The bypass channel exit distributions of total pressure, total temperature, and polytropic efficiency are compared with the design





BLADE STRAIN  
GAGE LEADS



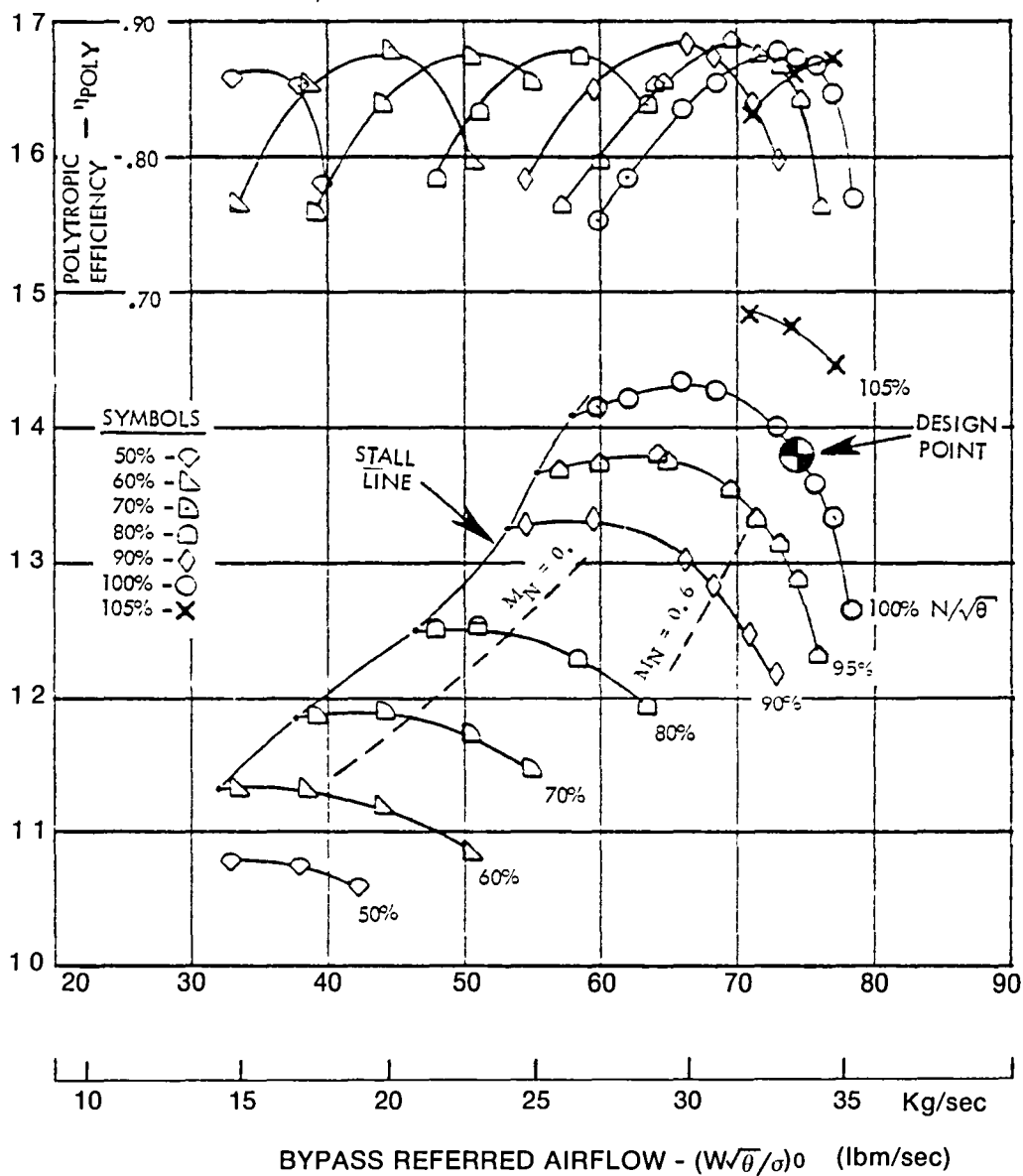
ROTOR  
CASING

INLET  
PLENUM



Figure 64. QCGAT Fan Module - Testway Installation.

TEST - 01  
 100%  $N/\sqrt{\theta} = 11200$  RPM



Note Dashed lines indicate engine operating lines for sea-level static ( $MN=0$ ) and altitude cruise ( $MN=0.6$ ) conditions

Figure 65. QCGAT Fan Module Baseline Test - Bypass Overall Performance Map

TEST - 01  
 100%  $N\sqrt{\theta} = 11200$  RPM

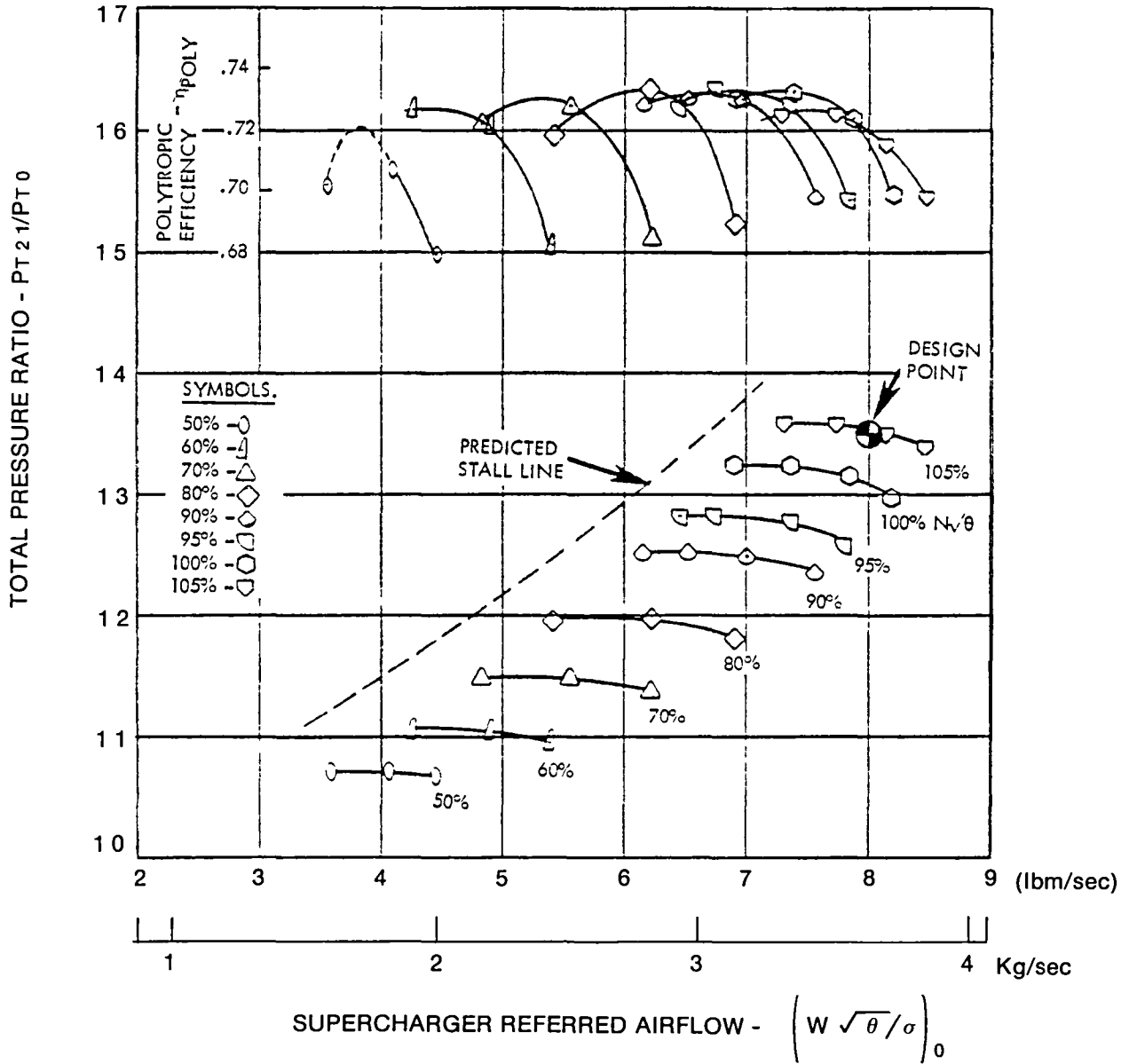


Figure 66. QCGAT Fan Module Baseline Test - Supercharger Overall Performance Map

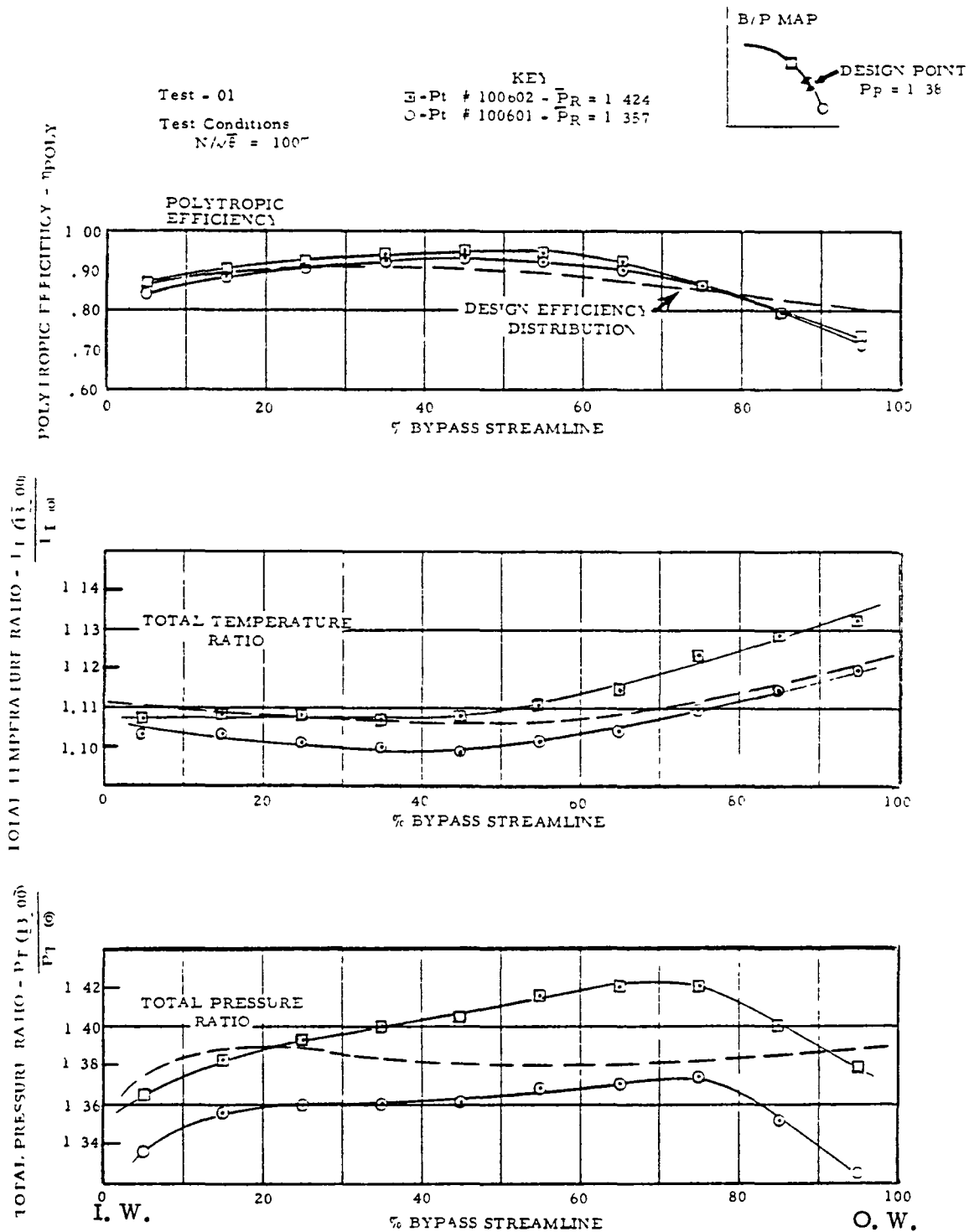


Figure 67. Bypass Exit Plane Profile Data

Test -01 Point # 100602 -  $\bar{P}_R = 1.311$   
 Test Conditions  
 $N/\sqrt{5} = 100\%$

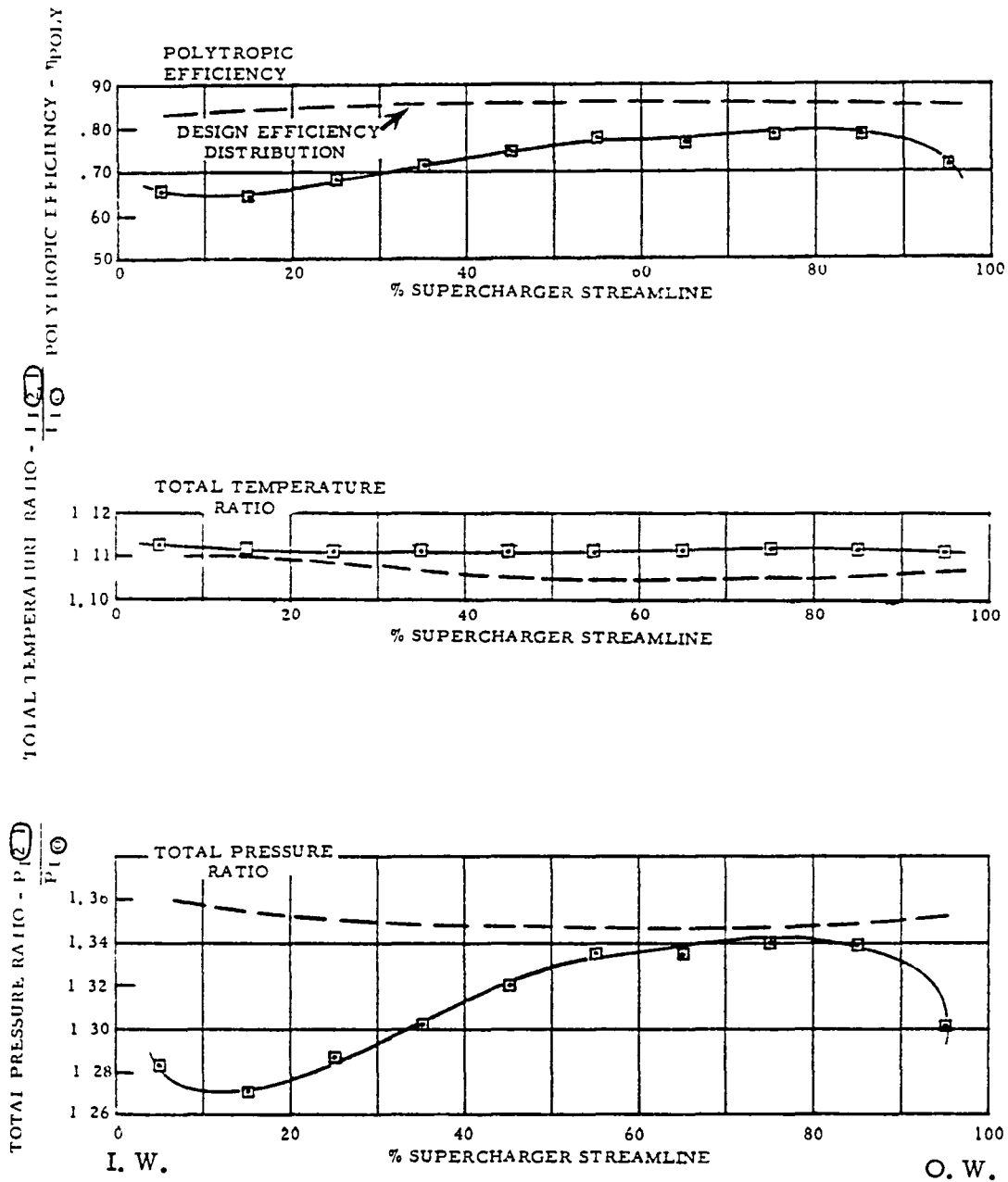
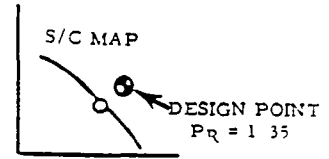


Figure 68. Supercharger Exit Plane Profile Data

profiles. The blade pressure levels in the 60 to 80-percent streamline portion are greater than design thereby yielding the higher than design efficiency.

This pressure profile trend was later corroborated with rotor-exit survey measurements. The same profiles for the supercharger show a substantial deficit in total pressure from the hub to mid-stream. Follow-on tests showed that the observed efficiency deficit is largely associated with the total pressure loss through the supercharger vane assembly and duct system.

The two major factors influencing the supercharger total pressure ratio are:

1. Geometry of the fan blade hub section velocity triangles is such that relative flow is turned by the rotor to the axial direction. A decrease in flow causes a small change in work output. The resulting flat map characteristic yields little or no pressure change with loading.
2. The splitter was placed relatively far aft of the rotor; this coupled with a high bypass ratio design allows air flow to divert to the bypass channel as loading is increased in the supercharger.

The second test phase isolated the supercharger performance loss to be attributed to the vane assembly and interconnecting duct. The efficiency deficit was a result of sensitivity to pressure loss at low pressure levels. Subsequently, the supercharger vane assembly was redesigned to minimize these losses.

#### 4.5.2 Distorted Inlet Test Results

The response of a turbofan to inlet distortion is of prime importance from the viewpoint of aerodynamic performance and mechanical integrity of the blades. Significant distortions frequently occur in aircraft installations as a result of intake flow separation induced either by crosswinds or high angles of attack.

The bypass map characteristic is generally flat once the peak pressure ratio has been reached; moderate amounts of circumferential distortion may cause the stall line to deteriorate and simultaneously raise the engine operating line.

In order to produce a crosswind type of distortion artificially, a crescent-shaped solid plate was placed about 1.4 diameters upstream of the rotor. Area blockage for this plate was 15 percent. Figure 69 shows the relationship of this plate to the channel and also the resulting distortion pattern which was obtained at 90 percent speed. The Lycoming distortion index definition is defined as follows:

Distortion Index

$$DI = \frac{(P_T \text{ mean} - P_T \text{ low mean})}{P_T \text{ mean}} [K_P]$$

where  $P_T$  mean = avg. total pressure at the measurement plane based on an area weighted average.

$P_T$  low mean = avg. total pressure area-averaged over all regions where  $P_T < P_T$  mean

$K_P$  = Factor accounting for profile and extent of distortion

$K_P$  =  $\sqrt{MER}$

$M$  = Magnitude of the peak distortion relative the average in the depressed region.

$M$  =  $6.0 \frac{P_T \text{ MEAN} - P_T \text{ low mean}}{P_T \text{ mean} - P_T \text{ low min}}$

$P_T$  low min = Minimum total pressure level

$E$  = Extent of distorted region

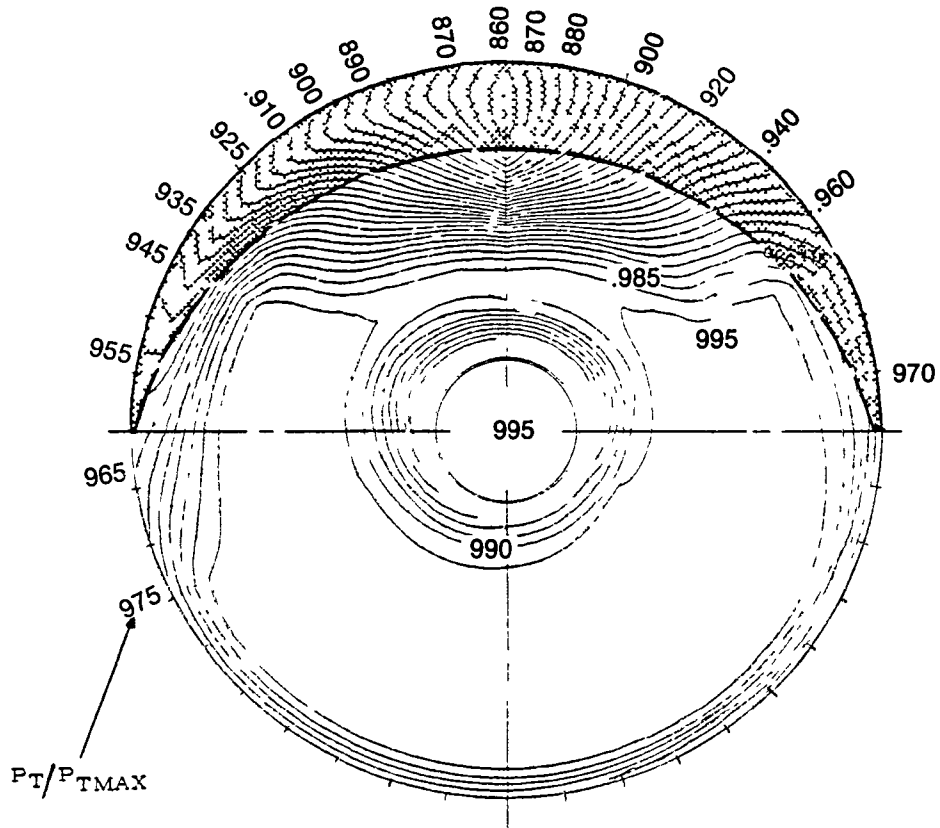
$E$  =  $\frac{2A_L}{A_{tot}}$

$A_L$  = Total annulus area

$R$  = Radial distortion sensitivity factor

$R$  =  $1 + \left| \frac{(2A_L \text{ hub} - 1)}{A_L} \right|$

$A_L$  hub = The area extent of low pressure regions which fall in the inner (hub) 50% annulus area.



D.I. - 0.057

CONTOUR INTERVAL - .005

$P_{T_{MAX}} = 13.53$

$\frac{P_{T_{MEAN}}}{P_{T_{MAX}}} = .975$

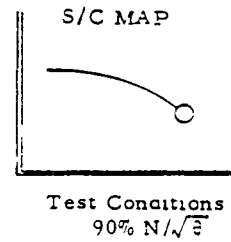


Figure 69. Area Blockage (15 Percent) Inlet Distortion Plate with Resultant Total Pressure Contours



Using the Lycoming D.I. as a descriptor to quantify the level of distortion, the QCGAT fan was tested up to an index of 0.06. Since this level is quite severe and well above limits generally set for satisfactory turbofan performance, the testing was not continued beyond 90 percent speed. A plot of distortion index versus total airflow is shown on Figure 70.

The effect upon overall performance of the combined radial/circumferential distortion pattern is shown on Figure 71.

At 80 percent speed, the stall margin (S.M.) for the bypass is reduced from 13 to 9.0 percent.

$$\text{Percentage S.M.} = \left[ 1 - \frac{(W/PR)_{\text{stall}}}{(W/PR)_{\text{op. line}}} \right] \times 100$$

The level of distortion at the 80 and 90 percent speed stall point was 0.03 D.I.

Peak efficiency at 80 and 90 percent speed decreased approximately 4 to 5 points.

Blade stresses remained at acceptable levels throughout the entire test.

In summary, the QCGAT rotor demonstrated satisfactory aerodynamic performance and excellent mechanical performance under inlet distortion conditions that are representative or in excess of those found in typical turbofan installations.

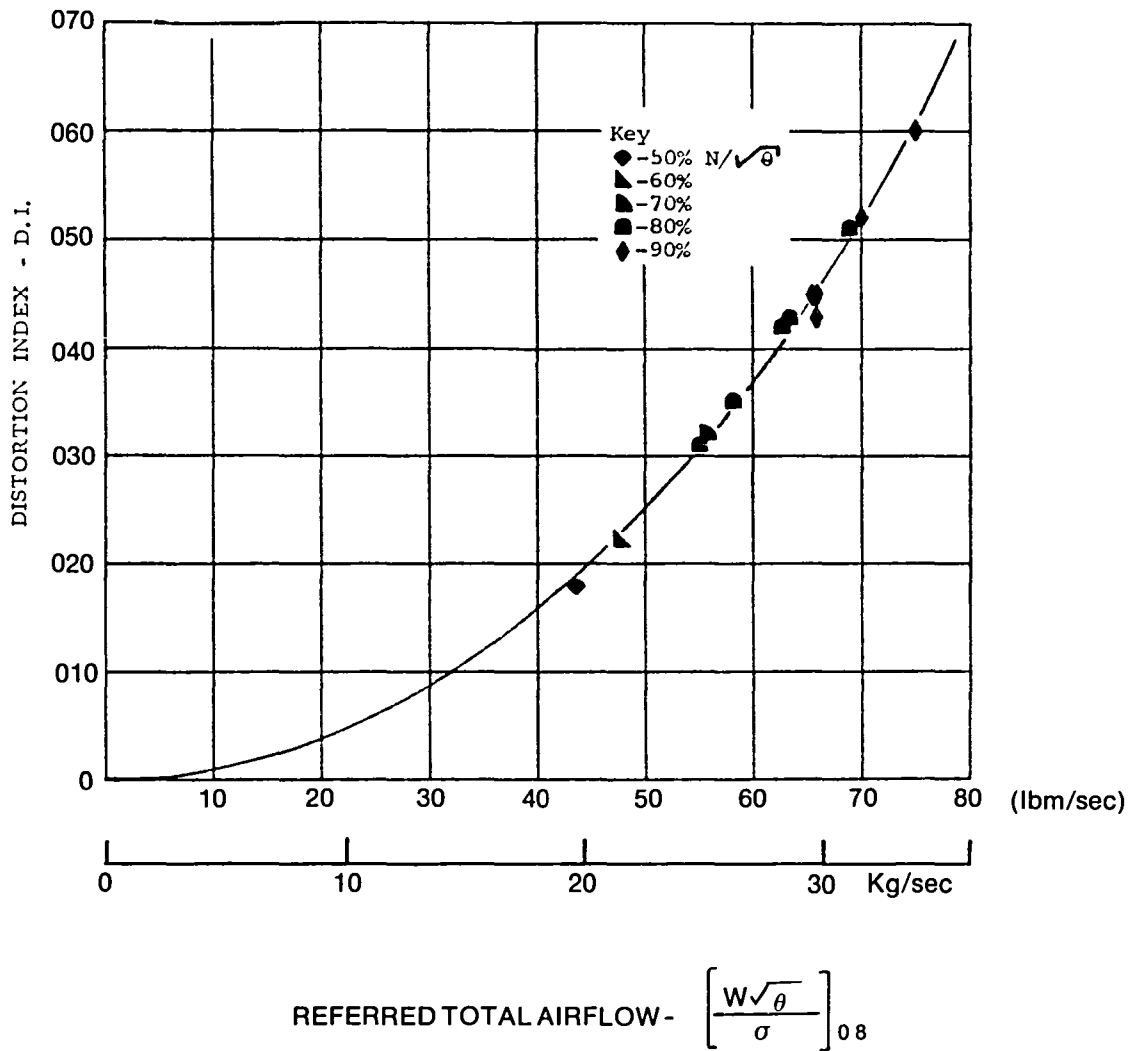


Figure 70. Distortion Index as a Function of Total Referred Airflow

TEST - 01  
 100%  $N/\sqrt{\theta} = 11200$  RPM

**DARK SYMBOL OVERLAY:**  
 (INLET DISTORTION)

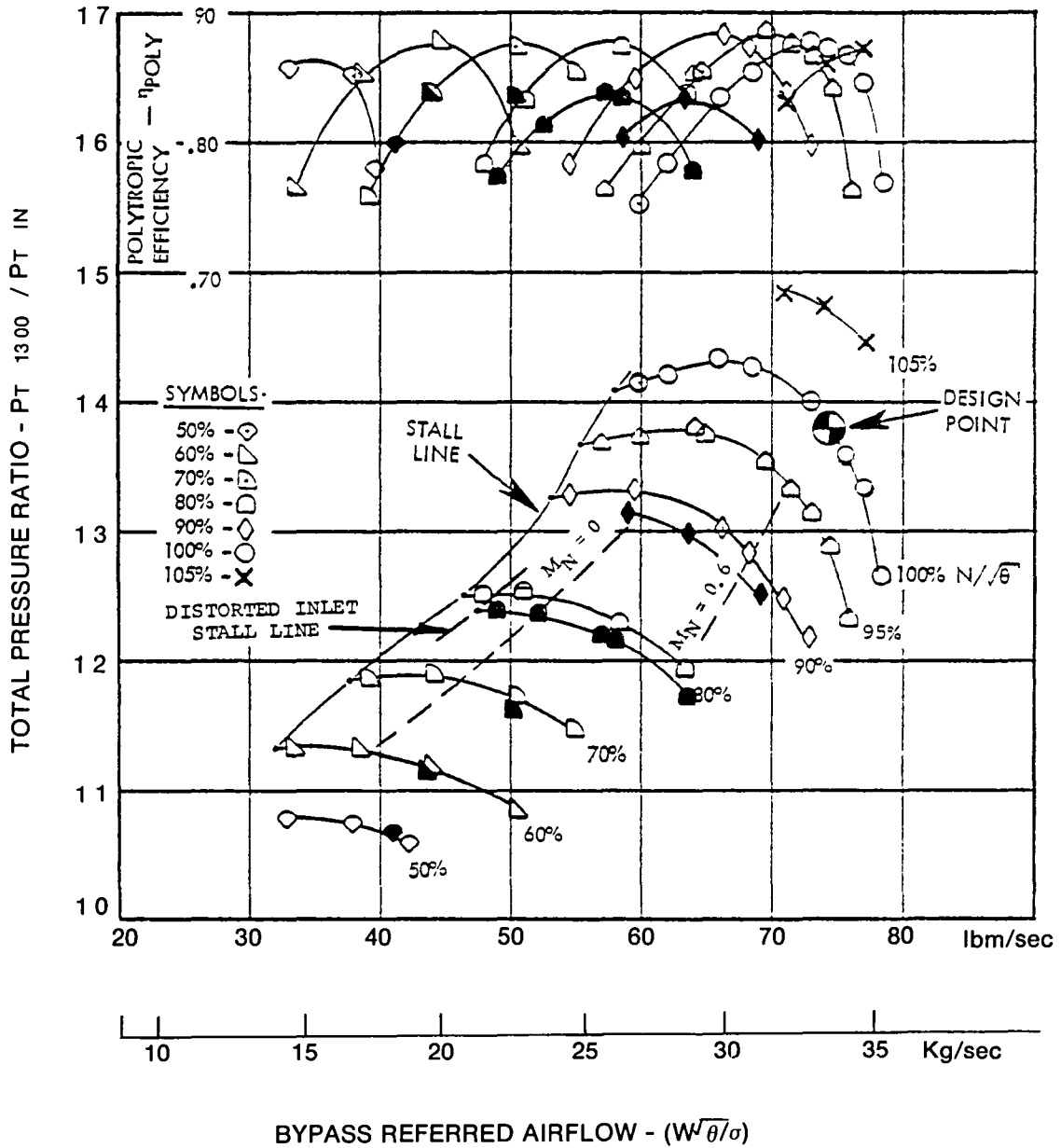


Figure 71. Bypass Overall Performance with Inlet Distortion

## 4.6 COMBUSTOR MODULE

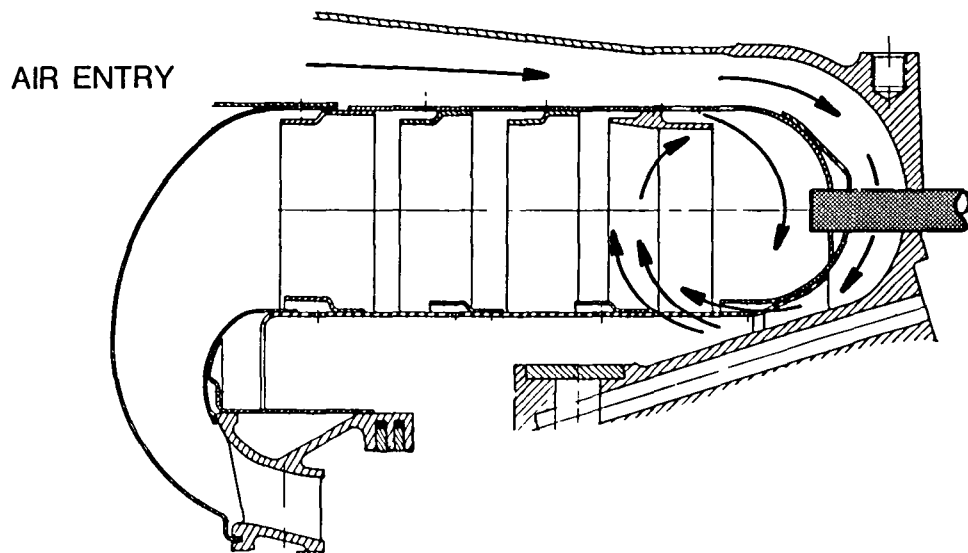
The Lycoming LTS 101 combustor has demonstrated exceptionally low emissions by comparison with conventional combustors of similar size. Several design changes were required to adapt the combustor to the QCGAT turbofan design. A new outer curl with improved cooling was designed, and the liner-to-curl seals were redesigned because of the higher pressure and temperature requirements of a fan engine design. Airblast fuel injectors from the ALF 502 fan engine were installed, and a new flow divider with the same relative flow schedule as the ALF 502 was designed and tested. A comparison of the basic LTS 101 combustor and the QCGAT development configuration are shown schematically in Figure 72.

During the iterations that optimize an engine performance cycle, continuous attention is required to avoid adverse impact on emissions characteristics. A summary of the primary causes for emissions in conjunction with engine parameters that have a beneficial influence are as follows:

<u>Emissions</u>	<u>Cause</u>
Unburned Hydrocarbons, UHC	Combustion Inefficiency
Carbon Monoxide, CO	Inadequate Residence Time, Temperature, Efficiency
Oxides of Nitrogen, NO <sub>x</sub>	High Residence Time/Temperature
Smoke	Local Rich Zones

Unburned hydrocarbons and carbon monoxide emissions are primarily a reflection of poor combustor efficiency at idle. Low combustor inlet temperature at idle aggravates the carbon monoxide emissions. To reduce these two constituents, one would strive for very high combustor efficiency at idle, combined with elevated combustor inlet temperature. To achieve the higher inlet temperature, a compressor with poor efficiency at low speed is desired. Whereas idle conditions have the primary influence on UHC and CO, take-off conditions predominate in the creation of NO<sub>x</sub>. Generally, the higher the combustor inlet temperature at take-off the more difficult the problem is with NO<sub>x</sub>. An important axiom is that NO<sub>x</sub> and CO can usually be traded through combustor design modification. Either emission can be improved at the

# LTS 101 COMBUSTOR



# QCGAT COMBUSTOR ASSEMBLY

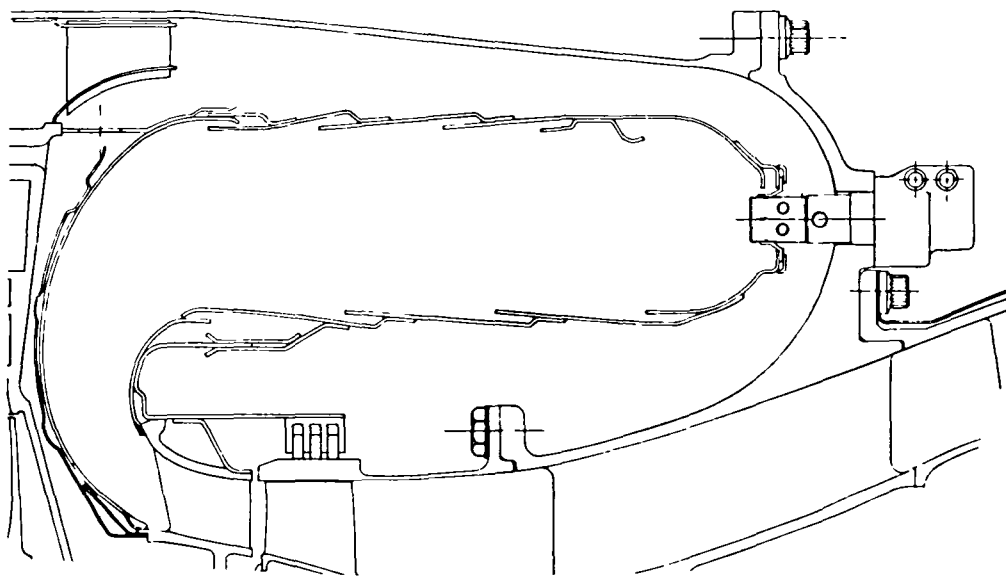


Figure 72. Comparison of the LTS101 Combustor with the QCGAT Combustor

expense of the other to achieve the desired combination.

The NO<sub>x</sub> emission goal was considered the most difficult to achieve. Because these emissions increase with pressure ratio, the 10:1 pressure ratio was a main consideration for the QCGAT compressor design. The high-bypass ratio also favors lower emissions for a given thrust rating.

The final combustor configuration culminated in a design that incorporated the optimum cycle characteristics, along with a unique vortex recirculation pattern that results in a lower rate of NO<sub>x</sub> increase with increasing combustor inlet temperature than for conventional combustors. This characteristic permits selection of high combustor efficiencies at idle with resulting low UHC and CO values without exceeding NO<sub>x</sub> values at high power settings. Typical combustion flow pattern and air distribution are shown in Figure 73.

#### 4.6.1 Test Rig and Facilities

Limited development effort was required to meet the emission goals and obtain a good turbine inlet temperature distribution, while maintaining adequate liner life.

The combustor test rig is shown schematically in Figure 74; a view of a cell installation is included. Instrumentation locations that can also be seen include pressure and temperature at the inlet and exit planes. A rotating drum arrangement was used in the exit plane as a traversing mechanism to obtain temperature data.

Airflow was supplied at engine operating pressures and temperatures by the facility compressors. Airflow measurement was accomplished with a standard ASME orifice arrangement. Fuel flow was measured with turbine flow meters. Exhaust emissions analysis equipment that was used complied with EPA Standard 40 CFR, Part 87 and was used to calculate combustion efficiency, as well as measure unburned hydrocarbon, carbon dioxide, oxides of nitrogen, and carbon monoxide. Carbon balance calculations were made and compared with fuel and air measurements to verify a representative sample.

#### 4.6.2 Test Sequence

The initial test was conducted with an existing LTS 101 liner to determine the optimal injector immersion and the flow-divider split. Also, the effects of combustor airbleed at idle and liner wall temperature

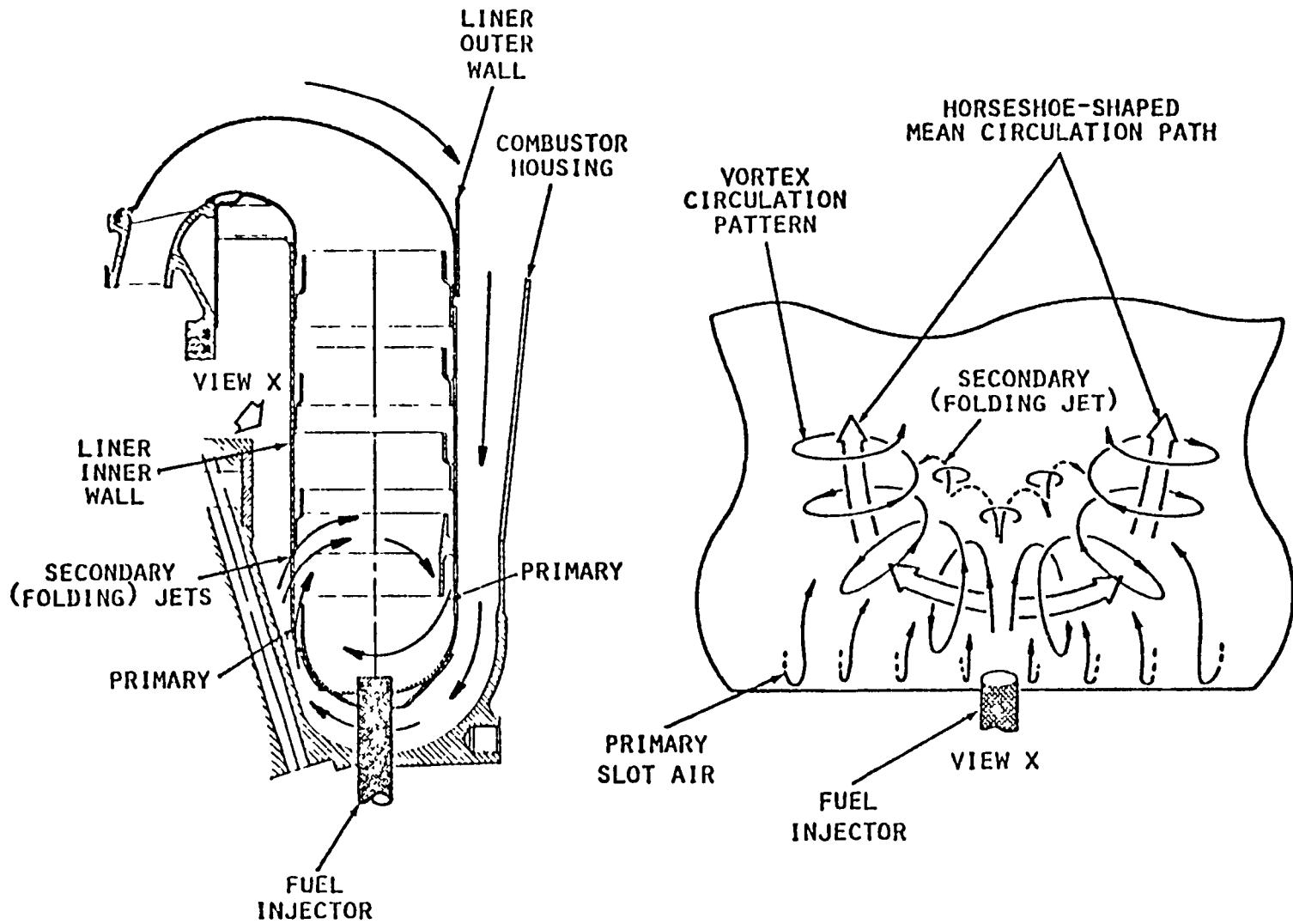


Figure 73. Circumferentially Stirred Combustor Flow Pattern

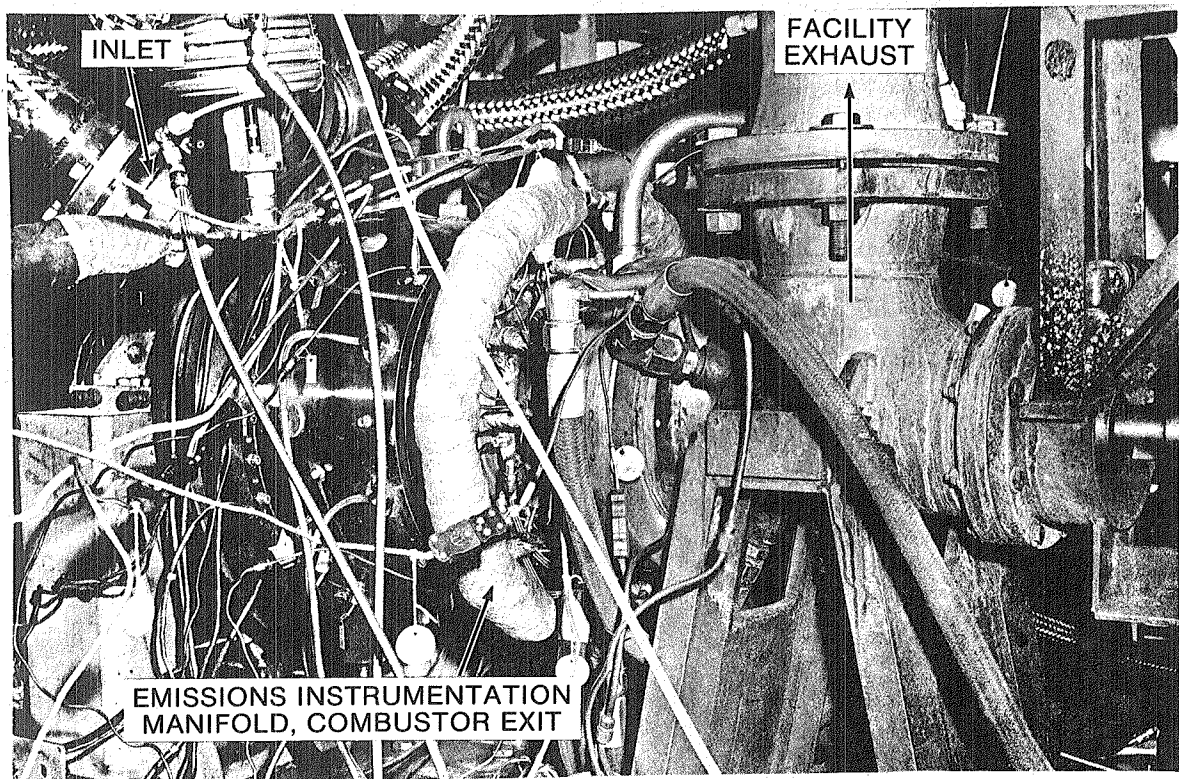
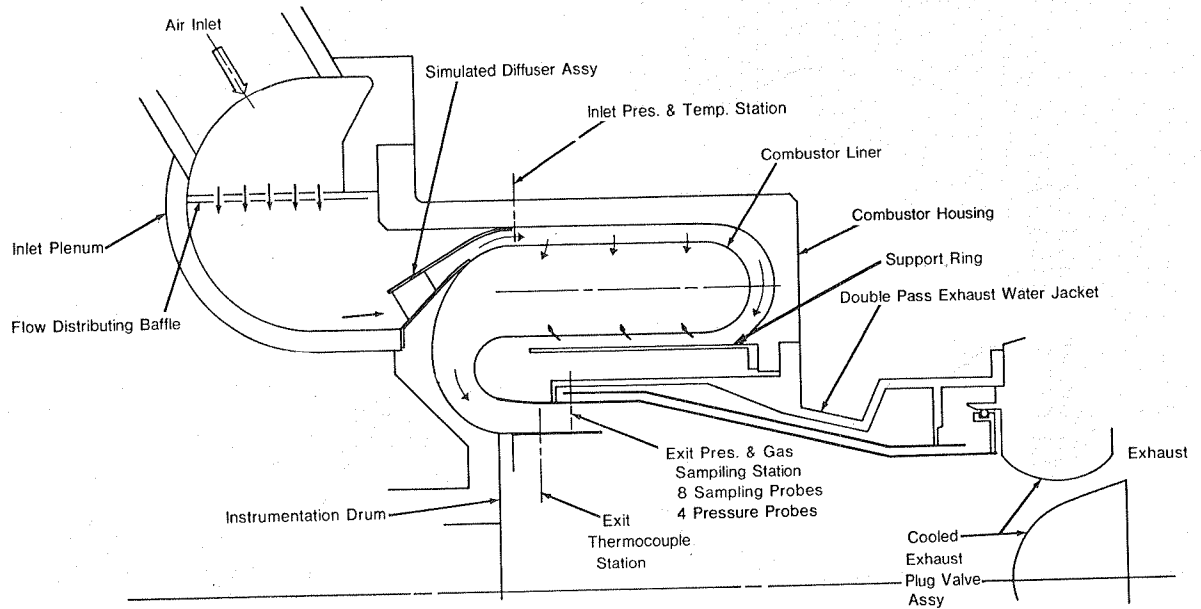


Figure 74. QCGAT Annular Combustor Test Rig and Test Cell Installation



were evaluated. Test points were those defined by the EPA; these included idle, approach power, 90 percent and take-off powers.

The next test phase was conducted with a liner modified in accordance with the initial test results. The effects of changes in the cooling flow network by air partitioning on emissions at all engine operating conditions were evaluated. Liner temperature measurements and temperature paint tests were made at take-off power. Liner and curl durability were evaluated after each high-pressure test.

#### 4.6.3 Test Results

Emission calculations using the taxi-idle and take-off power test points gave EPAP values equivalent to 45 percent of the UHC, 88 percent of the CO, and 101 percent of the NO<sub>x</sub> requirements. Figure 75 presents the effect of air-partition modifications on NO<sub>x</sub>. Initial tests indicated the NO<sub>x</sub> results were within design goals. However, as the combustor pressure drop was increased to reduce smoke, levels increased. The cooling flow network was then modified by air partitioning to meet the NO<sub>x</sub> emission goal.

The QCGAT liner finally selected to meet design goal has a slightly steeper slope, as depicted in Figure 75. The Lipert correlation, (Reference 9) for conventional combustors is for comparison.

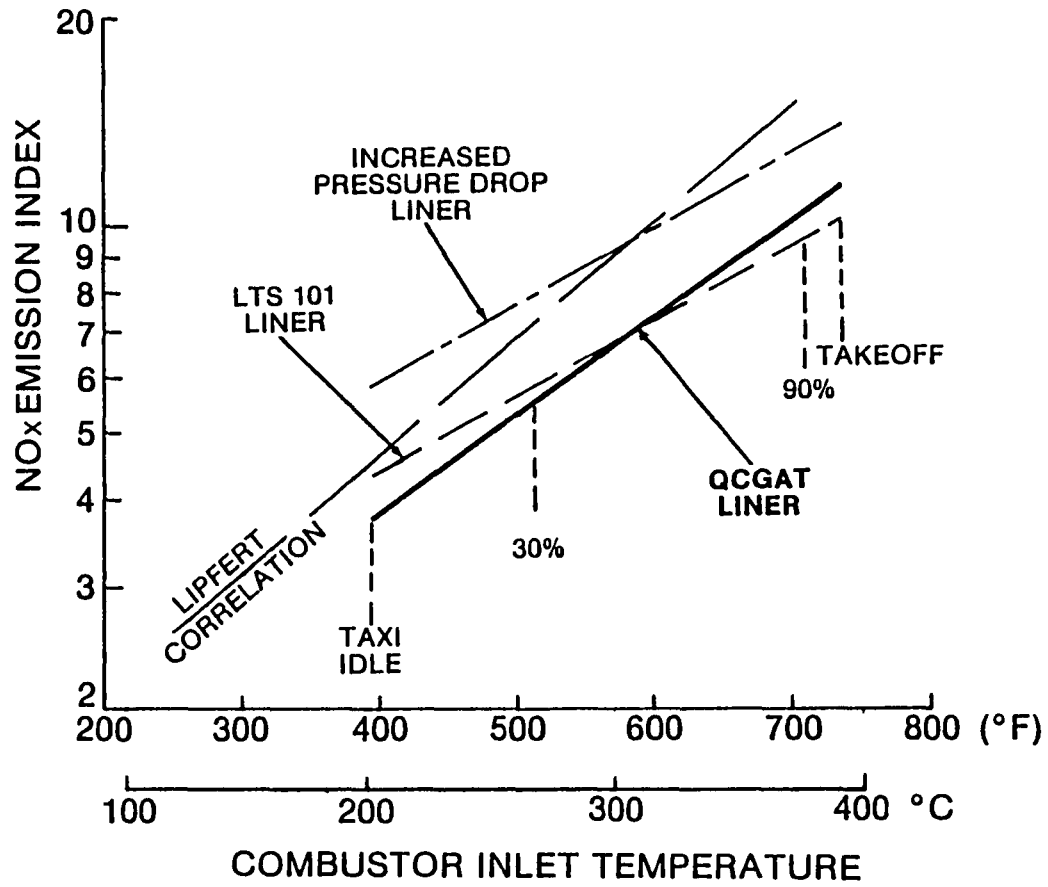


Figure 75. NO<sub>x</sub> Versus Combustor Inlet Temperature

## 5.0 ENGINE/NACELLE SYSTEMS PERFORMANCE

### 5.1 OVERALL PERFORMANCE

The QCGAT engine was configured to reduce overall emissions and noise levels without seriously impacting the advanced performance goals for the cycle. The design objective for the QCGAT engine program was to provide a minimal fuel consumption in a cruise condition of 7620m (25,000 ft) altitude at a Mach No. of 0.6 without sacrificing one-engine inoperative capabilities. Design and trade-off studies were performed to define the optimum cycle in terms of noise, emissions, and performance. The selected design cycle, resulting from the study, is presented in Table 3.

The QCGAT engine installed performance goals for the two prime flight conditions are shown in Table 4. This installed performance is with the nacelle system including the flight lip, mixer nozzle and acoustic treatment. The sea level static takeoff thrust is 7166 N (1611 lbf) and specific fuel consumption is 0.037 kg/hr/N (0.363 lbf/hr/lbf). For the 7620 m (25,000 ft) Mach 0.6 cruise, the thrust is 2157 N (485 lbf) and specific fuel consumption is 0.064 kg/hr/N (0.628 lbf/hr/lbf).

A mixer nozzle, Reference 8, was chosen for the engine configuration because of acoustic and performance reasons. Figure 76 presents the estimated variations of specific fuel consumption, along an engine operating line, with total net thrust at the selected cruise condition, for the split and forced mixer exhaust systems. As shown, a potential performance gain, at the cruise thrust, of approximately 3.0 percent could be realized with a mixer.

#### 5.1.1 Component Performance

The Avco Lycoming LTS 101 turboshaft engine was selected as the basic core for QCGAT engine. Core component modifications, required to meet QCGAT design goals, were Lycoming funded. The major components developed, under the NASA contract, were the fan module, reduction gearing, and the nacelle system which includes the forced mixer nozzle. The fan and nacelle were designed with low noise as a primary criteria. In addition, combustor system modifications were made, as required, to meet the emissions goals.

The core compressor was tested to establish mechanical and aerodynamic performance with the turbofan inlet duct. The compressor per-

TABLE 3. RESULTS OF DESIGN STUDY

**ALTITUDE = 7620m(25,000 FT), MACH = 0.6**

	<u>SELECTED DESIGN</u>
Fan Pressure Ratio	1.36
Cycle Pressure Ratio	13.7
Core Compressor Pressure Ratio	10.3
Thrust/Total Airflow, N/kg/sec(lbf/lbm/sec)	113.7(11.6)
Bypass Ratio	9.4

TABLE 4. QCGAT PERFORMANCE GOALS

**(STANDARD DAY, INSTALLED)**

Rating	<u>SEA LEVEL STATIC</u>	<u>7620m(25,000 ft) MACH = 0.6</u>
	Takeoff	Cruise
Thrust, N(lbf)	7166(1611)	2157(485)
SFC, kg/hr/N(lbm/hr/lbf)	0.0370(0.363)	0.0640(0.628)

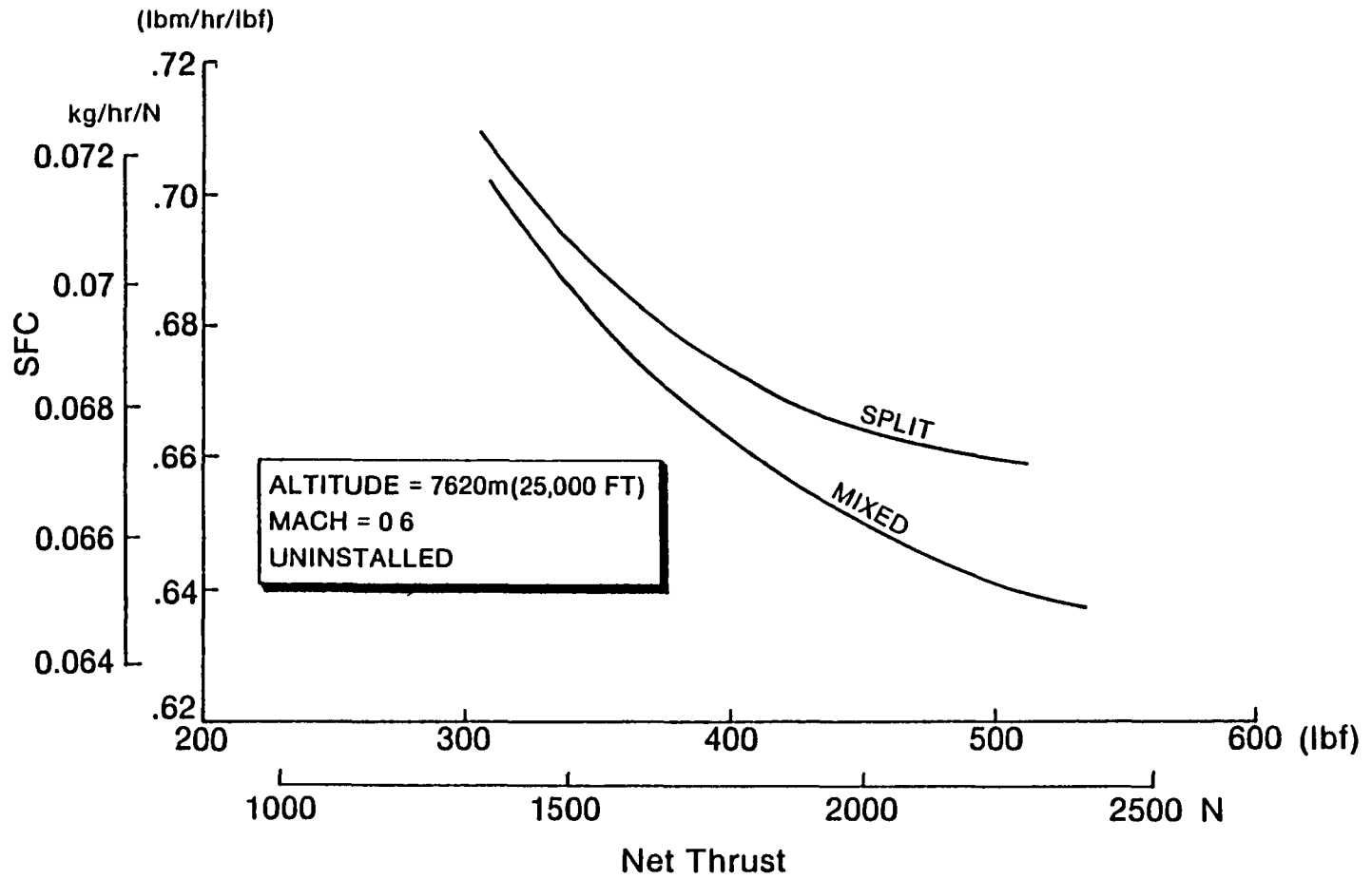


Figure 76. Predicted Influence of the Mixer

formance and surge characteristics with pressure distortion as measured during the fan component testing were also established. The rig test results showed that the compressor efficiency was within 1.0 percent of the design goal. The compressor showed high tolerance to pressure distortion produced by the fan. Also, the turbofan inlet duct caused a reduction in airflow to the compressor of 1.0 percent at the QCGAT operating conditions.

Rig tests on the initial gas producer turbine hardware confirmed that the design efficiency of this stage was met within 1.0 percent. However, the nozzles were substantially larger in flow area than design. An attempt was made to correct for flow size, by reducing the annulus area formed by the inner and outer wall contour. This corrected the flow area problem but caused cascade losses which reduced stage performance by approximately 3 points.

In addition, the interturbine duct pressure losses increased because of a resulting change in the turbine exit swirl angle. A redesign of the nozzle and rotor, to recover gas producer efficiency, was completed, and further component and engine performance verification program is continuing.

An experimental evaluation of the QCGAT fan module has shown that the bypass performance has exceeded design goals. (See discussion in Section 4.5 ). At the design pressure ratio (1.38) and speed (11,200 rpm), stage polytropic efficiency of 0.875 was demonstrated. This exceeded the design goal efficiency of 0.870. Bypass airflow at this point was 33.7 kg/sec (74.3 lbm/sec) compared with a goal of 33.6 kg/sec (74.0 lbm/sec).

The low pressure turbine, which was not rig tested, appeared to perform as anticipated based on measured engine data.

Engine performance estimates obtained from math model simulations, based upon component test results, showed that further component development of the core, was required to achieve performance goals. Lycoming is continuing the core development.

However, as a result of the analysis, it was concluded that the Lycoming QCGAT engine was a viable vehicle for demonstrating noise, emissions and specific fuel consumption improvements which were the program's prime objectives.

## 5.1.2 Full Engine Tests

### 5.1.2.1 Engine Configurations and Test Plan

Following the component rig tests, the full engine and nacelle system tests were conducted. Two engine configurations have been tested. The referee configuration consists of a calibrated bellmouth followed by a straight inlet duct to the fan shroud as shown in Figure 77.

In the exhaust system, the bypass and core flows are physically separated, (See Figure 78). Separate exhaust nozzles permit individual change of fan pressure ratio and variation of the power split between the fan and core.

The QCGAT test nacelle configuration, shown in Figure 79, has the flight inlet lip and diffusing duct mounted to the fan shroud. The flight lip can be readily interchanged with the bellmouth or the approach simulator inlets. (See Figure 80) Details of the test nacelle are shown in Figure 81. The diffusing duct following the inlet contains interchangeable hardwall or acoustically treated softwall liners. The nacelle rear section consists of a core cowl covering the core engine while providing a smooth aerodynamic inner wall contour for the fan flow surrounding the core. The common mixed exhaust nozzle clamps to the rear face of the fan frame and contains the removable duct portion of either hardwall or softwall panels.

Various combinations of the two basic engine configurations, the referee and test nacelle, were tested during the performance calibration sequence. Table 5 shows an overview of the seven prime engine configurations which were tested in order to determine the performance characteristics of the engine and nacelle system components. Prior to these tests, a baseline engine configuration was tested with a calibrated bellmouth coupled to a constant area duct and split exhaust.

The first three configurations, listed Table 5 with the split, or referee exhaust system, were tested with the diffusing flight inlet duct and the various interchangeable inlet lips.

All tests with the split exhaust were performed without the acoustic panels. The referee configuration with a bellmouth inlet was also used for the emissions sampling.



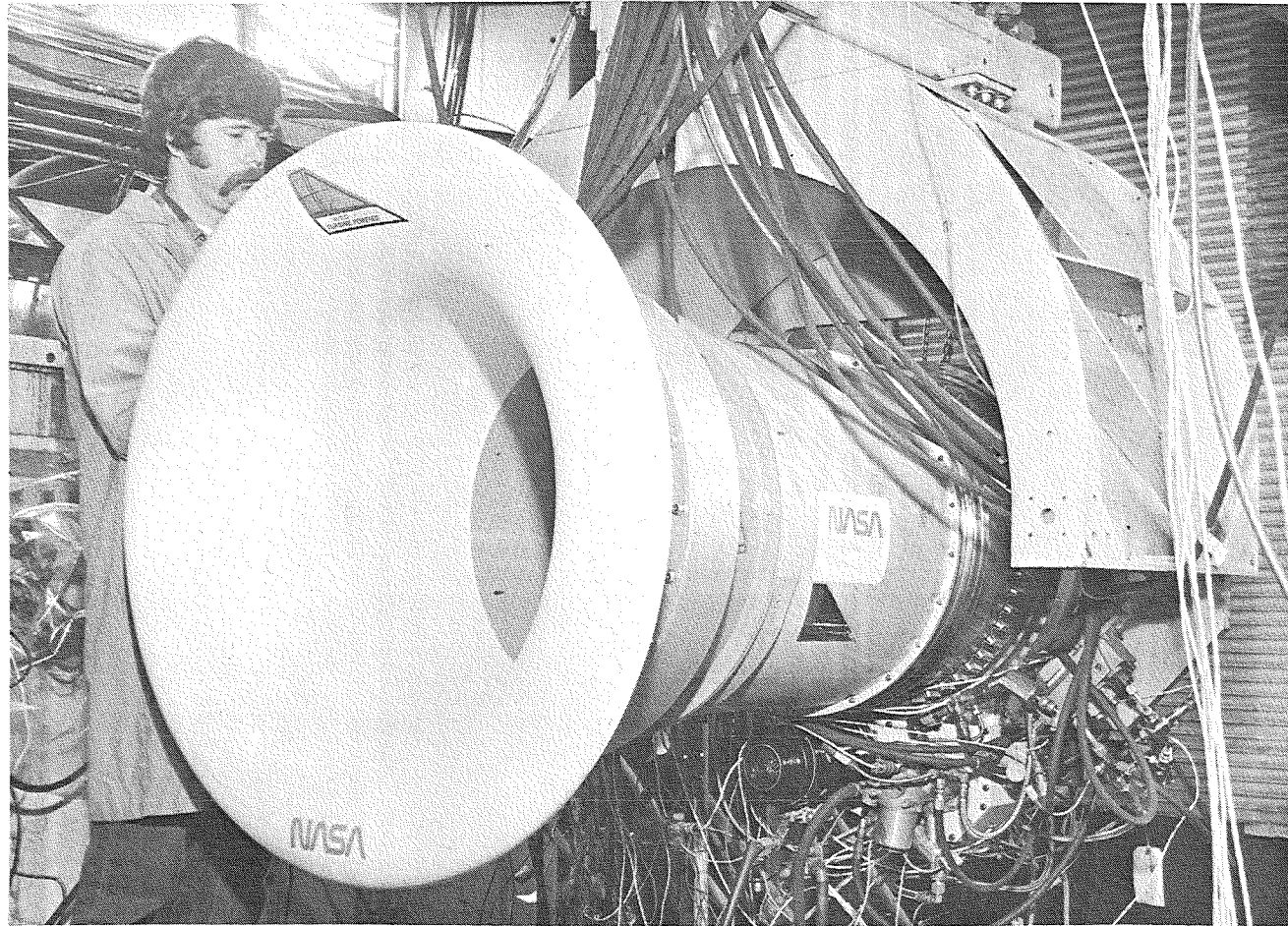


Figure 77. QCGAT Referee Configuration - Inlet

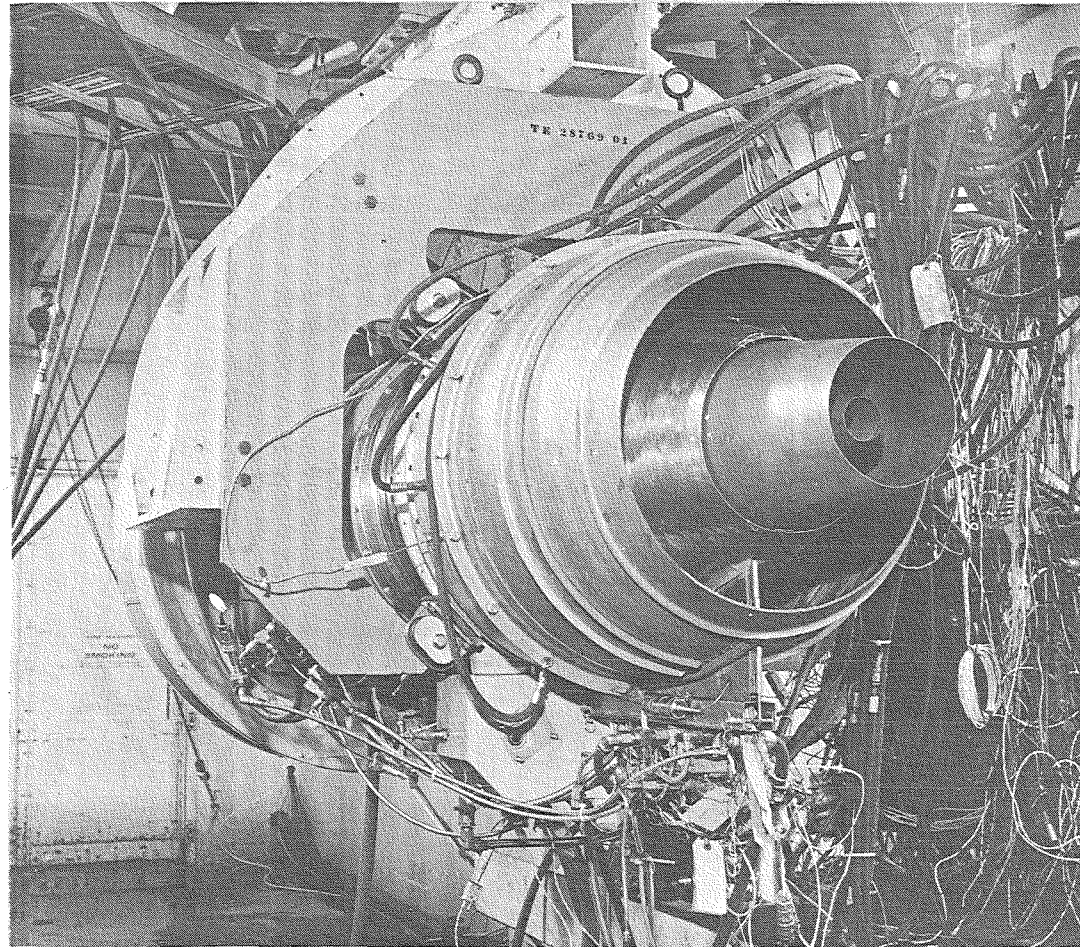


Figure 78. QCGAT Referee Configuration - Exit

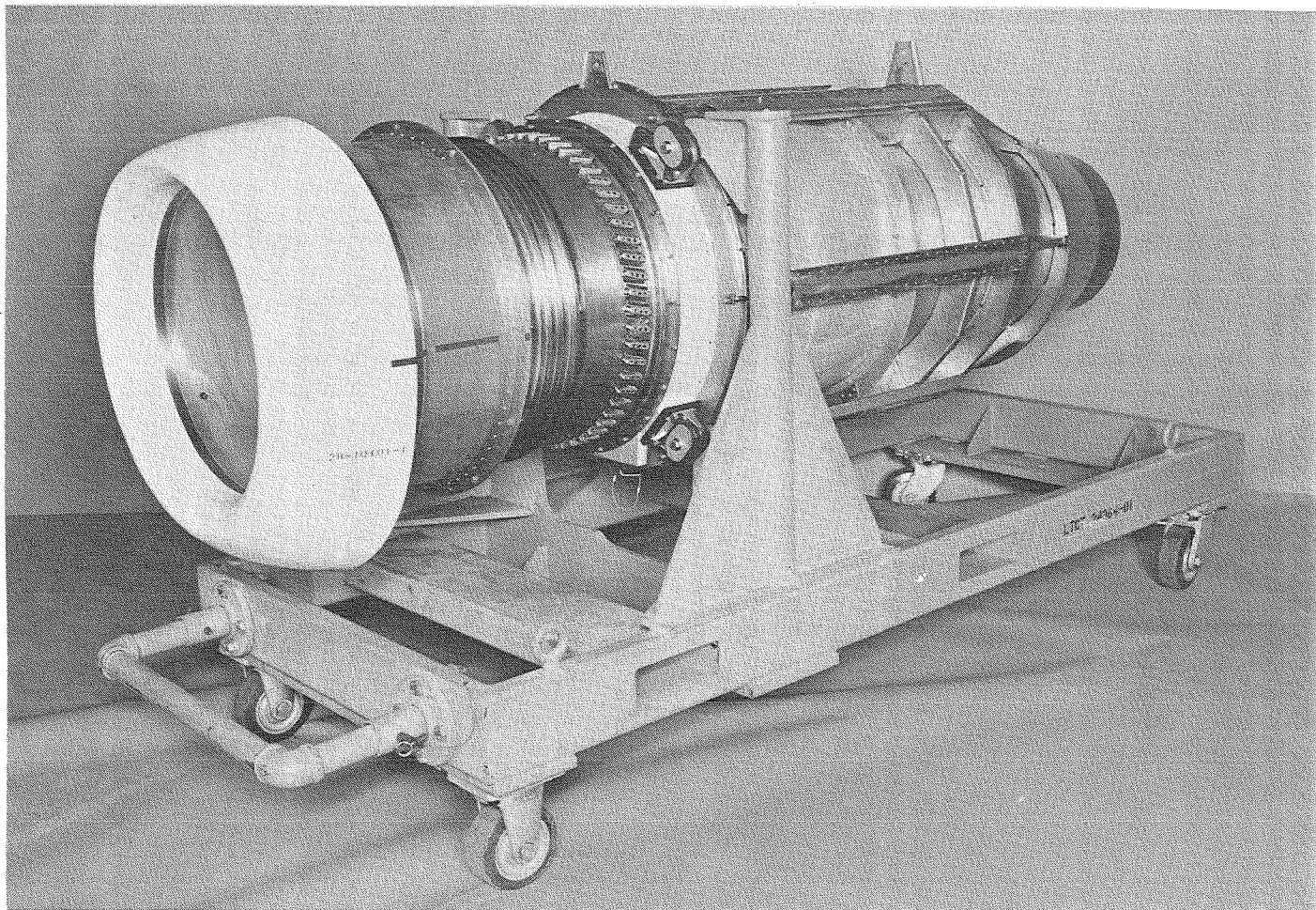
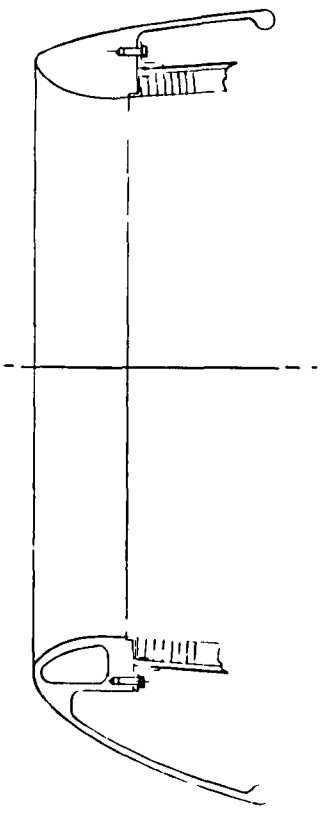
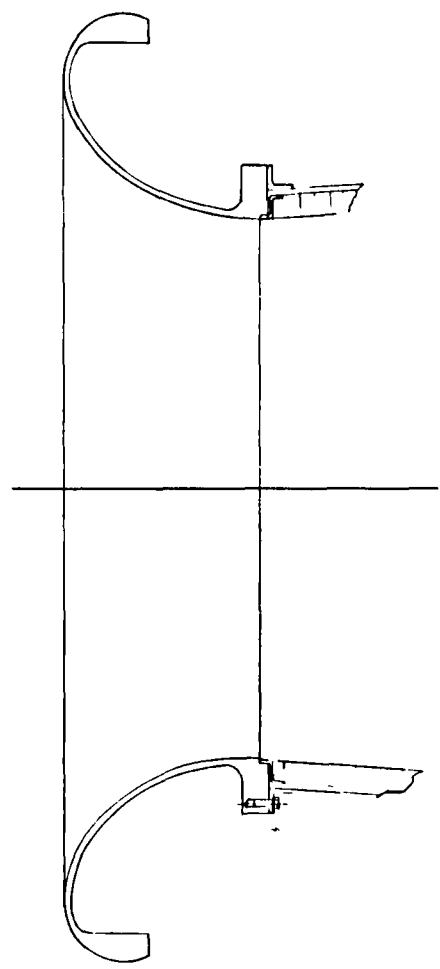


Figure 79. QCGAT Test Nacelle

**FLIGHT  
NACELLE**



**SYMETRICAL  
BELLMOUTH**



**APPROACH  
SIMULATOR**

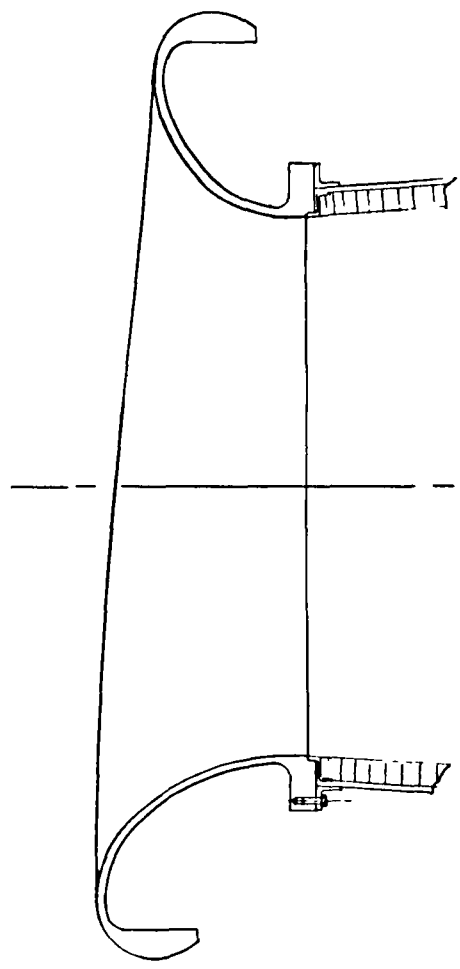


Figure 80. Replaceable Inlet Lips

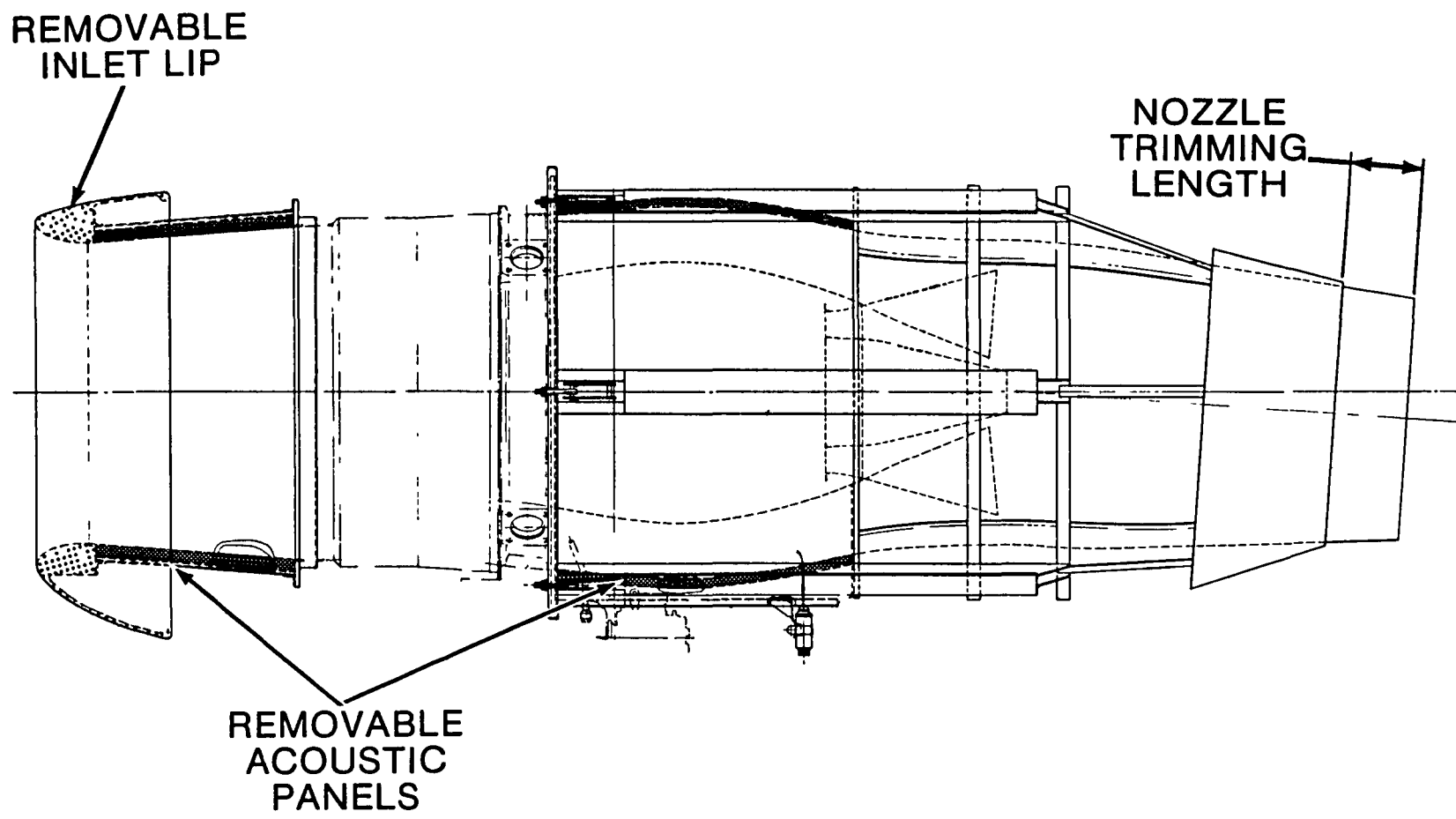


Figure 81. Details of the Test Nacelle

TABLE 5. ENGINE CONFIGURATIONS TESTED

**(PERFORMANCE TESTS)**

<u>ENGINE CONFIGURATION</u>		<u>ACOUSTIC TREATMENT</u>	
<u>INLET</u>	<u>EXHAUST</u>	<u>INLET</u>	<u>BYPASS</u>
<b>REFEREE CONFIGURATION</b>			
*Bellmouth	Split	Hardwall	Hardwall
Flight	Split	Hardwall	Hardwall
Approach Simulator	Split	Hardwall	Hardwall
<b>TEST NACELLE</b>			
Bellmouth	Mixer	Hardwall	Hardwall
Bellmouth	Mixer	Softwall	Hardwall
Bellmouth	Mixer	Softwall	Softwall
Flight	Mixer	Softwall	Softwall

\*Emission Test Configuration

The test nacelle configuration with the mixed exhaust was initially tested, for performance purposes, only with the bellmouth inlet. First, tests were conducted with hardwall panels in the inlet and fan bypass exhaust. Then, acoustic panels were placed in the inlet only. Finally, the engine was tested with acoustic panels in both the inlet and fan bypass exhaust. The installed performance demonstration was with the flight nacelle inlet, mixer nozzle and full acoustic treatment.

#### 5.1.2.2 Engine Tests Results

The purpose of the initial tests with the referee configuration was to evaluate mechanical engine operation and stress levels on fan and gear components.

Subsequent tests using the referee system, were conducted to evaluate overall engine and component performance prior to evaluating losses associated with acoustically treated nacelle system. Variations in performance attributed to the mixer system were also to be determined.

The purpose of these tests were twofold: First, to establish a base calibration for determining component performance. Second, to evaluate inlet pressure losses associated with the diffusing duct coupled to the various inlet lips.

Engine test data with the various inlet lips are presented in Figure 82 through 87. As previously stated, the engine tests, with the various inlet lips, were conducted in the early phases of the test program. Although the data, obtained from the initial tests, does not reflect the final performance characteristics of the engine, the data is valid for evaluating the impact of the inlet lips on the overall engine performance.

Detailed analysis of the test data has indicated that the diffusing duct and various inlet lips had a negligible impact on the overall engine performance.

Following the referee system performance and emissions tests, the installed nacelle test sequence was conducted. The purpose of these tests was two fold: first, to establish engine performance with a mixer nozzle; second, to evaluate the impact of the inlet and fan bypass exhaust acoustical panels on engine performance. The engine test results, as shown in Figures 88-93, indicated that the acoustical panels, used for noise reduction had a negligible influence on the overall engine performance. After the performance evaluation tests, the engine was

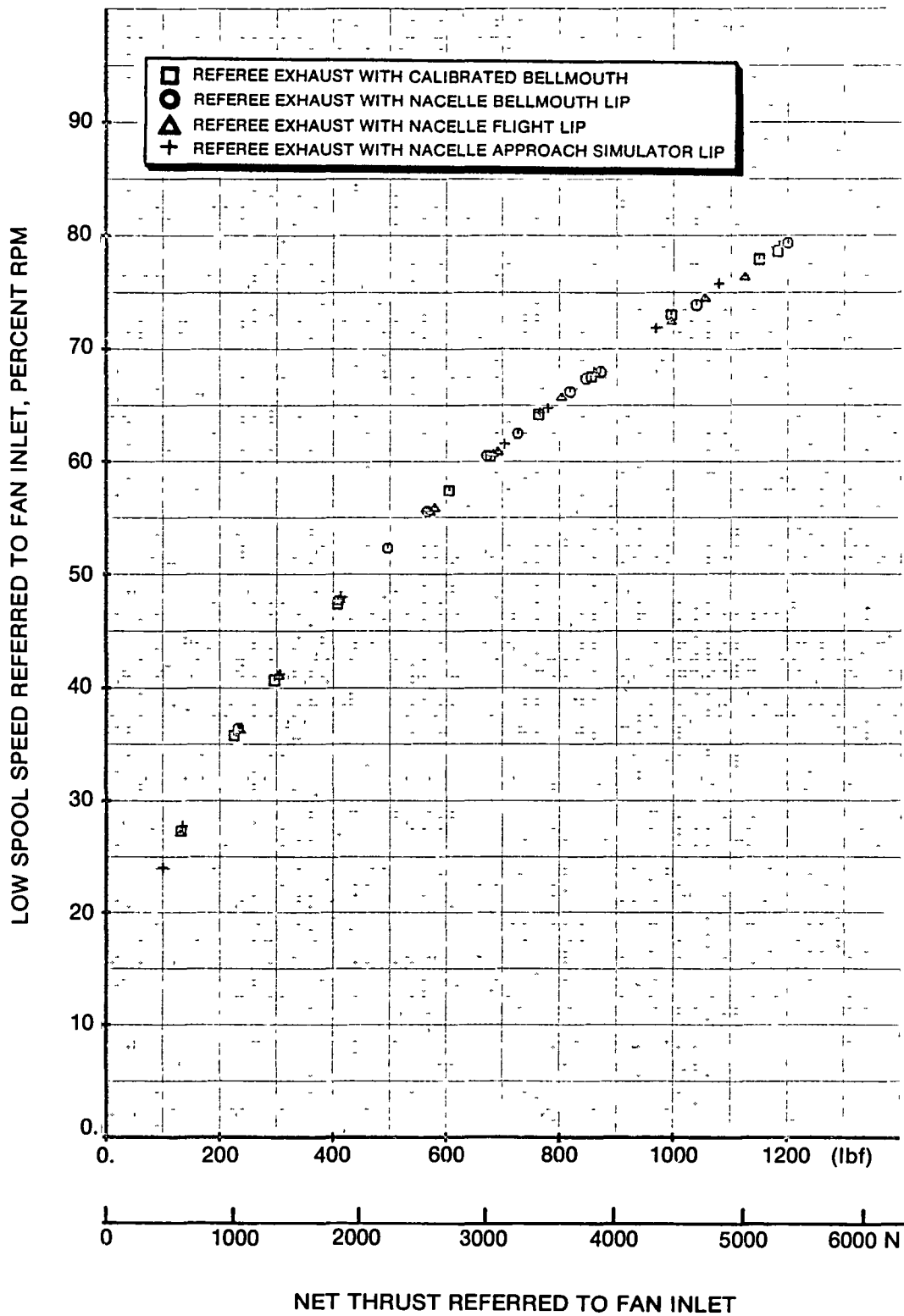
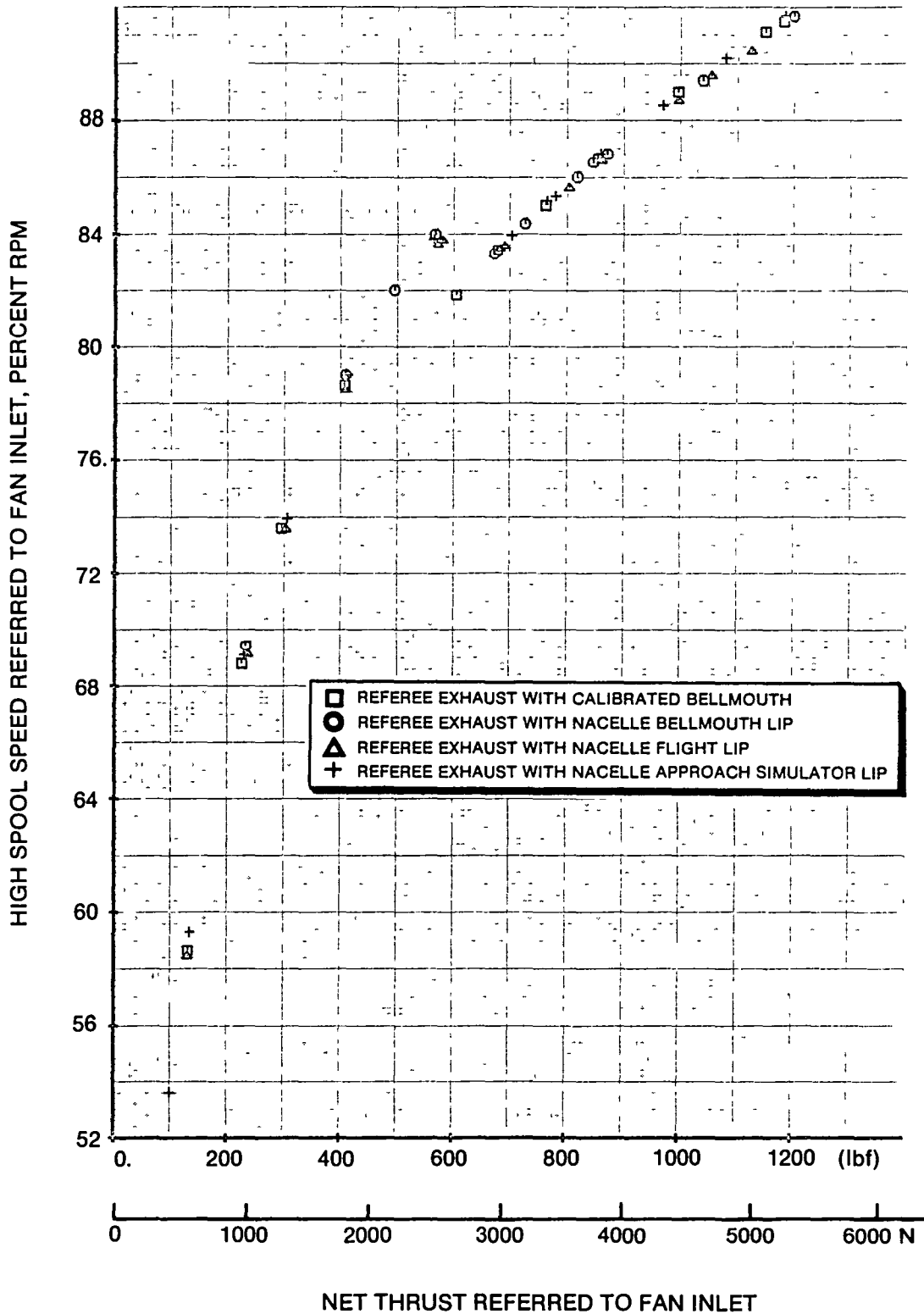
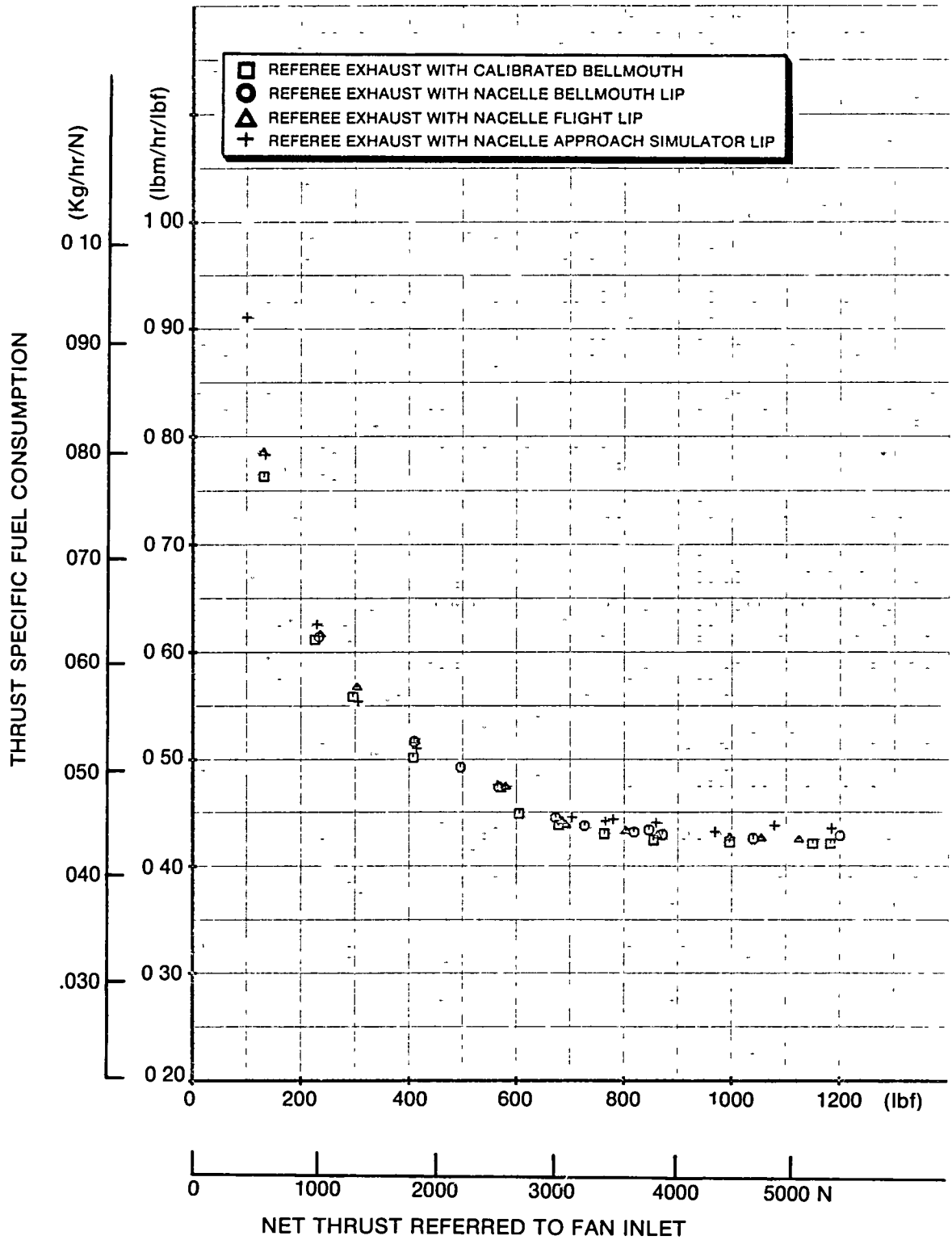


Figure 82. Low Spool Speed Versus Net Thrust







NET THRUST REFERRED TO FAN INLET  
 Figure 84. Thrust Specific Fuel Consumption Versus Net Thrust

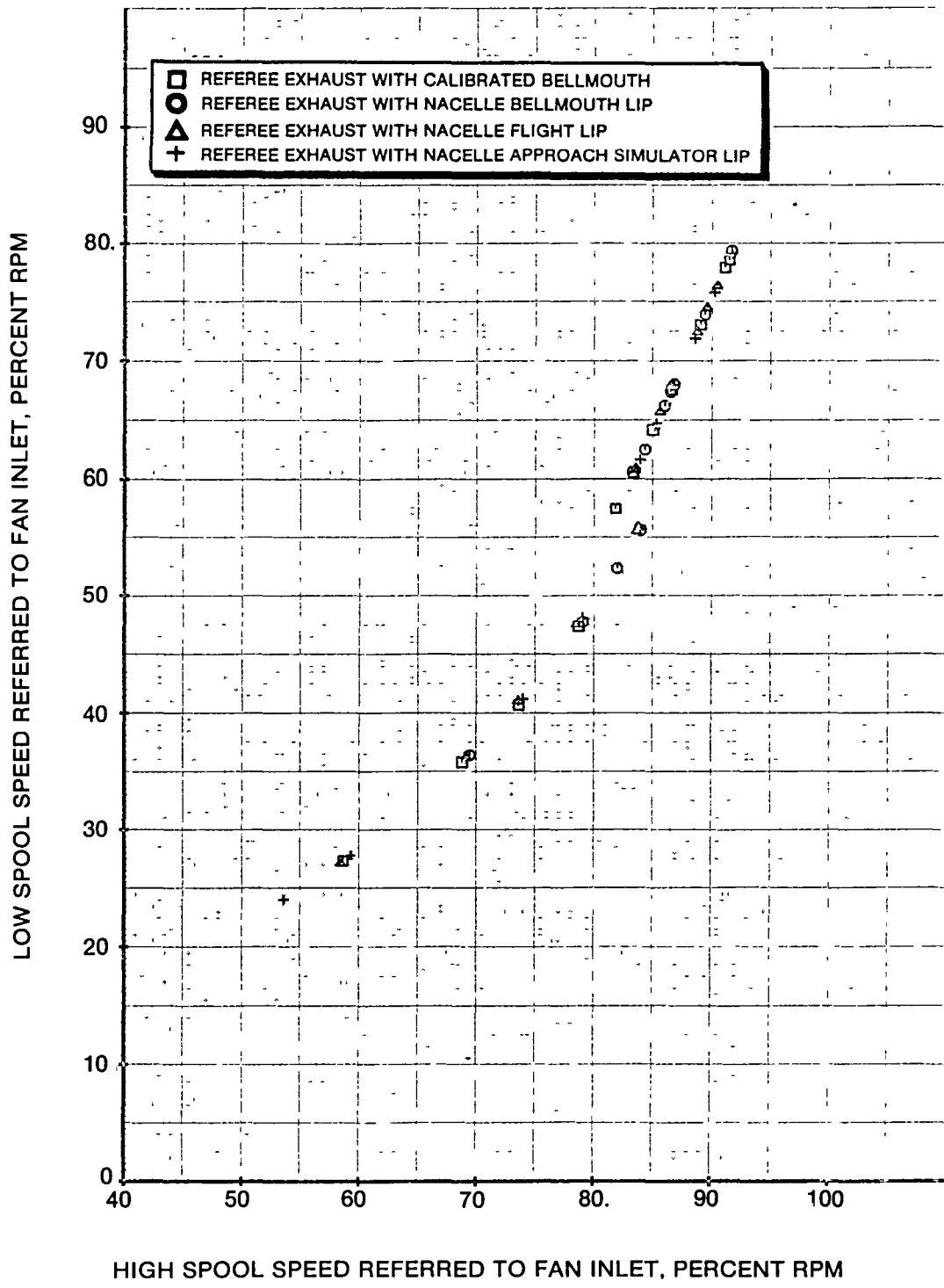


Figure 85. Low Spool Speed Versus High Spool Speed

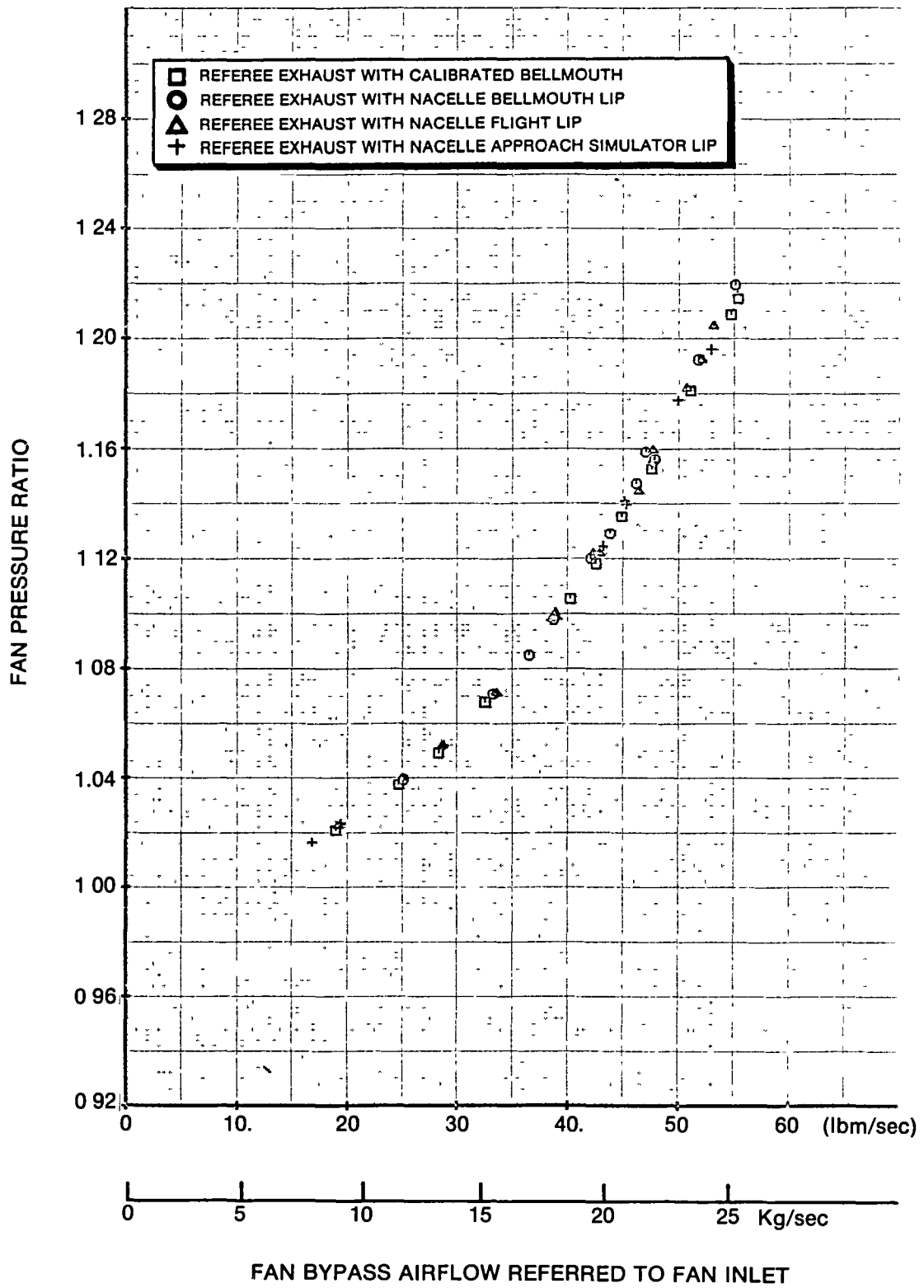


Figure 86. Fan Pressure Ratio Versus Fan Bypass Airflow

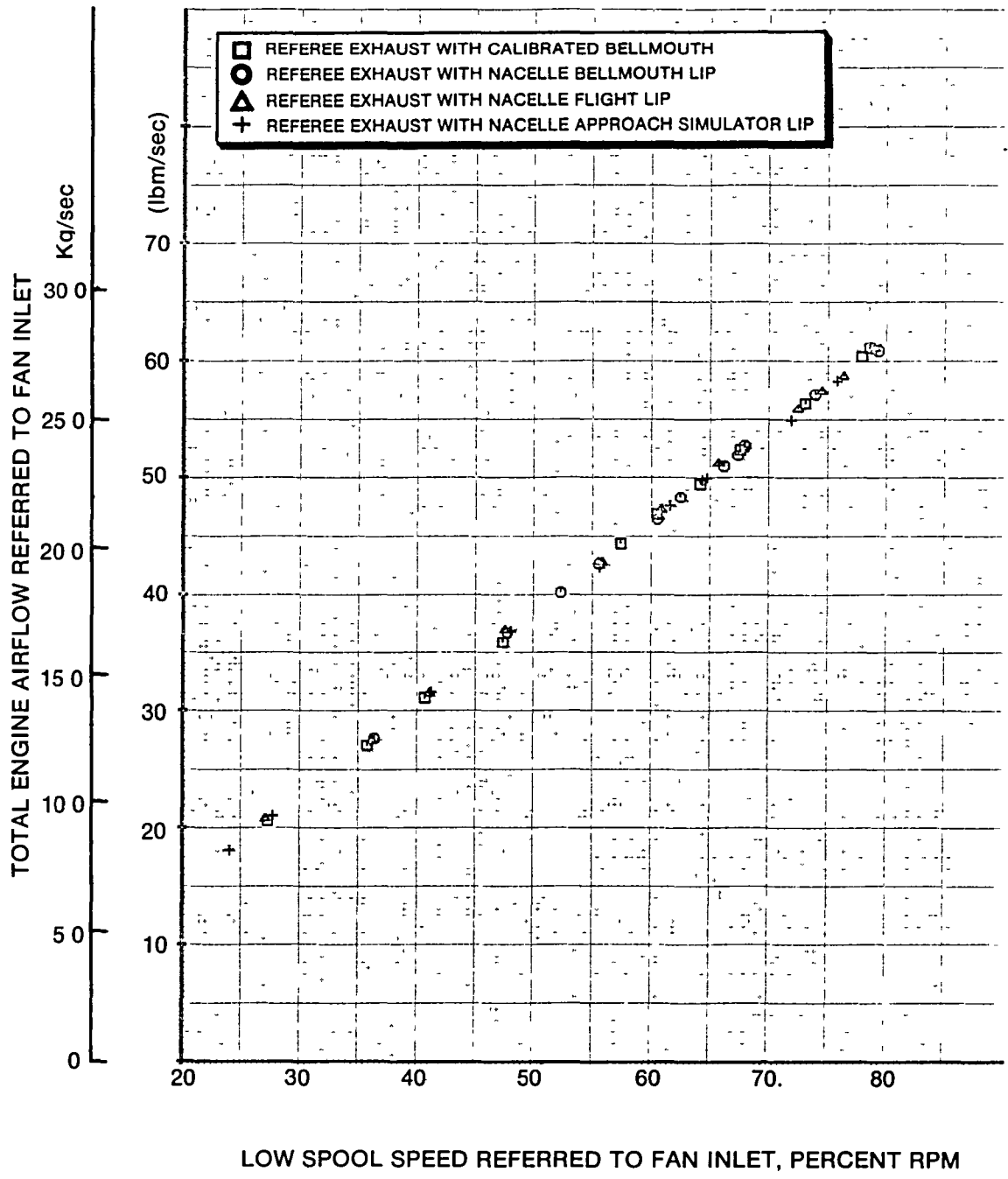


Figure 87. Total Engine Airflow Versus Low Spool Speed

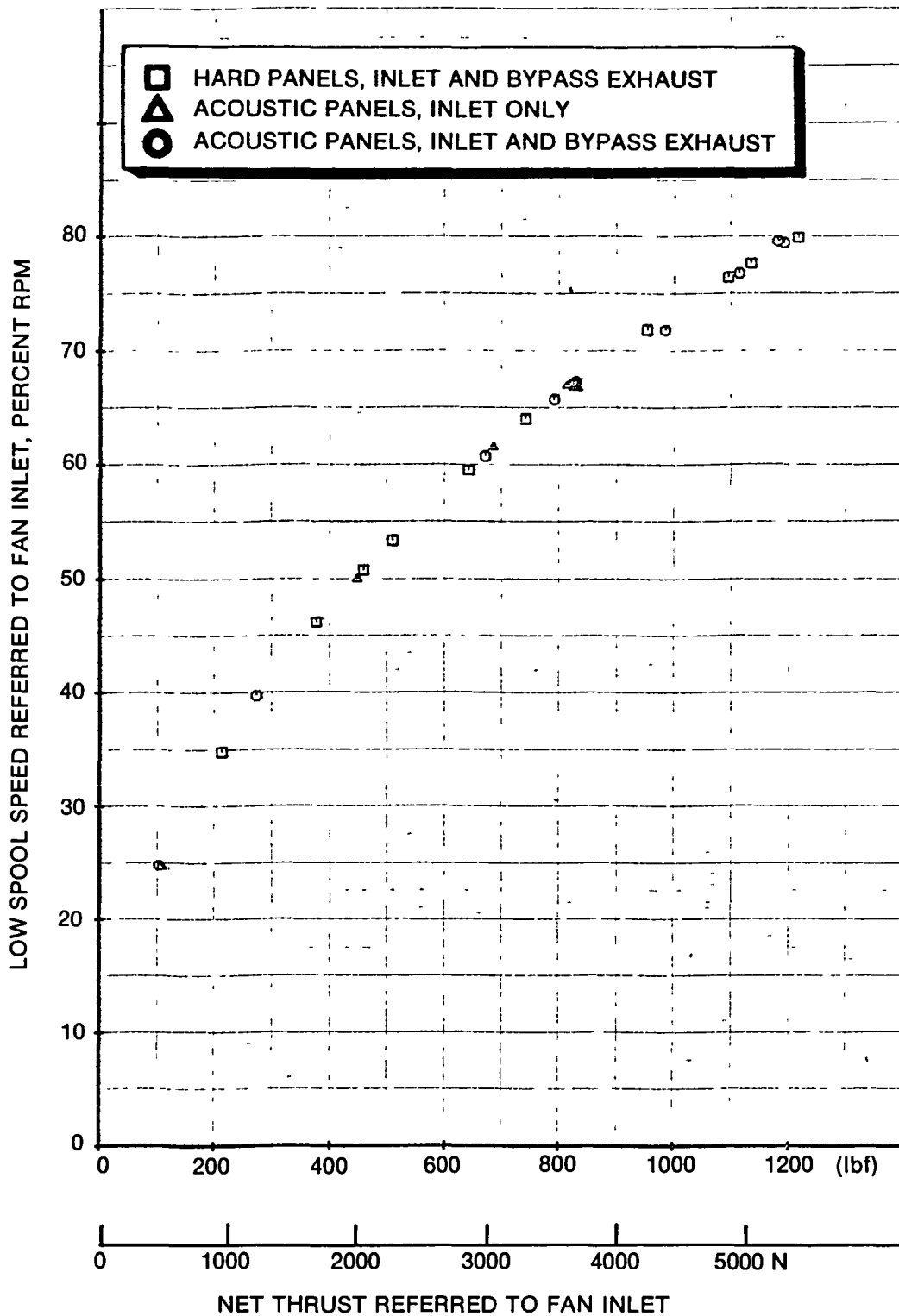


Figure 88. Low Spool Speed Versus Net Thrust - Nacelle Installed

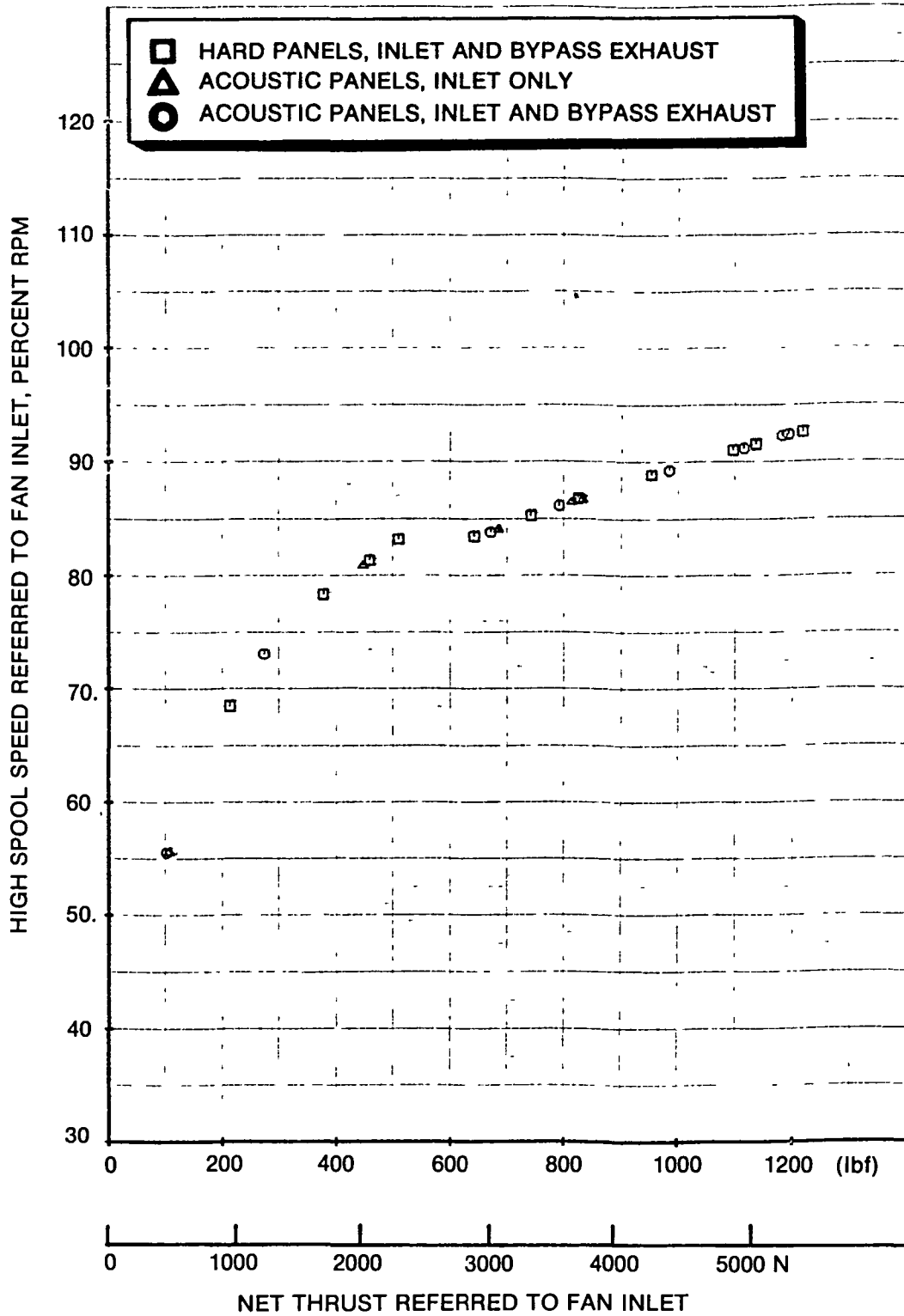


Figure 89. High Spool Speed Versus Net Thrust - Nacelle Installed

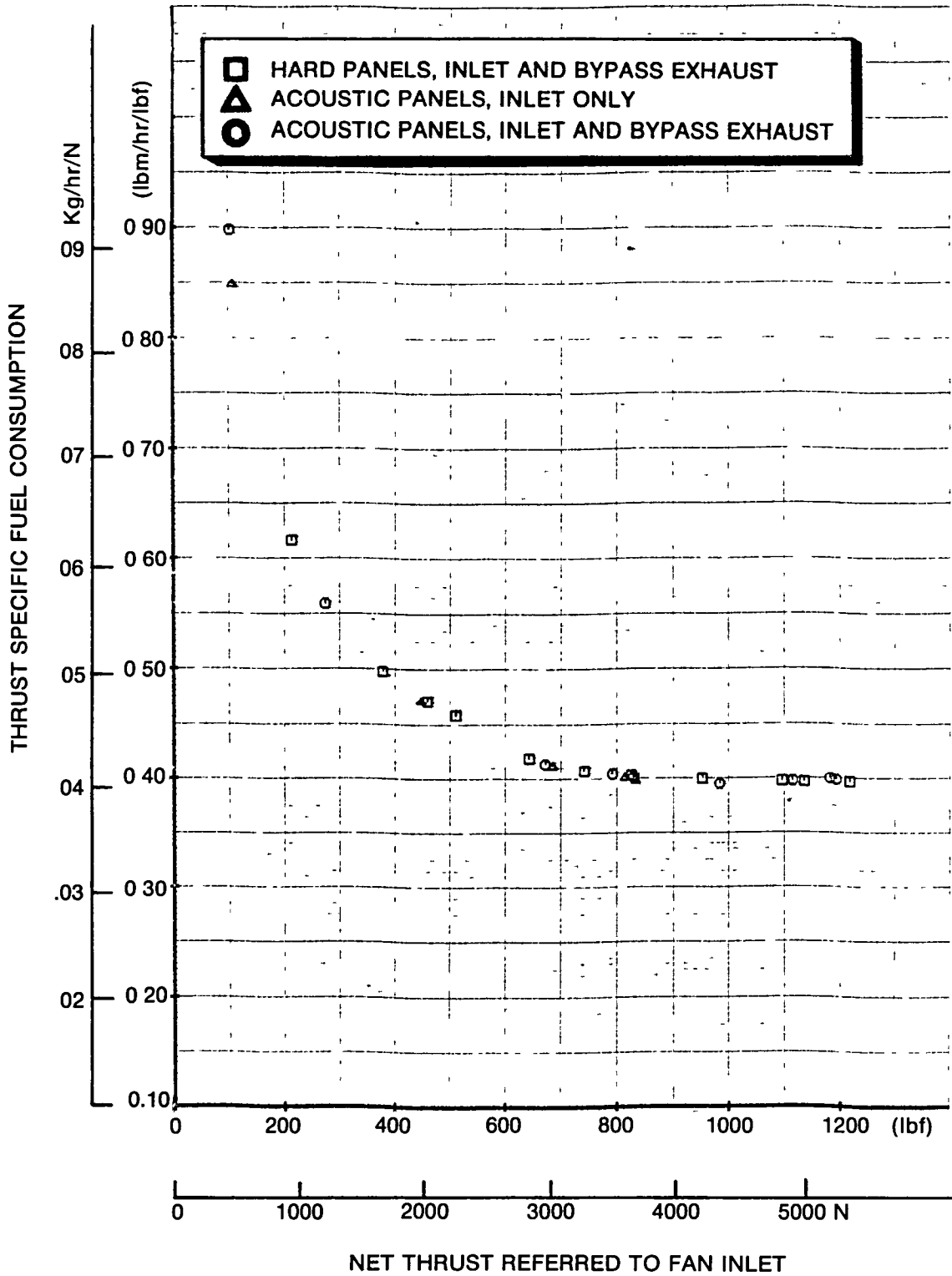


Figure 90. Thrust Specific Fuel Consumption Versus Net Thrust - Nacelle Installed



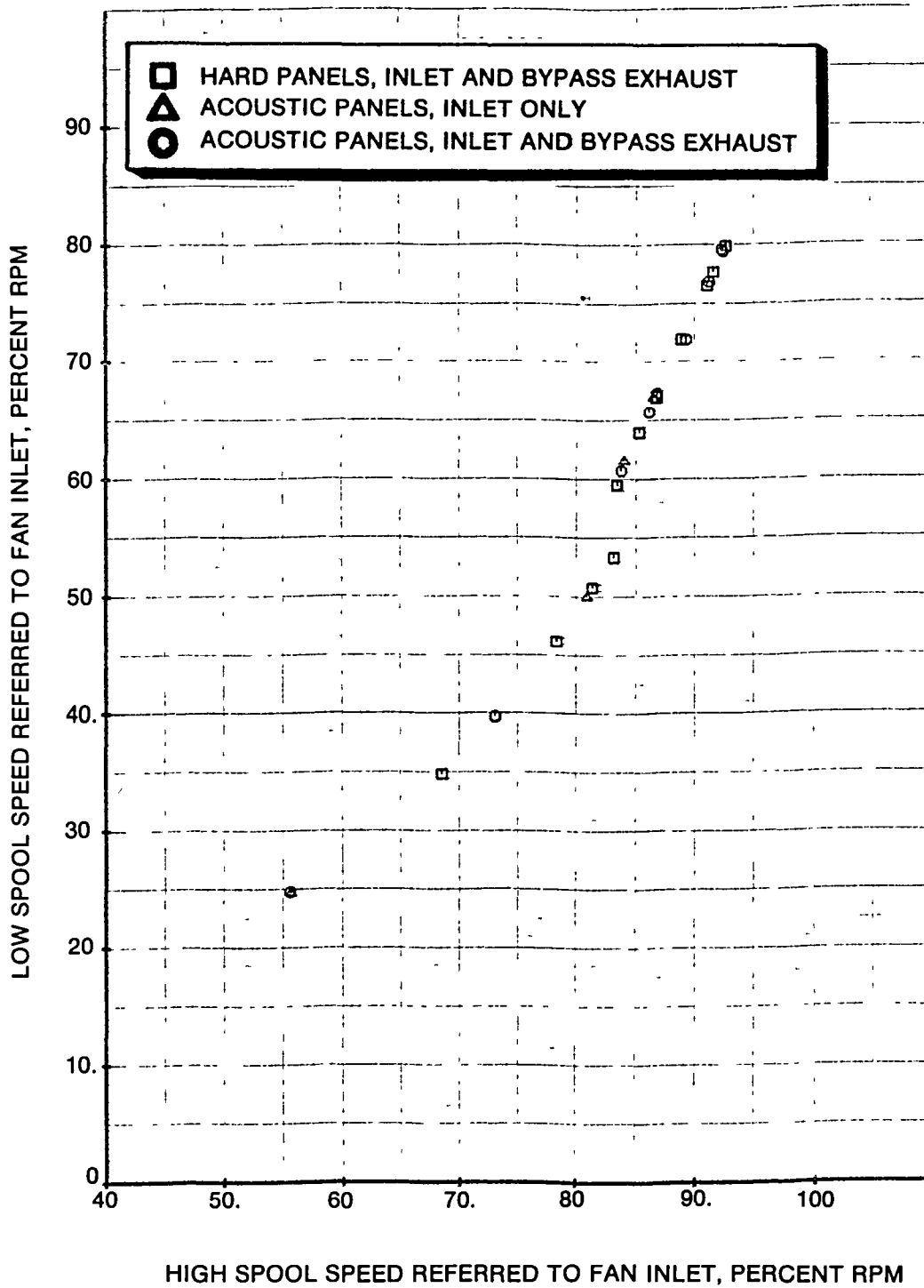


Figure 91. Low Spool Speed Versus High Spool Speed - Nacelle Installed

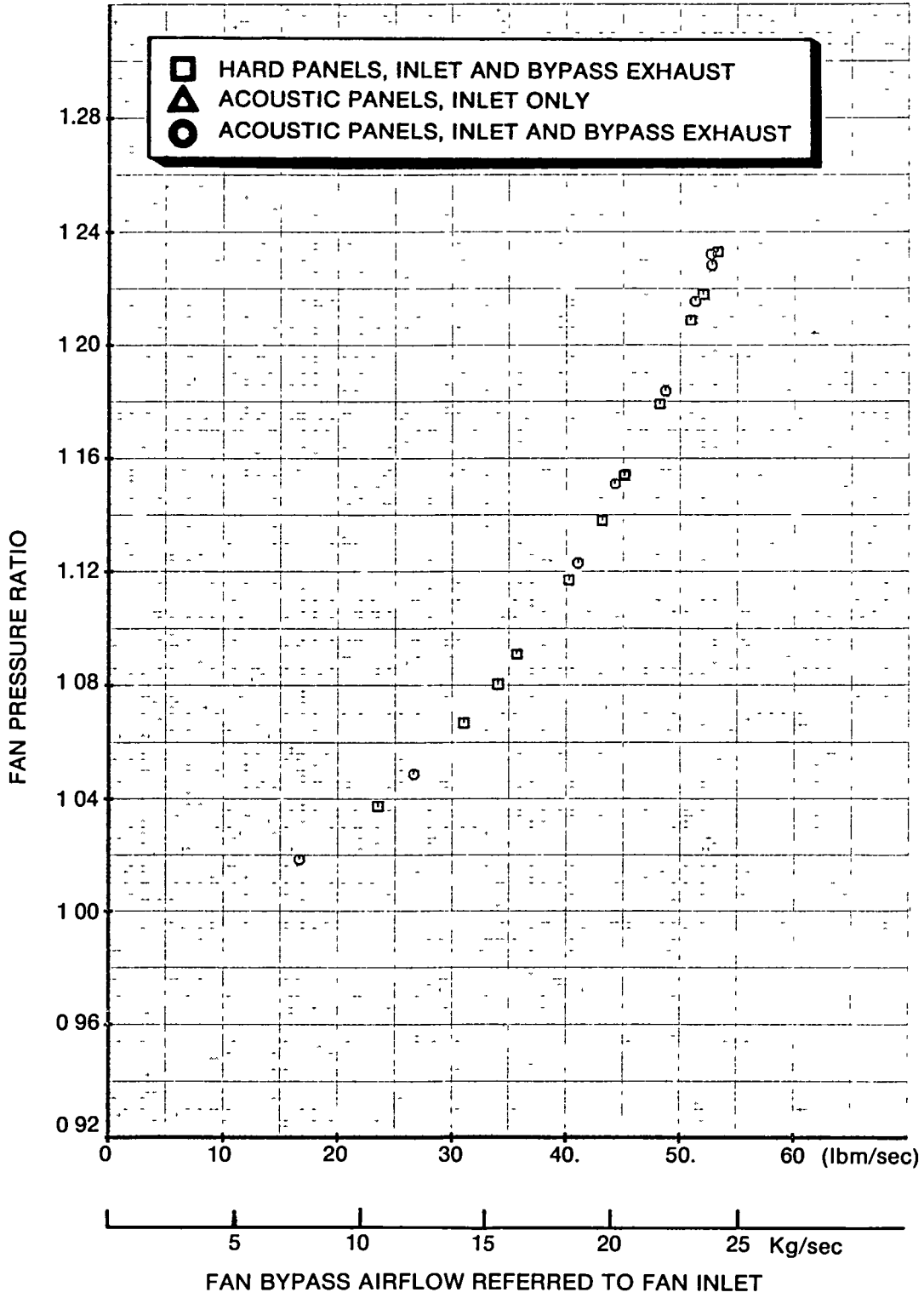


Figure 92. Fan Pressure Ratio Versus Bypass Airflow - Nacelle Installed

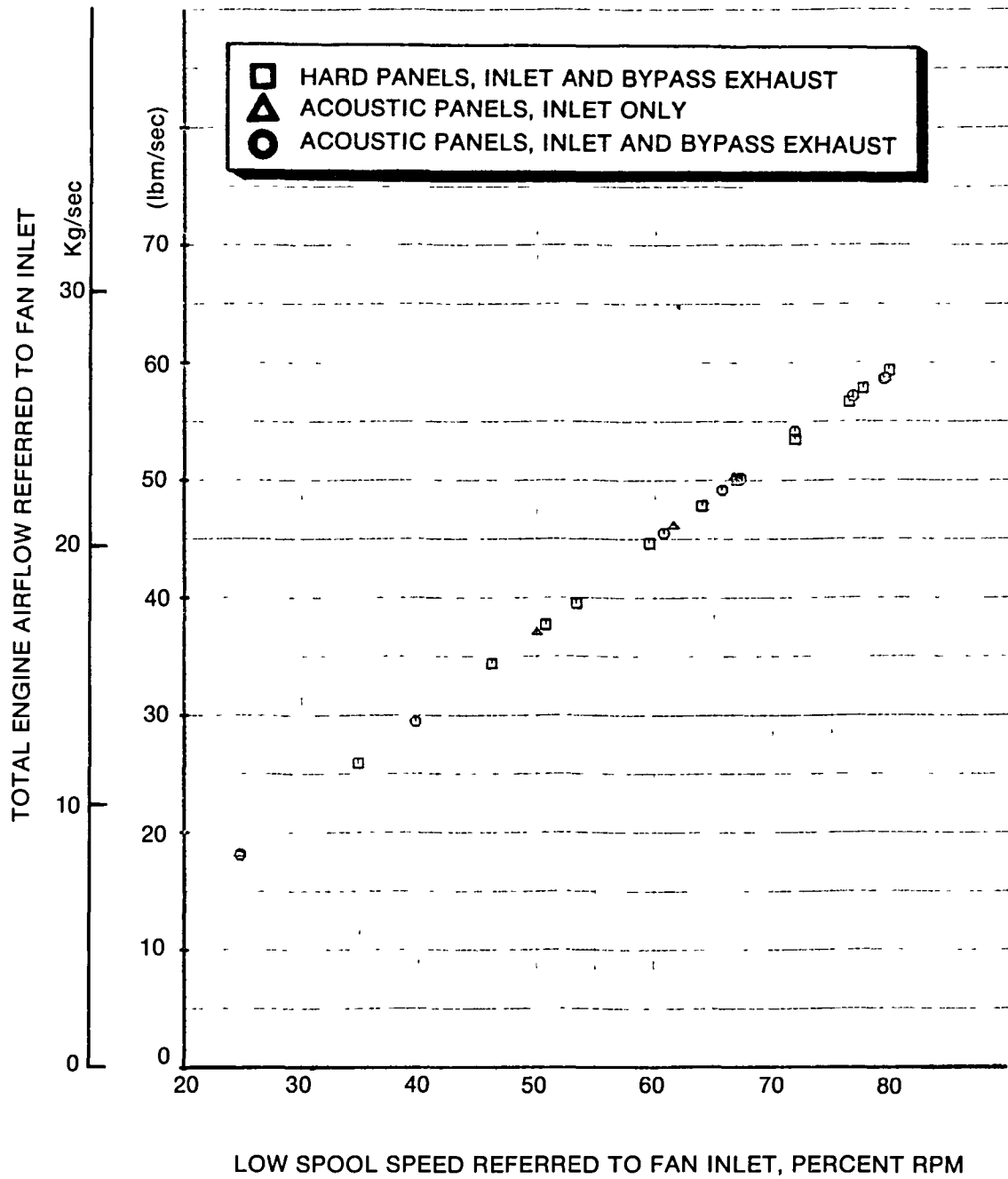


Figure 93. Total Engine Airflow Versus Low Spool Speed - Nacelle Installed

transferred to the acoustic test site for noise evaluation.

Table 6 shows a comparison between the demonstrated installed engine thrust and specific fuel consumption with the design goals. The measured static thrust and specific fuel consumption are 6485 N (1458 lbf) and 0.0400 kg/hr/N (0.392 lbf/hr/lbf). The cruise performance was estimated based upon engine static test data and component rig test results.

### 5.1.2.3 Engine Performance Test Summary

The estimated cruise performance of the Avco Lycoming QCGAT engine, in terms of specific fuel consumption, is approximately a 10.0 percent improvement over currently available small turbofan engines in the 13,344 N (3000 lbf) or less thrust class.

The performance goals were ambitious and certainly achievable with today's existing technology. Although the program performance goals were not achieved, the loss in engine performance has been identified as deficiencies in the turbine section of the core engine. A redesign of the affected hardware has begun under a separate Lycoming funded program, and further development testing will be conducted as necessary.

## 5.2 EMISSIONS TEST RESULTS

In 1970, Congress passed the Clean Air Act. This Act, which was to be effective in 1979, directed the Environmental Protection Agency to establish emissions standards applicable to aircraft. These standards, Reference 10, for small turbofan aircraft, which have now been abandoned by the EPA, were kept as NASA goals for the QCGAT engine program. To achieve these emissions limits, the basic combustor design used in the LTS 101 engine, References 11 and 12, were selected.

### 5.2.1 Design and Emissions Projections

This design, which is a circumferentially stirred combustor, is shown in Figure 94. In principle, the primary air is admitted through slots in the liner header producing flow circulation about a circumferential mean line. Air jets, called "folding jets" entering through the inner wall reinforce the primary zone recirculation, and the vortex fills the full annular height of the liner.

TABLE 6. QCGAT PERFORMANCE

**(STANDARD DAY, INSTALLED)**

	<u>GOAL</u>	<u>DEMONSTRATED</u>
<b>SEA LEVEL, TAKEOFF</b>		
Thrust, N(lbf)	7166(1611)	6485(1458)
SFC, kg/hr/N(lbm/hr/lbf)	0.0370(0.363)	0.0400(0.392)
<b>DESIGN CRUISE, 7620m(25,000 ft) MACH = 0.6</b>		
Thrust, N(lbf)	2157(485)	1850(416)*
SFC, kg/hr/N(lbm/hr/lbf)	0.064(0.628)	0.074(0.723)*

\*Estimated from Static Data

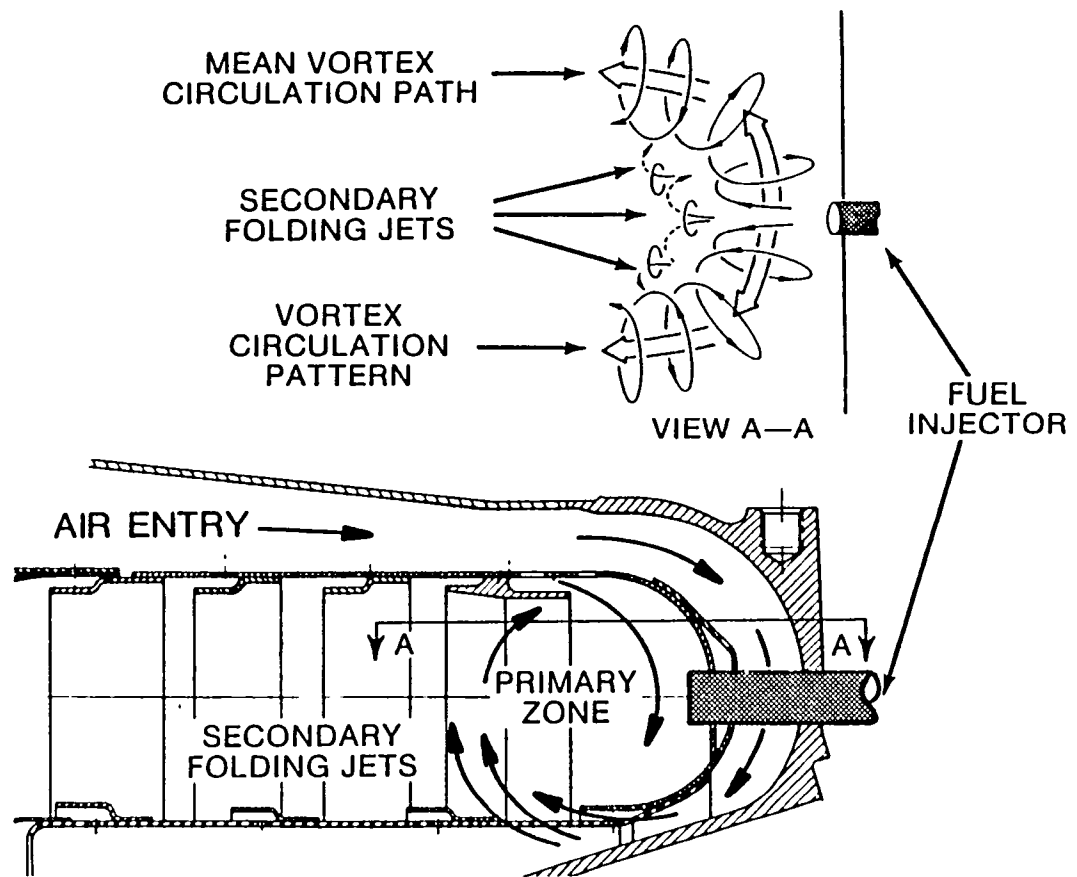


Figure 94. QCGAT Combustor

The vortex spreads circumferentially in both directions and is forced to turn in the axial direction on either side of the folding jets and the mean path of the combustion zone flow vortex takes the shape of a horseshoe. The number of fuel injectors is thereby reduced by one half, compared with normal practice, because of this unique combustor primary zone aerodynamic concept.

Emission measurements, for this type of combustor, attained from the LTS 101 engine were available for use in predicting emissions for the QCGAT performance cycle. Table 7 shows the estimated emissions values, for the QCGAT cycle, with the production LTS 101 combustor. These EPA parameters were generated for a takeoff and landing cycle for class T1 aircraft, (Reference 10).

These emissions projections indicated that further development of the LTS 101 combustor was required to reduce smoke.

Airblast injectors, which replaced the dual orifice injectors, were selected to reduce smoke. The introduction of the airblast injectors also increased combustor efficiency and oxides of nitrogen (NOx) at idle.

Increasing the combustor pressure drop for temperature distribution control, also increased NOx and combustor efficiency while appreciably decreasing carbon monoxide and unburned hydrocarbons. This is typical of the improved primary zone mixing, which results from the higher pressure drop. Air partition modifications were then made, as required, to meet the design goals for NOx. Figure 95 presents the effect of air partition modifications on NOx. Unburned hydrocarbons and carbon monoxide were within the goals in all tests. Initially, the NOx slope for the LTS 101 combustor was as predicted, and met the goal. However, as the combustor pressure drop was increased to reduce smoke, NOx increased.

Air partition modifications, as previously stated, were then made to meet the NOx emissions goal.

The final selected QCGAT liner, which met the goal, has a slightly steeper slope than the initial configuration. The Lipfert correlation, Reference 9, for conventional combustors is shown for comparison.

TABLE 7. INITIAL ESTIMATED QCGAT EMISSIONS

**LTS 101 COMBUSTOR**

	<u>UHC</u>	<u>CO</u>	<u>NOx</u>	<u>SMOKE NUMBER</u>
Estimated Values*	0.034 (1.2)	0.238 (8.4)	0.096 (3.4)	70.0
NASA Goals*	0.045 (1.6)	0.266 (9.4)	0.105 (3.7)	45.0

\*g/kNs (lbm/1000 lbf thrust hr-cycle)



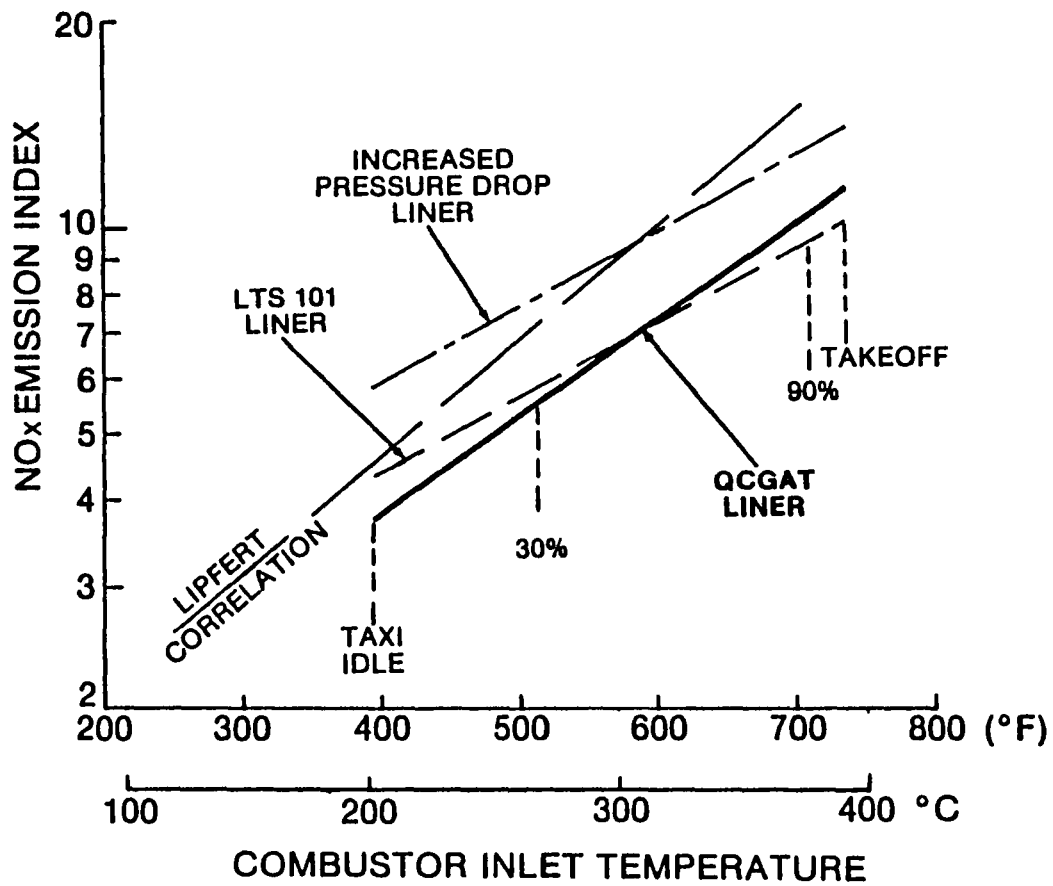


Figure 95. NO<sub>x</sub> Versus Combustor Inlet Temperature

### 5.2.2 Emissions Sampling

Development and initial emissions testing of the combustor was conducted in the laboratory. (See discussion in Section 4.2.) After the laboratory tests, the QCGAT liner was transferred to the engine for demonstrated emissions sampling.

The emissions test probes were installed as shown in Figure 96. The probes, which are cruciform-shaped, were set at two angular positions. One probe measured along the horizontal and vertical axes. The other probe was rotated 45 degrees.

Table 8 is a comparison of the emissions test results with the NASA goals. Measurements from the engine test showed that the unburned hydrocarbons were 60 percent lower than required. The carbon monoxide was 30 percent lower, oxides of nitrogen 1.0 percent higher and the smoke number 50 percent lower than the goal.

### 5.2.3 Emissions Summary

The emissions requirements of the QCGAT engine have been met and, in most cases, surpassed. The QCGAT combustor provides substantial margin for carbon monoxide and unburned hydrocarbons emissions while meeting the goal for NO<sub>x</sub> within the scope of the program.

The combustor system modifications required to meet the emissions goals had a negligible effect on engine performance.

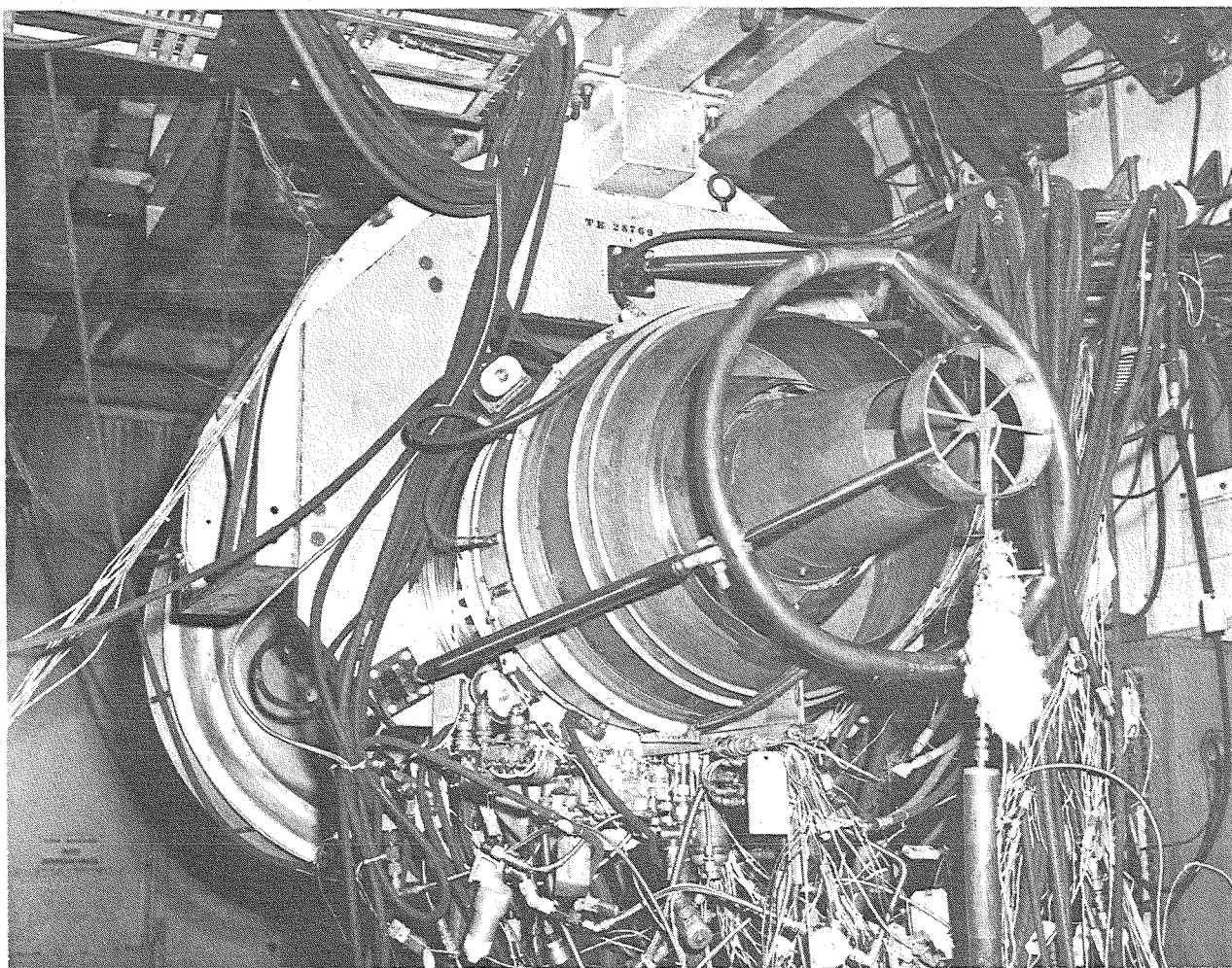


Figure 96. Engine Emissions Sampling Test Probes

TABLE 8. QCGAT EMISSIONS RESULTS

	<u>UHC</u>	<u>CO</u>	<u>NO<sub>x</sub></u>	<u>SMOKE NUMBER</u>
Goal*	0.045 (1.6)	0.266 (9.4)	0.105 (3.7)	45
Engine Test*	0.017 (0.6)	0.193 (6.8)	0.106 (3.75)	24
Engine Test/Goal	0.4	0.7	1.01	0.5

\*g/kNs (lbm/1000 lbf thrust hr-cycle)

### 5.3 ACOUSTICAL PERFORMANCE

Avco Lycoming participated in the NASA QCGAT program by developing a fan module based upon an existing turboshaft engine. The fan was designed using the latest in large engine noise control technology and a mixer that was added to reduce the already low exhaust-gas velocity. A nacelle incorporating sound treatment was also provided for the test engine. A noise prediction model was used throughout the design effort to evaluate various design alternative. Acoustic tests were then made to verify the prediction and identify the noise characteristics of the fan, core, jet, and sound treatment. Analysis of the recorded data yielded close agreement with the expected results. As anticipated, core noise was the predominant source of noise produced by the QCGAT engine. Flyover noise predictions made indicated that the Avco Lycoming QCGAT engine would meet the goals defined for the QCGAT program.

#### 5.3.1 Background

The Avco Lycoming Quiet Clean General Aviation Turbofan engine program was designed to demonstrate the latest control technology for gas turbine noise in a general aviation size engine. A considerable amount of effort was required to identify the design features that offset the generation of noise. This work is still in progress, as can be witnessed by the complexity of the facilities at Lewis Research Center and elsewhere. Most of this work, however, has been directed towards the commercial transport class of engines. The QCGAT program was designed to broaden the scope of subject effort to include the general aviation size engine.

The significant features of the QCGAT engine shown on Figure 97, are:

- o Low exhaust velocity achieved by a high bypass fan design
- o Use of an exhaust mixer
- o No fan inlet guide vanes
- o Subsonic fan blade design
- o Large fan blade to vane spacing

# AVCO LYCOMING QCGAT ENGINE

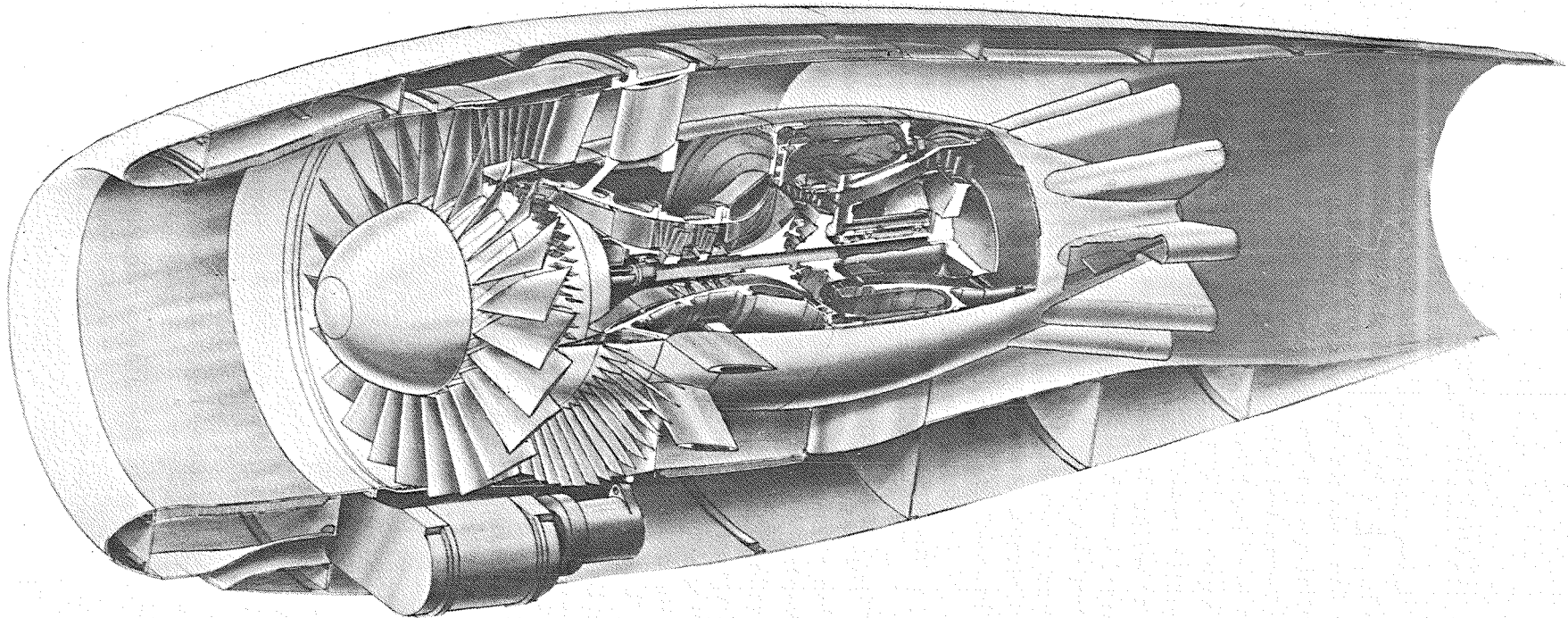


Figure 97. Cross Section of the Engine with Cutaway

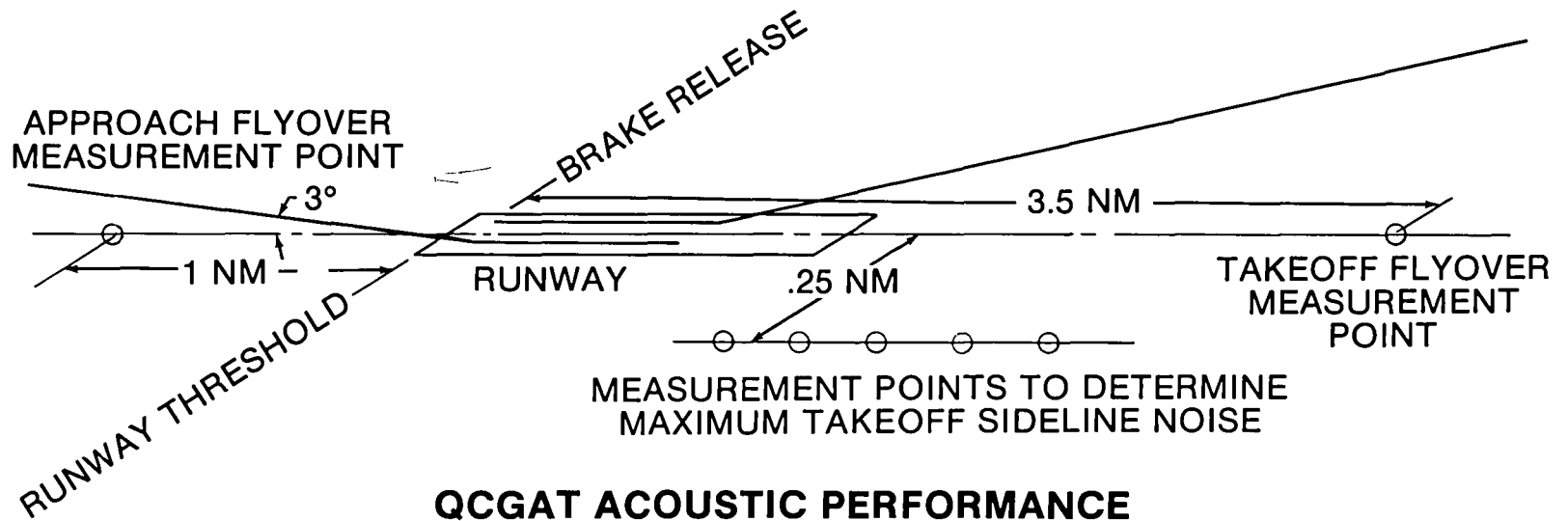
- o High fan blade to vane ratio
- o Acoustical lining of the fan inlet and discharge ducts .

Nacelle and aircraft configurations play an important role in incorporating the above features in the overall acoustic design. For example, the mixer is enclosed in a shroud formed by the nacelle. Also, the fact that forward airspeed mitigates the amount of jet noise generated has been factored into the design. Based upon the results of the prediction of the acoustical performance of the engine aircraft system and the impact of each component on the overall design, the above features were optimized for the QCGAT aircraft.

QCGAT noise goals were selected by NASA to create a design that included the latest noise control technology. Avco Lycoming's QCGAT engine design entailed the addition of a new fan design module that incorporates the latest noise techniques to an existing turboshaft engine.

Original estimates of the engine noise emissions, based upon that design, are shown in Figure 98 along with the relevant measurement locations. This analysis indicated that takeoff noise levels would be 4 EPNdB below the goal, sideline 6 EPNdB below goal and approach to be 9 EPNdB. The prediction also indicated that the core would be the dominant source of noise at each measurement position, with the fan contributing to the approach noise and the jet contributing to the takeoff noise levels.

Notice that the goals are given in terms of aircraft flyover noise. From the point of brake release and with the aircraft flying directly overhead, the takeoff measurement point lies 6500m (3.5 nautical miles) down range. The sideline measurement point also lies down range on a takeoff but is displaced 460m (1/4 of a nautical mile) to the side and consists of a series of points in order to determine maximum noise level. The approach measurement point is located under the landing flight path at a point one nautical mile from the runway threshold. Since the approach glide slope is defined as 3 degrees, the altitude of the aircraft over the measurement point is fixed at 112m (370 feet), (Reference 13). Thus, aircraft performance had to be considered in the engine design. Beech Aircraft Company was contracted to define the characteristics of a twin-engine QCGAT-powered aircraft. With respect to noise, the rate of climb at takeoff, the power required at approach, and the geometry of the wing were determined. Airframe noise, however, was not included in the noise estimates.



### QCGAT ACOUSTIC PERFORMANCE

<u>CONDITION</u>	<u>EPNL GOAL EPNdB</u>	<u>PREDICTED ENGINE EPNL, EPNdB</u>
Takeoff Flyover	69.4	64.8
Takeoff Sideline	78.4	71.7
Approach Flyover	83.4	73.8

Figure 98. QCGAT Noise Goals



The design and performance of subject aircraft plays an important part in the noise emissions of the QCGAT engines. That is, the approach speed and takeoff performance of the aircraft can be varied to meet market requirements. For example, a lower approach power could be used that would result in lower approach noise levels but would require more runway length. Because the approach noise levels were predicted to be low, a small penalty was accepted to reduce field length requirements. This will allow the aircraft to be certified for use at most air fields in the United States.

Gas turbine engine noise-source identification and control (Figure 99) starts with the engine. Given the geometric and performance characteristics of the engine, prediction of an engine's noise emissions can be made. Engine noise is subdivided into five distinct noise generating mechanisms: 1) fan, 2) compressor, 3) combustion process, 4) power turbines, and 5) the turbulent mixing of the exhaust jet with the ambient air. The majority of the work accomplished to advance the state-of-the-art for gas turbine and aircraft noise identification and prediction was and is presently being carried out by NASA as part of their Aircraft Noise Prediction Procedures (ANOPP) (References 14 thru 17). This work served as the basis of noise prediction efforts used in this program. Certain modifications were made in order to more accurately reflect the experiences at Avco Lycoming with engine noise predictions. Then by using this aircraft performance and applying flight effects, aircraft flyover noises were calculated.

### 5.3.2 Engine Design and Noise Prediction

#### 5.3.2.1 Fan Design

The first task required to design a fan module for an existing turboshaft engine involved several iterations to assess the design alternatives. Reduction of noise was achieved through the use of a low-pressure ratio fan to reduce blade loading and noise generation, which was part of the fan design from its conception. Other design features also shown to have resulted in quieter fan designs for the large turbofan engines are as follows:

- o Low Blade Loading
- o Subsonic Blade Tip Speed

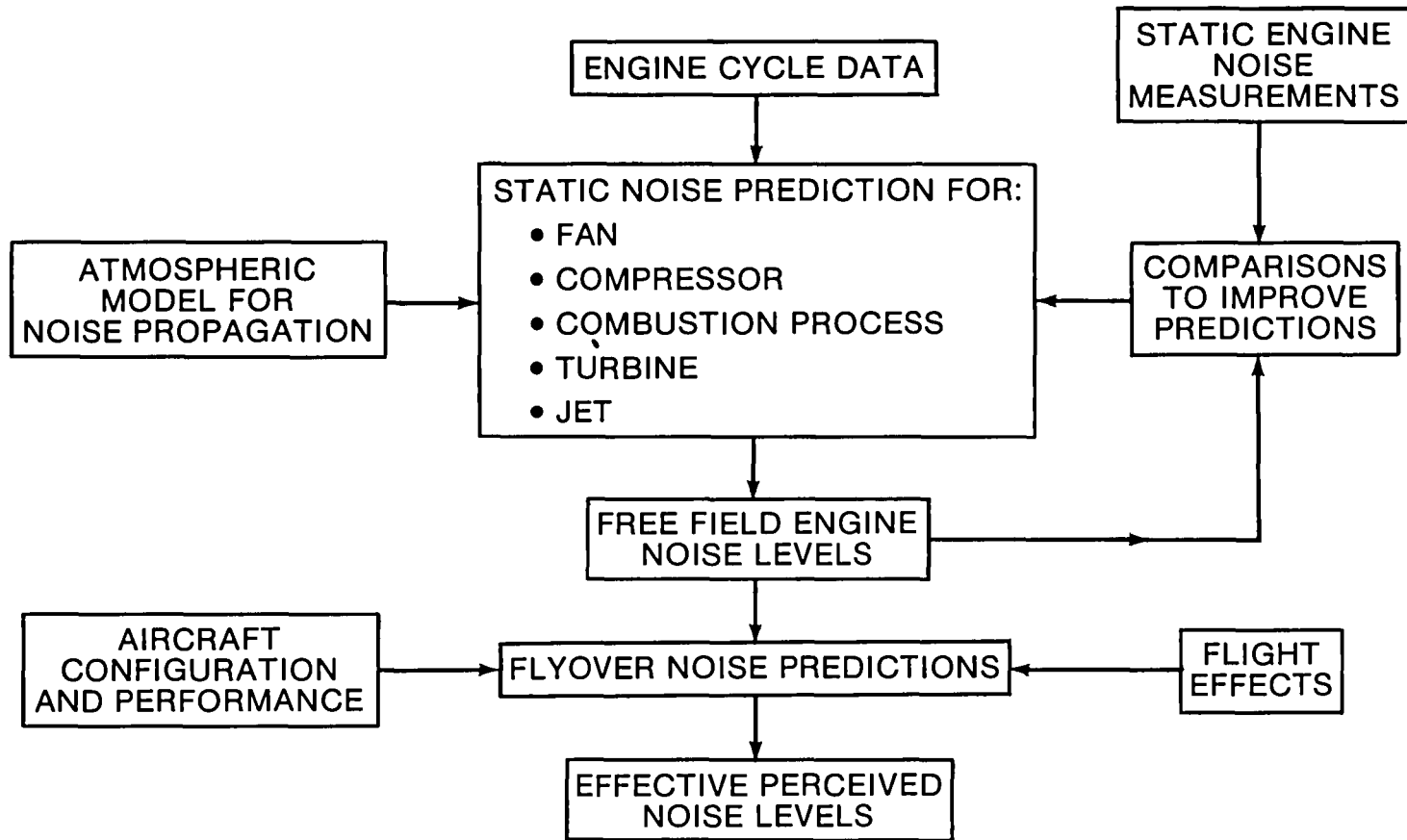


Figure 99. Noise Prediction Procedures

- o Blade to Vane Spacing Greater 2 Blade Widths
- o Vane to Blade Ratio Greater than 2
- o No Inlet Guide Vanes

Because fan blade tip speed was designed to be subsonic, multiple pure tones or "Buzz Saw Noise" were eliminated altogether. The design relative-tip Mach number for the QCGAT engine is 1.13; this yields a subsonic value at all sea-level operating points. The distance separating the fan blades from the fan exit guide vanes is great when compared with the blade width in order to reduce rotor-stator interaction noise that is expressed as fan broadband noise. A value of 2.3 was used for this ratio. The ratio of fan vanes-to-blades optimized at a value of 2.5 eliminates what is known as spinning modes that propagate at the blade passing frequency fundamental. In addition, inlet guide vanes were not used in the fan design. To further insure that inlet turbulence was reduced, a long inlet duct was included in the nacelle design. These features were accounted for in the prediction of the fan noise levels. The noise prediction indicated that the fan would be a contributor, along with the core, to only the approach power levels. By identifying the effect of the various alternatives with the aid of our prediction procedures, a balance was maintained that achieved a low-noise signature at approach.

The model for fan noise prediction was derived from Reference 16, in which fan noise is considered to be composed of five sources.

1. Fan inlet broadband
2. Fan discharge broadband
3. Fan inlet discrete tone
4. Fan discharge discrete tone
5. Fan inlet combined tone.

Combined tones do not propagate below cutoff and do not come into play for the QCGAT engine.

The basic features of the prediction program are outlined in Figure 100, where each factor is part of the equation

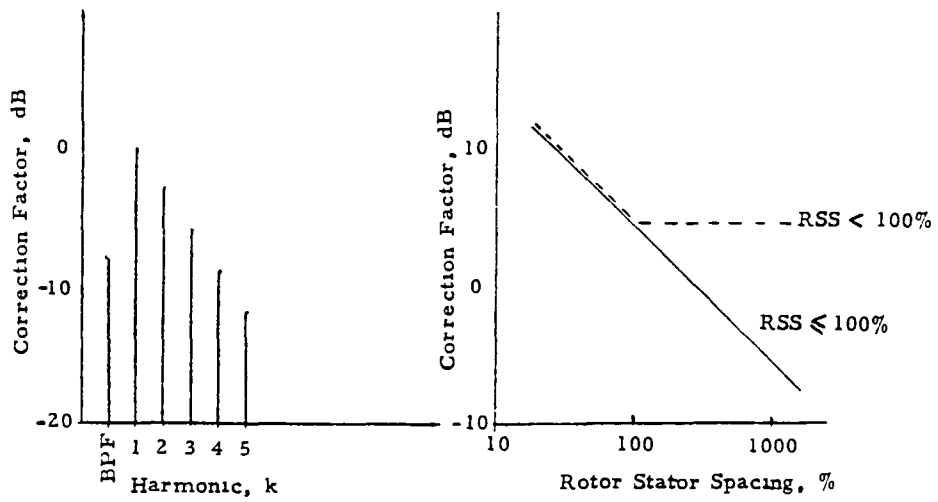
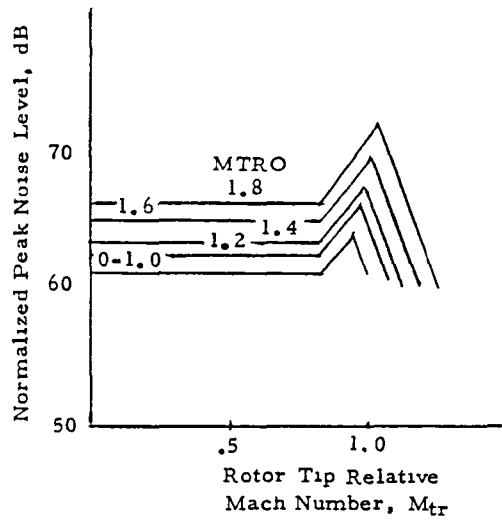


Figure 100. Fan Noise Components (Ref. 16)

$$L_c = 20 \log \left( \frac{\text{Temp Rise}}{\text{Ref Temp}} \right) + 10 \log \left( \frac{\text{Mass flow}}{\text{Ref Mass flow}} \right) +$$

f (Relative Tip Mach No.) + f (Blade-to-vane spacing) + Directivity  
+ Spectrum Correction

The result was then extrapolated to the corresponding free-field location for comparison with test-stand data.

### 5.3.2.2 Jet Noise

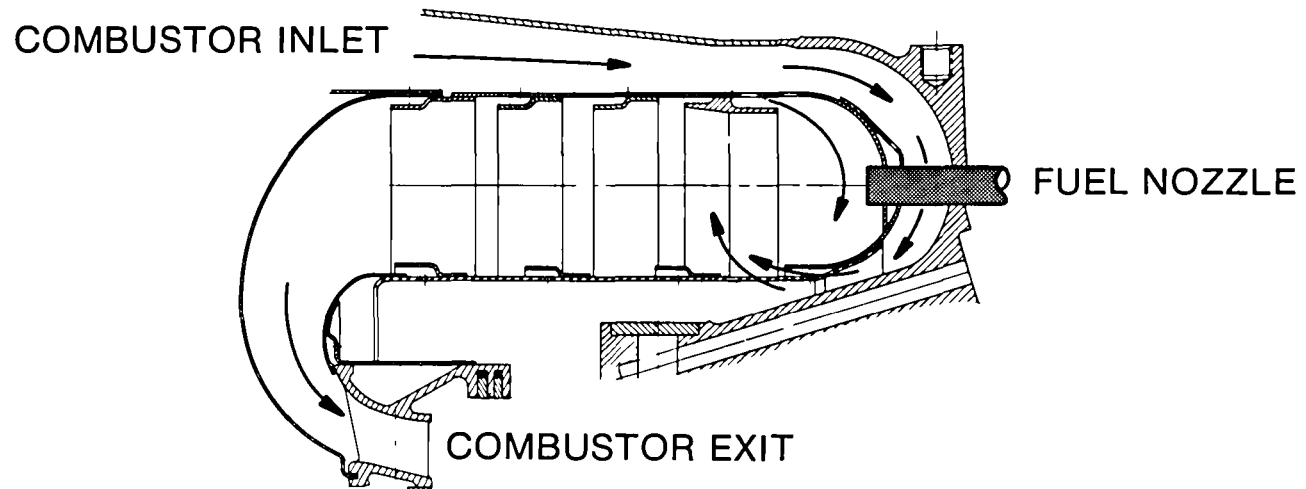
Jet noise is the second major element in the QCGAT engine design. A high-bypass fan design is used to reduce the exhaust velocity, thereby reducing the noise generated by the turbulent mixing of a high-velocity jet.

To further reduce jet noise, a six-element mixer was designed to mix the core engine and fan exhaust gas to yield a single low-velocity exhaust jet. (See Reference 8 for details of the mixer design.) The mixer, however, is not entirely free of side effects. Pre- and post-mixing turbulence can be an additional source of noise that must be dealt with. These noise sources can be reduced by the addition of a shroud. The shroud effect was incorporated by the extended mixing section of the final nozzle.

### 5.3.2.3 Core Noise

The high-bypass fan and mixer were designed to reduce the jet noise component to a noise level below that of the core when forward flight effects cause a reduction to occur in the jet noise that leaves the core noise component. Core noise is the noise generated by the combustion process. Engine compressor and turbine noises were predicted to be above the audible range. Thus, these noise sources which do not contribute to the perceived noise of the QCGAT engine were not considered in the design.

Core noise models for the most part have been empirically derived. The ANOPP routine has been found to be adequate for the core turboshaft engine (Reference 15). This prediction model uses combustor mass flow, temperature rise, and pressure drop as the basis for predicting core noise. (See Figure 101.) Empirical data also suggest a 7 to 10 dB reduction for the turbofan version of this model (Reference 6). Core noise is now recognized as a major

**(GOOD AGREEMENT FOR TURBOSHAFT ENGINES)**

Noise a Function of:

- Mass Flow
- Temperature Rise
- Pressure Drop

Figure 101. Core Noise Model

source in turbofan engine noise and is the focal point of much research; however, core-noise control was not part of this program. As predicted, the core was a significant contributor to the noise characteristics of the aircraft. Consequently, further fan and jet noise reduction would have to be unwarranted.

#### 5.3.2.4 Flight Effects

An aircraft engine operates differently in flight than when it is tied down to a test stand. Engine noise characteristics also change. In flight, the air inflow is streamlined because of the flight cleanup effects of the forward airspeed and the absence of ground turbulence that influence the generation of fan noise, particularly the tone at the blade-passing frequency. Forward flight, however, has its greatest impact on the generation of jet noise. In flight, the relative velocity between the exhaust and the ambient air is reduced. This plays an important part in the overall design of the engine aircraft system. For example, the airspeed at takeoff is, in part, determined by available runway length. A longer takeoff roll would permit a higher takeoff speed. Consequently, the same jet noise level and relative jet velocity could have been achieved by using a higher exhaust velocity and a higher takeoff air speed.

As the aircraft flies past the observer, the sound varies both in time and spectral content. Dynamic amplification acts to increase the noise level as the aircraft approaches and reduces in noise levels as it recedes. There is then, the doppler effect that imparts a frequency shift to the noise spectrum as the aircraft flies by. These phenomena must be accounted for to accurately predict the perceived noise of the aircraft.

#### 5.3.3 Sound Treatment Design

It has been recognized for sometime that the fan inlet and discharge ducts of an engine nacelle (Figure 102) offer ideal locations for the installation of sound treatment materials are particularly efficient generated by the fan. Absorptive material are particularly efficient in absorbing sound energy in the high-frequency region where much of the acoustical power radiated by the fan is concentrated. In addition, the treatment of sound can be accomplished by the use of flight-worthy materials that add minimal weight to the aircraft. Finally, the theory and experience of designing sound-treatment panels are sufficiently sophisticated to accurately predict the results that will be

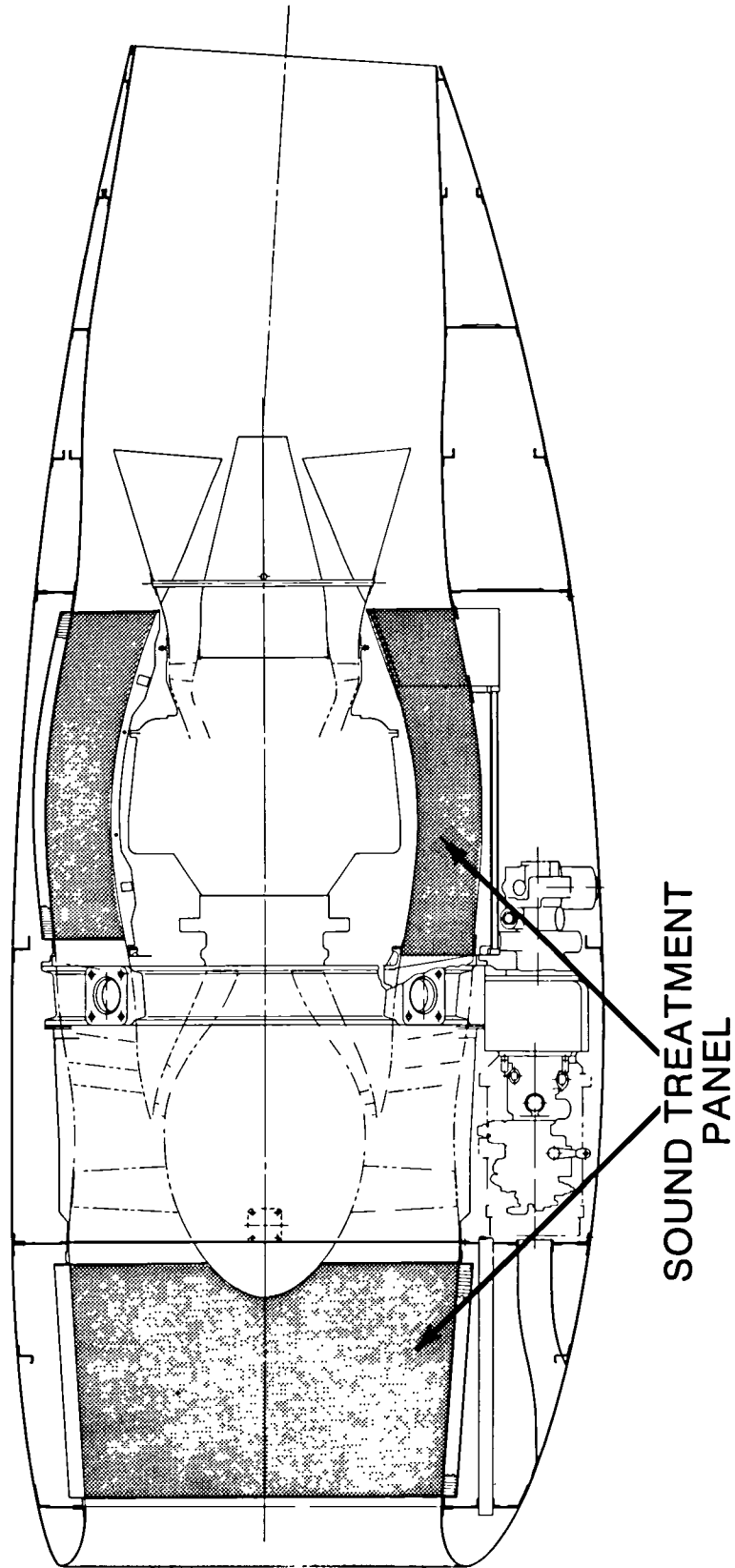


Figure 102. Sound Treatment Locations



achieved with a particular design. Sound-treatment panels were, therefore, installed in the QCGAT engine nacelle to determine the benefits that would be derived from their use in an aircraft design and to evaluate the manufacturing tolerances of the sizes required for the QCGAT engine.

Sound attenuation requirements were determined by comparing the predicted noise levels with the QCGAT program goals. Aircraft approach represented the only condition where the fan noise was predicted to contribute significantly to the aircraft noise levels. In addition, the frequency of the blade-passing tone at approach occurs in the more heavily weighted part of the audible spectrum. Consequently, the approach power point was selected for the design of sound treatment. At other conditions, the fan does not contribute significantly to the aircraft noise levels.

The Lockheed California Company was contracted to design the sound treatment arrangement for the nacelle. Given the dimensional limitations, the nacelle needing sound treatment, and engine operating parameters at approach, Lockheed generated a set of design curves from which the sound treatment was designed (Reference 1).

These curves were based upon an analytical and empirically derived solution to what are known as the convected wave equations. These equations describe the sound generated by the fan as modes of acoustic energy rotating with and against the fan. This acoustic energy can only propagate under certain boundary conditions. The physical characteristics and operating parameters form these boundary conditions and determine which modes will propagate. Lockheed performed this analysis and recommended a design.

Recommendations based on the Lockheed design, shown in Figure 103, were for a single degree of freedom panel for both the inlet and discharge ducts. The Lockheed design consists of a solid backing plate held 16 mm (5/8 in.) off an inner plate that is perforated to achieve a 5 percent open area. A honeycomb cell-structure material separates the inner and outer plates. The inlet panel, 330 mm (13 in.) long, fulfills the available space in the inlet duct. The discharge sound treatment consists of a 45.7 mm (1.8 in.) long panel on the outer duct wall. The inner duct wall formed by the core cowl was not treated. The discharge panel was terminated before the start of the mixer to simplify the design. Otherwise, the radiant heat from the mixer would have required the selection of more expensive materials and fabrication techniques.

	<u>THICKNESS</u>	<u>LENGTH</u>	<u>OPEN AREA</u>
Fan Inlet	0.63 IN.	13 IN.	5%
Fan Discharge	0.63 IN.	18 IN.	5%

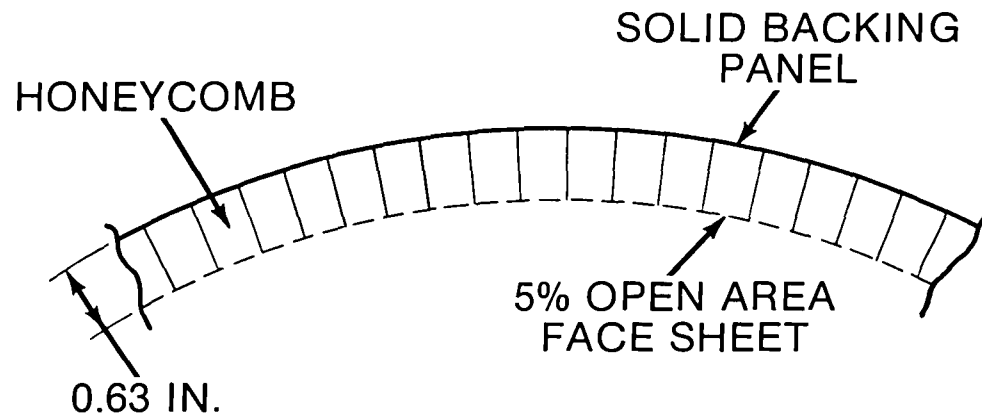


Figure 103. Sound Treatment Design

The predicted insertion losses for the fan inlet sound treatment panel at the approach and takeoff points are shown in Figure 104. The sound treatment, as discussed earlier, was designed for the approach condition. At this power setting, the peak attenuation is made to coincide with the blade-passing frequency. The insertion loss is higher at the takeoff condition because of the increase in airflow through the engine. The blade-passing frequency at takeoff is also higher. The result is an attenuation that is approximately the same as that for the approach condition.

The predicted attenuation for the fan discharge treatment is shown in Figure 105. The duct width between the inner and outer wall makes the treatment more effective, even though the inner wall is not treated.

The test nacelle and sound treatment panels were fabricated by Avco Aerostructures in Nashville, Tenn. The test nacelle was designed to take insert panels in the fan inlet and discharge ducts where ordinarily the sound treatment would have been made integral with the nacelle. Two sets of inserts were fabricated. Each set was designed to be of one piece for easy removal and installation during testing and to be rigid enough to maintain the desired wall contours. The panels were of a sandwich-type construction with a honeycomb structure separating the inner and outer plates. The thickness of the honeycomb was determined by Lockheed's sound attenuation requirements. One set was fabricated with a solid inner plate, and one set (Figure 106) was fabricated with an inner plate perforated to achieve a 5-percent open area. In this way, the engine could be tested with and without sound treatment in the nacelle.

The small radius of the inlet and discharge duct was limited to the depth of honeycomb that could be used without warping the cell structure walls. The selected honeycomb material used a small cell pattern in order to be flexible enough to accommodate the curvature. This, however, meant that there would be fewer holes per cell and potentially have more holes blocked by the cell walls as the honeycomb was laid over the perforated plate. The minimum hole sizes available dictated a wide diversion of holes. A special adhesive was used that migrated up the cell walls during the curing process and did not plug holes. The perforated plate was punched to a 6-percent open area. Then when the honeycomb was bonded to the plate, the open area was reduced to the designed 5 percent.

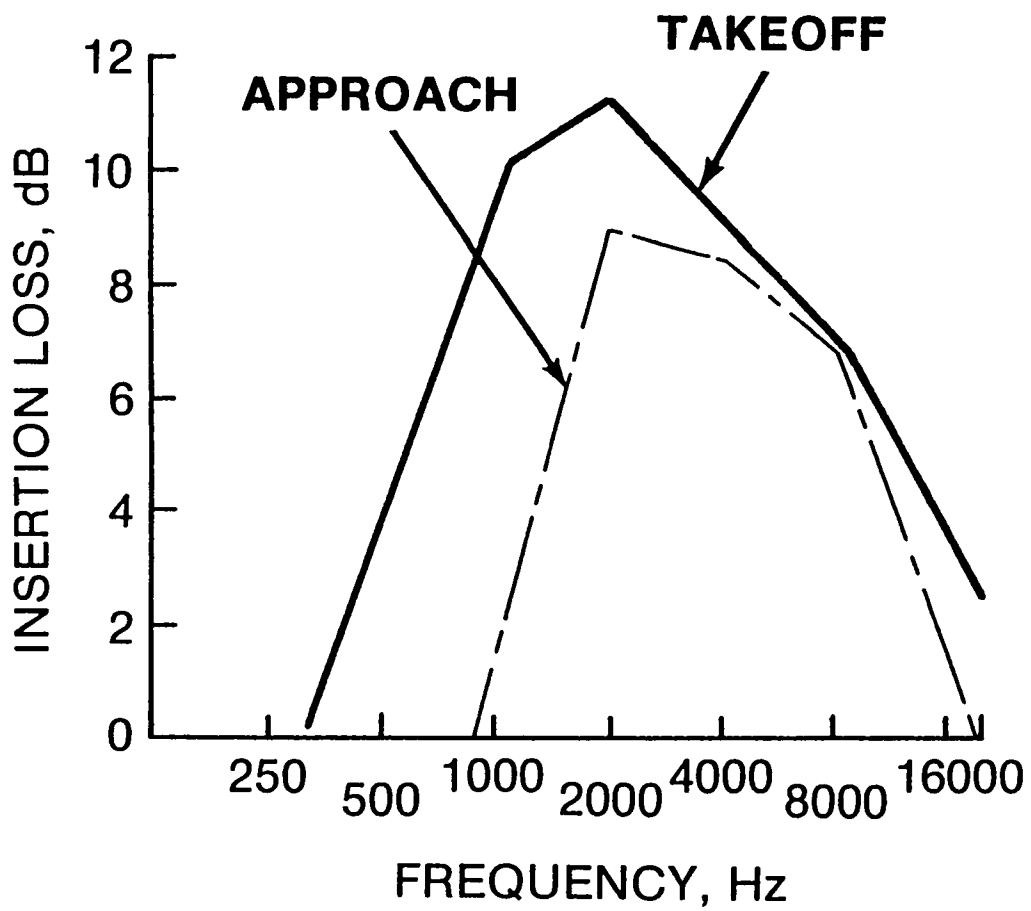


Figure 104. Inlet Attenuation

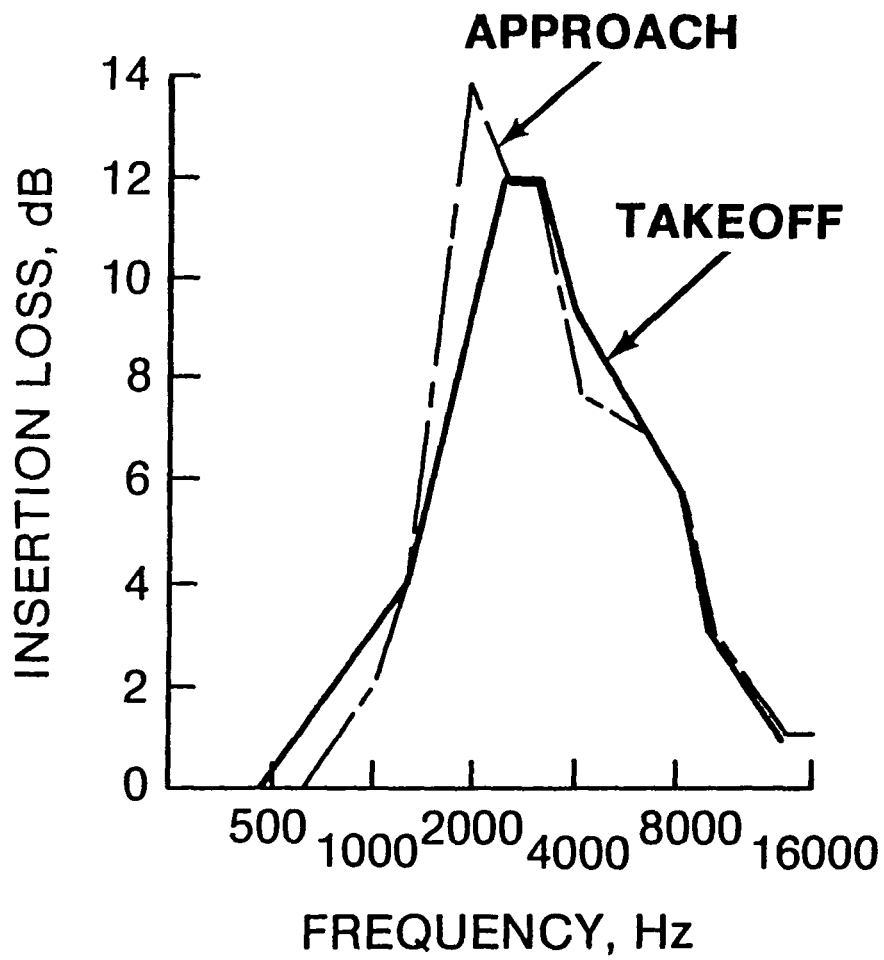
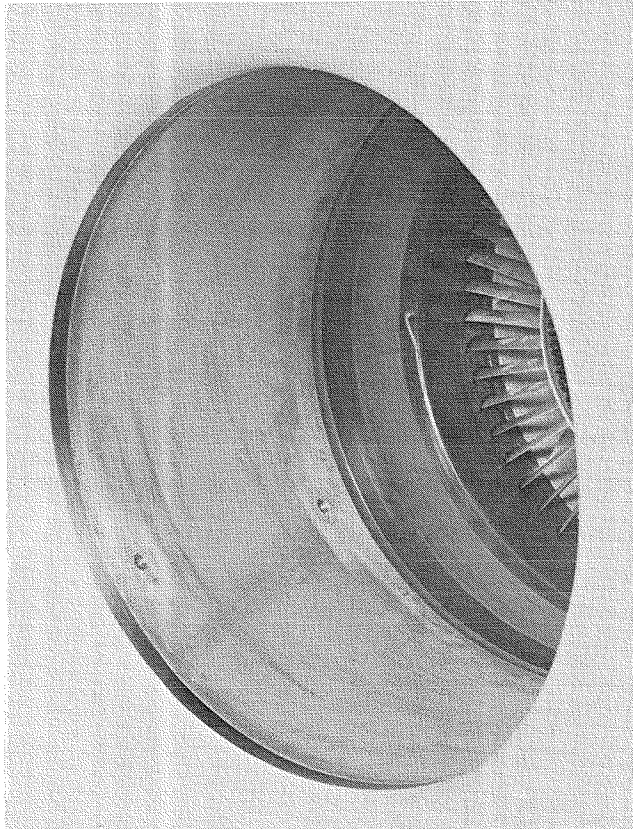


Figure 105. Exhaust Attenuation

**INLET PANEL**



**DISCHARGE PANEL**

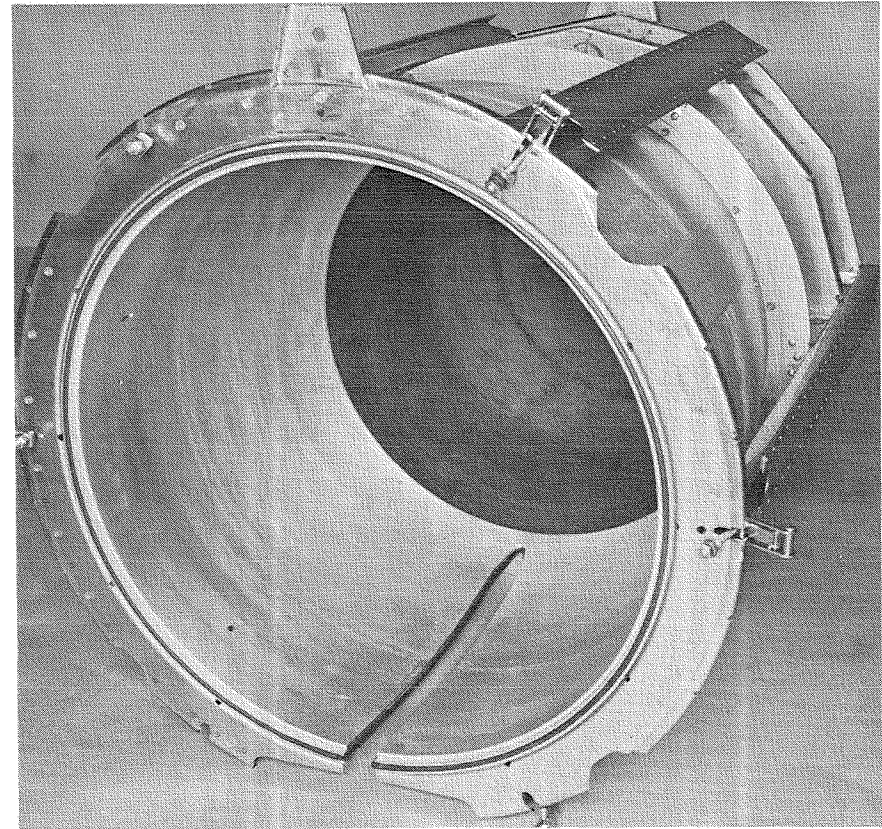


Figure 106. Sound Treatment Panels

#### 5.3.4 Wing Shielding

The program goals are given in terms of aircraft flyover noise parameters. Experience has shown that when the engine is placed above the wing, the wing serves as a barrier. A barrier-attenuation routine was included in the aircraft noise model to account for this effect. As shown in Figure 107, the wing creates a shadow zone that moves in conjunction with the aircraft. Since only a small fraction of the noise is refracted around the leading and trailing edges of the wing, the forward radiated fan noise will not reach the ground as the shadow zone passes an observer.

#### 5.3.5 Acoustic Test Phase

The goals of the test program were to verify the noise predictions by comparison with measured data to determine the noise reduction of the mixer and to determine the effectiveness of the sound-treatment panels.

The normal method of recording noise emitted by an engine is to record the 1/3 octave band sound pressure levels at nineteen positions located on an arc 30 meters (100 feet) from the engine. A full set of data over an arc of 180 degrees can be obtained with microphones located every 10 degrees. Four power settings corresponding to the operating envelope of the engine were used. In addition to the far-field microphones, acoustic probes were placed on the engine to aid in identifying core and mixer components and the noise reduction of the sound treatment. A barrier was also used during a part of the testing to aid in isolating the fan inlet and discharge component sound levels.

Three separate engine configurations used during the acoustic testing of the QCGAT engine were: 1) a split-flow exhaust nozzle configuration called the referee system; 2) the hardwall nacelle configuration in which the test nacelle, mixer, and hardwall fan inlet and discharge panels were used, and 3) the softwall nacelle configuration in which the hardwall panels were replaced with the sound treatment panels. Each configuration was tested to record the engine noise at four power settings. The QCGAT engine was mounted in a test frame and after a test cell series, it was moved to the free-field test site. This site is located remotely from the plant in an area free of most noise intrusions and where testing does not affect the local community.

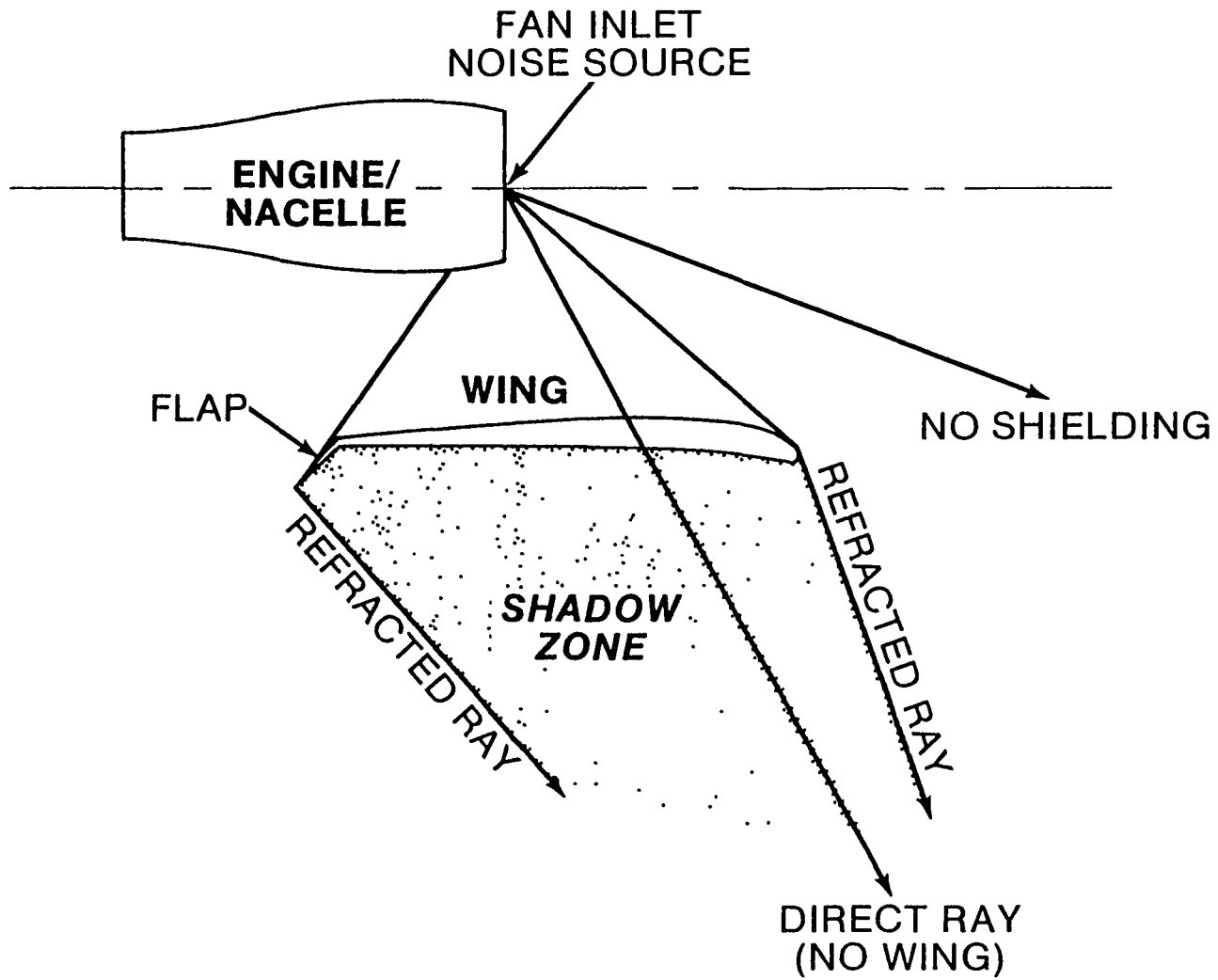


Figure 107. Wing Shielding



The engine (in the nacelle and test frame) was installed on a rotating test stand that is capable of rotating a full 360 degrees. The normal method of testing is to record engine noise on an arc 30 meters (100 feet) from the engine by means of five microphones placed 10 degrees apart, as shown on Figure 108. By rotating the engine and repeating the test points, a full 180 degrees of noise can be obtained with some overlap. The microphones located at the 170- and 180-degree points in exhaust stream were not used for most runs.

One-half inch condenser microphones fitted with wind screens placed on the ground were used as recommended by NASA. This allowed 6 dB correction to be used when correcting the data recorded over a reflecting plane to free-field conditions for comparison with the predicted noise levels. The microphone placement is shown in Figure 109. Signal conditioning instrumentation was located in an acoustic data acquisition trailer where the data were recorded on magnetic tape for later analysis.

The test data were recorded on magnetic tape in 2-minute segments. The instrumentation setup for the acquisition of the acoustic data is shown on Figure 110. The tape-recorded data were then played back through a 1/3-octave band digital frequency analyzer to obtain the 1/3-octave band sound pressure levels for each run. An averaging technique was used to average out the random fluctuations in the data so as to yield a steady-state value for the 2-minute sample. The data were first corrected to standard acoustic day conditions and free field conditions. They were then organized and tabulated by frequency-versus-angle from the engine inlet for each operating condition and configuration.

At each test point, a complete set of engine performance data was recorded for use in predicting the engine static noise levels for comparison with the measured sound levels. The ambient pressure, temperature, and relative humidity were also recorded.

Fan noise radiates both from the inlet and the exhaust. Near the inlet axis, inlet fan noise dominates, and near the exhaust axis exhaust fan noise dominates. However, near 90 degrees, the two blend together. To isolate the fan inlet noise from the fan discharge noise, a barrier was physically placed between them. This was accomplished at the freefield test site with the barrier as shown on Figure 111. The barrier was constructed of a fixed partition 4.3 meters (14 feet)

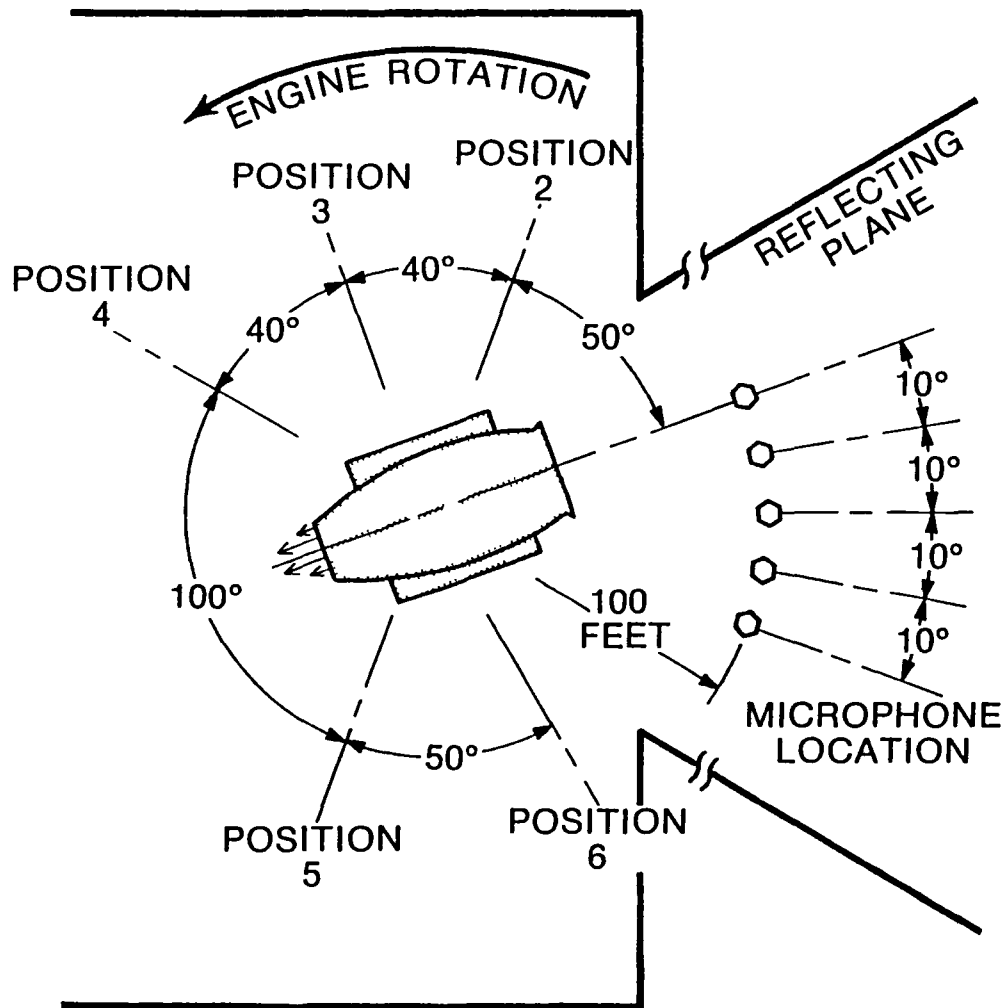


Figure 108. Microphone Arrangement

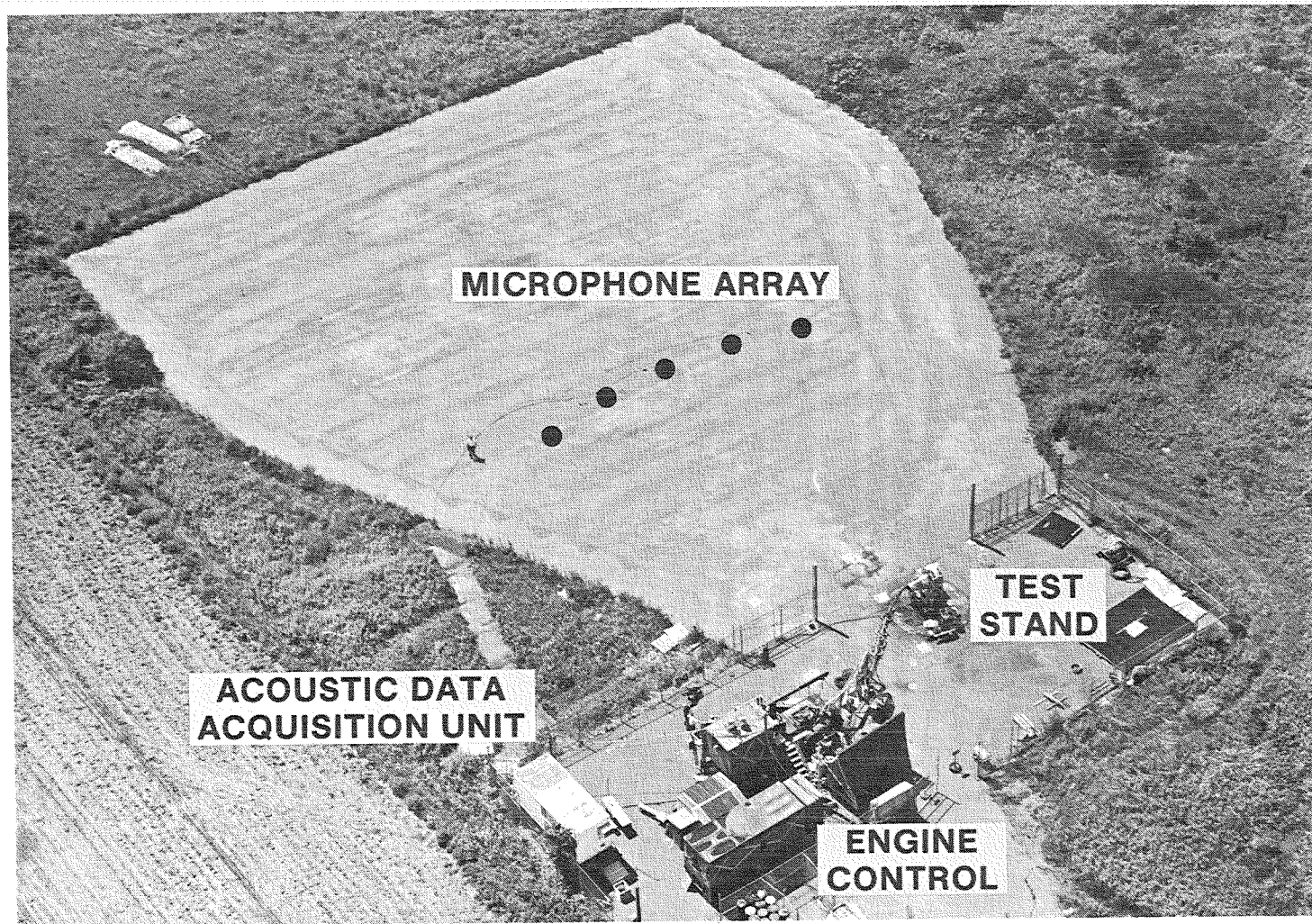


Figure 109. Test Site

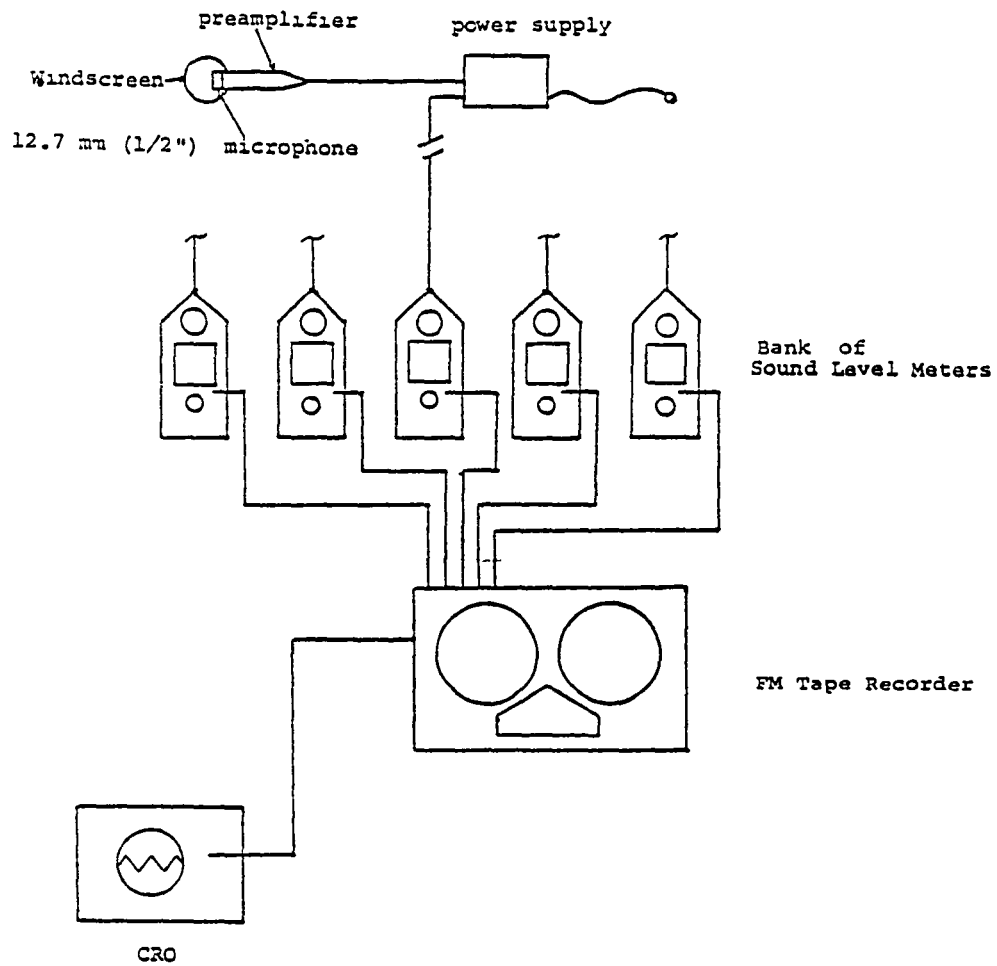


Figure 110. Instrumentation Setup for the Acquisition of the Acoustic Data

**(ISOLATE FORWARD AND AFT RADIATED FAN TONES)**

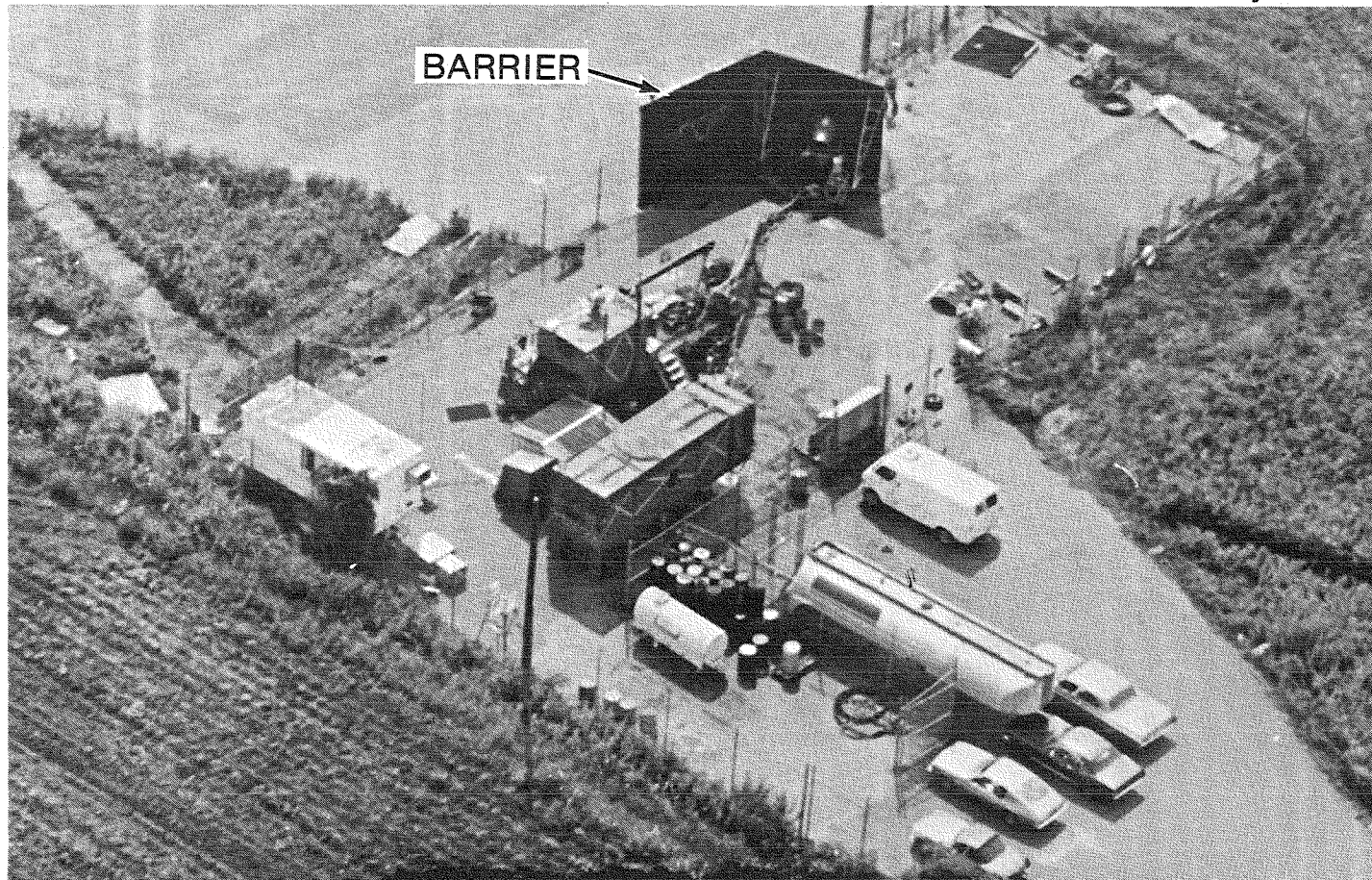


Figure 111. Barrier

high by 6 meters (20 feet) long and a movable partition through which the engine inlet protruded. This effectively removed the fan discharge noise from the measurements. Data were then recorded over an arc of 80 degrees. The movable partition was then removed, and the engine was rotated 180 degrees so that the exhaust protruded through the barrier when it was moved back into position. The fan discharge noise was then recorded without fan inlet noise contributions. Both of these tests were run at the same four-power setting with the hard-wall and the softwall nacelles installed on the engine.

Locations of engine-mounted probes are shown in Figure 112. Half-inch condenser microphones were located both upstream and downstream of the inlet sound treatment to measure the noise reduction across the inlet sound treatment panels. Semi-infinite wave guide probes, supplied by NASA, were used to sample the acoustic pressure levels in the primary engine exhaust and at the mixer exhaust plane. These probes consisted of 6.35 mm (1/4 inch) condenser microphones in a sealed tube (See Reference 7.) A low-volume flow of nitrogen at a pressure just above that in the duct provided a gas seal to prevent hot exhaust gas from entering the tube where it could damage the microphone.

The probes were designed to record the acoustic pressure levels at the indicated probe locations. They were to be used in coherence analyses if it became necessary to determine what part of the noise in the far-field originated from within the engine.

The split-flow nozzle configuration with the semi-infinite waveguide probes installed in the primary exhaust nozzle is shown on Figure 113. This configuration was used to obtain baseline data for comparison with the mixer nozzle noise levels.

### 5.3.6 Data Analysis

5.3.6.1 Static Test Conditions - During the individual test runs, engine performance was monitored, and relevant ambient and operating parameters were recorded. Using these data and the appropriate cycle sheet data, predictions of the expected sound pressure levels were computed. These were then compared point by point, frequency by frequency, and angle by angle with the measured sound pressure

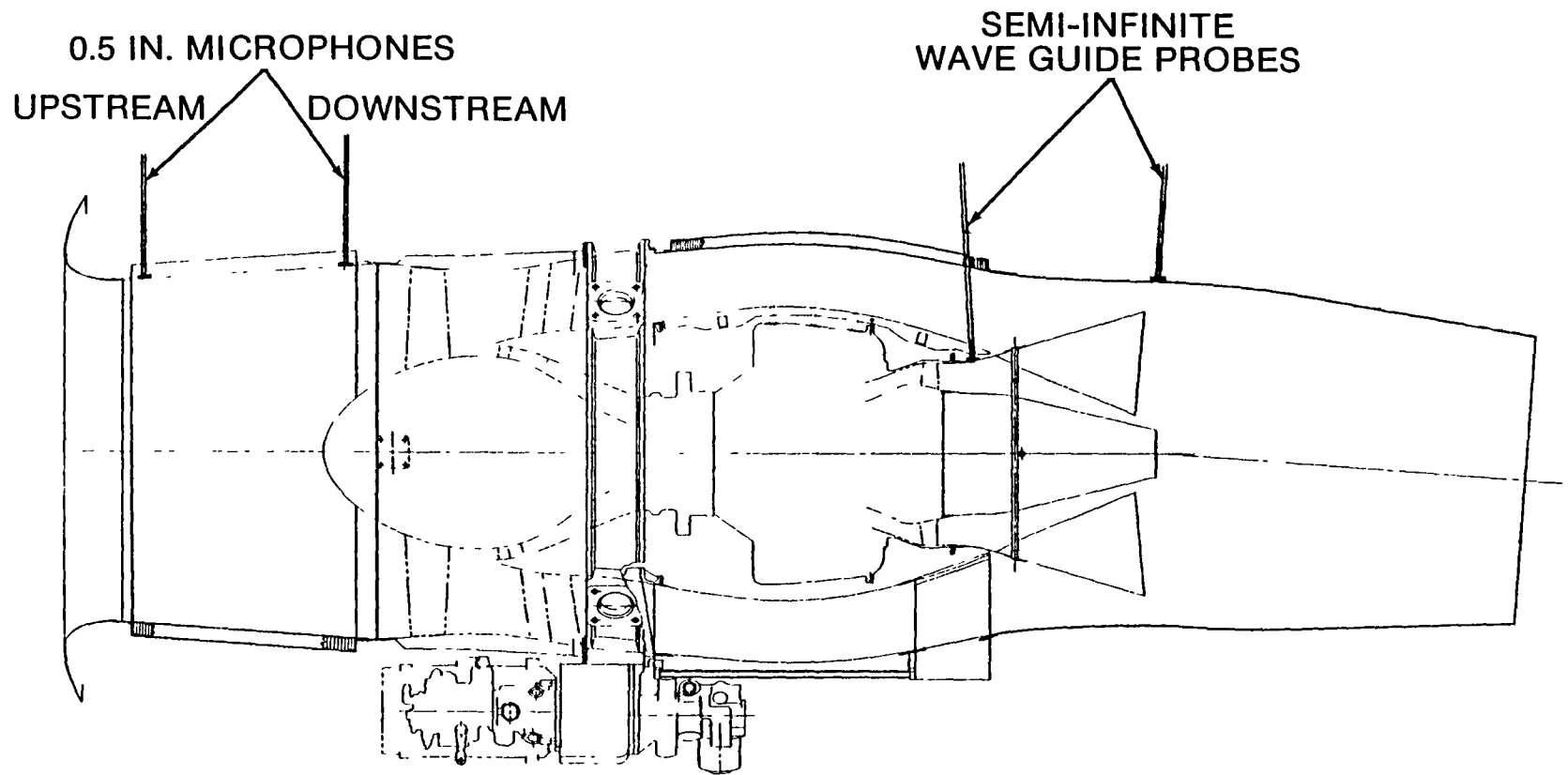


Figure 112. Probe Locations

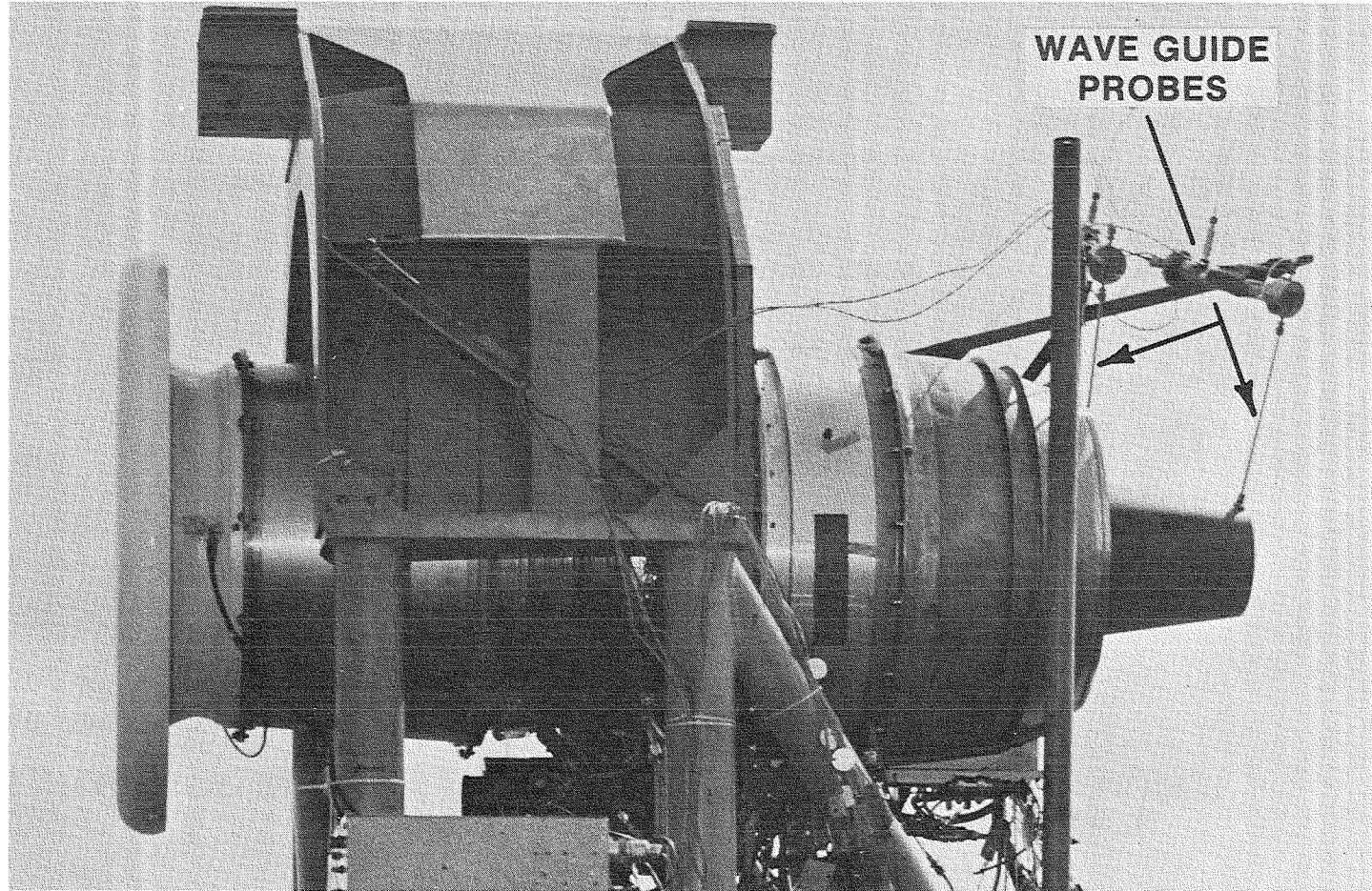


Figure 113. Reference System



levels. In this manner, estimates of the contribution of each component to the overall noise levels at each power setting were made. The predictions were then adjusted to reflect this comparison, and the correlation was run again. The insertion loss of the sound treatment was determined along with the mixer noise reduction.

The individual component contribution to the overall noise levels was determined on a spectrum basis, as shown on Figure 114. This plot consists of the one-third octave band sound pressure levels over a frequency range from 25 to 20,000 Hz. The predicted fan noise contribution was then overlaid. The calculations correctly located the blade passing tone, its harmonics, and the broadband component. The magnitude of the blade passing-tone fundamental, however, was underpredicted. Next, the predicted jet noise component was added as shown on Figure 115. As expected, the jet component does not contribute directly to the noise levels at the low-power setting. When the predicted core noise component is added to the noise spectrum as shown on Figure 116, the predicted spectra match the measured spectral shape. The agreement, however, is only fair in the mid-frequency region through the blade passing-tone fundamental. This same analysis was carried out for the softwall and split-flow configuration. The analysis was also carried out at each power setting. The high-power setting is shown on Figure 117. Notice that the agreement is only fair across the mid- and high-frequency regions of the spectrum. The low frequency part of the spectra appear to be in close agreement. Here, the jet noise component is predicted to be the predominant source. Based upon this comparison and similar ones at other power settings and configuration, it appears that the jet-noise prediction model used is adequate for the QCGAT program. Consequently, the predicted jet-noise levels could be analytically removed from the measured data. The remaining noise levels would then be those composed of the core and fan components. Once the jet component has been removed, the sound power levels attributed to the core were then compared with the predicted-core sound power levels, as shown in Figure 118. Also plotted are the sound power levels derived from the acoustic probes located in the primary exhaust. The probe data are shown more as a confirmation of the slope, rather than the sound power levels correctly calculated. These data indicate that the core noise model underpredicts the core noise level by roughly 3 dB. This underprediction appears to be independent to the power setting of the engine. Therefore, a simple

**LOW POWER SETTING - HARDWALL CONFIGURATION**

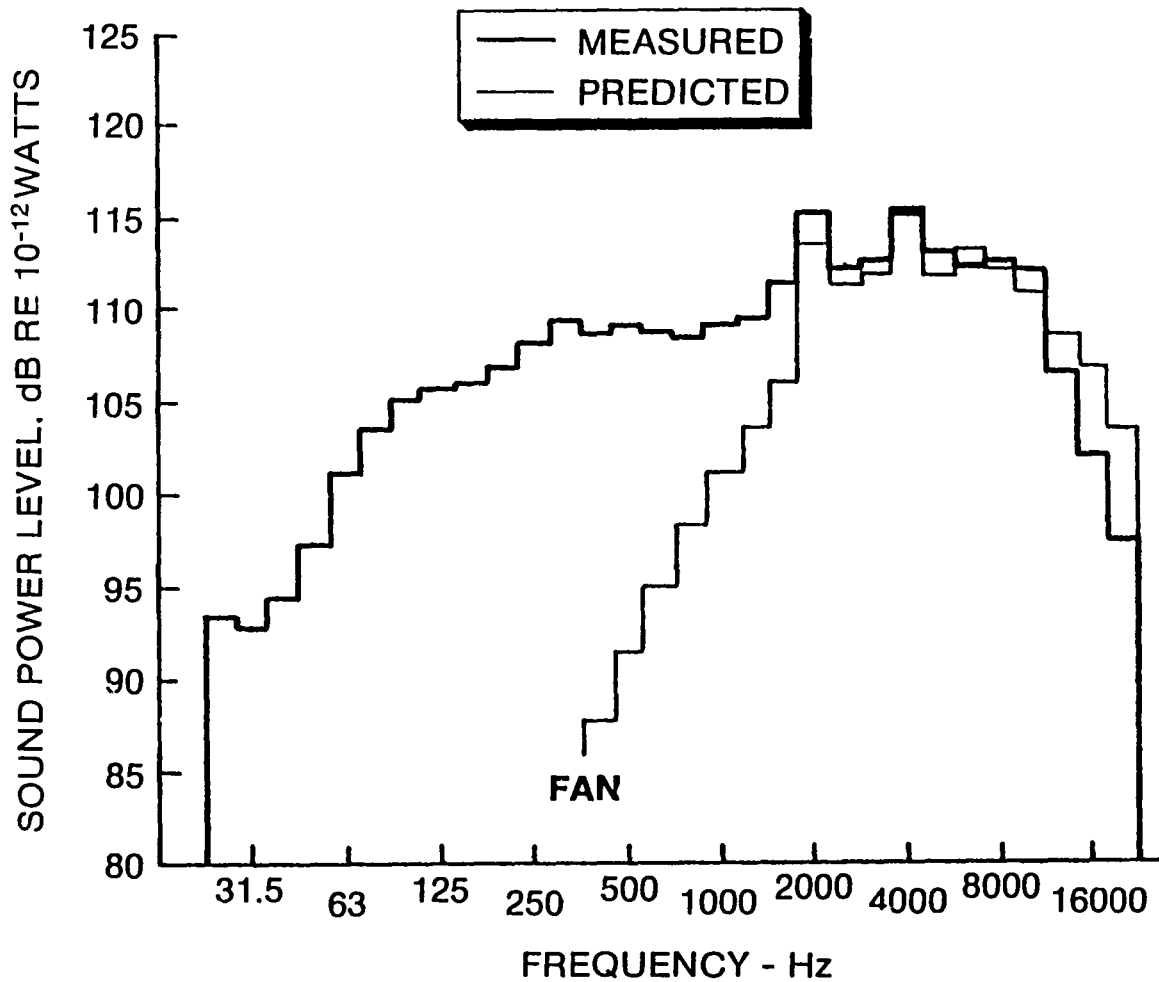


Figure 114. Measurements with Predicted Fan

**LOW POWER SETTING - HARDWALL CONFIGURATION**

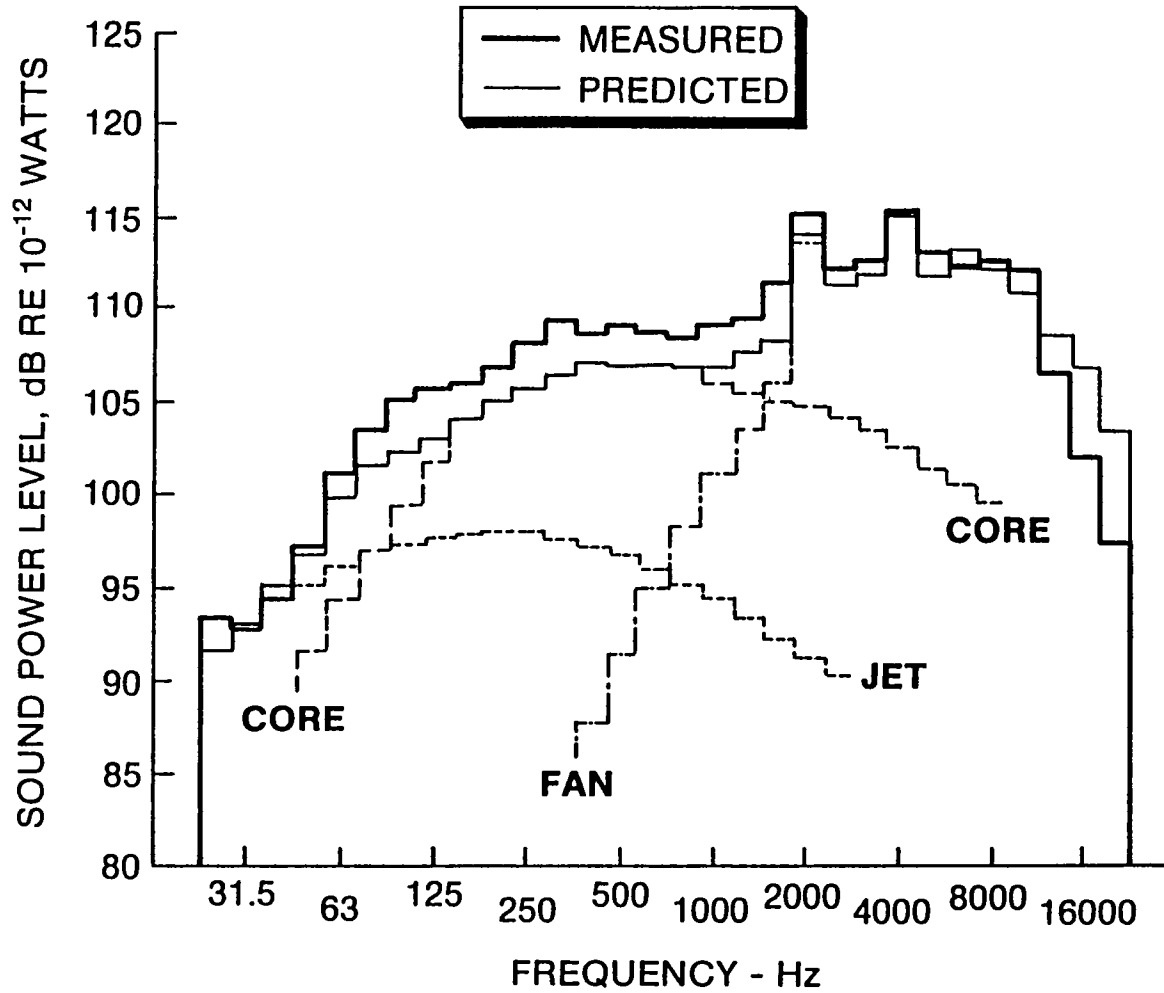


Figure 115. Measurements with Jet Added

**LOW POWER SETTING - HARDWALL CONFIGURATION**

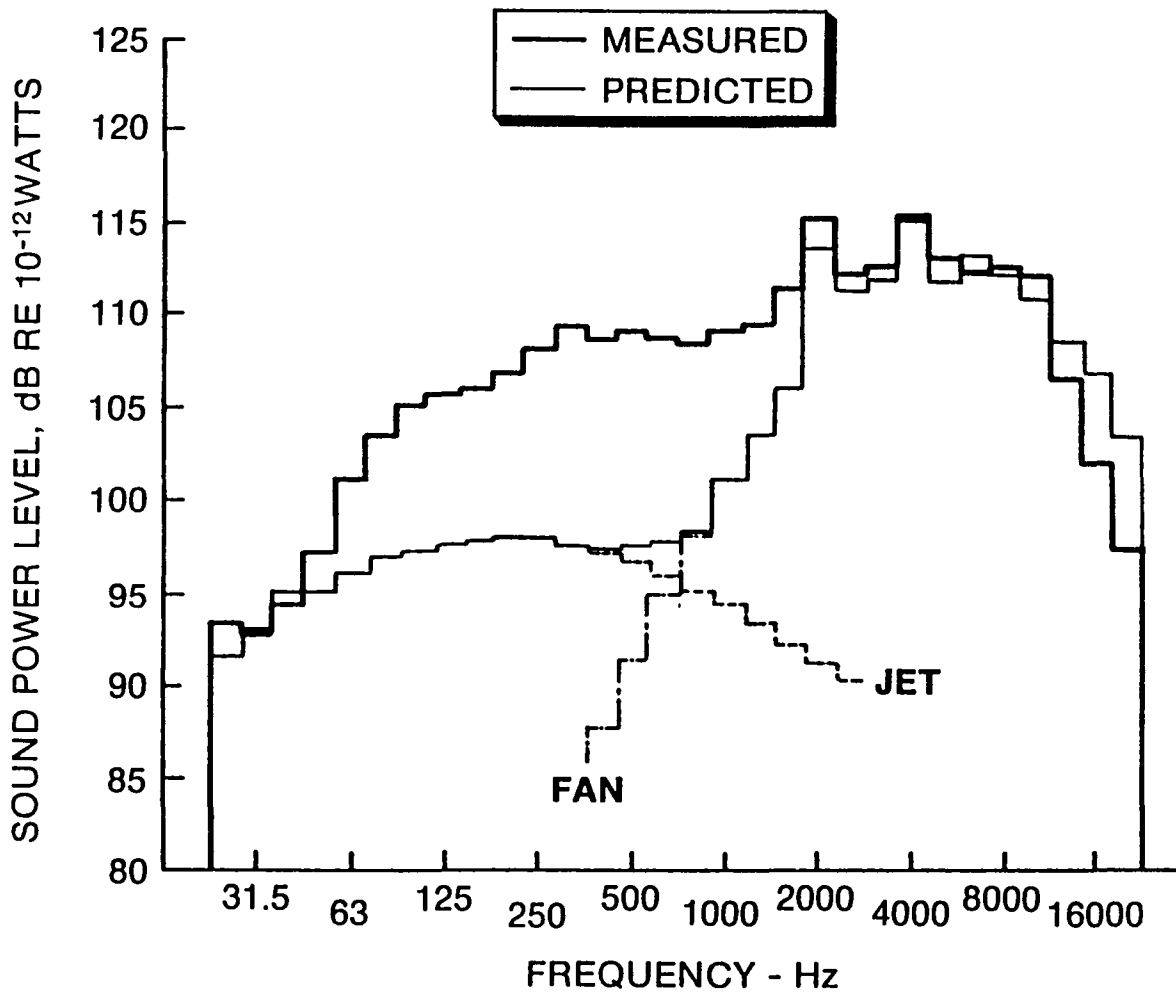


Figure 116. Core Added to Measured

**HIGH POWER SETTING - HARDWALL CONFIGURATION**

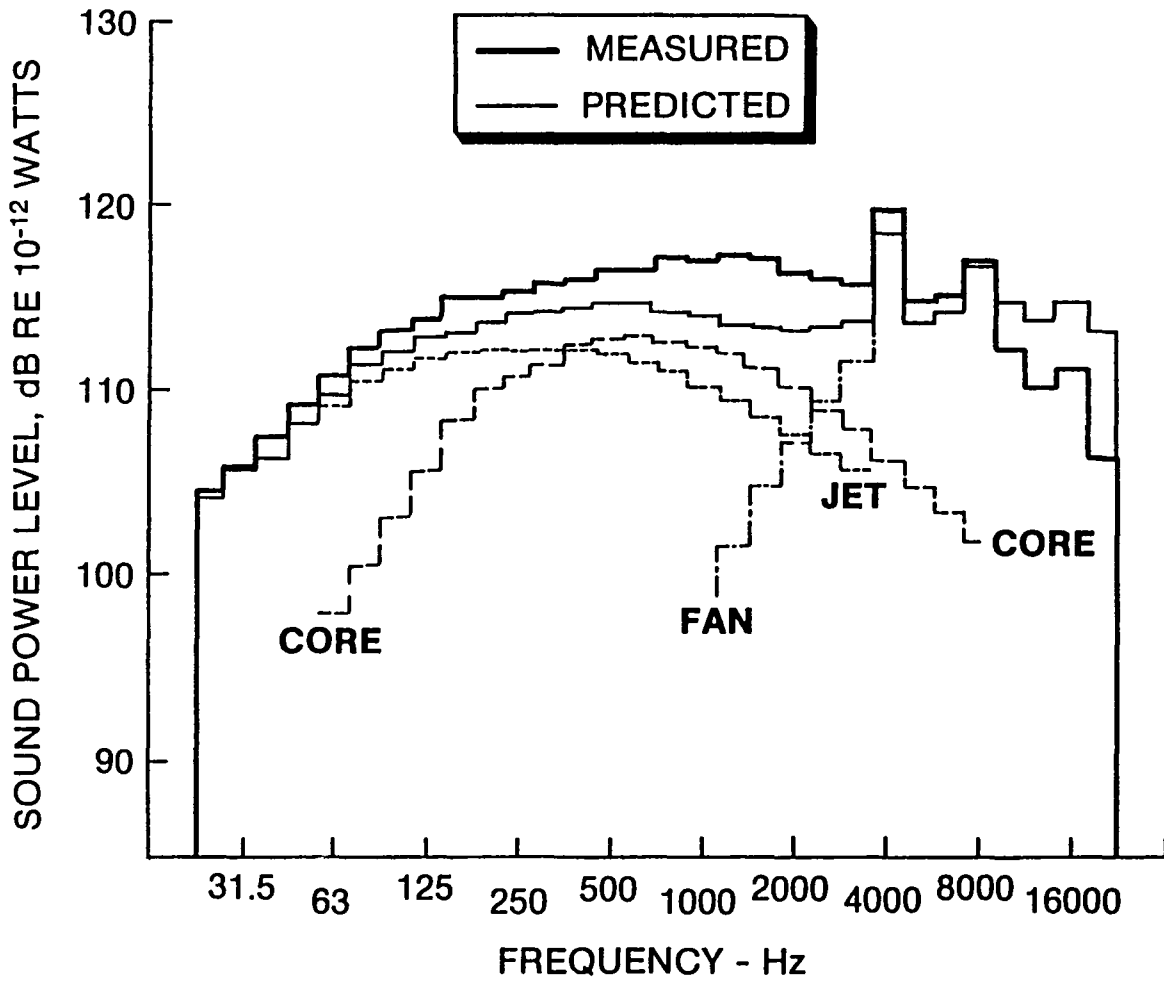
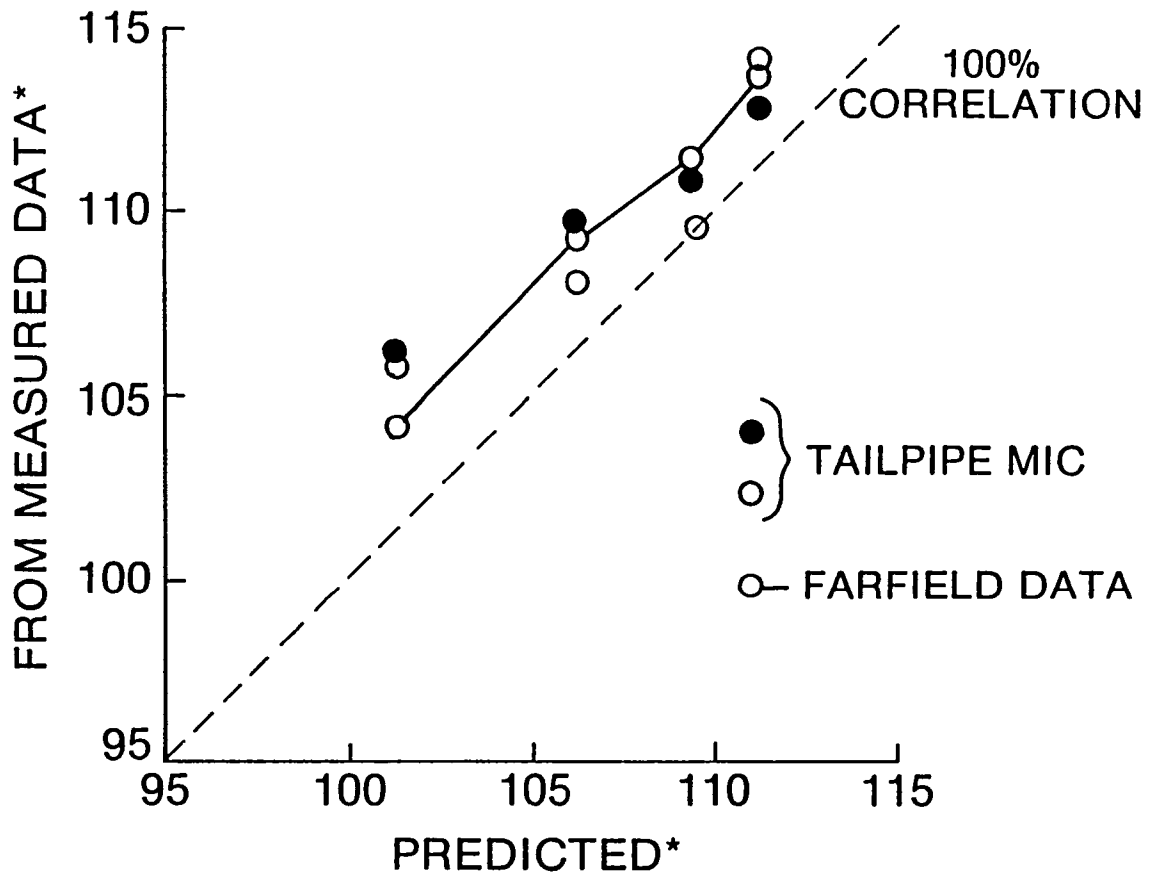


Figure 117. High Power Setting



\*Sound Power Level, dB RE 10<sup>-12</sup> Watts

Figure 118. Core Comparison

3 dB correction factor could be applied to the core noise prediction procedures. After making this refinement to the core noise model, the predicted-to-measured correlation was then rerun. Figure 119 shows this comparison. The spectral agreement between the measured and predicted data is good over the frequency range of interest. It can be seen that the sound levels in the band containing the tone at blade passing are also in good agreement; this indicates that the core noise contributes across the spectrum. The dominance of the core noise can be seen in Figure 120. The noise levels in the discharge quadrant are dominated by the core component to the extent that the fan component is almost entirely masked. For this reason, the reduction in the fan noise levels by the sound treatment was difficult to discern. When the core noise component is removed from the 1/3 octave band containing the blade passing tone, and the resulting blade passing tone is plotted against the angle from the inlet, as shown on Figure 121, a fan-tone directivity plot is formed. The predicted sound-pressure levels at the peak angles are also shown for the inlet and discharge quadrants. The expected results with the barrier in place come from the prediction procedures. Only when the barrier is in place will the measured data approach these lines, which it does as can be seen by the dotted lines. This plot shows how the fan noise contributes to the forward-and aft-radiated engine noise levels. If an observer was to move past the engine, the noise levels experienced would first rise and then fall off as the observer moved past. Once past the engine, the noise levels would then rise again as the discharge fan noise reached the observer. This is roughly how the static data were converted to observed-flight sound levels. At the high power setting (Figure 122), the core noise obscures the aft fan tone from the analysis. A small adjustment was made to the fan noise model from which these data were derived. This adjustment had to do with the effect of relative blade tip design Mach number. With this adjustment, we concluded from the agreement shown here and on the previous figure that the fan noise model accurately computes the fan noise levels. The sharp dip at the 60-degree point results from the fact that the data from 0 to 40 degrees were recorded at slightly different power settings than the data from 50 to 90 degrees. The predicted data show this same dip. This is an artifact of the data acquisition process and is not a characteristic of the fan noise. The individual component contributions appear to be adequately predicted once the noted corrections have been made. Figure 123 shows a final comparison of the measured

**HIGH POWER SETTING - HARDWALL CONFIGURATION**

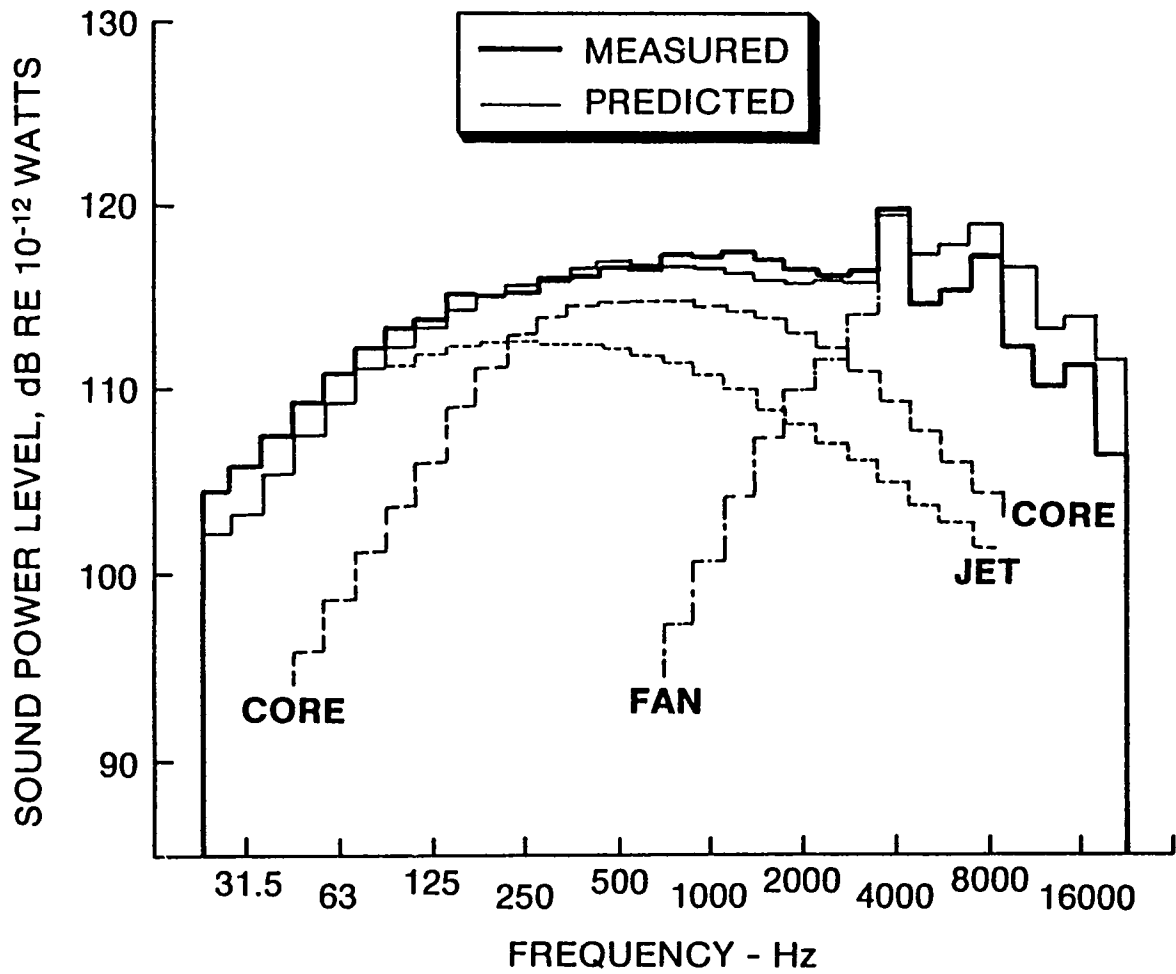


Figure 119. Revised Core Comparison



- Fan Tone Masked By Core Noise

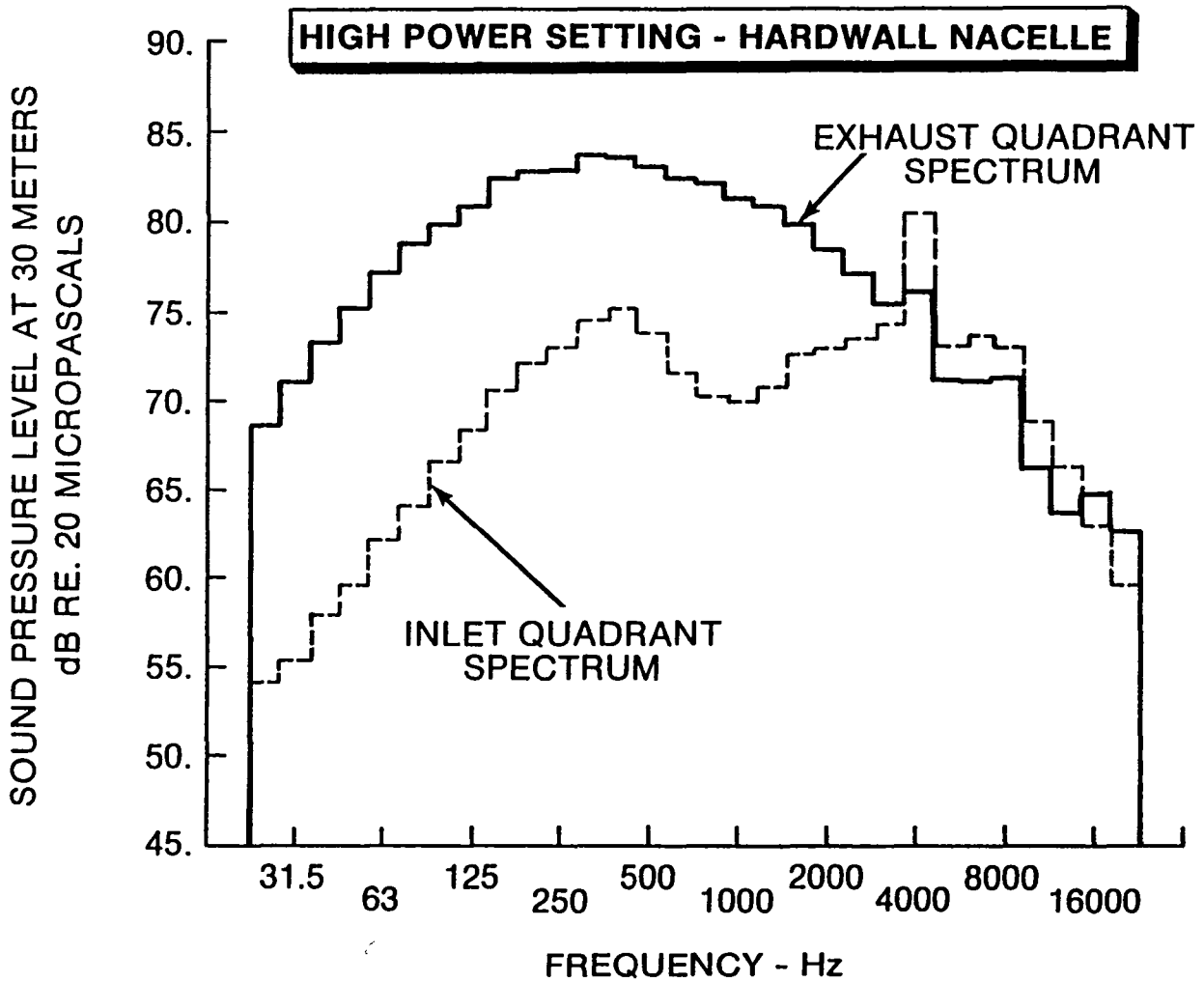


Figure 120. Core Noise Dominance

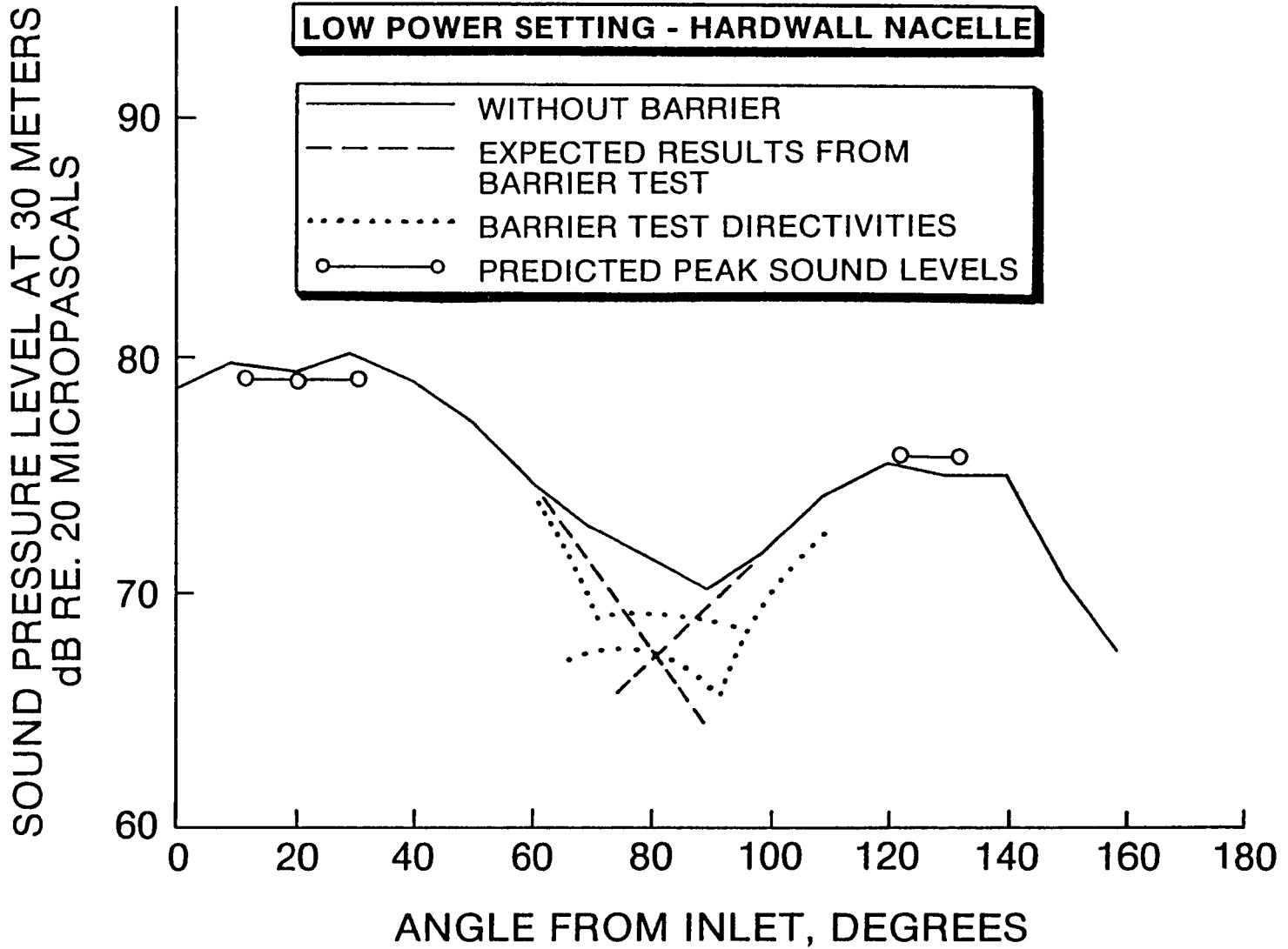


Figure 121. Fan Directivity Plots

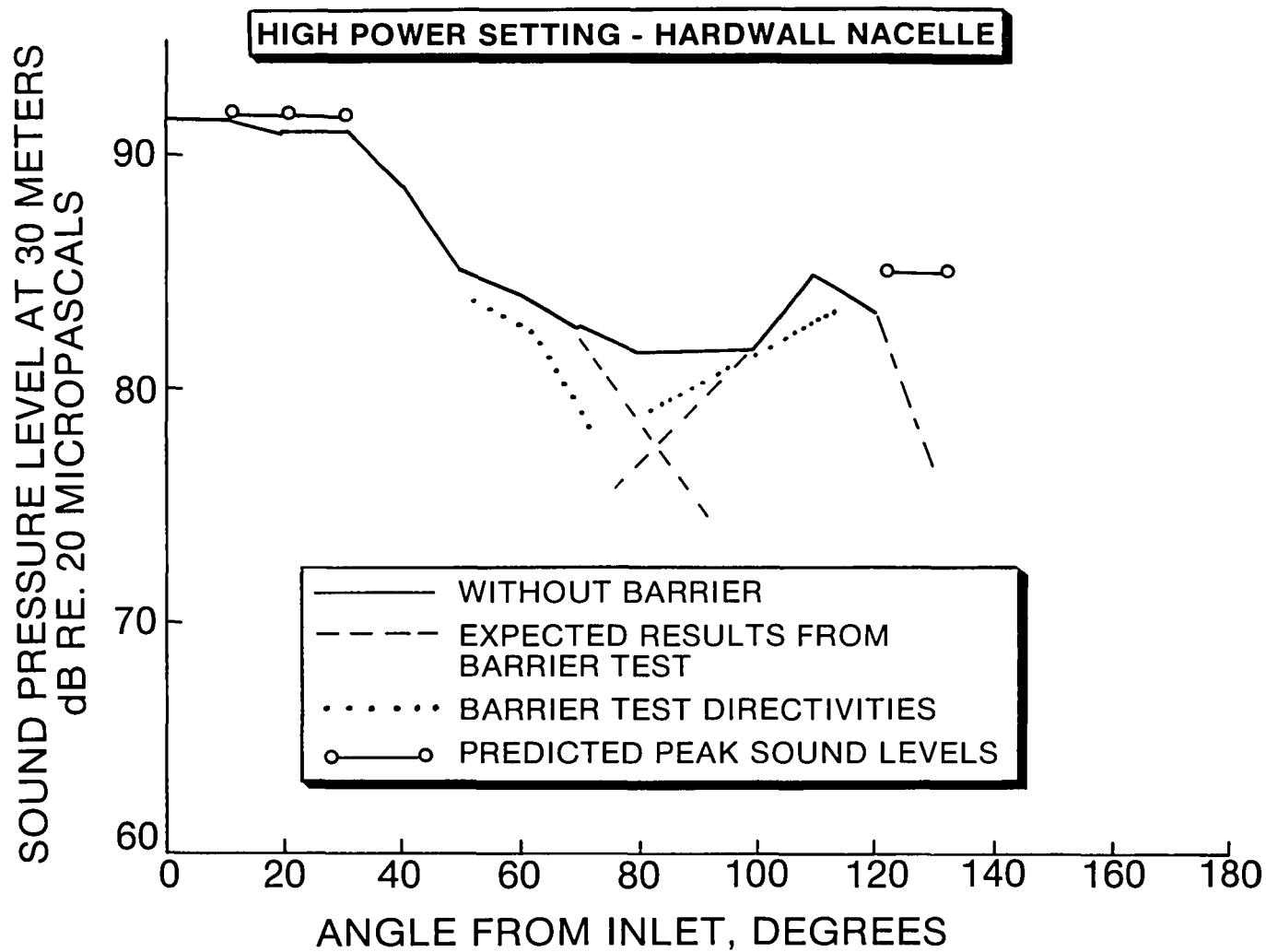


Figure 122. High Fan Directivity

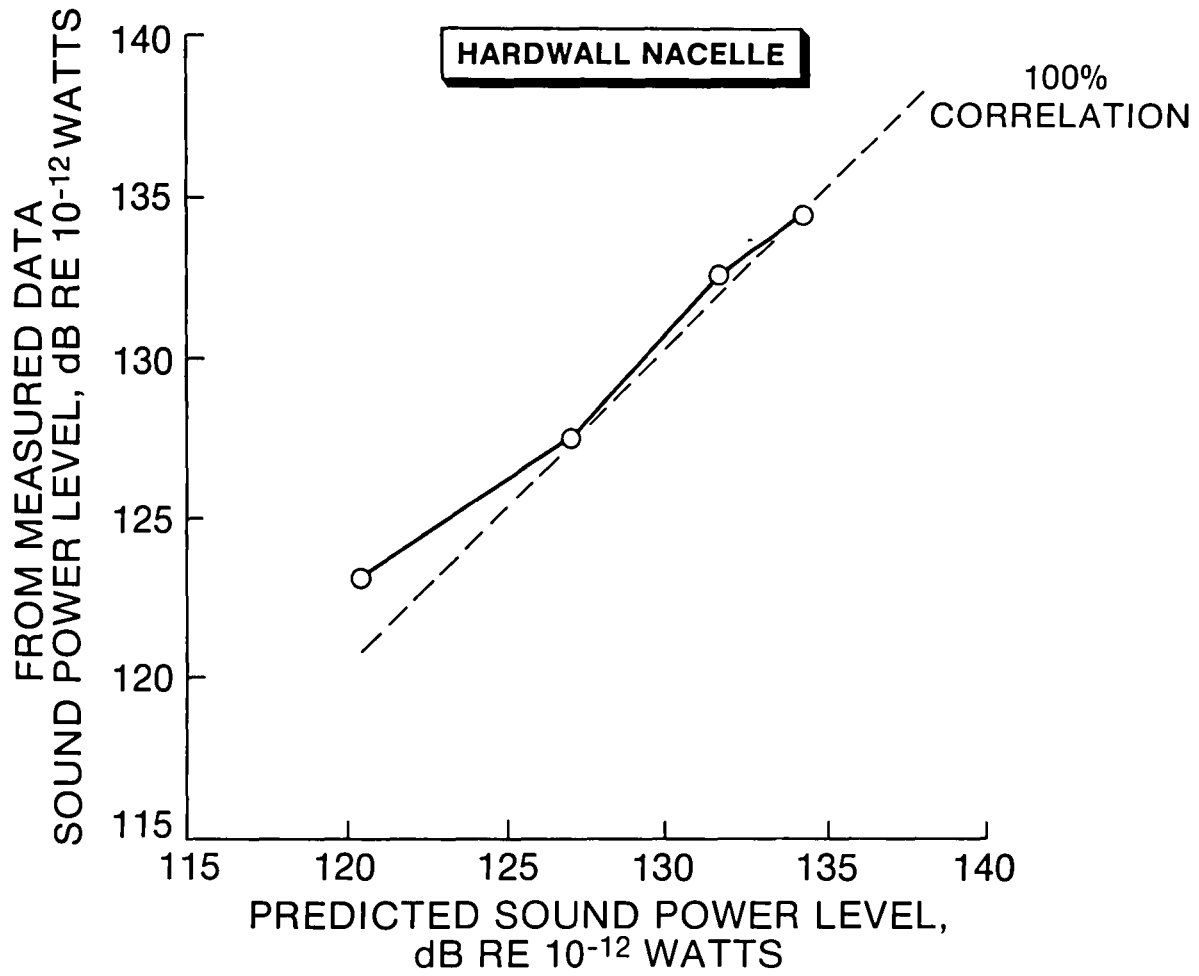


Figure 123. Final Comparison

and predicted overall sound power levels. This plot was generated to verify the accuracy of the prediction techniques for the static case before proceeding to the flyover analysis. The agreement shown indicates that the updated noise prediction model accurately reflects the static noise emissions of the QCGAT engine.

As noted earlier, it was difficult to discern the noise reduction of the sound-treatment panels from the far-field data. Figure 124 shows the one-third octave band sound pressure levels at the upstream and downstream microphone locations in the inlet. Here, the acoustic energy is propagating against the airflow in the inlet duct. The upstream microphone then recorded the inlet noise after it passed through the treated part of the inlet duct. Figure 125 shows the expected insertion loss and the insertion loss derived from the test data; these are the values that will be used in the flyover noise estimates. Figure 126 shows the expected and estimated insertion loss for the fan discharge-duct sound-treatment panels. The discharge panels had no provision for microphones and high core noise levels precluded a determination of its noise reduction. It is assumed that the treatment was functioning properly. The estimated values for the discharge sound-treatment panels are shown on Figure 124.

The jet noise levels were predicted to be low because of the use of a high bypass-ratio fan. Figure 127 shows the difference between the noise spectra of such an engine fitted with the split-flow nozzle configuration and with the mixer nacelle configuration. The shaded area represents the static noise reduction of the mixer.

Above 250 hertz, the core noise-source starts to mask the jet noise, and above 1000 hertz the fan is dominant. When flight effects are added, both the mixed and split-flow jet components will drop leaving the mixed-flow jet noise levels below the core noise levels. The split-flow noise levels would drop and be roughly equal in magnitude to static jet-noise levels.

5.3.6.2 Flight Predictions - The procedures employed (Figure 128) in the QCGAT program to assess the noise emissions of a QCGAT powered aircraft are the Federal Aviation Administration's certification procedures for turbojet-powered aircraft (Reference 13). This is a very rigorous method. Basically, the FAA requirements call for measuring the aircraft's noise every one-half second as the aircraft flies over the measurement point. For this analysis, predicted data were substituted for the actual measurement. The dem-

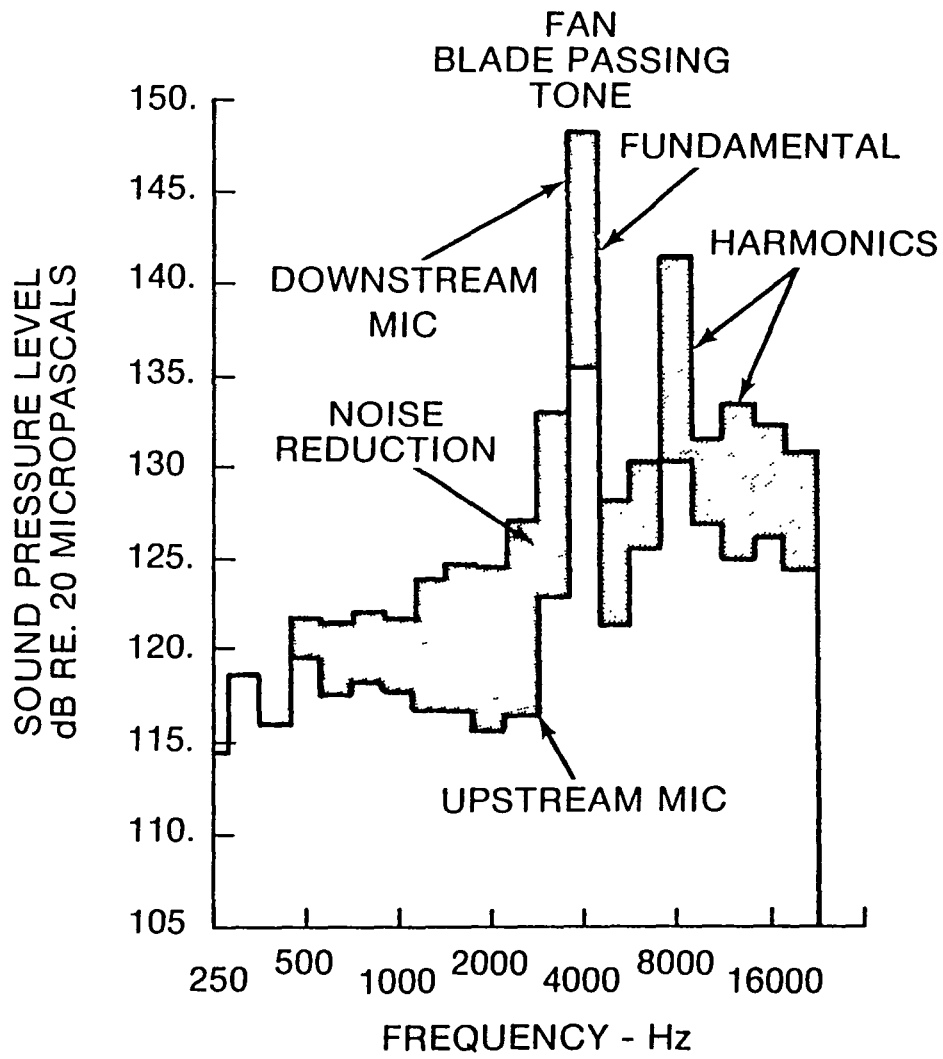


Figure 124. Sound Treatment

- Treatment Estimated to Meet Design Specifications
- Analysis Limited By Low Fan Sound Levels

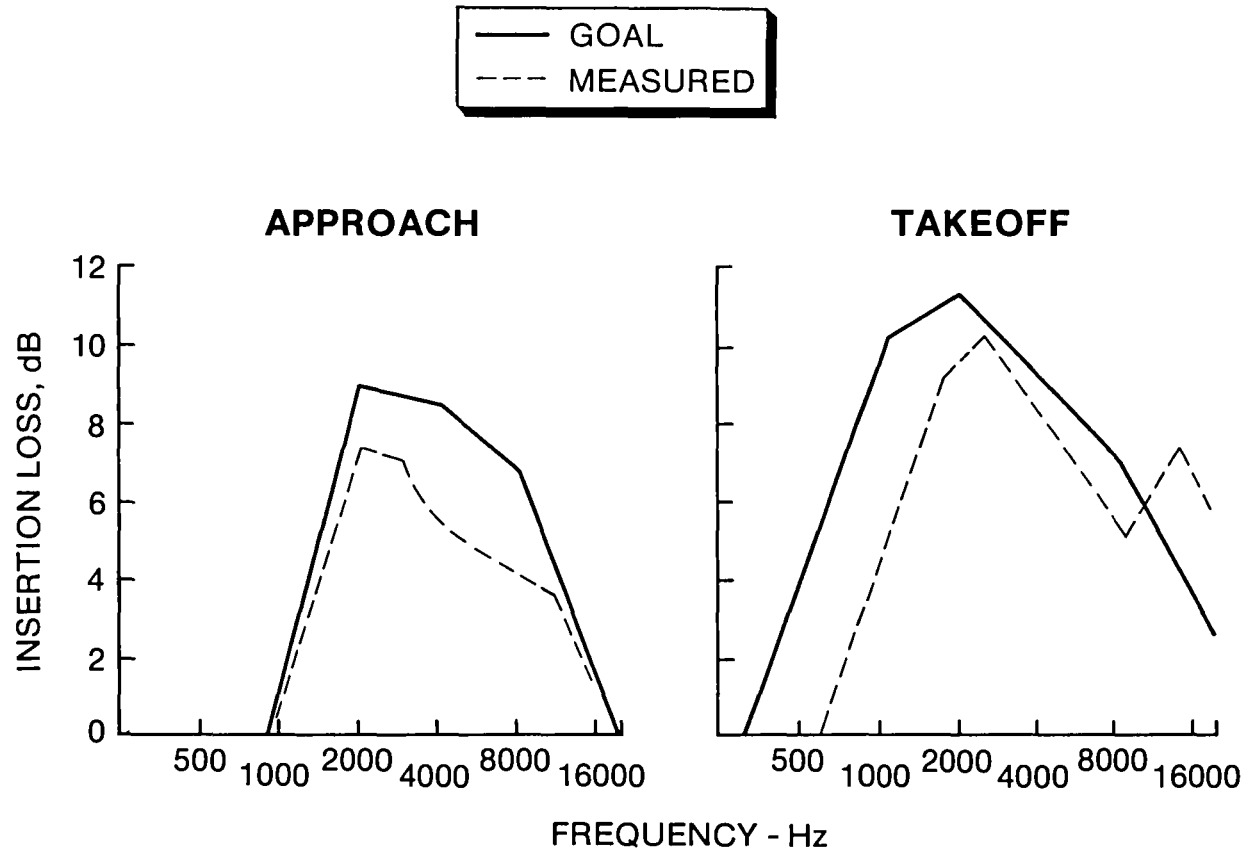


Figure 125. Insertion Loss-Inlet

- Treatment Estimated to Meet Design Specification
- Analysis Limited By Low Fan Sound Levels

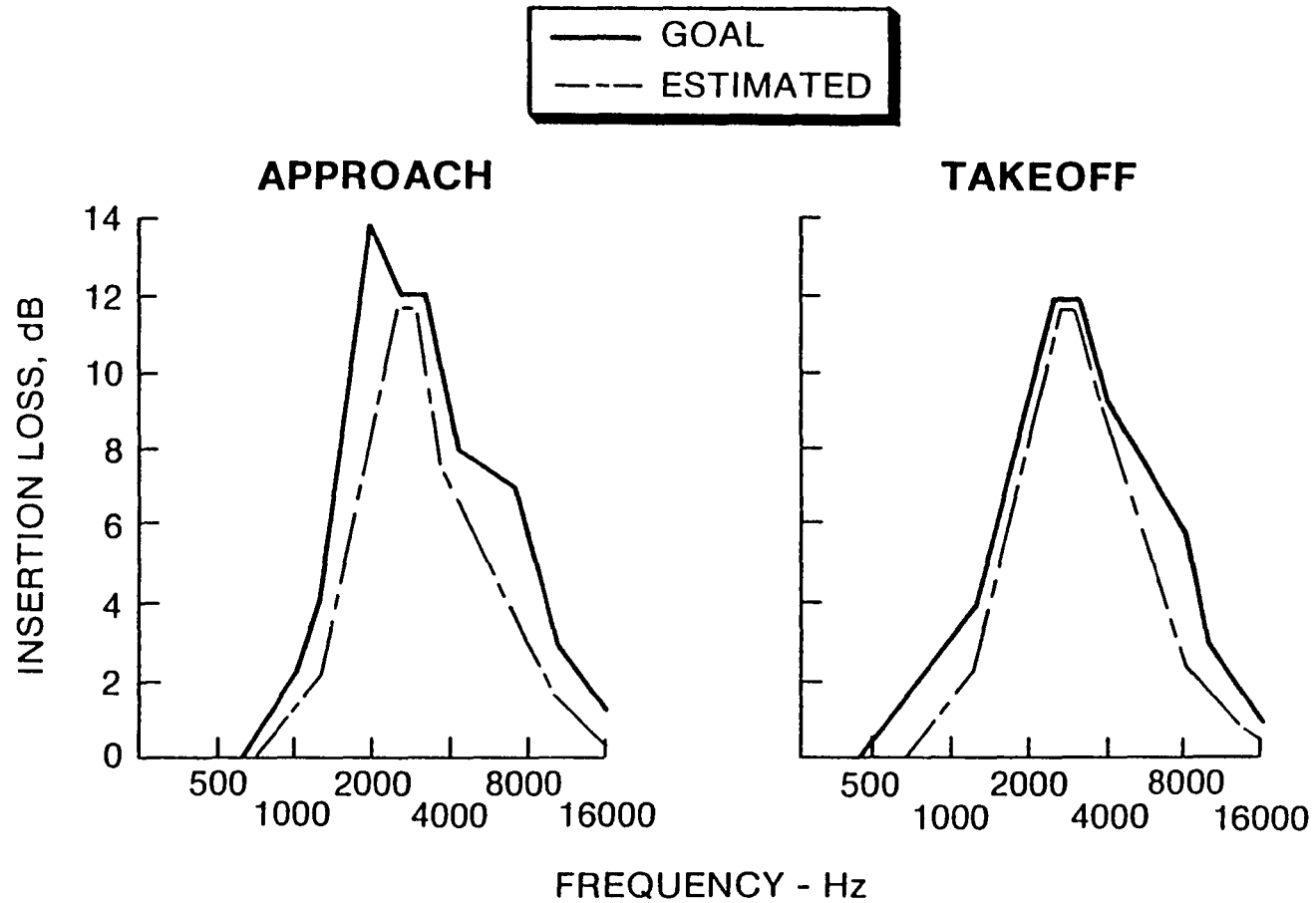


Figure 126. Insertion Loss - Discharge



- Greater Than 5 dB
- Coincides with Predicted Results

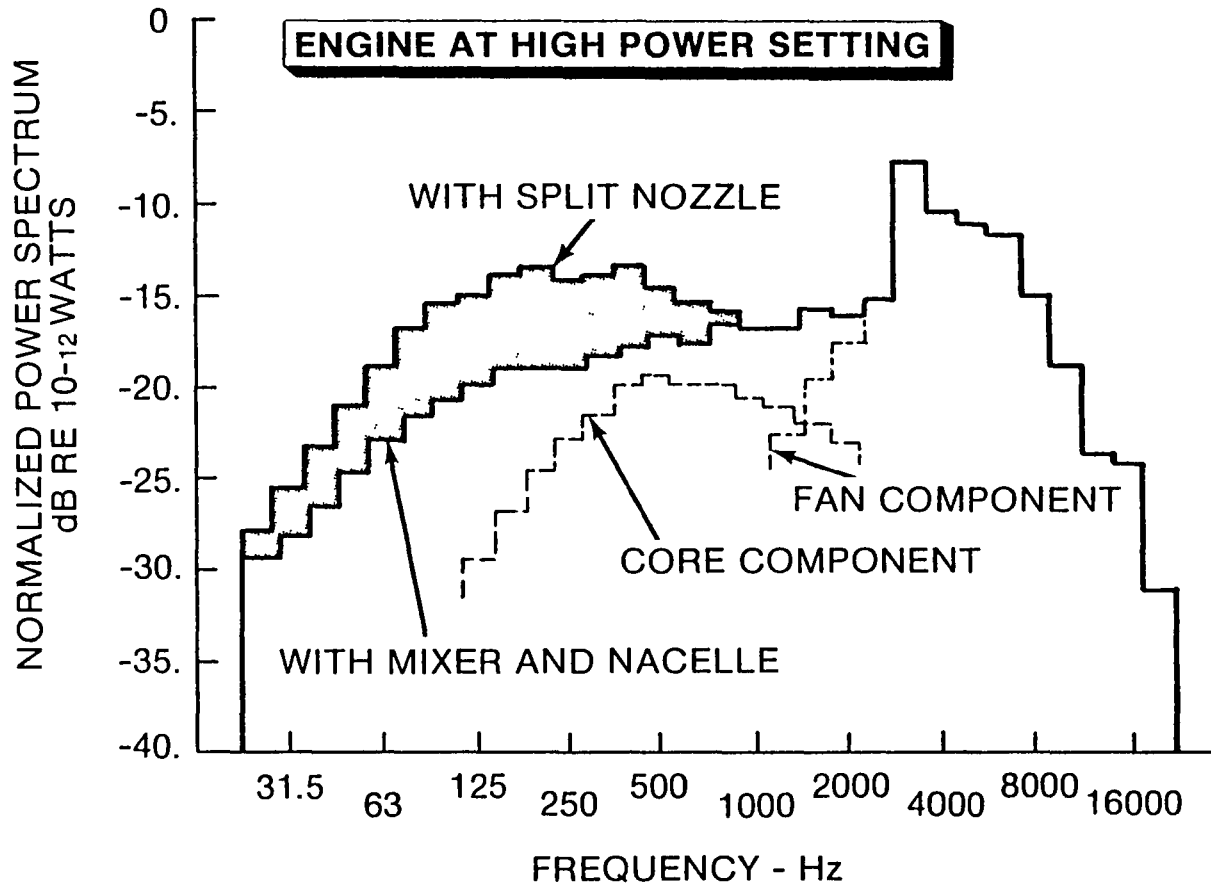


Figure 127. Jet Spectra

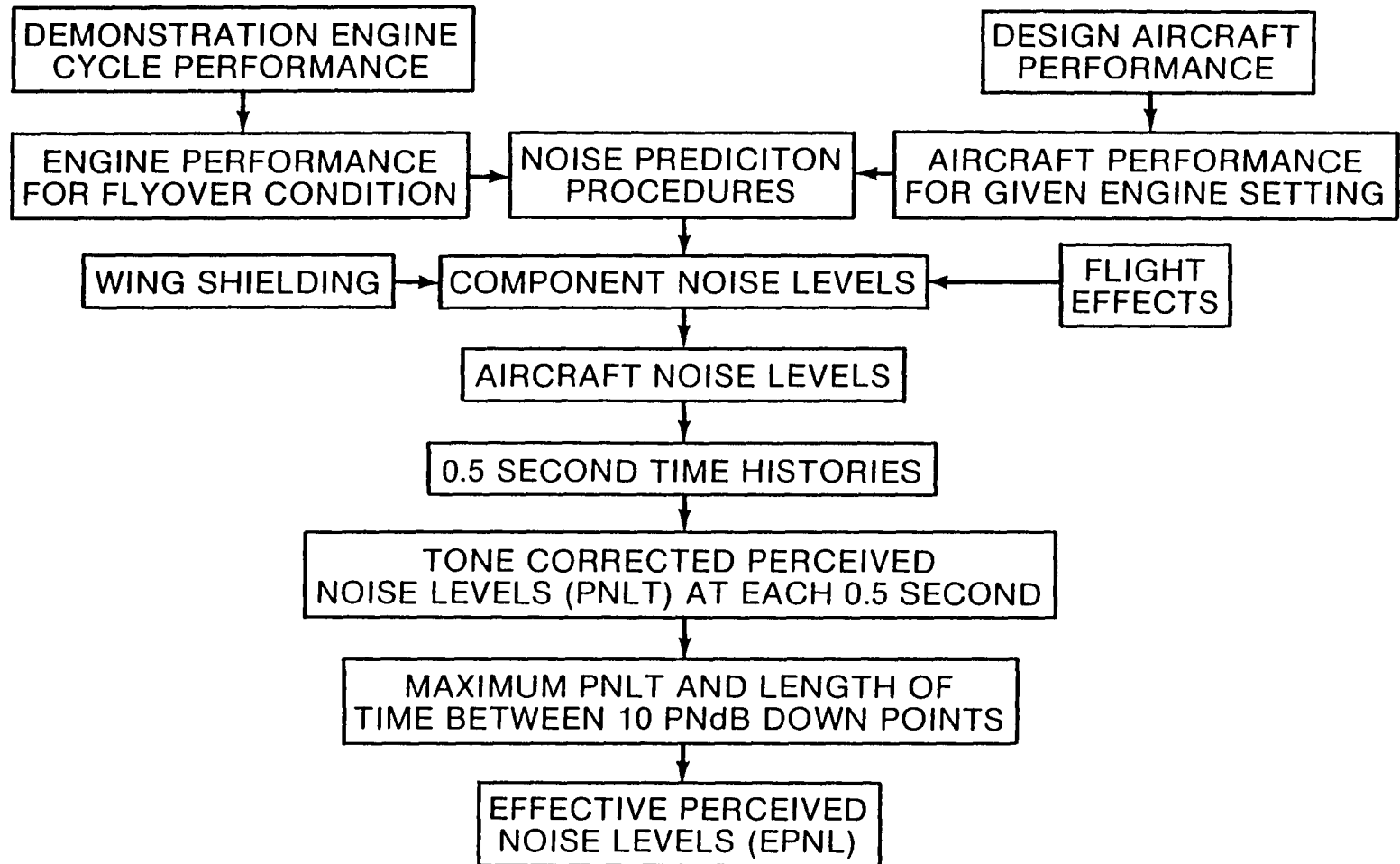


Figure 128. Flyover Procedures

onstrated engine performance and the Beech aircraft design were used to compute the individual test point performances. These data were then entered into the prediction procedures. The appropriate flight and wing shielding effects were then applied to the individual component noise predictions. The aircraft noise signature was then derived by combining these into a table of aircraft noise. Then by analytically moving the aircraft noise table past the measurement point, the time history of the flyover could be constructed for each half-second interval. These sound levels were then used to compute the tone corrected perceived noise levels for the flyout event. The maximum tone-corrected perceived noise levels were then found along with the time the aircraft noise was within 10 PNdB of the maximum. The effective perceived noise levels were calculated from these data.

Figure 129 shows the tone-corrected perceived noise levels versus time for the approach flyover. The maximum tone-corrected perceived noise level, labeled PNLT<sub>M</sub>, would occur after the aircraft had passed directly overhead. The time that the PNLT was within 10 PNdB of the value would be 8.5 seconds. This plot also shows that the fan inlet and discharge noise would be heard at separate times. The valley between the peaks was caused by the lower sound levels generated at the sideline positions. Wing shielding, the shaded portion, would act to cut the inlet peak off early and make the valley deeper. The core noise component would be heard after the aircraft passed, as most of the core noise is in the aft quadrant of the engine. Because of the duration correction, the fan component noise levels are higher and contribute more to the effective perceived noise levels.

The takeoff flyover tone-corrected perceived noise level time history is shown similarly in Figure 130. The time interval that the noise was within 10 PNdB of the maximum would be much longer. At the approach condition, the altitude at flyover would be 113 meters (370 feet). For the takeoff condition, it would be 792 meters (2600 feet). Consequently, the time the aircraft requires to fly past would be considerably longer. The maximum tone-corrected perceived noise level would also occur much later as the sound would take longer to reach the observer because the dominant noise sources are the core and jet. These components radiate most of their acoustic energy to rear quadrants and, as such, it would not be heard until the aircraft has flown past the observer. Also shown here are the higher noise levels of a split-flow nozzle configured aircraft. Here the jet component would contribute more to the aircraft noise levels in both

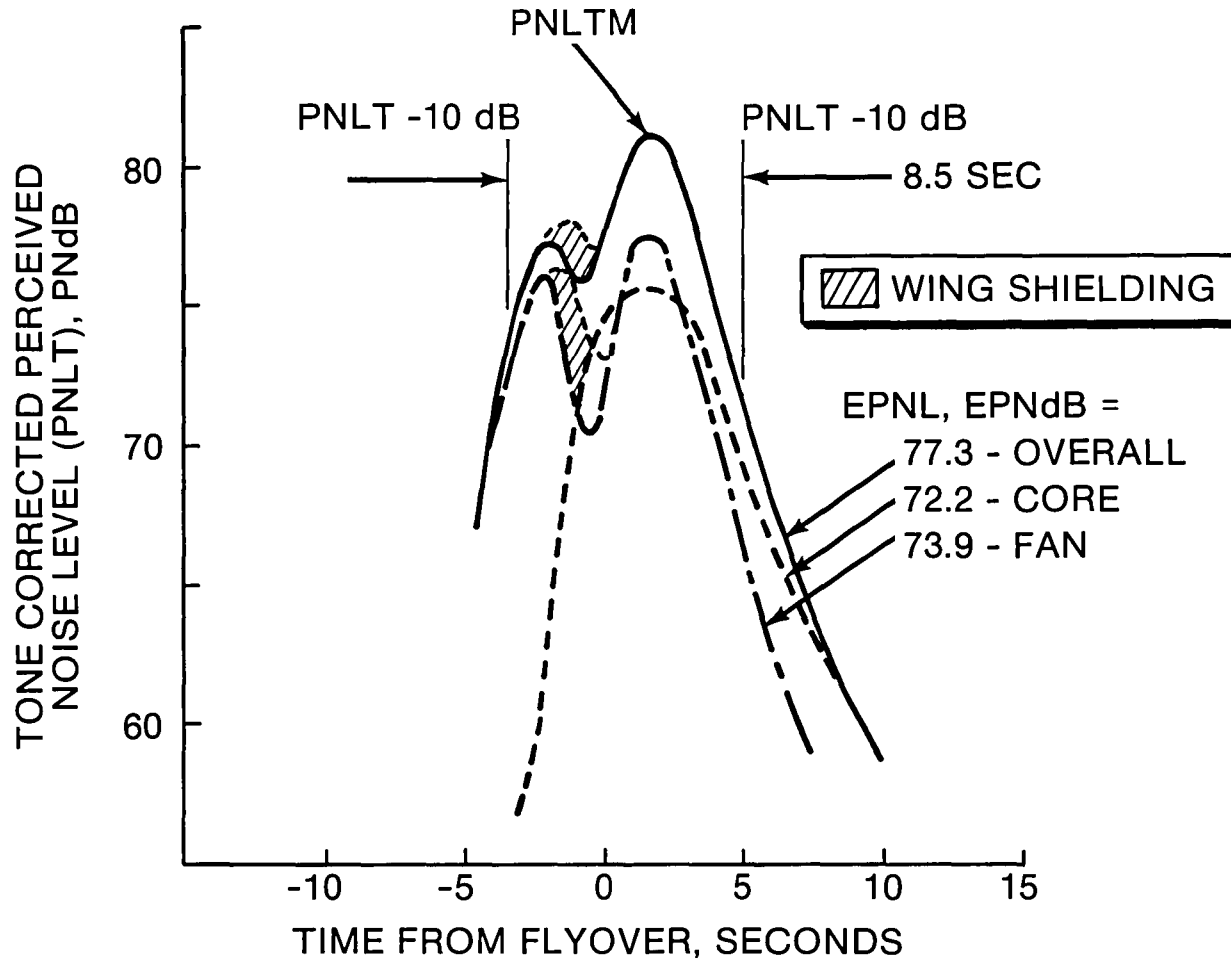
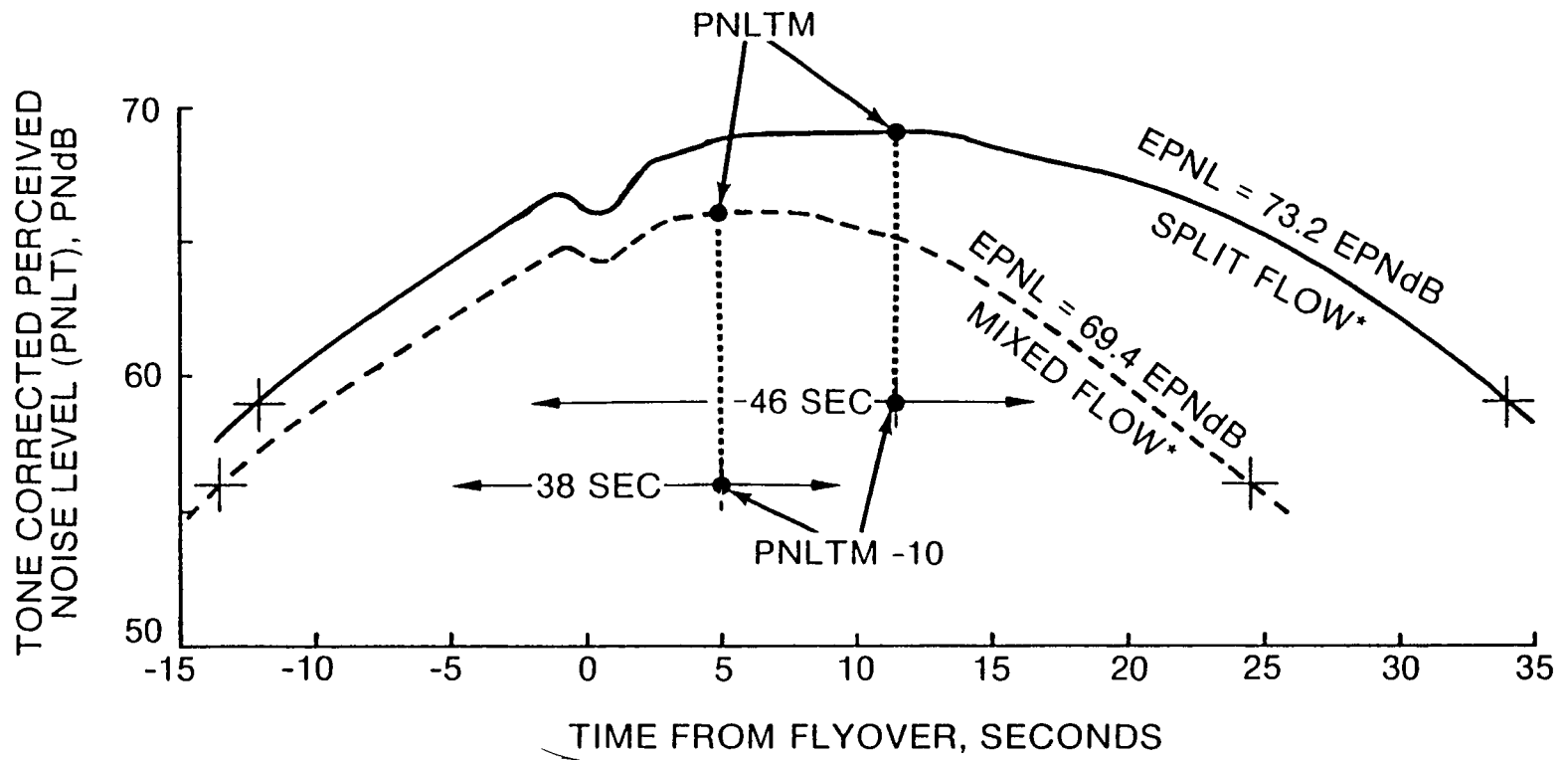


Figure 129. Component Contribution - Approach Noise



Takeoff Flyover Noise Time History  
at Observer Location 3.5 Nautical  
Miles Down Range from Brake Release

\*No Sound Treatment

Figure 130. Component Contribution - Takeoff Noise

magnitude and duration. The duration would be increased because the jet noise peaks further aft than the core noise. This means that the peak noise would occur later in the flyover. Thus, the addition of the mixer not only reduces the aircraft flyover noise levels, the aircraft noise does not linger as long.

### 5.3.7 Conclusion

For an aircraft powered by two Avco Lycoming QCGAT engines installed in a nacelle that includes a mixer, fan inlet and discharge sound-treatment panels, and mounted over the wings, the effective perceived noise levels for the takeoff, sideline, and approach conditions would be 68.4, 70.6, and 77.3 EPNdB, respectively. These noise levels, shown in Figure 131, are below the limits set by the QCGAT program goals. In the analysis, the effect of several alternative engine configurations on the aircraft noise was assessed. For example, removal of the sound-treatment panels would add 2 EPNdB to the approach noise levels and still be below the QCGAT goals. The other positions would not be affected appreciably.

When the iterations are completed for this engine design, the increased thrust of the engine means that the aircraft will achieve an altitude of 3600 feet over the takeoff point versus the present 2600 feet. This will result in a 3 EPNdB reduction in the takeoff noise levels and a 1 EPNdB reduction in the sideline noise levels. In this case, the split-flow exhaust nozzle configuration would be within 1 EPNdB of the QCGAT goals. Figure 132 shows that the Avco Lycoming QCGAT engine's effective perceived noise levels plotted against the Federal Aviation Administration's Stage III noise standards and the high technology levels that were used by NASA for the QCGAT program goals. This demonstrates that the technology which has worked for the large engine can be applied to the general-aviation size engine.

In summary, large turbofan noise-control technology was successfully applied to a general-aviation size engine. The stringent program goals set by NASA forced a concept that required integration of a quiet fan design with the nacelle and aircraft to provide an efficient propulsion system.

Static noise tests have demonstrated that the QCGAT program goals can be met with the latest noise-control techniques without incurring a performance penalty.



### QCGAT ACOUSTIC PERFORMANCE

<u>CONDITION</u>	<u>EPNL GOAL EPNdB</u>	<u>DELIVERED ENGINE EPNL, EPNdB</u>
Takeoff Flyover	69.4	68.4
Takeoff Sideline	78.4	70.6
Approach Flyover	83.4	77.3

Figure 131. Noise Levels - QCGAT Goals

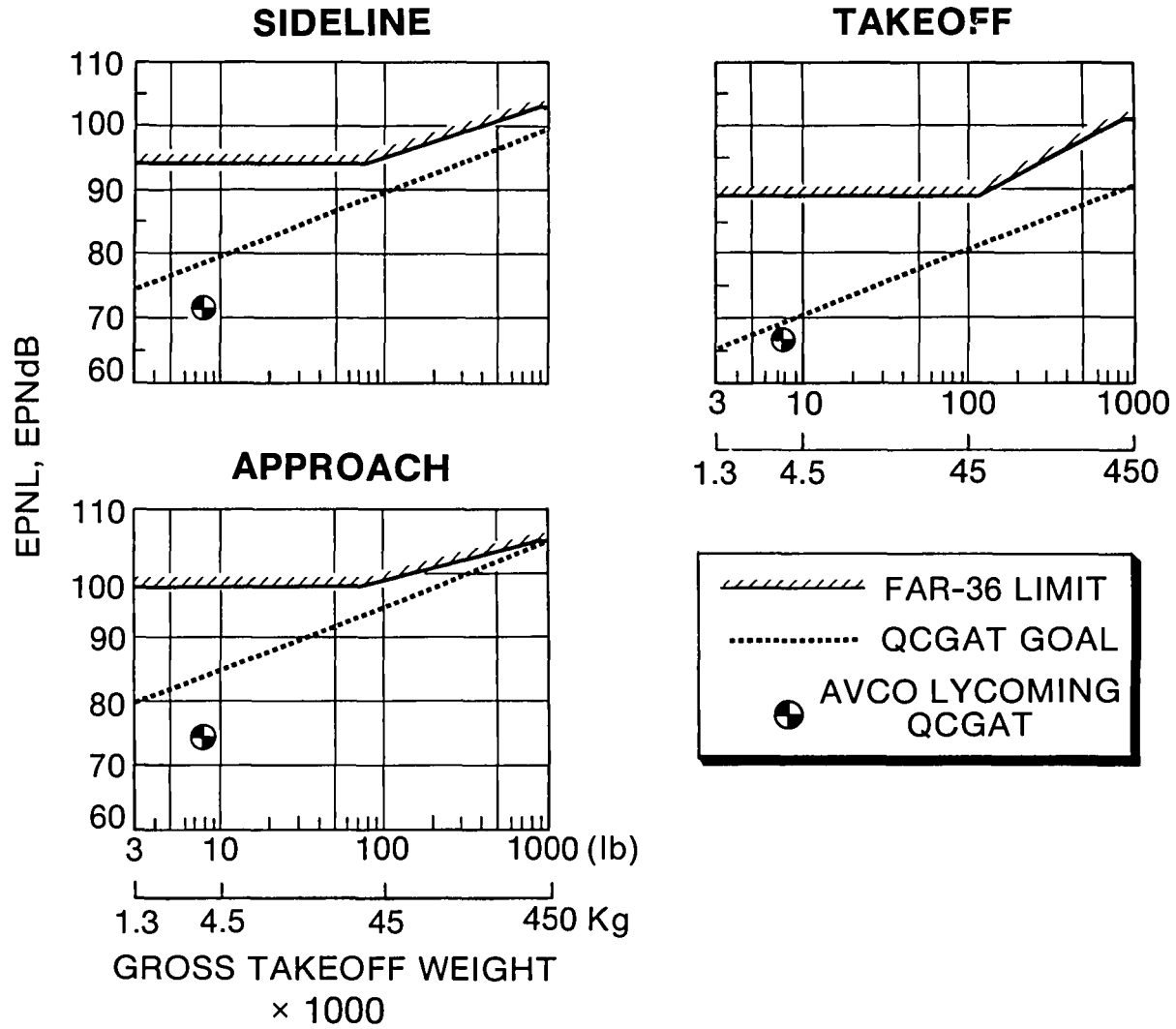


Figure 132. Noise Levels - FAA Standards



## 6.0 SUMMARY OF RESULTS

### 6.1 OBJECTIVES

The objective of the NASA Quiet, Clean General Aviation Turbofan (QCGAT) engine program was to demonstrate the applicability of large turbofan engine technology to small general aviation engines. Specifically, reduction in the levels of noise and pollutant emissions, along with fuel consumption, were addressed.

Avco Lycoming participated in the NASA QCGAT engine program by designing and developing a 7,000 N (1,600 lbf) thrust turbofan that used the Lycoming LTS 101 as a core engine. The prime areas investigated in order to meet the NASA requirements were:

1. Define the engine and determine its characteristics and requirements for a QCGAT engine applicable to general aviation aircraft. (This included a preliminary design of an aircraft by the Beech Aircraft Corporation).
2. Design and fabricate the new and modified parts required to be used with an existing gas generator core in the turbofan engine.
3. Perform evaluation test of critical components
4. Perform evaluation tests of the QCGAT engine
5. Design and fabrication of an acoustically treated nacelle
6. Measure engine noise, emissions, and sea level static overall engine performance to establish validity of predictions prior to engine delivery to NASA.
7. Deliver a quiet, clean, turbofan engine, an acoustically treated nacelle, and engine test support hardware to NASA.

### 6.2 TEST RESULTS

QCGAT engine test results compared with the predicted design performance goals are tabulated below.

### 6.2.1 Overall Engine Performance Demonstrated

<u>Sea Level Takeoff</u> <u>(Standard Day Installed)</u>		<u>Goal</u>	<u>Test</u>	<u>Deviation from</u> <u>Design (%)</u>
Thrust	N (lbf)	7166 (1611)	6485 (1458)	-9.5
Specific Fuel Consumption				
	Kg/N-hr	0.0370	0.0400	+9.5
	lbm/lbf-hr	(0.363)	(0.392)	
<u>Design Cruise</u> <u>7620 M (25,000 ft), Mach 0.6</u>				
Thrust	N (lbf)	2157 (485)	1850 (416)	* -14.2
Specific Fuel Consumption				
	Kg/N-hr	0.064	0.074	* +15.1
	lbm/lbf-hr	(0.628)	(0.723)	

\* Estimated from Static Data

The overall performance did not meet the desired goals. However, subsequent component testing has identified the deficiency to be in the matching of the high-pressure turbine and the power turbine. Since the hardware design and procurement were not within the NASA timeframe, the engine performance demonstration test was conducted with existing hardware. The design goals are viable and achievable with the Lycoming QCGAT engine.

### 6.2.2 Emissions

	<u>Goal*</u>	<u>Test *</u>	<u>Deviation</u>
Unburned Hydrocarbons (UHC)	.045 (1.6)	.017 (.62)	-62.2%
Carbon Monoxide (CO)	.266 (9.4)	.193 (6.8)	-27.4%

	<u>Goal*</u>	<u>Test*</u>	<u>Deviation</u>
Oxides of Nitrogen (NO <sub>x</sub> )	.105 (3.7)	.106 (3.75)	+1%
Smoke Number	45	24	-46.7%

\* - Units gm/KNsec

(lbm/1000 lbf Thrust hr-Cycle)

The Lycoming QCGAT engine test demonstrated that all emission goals were easily achievable with the exception of NO<sub>x</sub> which was slightly over the design estimated goal.

### 6.2.3 Acoustics

The NASA program goals were 15 to 20 EPNdB below the FAR Part 36 noise levels. The high technology levels of the Lycoming QCGAT program demonstrated performance levels better than the goals, as tabulated below:

<u>Condition</u>	<u>Goal (EPNLdB)</u>	<u>Measure (EPNLdB)</u>	<u>Noise Improvement (dB)</u>
Takeoff Flyover	<sup>64.4</sup> 64.4	68.4	1.0
Takeoff Sideline	78.4	70.6	7.8
Approach Flyover	83.4	77.3	6.1

### 6.3 CONCLUDING REMARKS

Efforts of the NASA/QCGAT program have contributed to a new engine that is designed to serve the needs of the general aviation industry in the 1980's. The engine and nacelle designs have demonstrated the primary program objectives. Technology to reduce engine noise has been successfully applied to the general aviation size engine to obtain the acoustic goals with margin. Any foreseeable acoustic or pollutant emission requirements will offer no major constraint.

Challenging objectives for a fuel-efficient, ecological aircraft were set for the preliminary design to respond to our assessment of general aviation market needs for the next decade. The aircraft design achieves these objectives to provide a truly quiet, clean, six-place, long-range capability that will be attractive to both the user and suburban community.

## REFERENCES

1. Wharton, H. E., AVCO LYCOMING QUIET CLEAN GENERAL AVIATION TURBOFAN (QCGAT) ENGINE NACELLE SOUND ABSORPTION PANEL DESIGN, Lockheed California Co. Report LR 28254, July 20, 1977.
2. Tyler, J. M. and Sofrin, T. G., AXIAL FLOW COMPRESSOR NOISE STUDIES, SAE345D, 1961.
3. Ko, S. H., SOUND ATTENUATION IN ACOUSTICALLY LINED CIRCULAR DUCTS IN THE PRESENCE OF UNIFORM FLOW AND SHEAR FLOW, Journal of Sound and Vibration, Vol. 22 (2), pp. 193-210, 1972.
4. Rice, E., SPINNING MODE SOUND PROPAGATION IN DUCTS WITH ACOUSTIC TREATMENT AND SHEARED FLOW, AIAA Paper 75-519, March 1975.
5. Prydz, R. A., BOUNDARY LAYER CONSIDERATIONS FOR OPTIMIZATION OF ACOUSTIC LINERS FOR AIRCRAFT ENGINE DUCTS, SAE Paper 760896, November 1976.
6. Dunn, D.G. and Peart, N.A., AIRCRAFT NOISE SOURCE AND CONTOUR ESTIMATION, NASA CR 114649, July 1973.
7. Laurence, J. C. and Benninghoff, J. M., TURBULENCE MEASUREMENTS IN MULTIPLE INTERFACING AIR JETS, NASA TN 4029.
8. Hurley, J. F., Hanson, L. and Wilson, C. A., DESIGN OF AN EXHAUST MIXER NOZZLE FOR THE AVCO LYCOMING QUIET CLEAN GENERAL AVIATION TURBOFAN (QCGAT), NASA-CR-159426, August 1978.
9. Lipert, F. W., CORRELATION OF GAS TURBINE EMISSIONS DATA, ASME 72-GT-60.
10. EMISSIONS STANDARDS AND TEST PROCEDURES, Title 40, CFR Part 87, published in the Federal Register, July 17, 1973.
11. U. S. Patent 3,671,171, ANNULAR COMBUSTORS, Brian W. Doyle.

12. U. S. Patent 3,645,095, ANNULAR COMBUSTOR, Jerry O. Melconian.
13. FEDERAL AVIATION ADMINISTRATION NOISE STANDARDS  
Title 14, Code of Federal Regulation, Chapter I. Part 36  
Amendment 7.
14. Stone, J. R., INTERIM PREDICTION METHOD FOR JET NOISE,  
NASA T MX-71618 (1974).
15. Huff, R.G., Clark, B.J., and Dorsch, R.G., INTERIM  
PREDICTION METHOD FOR LOW FREQUENCY CORE ENGINE  
NOISE, NASA TMX-71627 (Nov. 1974).
16. Heidmann, M. F., INTERIM PREDICTION METHOD FOR FAN  
AND COMPRESSOR NOISE SOURCE, NASA TX-71763 (June 1975).
17. Gilliam, R. E., et al, ANOPP USERS MANUAL, (July 1978).

Distribution List - QCGAT Final Report

<u>Addressee</u>	<u>Number of Copies</u>
1. NASA Scientific and Technical Information Facility P.O. Box 8757 Bal't/Wash. International Airport MD 21240 Attn: Accessioning Dept.	25
2. NASA Lewis Research Center 21000 Brookpark Road Cleveland, Ohio 44135 Attn: G. K. Sievers MS 301-2	
-NASA Project Manager	1
L. Schopen MS 500-305	
-NASA Lewis Contracting Officer	1
Lewis Library MS 60-3	2
Report Control Office MS 5-5	1
J.F. McCarthy, Jr. MS 3-2	1
J.M Klineberg MS 3-3	1
W.L. Stewart MS 3-5	1
D. Poferl MS 500-207	1
J.R. Esterly MS 500-207	1
C.E. Feiler MS 54-3	1
J.F. Groeneweg MS 54-3	1
E.J. Rice MS 54-3	1
W.L. Jones MS 500-208	1
J.G. McArdle MS 500-208	1
U.H. von Glahn MS 54-3	1
J.R. Stone MS 54-3	1
M. Reshotko MS 54-3	1
J.A. Yuska MS 500-208	1
W.H. Fenning MS 500-208	1
A.S. Moore MS 500-208	1
D.D. Chrulski MS 500-208	1
R.J. Weber MS 501-10	1
K.L. Abdalla MS 500-127	10
D.L. Bresnahan MS 500-127	1

AddresseeNumber of Copies

## NASA Lewis Research Center (cont'd)

E.A. Krejsa	MS 54-3	1
D.A. Petrash	MS 60-6	1
R.E. Jones	MS 60-6	1
E.A. Lezberg	MS 60-4	1
J.S. Fear	MS 54-6	1
M.A. Beheim	MS 86-1	1
D. Drain	MS 100-1	1
D.L. Nored	MS 301-2	1
M.R. Vanco	MS 301-4	1
R. Rudey	MS 60-4	1
M.J. Hartmann	MS 5-3	1
W.J. Anderson	MS 23-2	1
L.P. Ludwig	MS 23-2	1
D.P. Townsend	MS 6-1	1
C.L. Ball	MS 5-9	1
L. Reid	MS 5-9	1
R.D. Moore	MS 5-9	1
H.E. Rohilk	MS 77-2	1
R.Y. Wong	MS 77-2	1
F.S. Stepka	MS 77-2	1
R.C. Bill	MS 23-2	1
J.J. Coy	MS 6-1	1
P.L. Meitner	MS 77-2	1
C.P. Blankenship	MS 105-1	1
L.M. Hibben	MS 500-211	1
E.R. Hersman	MS 21-4	1
L.A. Povinelli	MS 86-1	1
3. NASA Headquarters		
600 Independence Avenue SW		
Washington, D.C. 20546		
Attn: Assoc. Admin, OAST	Code R-1	1
W.B. Olstad	Code RD	1
-Dep. Assoc.		
Admin		
W.S. Aiken, Jr.	Code RJ-2	1
H. Johnson	Code RJG-4	3
R. Rose	Code RJG-4	1
G. Banerian	Code RTP-6	1
4. NASA Langley Research Center		
Hampton, Virginia 23365		
Attn: O.W. Nicks	MS 103A	1

AddresseeNumber of Copies

## NASA Langley Research Center (cont'd)

	J. P. Raney	MS 461	1
	J. W. Stickle	MS 246A	1
	B. J. Holmes	MS 247	1
5.	NASA Ames Research Center		
	Moffett Field, California 94035		
	Attn: L. Roberts	MS 200-3	1
	T. L. Galloway	MS 237-9	1
	M. D. Shovlin	MS 237-10	1
6.	NASA Dryden Flight Research Center		
	P. O. Box 273		
	Edwards, California 93523		
	Attn: I. T. Gillam		1
7.	Environmental Protection Agency		
	Crystal Mall, Bldg. 2		
	1921 Jefferson Davis Highway		
	Arlington, Virginia 20460		
	Attn: H. J. Nozick		1
	J. Shettino		1
	W. Sperry		1
8.	Dept. of Transportation		
	ARD 500		
	Washington, D. C. 20591		
	Attn: H. True		1
9.	DOT/FAA		
	800 Independence Ave, SW		
	Washington, D. C. 20591		
	Attn: J. O. Powers		1
	C. Foster		1
	R. N. Tedrick		1
10.	DOT/FAA		
	Nat'l Av. Fac. Exp.		
	Atlantic City, New Jersey 08405		
	Attn: J. F. Woodall		1
11.	AF Systems Command Liaison Office		
	Lewis Research Center, NASA		
	2100 Brookpark Rd.		
	Cleveland, Ohio 44135		
	Attn: Maj. A. J. Willoughby		1



AddresseeNumber of Copies

12.	Propulsion Laboratory US Army Res. & Tech. Laboratories Lewis Research Center, NASA 21000 Brookpark Road Cleveland, Ohio 44135 Attn: J. Acurio		1
13.	E.E. Bailey Technical Liaison AFAPL/DO Wright Patterson AFB, Ohio 45433		2
14.	Wright Patterson AF Base Dayton, Ohio 45433 Attn: W.C. Elrod E. Klenke E. Lake R.L. Spencer	AFIT/ENY ASD/ENFP AFAPL/POP1 AFAPL/TBD	1 1 1 1
15.	US Army Res. & Techn. Lab Applied Technology Lab Ft. Eustis, Virginia 23604 Attn: C.A. Elliot H. Morrow		1 1
16.	Naval Air Development Center Warminster, Pennsylvania 18974 Attn: S.R. Shapiro		1
17.	Air Research Manufacturing Co. 402 South 36 Street Phoenix, Arizona 85010 Attn: F.B. Wallace R. Heldenbrand W. Norgren L. Kisner W. Blackmore F. Lewis		1 1 1 1 1 1
18.	Garrett Corporation P.O. Box 92248 Los Angeles, California 90009 Attn: I.E. Spear J. Mason		1 1
19.	Garrett Corporation 19201 Susana Road Compton, California 90221 Attn: G. Paden		1

AddresseeNumber of Copies

20.	Garrett Corporation Dayton Office 333 West First Street Dayton, Ohio 45402 Attn: B. Tyson	1
21.	Garrett Corporation Suite 419 1625 I Street, NW Washington, D. C. 20006 Attn: M. S. Rachlin	1
22.	Boeing Commercial Airplane Co. P. O. Box 3707 Renton, Washington 98124 Attn: C. G. Hodge	1
23.	The Boeing Company 3801 S. Oliver Street Wichita, Kansas 67210 Attn: M. D. Nelson	1
24.	Beech Aircraft Corp. 9709 East Central Wichita, Kansas 67201 Attn: R. L. Benefiel R. C. Umcheidt W. D. Wise	1 1 1
25.	Bolt, Beranek & Newman, Inc. 21120 Vanowen St. Canoga Park, California 91303 Attn: W. J. Galloway J. F. Wilby	1 1
26.	Cessna Aircraft Company P. O. Box 1521 Wichita, Kansas 67201 Attn: M. S. Harned	1
27.	Cessna Aircraft Company Pawnee Division Wichita, Kansas 67201 Attn: A. Asher	1
28.	Cessna Aircraft Company Wallace Division P. O. Box 7704 Wichita, Kansas 67201 Attn: E. Kraus	1

<u>Addressee</u>	<u>Number of Copies</u>
29. Detroit Diesel Allison Division of General Motors Suite 312 333 West First Street Dayton, Ohio 45402 Attn: F. Walters	1
30. Douglas Aircraft Company 3855 Lakewood Blvd. Long Beach, California 90846 Attn: R. Pendley	1
31. GAMA 1025 CT Ave. NW #1025 Washington, D.C. 20036 Attn.: S.J. Green	1
32. Gates Learjet Corporation P.O. Box 7707 Wichita, Kansas 67277 Attn: E. Schiller R.C. Scott	1 1
33. General Electric Co. P.O. Box 81186 Cleveland, Ohio 44181 Attn: M. H. Rudasil	2
34. General Electric Co. 1000 Western Ave. Lynn, Massashusetts 01910 Attn: A.J. Koschier	1
35. Grumman Aerospace Corp. Bethpage, New York 11714 Attn: C.A. Hoelzer	1
36. Gulfstream American Corp. P.O. Box 2206 Savannah, Georgia 31402 Attn: R.J. Stewart, MS D-04	1

<u>Addressee</u>	<u>Number of Copies</u>
37.    Learavia P.O. Box 6000 Reno, Nevada        89506 Attn:                I. Gilchrist	1
38.    Lockheed Georgia Co. 86 South Cobb Drive Marietta, Georgia    30063 Attn:                H. J. Rubel Dept. 72-73 W. A. French Dept. 72-47	1 1
39.    Piper Aircraft Corp. Lock Haven, Pennsylvania 17745 Attn:                C. L. Kuntz M. J. Dees, Jr.	1 1
40.    Pratt & Whitney Aircraft 20800 Center Ridge Road Rocky River, Ohio    44116 Attn:                J. C. Chew	2
41.    Rockwell International Corp. General Aviation Division 5001 North Rockwell Ave. Bethany, Oklahoma    73008 Attn:                L. L. McHughes	1
42.    Rohr Corporation P.O. Box 878 Chula Vista, California 92012 Attn:                F. Horn	1
43.    Solar Turbine International P.O. Box 80966 San Diego, California    92138 Attn:                G. Hosany    MZR1	1
44.    Teledyne CAE 1330 Laskey Road Toledo, Ohio    43601 Attn:                B. Signh R. Snook H. Paget E. Benstein	1 1 1 1

<u>Addressee</u>	<u>Number of Copies</u>
45. University of Oklahoma 865 ASP Norman, Oklahoma 73019 Attn: Dr. K.H. Bergey	1
46. Vought Corporation P.O. Box 5907 Dallas, Texas 75222 Attn: S. Laden	1
47. Williams Research Corp. 2280 West Maple Road P.O. Box 95 Walled Lake, Michigan 48088 Attn: E. Lays Library	1 1
48. University of Kansas Department of Aerospace Engineering Lawrence, Kansas 66045 Attn: J. Roskam	1
49. General Aviation Assoc., Inc. Basking Ridge, New Jersey 07920 Attn: J.W. Olcott	1
50. Aircraft Owners and Pilots Association 7315 Wisconsin Avenue, N.W. Washington, DC 20014 Attn: J.L. Baker	1
51. National Business Aircraft Association, Inc. One Farragut Square Washington, DC 20006 Attn: J.H. Winant	1
52. Avco Aerostructures Division P.O. Box 210 Nashville, Tennessee 37202 Attn: J. Burkard	1
53. Avco Lycoming Engine Group 652 Oliver Street Williamsport, Pennsylvania 17701 Attn: S. Jedrzejewski J. Duke	1 1
54. Lockheed California Company Burbank California 91503 Attn: H.E. Wharton	1

**End of Document**